

การเลื่อนตัวอายุอ่อนบริเวณรอยเลื่อนศรีสวัสดิ์ส่วนใต้ อำเภอศรีสวัสดิ์  
จังหวัดกาญจนบุรี และการหาอายุด้วยวิธีการเรืองแสงความร้อน



นายรัชชัช นันทิ

สถาบันวิทยบริการ

จุฬาลงกรณ์มหาวิทยาลัย

วิทยานิพนธ์นี้เป็นส่วนหนึ่งของการศึกษาตามหลักสูตรปริญญาวิทยาศาสตรมหาบัณฑิต

สาขาวิชาธรณีวิทยา ภาควิชาธรณีวิทยา

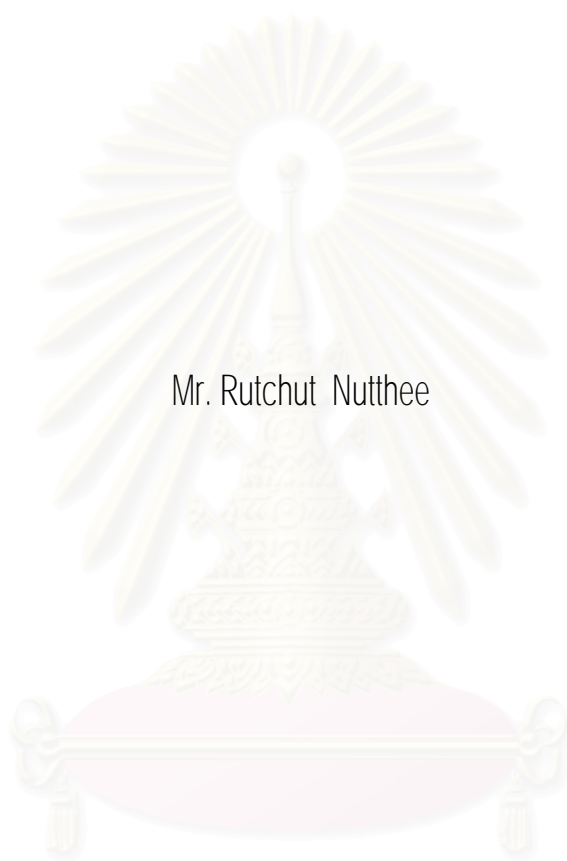
คณะวิทยาศาสตร์ จุฬาลงกรณ์มหาวิทยาลัย

ปีการศึกษา 2545

ISBN 974-17-1018-6

ลิขสิทธิ์ของจุฬาลงกรณ์มหาวิทยาลัย

YOUNG FAULT MOVEMENTS ALONG THE SOUTHERN SEGMENT OF SRI SAWAT FAULT,  
AMPHOE SRI SAWAT, CHANGWAT KANCHANABURI;  
AND THEIR TL-DATING RESULTS



Mr. Rutchut Nutthee

สถาบันวิทยบริการ  
จุฬาลงกรณ์มหาวิทยาลัย  
A Thesis Submitted in Partial Fulfillment of the Requirements  
for the Degree of Master of Science in Geology

Department of Geology  
Faculty of Science  
Chulalongkorn University  
Academic Year 2002  
ISBN 974-17-1018-6

Thesis Title                      Young faulting along the southern segment of Sri Sawat fault,  
Amphoe Sri Sawat, Changwat Kanchanaburi  
By                                      Mr. Rutchut Nutthee  
Field of Study                      Geology  
Thesis Advisor                      Assistance Professor Veerote Daorerk  
Thesis Co-advisor                      Assistance Professor Punya Charusiri, Ph.D.

---

Accepted by the Faculty of Science, Chulalongkorn University in Partial  
Fulfillment of the Requirements for the Master 's Degree

..... Dean of the Faculty of Science  
(Associate Professor Wanchai Phothiphichitr, Ph.D.)

THESIS COMMITTEE

..... Chairman  
(Assistance Professor Somchai Nakapadungrat, Ph.D.)

..... Thesis Advisor  
(Assistance Professor Veerote Daorerk, M.Sc.)

..... Thesis Co-advisor  
(Assistance Professor Punya Charusiri, Ph.D.)

..... Member  
(Assistance Professor Nopadon Muangnoicharoen, Ph.D.)

..... Member  
(Mr. Apichard Lumchaun, M.Sc.)

รัชชัช นัทธี : การเลื่อนตัวอายุอ่อนบริเวณรอยเลื่อนศรีสวัสดิ์ส่วนใต้ อำเภอศรีสวัสดิ์ จังหวัดกาญจนบุรี และการหาอายุด้วยวิธีการเรืองแสงความร้อน. (YOUNG FAULT MOVEMENTS ALONG THE SOUTHERN SEGMENT OF SRI SAWAT FAULT, AMPHOE SRI SAWAT, CHANGWAT KANCHANABURI; AND THEIR TL-DATING RESULTS) อ. ที่ปรึกษา : ผศ. ดร. วิโรจน์ ดาวฤกษ์, อ. ที่ปรึกษาร่วม : ผศ. ดร. ปัญญา จารุศิริ, 205 หน้า. ISBN 974-17-1018-6

การวิจัยนี้มีจุดประสงค์เพื่อศึกษารายละเอียดของแผ่นดินไหวในอดีตบริเวณรอยเลื่อนศรีสวัสดิ์ส่วนใต้ อันได้แก่ความต่อเนื่องของการไหวตัวจากอดีต หาอายุของการเคลื่อนที่ตามหลักฐานที่ปรากฏ พร้อมทั้งหาอัตราการเลื่อนตัวและการประมาณขนาดแผ่นดินไหวในอดีต เพื่อเป็นแนวทางกำหนดว่ารอยเลื่อนศรีสวัสดิ์เป็นรอยเลื่อนมีพลังหรือไม่

การศึกษาโดยข้อมูลจากระบบโทรสัมผัสพบว่าบริเวณส่วนใต้ของรอยเลื่อนศรีสวัสดิ์ แสดงแนวของรอยเลื่อนคมชัด มีลักษณะของรูปแบบธรณีฐานอันเกิดจากการเลื่อนตัวชัดเจน มีการเคลื่อนที่แบบขวาเข้าจากการศึกษาภาคสนามพบการสะสมตัวของตะกอนยุคอ่อน และตะกอนลานหินเชิงผา และการเลื่อนตัวของชั้นดินและเพดิเมนต์ที่ปรากฏจากชั้นหินโผล่ เป็นการเลื่อนตัวแบบย้อนกลับ ลักษณะของรอยเลื่อนศรีสวัสดิ์โดยสรุปจึงเป็นรอยเลื่อนตามแนวเฉียง

ตัวอย่างของตะกอนเชิงเขาที่สัมพันธ์กับรอยเลื่อนจำนวน 7 ตัวอย่างจากร่องสำรวจที่ขุด และอีก 10 ตัวอย่างจากร่องสำรวจที่เปิดหน้าดินไว้แล้ว ได้นำมาหาอายุโดยวิธีเรืองแสงความร้อน โดยใช้แร่ควอทซ์ที่คัดแยกออกมาจากตัวอย่างเพื่อวิเคราะห์ ซึ่บอกเหตุการณ์การเลื่อนตัวถึง 4 ครั้ง ได้แก่ อายุมากกว่า 80,400 ปี อายุระหว่าง 36,700 ถึง 49,300 ปี อายุระหว่าง 29,500 ถึง 30,000 ปี และ ระหว่าง 5,800 ถึง 9,200 ปี

อัตราการเลื่อนตัวของรอยเลื่อนศรีสวัสดิ์ซึ่งคำนวณจากวิธีของ McCalpin (1996) มีค่าประมาณ 0.672 มม/ปี และขนาดของแผ่นดินไหวคำนวณจากค่าความยาวของรอยเลื่อนโดยวิธีของ Wells and Coppersmith (1994) มีค่าประมาณ 6.3  $M_w$  ผลจากการหาอายุแสดงถึงการเลื่อนตัวของรอยเลื่อนศรีสวัสดิ์ส่วนใต้อยู่ในช่วงสมัยโฮโลซีน

ภาควิชา.....ธรณีวิทยา.....ลายมือชื่อนิสิต.....  
 สาขาวิชา.....ธรณีวิทยา.....ลายมือชื่ออาจารย์ที่ปรึกษา.....  
 ปีการศึกษา.....2545.....ลายมือชื่ออาจารย์ที่ปรึกษาร่วม.....

## 4272376123 : MAJOR GEOLOGY

KEY WORD: PALEOSEISMOLOGY / THERMOLUMINESCENCE / MORPHOTECTONIC / SRI SAWAT FAULT  
RUTCHUT NUTHEE : YOUNG FAULT MOVEMENTS ALONG THE SOUTHERN  
SEGMENT OF SRI SAWAT FAULT, AMPHOE SRI SAWAT, CHANGWAT KANCHANABURI;  
AND THEIR TL-DATING RESULTS.

THESIS ADVISOR : ASSISTANT PROFESSOR VEEROTE DAORERK, THESIS CO-  
ADVISOR : ASSISTANT PROFESSOR PUNYA CHARUSIRI, 205 pp. ISBN 974-17-1018-6

The purpose of this research is to clarify the paleoearthquakes along the southern segment of the Sri Sawat Fault (SSF), to determine the age of fault movements, to estimate their slip-rates and the magnitudes of paleoearthquakes, and to indicate whether this fault is still active.

By means of remote-sensing interpretation, the appearance of sharp lineaments are well observed together with morphotectonic features. These indicate the right-lateral displacement of SSF in the southern segment. Young deposition of sediments are found in field locations nearby SSF. In addition, the offset of top-soil and pediments observed from the recent road-cut exposures strongly indicate the local reverse fault movement of the SSF. Therefore, the fault is consequently regarded as the oblique slip fault.

Seven representative samples of colluvial sediments related to the SSF were collected from the Kaeng Khaep excavated trench and ten from Pha Tawan I and II trenches for thermoluminescence (TL) dating using particularly quartz concentrates extracted. However, the results indicate four faulting events, i.e., the prior 80.4 ka, the 36.7 to 49.3 ka, the 29.5 to 30.0 ka and 5.8 to 9.2 ka events.

The slip-rates of movements of SSF, based on the method of McCalpin (1996), is about 0.672 mm/year and its magnitude using surface rupture length (SRL), based on method described by Wells and Coppersmith (1994), is about 6.3  $M_w$ . The dating result shows the activeness of SSF within Holocene Epoch.

Department.....Geology.....Student's signature.....  
Field of study.....Geology.....Advisor's signature.....  
Academic year.....2002.....Co-advisor's signature.....

## ACKNOWLEDGEMENTS

Grateful acknowledgements are made to Electricity Generating Authority of Thailand; EGAT, and research fund from Ministry of Educational Affair for financial supports.

The author would like to express his deepest gratitude to Assist. Prof. Veerote Daorerk and Assist. Prof. Dr. Punya Charusiri, Department of Geology, Faculty of Science, Chulalongkorn University for valuable advice and encouragement throughout the study.

The author is highly indebted to Professor Dr. Isao Takashima, and Mr. Krit Won-In of the Research Institute of Materials and Resources, Akita University, for generousities and allowing to use the thermoluminescence equipment and beneficial comment for this research up to their helpful and take care while the author worked in Japan.

Thanks are also to Mr. Apichard Lumchaun, Mr. Suwith Kosuwan, and Mr. Preecha Saithong of the Geological Survey Division, Department of Mineral Resources (DMR), for their encouragements and providing all the necessary research facilities, Mr. Naramase Teerarungsigul and Mr. Santi Sri-chum for detailed survey facilities and Mrs. Suree Teerarungsigul for aerial photographs and remote sensing interpretation. Special recognition and thanks are extended to Mr. Chaiyan Hinthong for his valuable criticism, encouragement and reading of the manuscript, Mr. Puttana Asokanan and Mr. Chakawut Pinrote of Electricity Generating Authority of Thailand; EGAT, for providing grants and facilities.

Thank to Mr. Pisanuphong Kanchanapayon, Ms. Hathaitip Thassanapak, Mr. Mongkol Udchachon, Mr. Rottana Ladachart, Mr. Rattokorn Songmaung for field assistants and preparing the manuscript, and Mrs. Viyada Lamul for her helpful and facilities. Special thank to Ms. Titikan Mekjaruskul and for her suggestions, encouragement and manuscript preparation.

Thank to Police Captain, Dokmai Boonsilapa (Vice-gendarme of Amphoe Sri Sawat) and villagers at Tumbon Tha Kradan, Amphoe Sri Sawat, Changwat Kanchanabri for their welcome, helpful and providing facilities during the author's field work in the study area.

Finally, most sincere thanks are extended to his parents; Wing Commander Thong-kum and Mrs. Unchalee Nutthee, brothers, sister, and his family for their valuable loves, supporting and encouragement.

# CONTENTS

	Page
ABSTRACT IN THAI .....	iv
ABSTRACT IN ENGLISH .....	v
ACKNOWLEDGEMENTS .....	vi
CONTENTS .....	vii
LIST OF TABLES .....	xi
LIST OF FIGURES .....	xii
CHAPTER I INTRODUCTION .....	1
1.1 Background and research concept .....	1
1.1.1 Earthquakes in the World and Thailand .....	1
1.1.2 Earthquakes and Active Faults .....	2
1.1.3 Changwat Kanchanaburi and Sri Sawat Fault .....	4
1.2 Objectives .....	6
1.3 Methodology .....	8
1.3.1 Data Preparation and Locating Study area .....	10
1.3.2 Field Work Investigation .....	10
1.3.3 Laboratory Analysis .....	10
1.3.4 Discussion and Conclusion .....	10
1.4 Selected Literature Reviews and Previous work .....	10
CHAPTER II PALEOSEISMOLOGY AND RELATED OTHER TECTONICS STUDIES ..	18
2.1 Introduction to Paleoseismology .....	18
2.1.1 Definition .....	18
2.1.2 Relation of Paleoseismology and Other Neotectonic Studies ..	18
2.1.3 Application of Paleoseismics data to Seismic Hazard Assessment and Neotectonics Research .....	20
2.1.4 Field Techniques in Paleoseismology .....	21
2.1.4.1. Mapping Paleoseismic Landforms .....	21
2.1.4.2. Mapping Paleoseismic Stratigraphy .....	21
2.1.4.3 Geophysical Techniques in Paleoseismology.....	22

## CONTENTS (continued)

	Page
2.2 causes of Earthquake .....	22
2.3 Earthquake and Plate Tectonics Theory .....	23
2.3.1 Divergent Boundaries .....	27
2.3.2 Transform Boundaries .....	27
2.3.3 Convergent Boundaries .....	27
2.4 Seismotectonic Setting .....	30
 CHAPTER III SRI SAWAT FAULT .....	 35
3.1 The Studies of Sri Sawat Fault in Thailand .....	35
3.2 Segmentation of Sri Sawat Fault .....	36
3.2.1 Northern segment of Sri Sawat fault .....	38
3.2.2 Central segment of Sri Sawat fault .....	38
3.2.3 Southern segment of Sri Sawat fault .....	40
3.3 Locating Study Area .....	40
3.3.1 Area A; Srinakarind Dam .....	42
3.3.2 Area B; Ban Kaeng Khaep .....	43
3.3.3 Area C; Ban Tha Thung Na .....	50
3.4 General Geology of the Study Area .....	54
3.4.1 Geological Setting .....	54
3.4.2 Structural Setting .....	57
3.5 Field Work Investigation .....	58
3.5.1 Station 1 .....	58
3.5.2 Station 2 .....	61
3.5.3 Station 3 .....	68
3.5.4 Station 4 .....	68
3.5.5 Station 5 .....	70
3.5.6 Station 6 .....	70



## CONTENTS (continued)

	Page
CHAPTER IV Paleoseismic Study by Using Trenching Technique .....	72
4.1 Location of Trenches .....	72
4.2 Sample collection for Thermoluminescence (TL-) Dating .....	72
4.3 Ban Kaeng Khaep Trench .....	74
4.3.1 Mapping Units and Description .....	75
4.3.2 Fault description .....	82
4.3.3 Location of collected samples .....	85
4.4 Ban Pha Tawan Trench 1 .....	85
4.4.1 Mapping unit and description .....	92
4.4.1.1 Northwest trench wall .....	92
4.4.1.2 Southeast trench wall .....	93
4.4.2 Location of collected samples .....	93
4.5 Ban Pha Tawan Trench 2 .....	97
4.5.1 Mapping unit and description .....	97
4.5.2 Location of collected sample .....	99
CHAPTER V AGE DETERMINATION BY THERMOLUMINESCENCE DATING .....	102
5.1 The Thermoluminescence Process .....	102
5.2 Thermoluminescence Dating .....	103
5.2.1 The Age Equation .....	103
5.2.2 Events Dated by Thermoluminescence .....	105
5.3 Sample Preparation .....	107
5.3.1 Crushing and Sieving .....	107
5.3.2 Sample Washing and Purify Quart Grained .....	108
5.4 Sample Treatment .....	108
5.4.1 Water Content Determination .....	108
5.4.2 Annual Dose Determination .....	108
5.4.3 Reset existing TL signals to zero and Artificial Irradiation .....	111
5.4.4 Measurement of Thermoluminescence .....	111

## CONTENTS (continued)

	Page
5.5 Calculation of Thermoluminescence Age .....	114
5.5.1 Evaluation Paleodose .....	114
5.5.2 Correction of Dated sediments .....	116
5.5.2.1 The Basis of The Dating of sediments .....	116
5.5.2.2 Methods of Evaluation of the Accumulated Dose [D(I <sub>0</sub> )] After Deposit .....	124
5.6 Thermoluminescence Age Estimate .....	132
5.7 Thermoluminescence Age of Sedimentary Unit .....	132
5.7.1 Ban Kaeng Khaep Trench .....	134
5.7.2 Ban Pha Tawan Trench 1 .....	138
5.7.3 Ban Pha Tawan Trench 2 .....	138
5.8 Suggestion of TL Dating .....	140
 CHAPTER VI DISCUSSION AND CONCLUSION .....	 141
6.1 Behavior of Paleo-Movements of Southern Segment of Sri Sawat Fault ..	141
6.2 Sequence of Fault Movements .....	142
6.3 Relationship between TL Ages and Fault Movements .....	142
6.4 Calculation of Fault Slip Rate .....	148
6.5 Estimating Paleoearthquake Magnitude .....	148
 CHAPTER VII CONCLUSION AND RECOMMENDATION .....	 151
7.1 Conclusion .....	151
7.2 Recommendation .....	151
REFERENCES .....	153
APPENDICES .....	168
BIOGRAPHY .....	205

## LIST OF TABLES

	Page
Table 4.1	Summary of the description of mapped unit for both side wall of the Kaeng Khaep Trench ..... 77
Table 5.1	Results of water content, natural radioactive content (U, Th, K20) and annual dose for TL dating samples from Ban Kaeng Khaep and Ban Pha Tawan I and II Trench.....112
Table 5.2	Age estimates for samples from Ban Kaeng Khaep and Ban Pha Tawan I and II Trench.....135
Table 6.1	Empirical relationships between moment magnitude (M) and fault parameters (Wells and Coppersmith, 1994) ..... 150



สถาบันวิทยบริการ  
จุฬาลงกรณ์มหาวิทยาลัย

## LIST OF FIGURES

	Page
Figure 1.1	Index map of Thailand and neighboring countries showing epicentral distribution since 1456 to 2000 (Charusiri et al., 2001) ..... 5
Figure 1.2	Route map of western Thailand showing location of main roads, major towns/districts, and the study area (at southern end of Srinagarind Dam)..... 7
Figure 1.3	Flow chart showing the methodology applied in this study ..... 9
Figure 1.4	Seismic source zone of Myanmar-Thailand-Indochina (Nutalaya, 1987). 12
Figure 1.5	Seismotectonic map of parts of Myanmar and Thailand showing distribution of major fault (Modified from Nutalaya, 1986) ..... 13
Figure 2.1	World distribution of earthquakes recorded over a six-year period with focal depths between 0 and 700 kilometers, showing major earthquake belts (labeled) (Plummer et al., 2001) ..... 24
Figure 2.2	Major plates of the world in the theory of plate tectonics. Compare the locations of plate boundaries with earthquake locations shown in figure 2.1. Double lines show diverging plate boundaries, single lines show transform boundaries. Heavy lines with triangles show converging boundaries; triangles point down subduction zone (Plummer et al., 2001) ..... 25
Figure 2.3	An idealized cross-section illustrating the relationship between the lithosphere and the underlying asthenosphere and the three principal types of plate boundaries: divergent, convergent, and transform (after Monroe and Wicander, 1998) ..... 26
Figure 2.4	Divergent plate boundaries. (A) On the ocean floor. (B) On a continent. Each boundary is marked by a rift valley and narrow band of shallow-focus earthquakes (shown as stars). Depth of rift valleys is exaggerated (Plummer et al., 2001) ..... 28
Figure 2.5	Transform boundaries. (A) Narrow band of shallow-focus earthquakes shown as stars along single fault. (B) Broad band of earthquakes along a system of parallel faults (Plummer et al., 2001) ..... 28

## LIST OF FIGURES (Continued)

	Page	
Figure 2.6	(A) A vergent boundary marked by the collision of two continents. A very broad zone of shallow-focus earthquakes occurs along a complex system of faults. (B) A convergent boundary with ocean floor subducting plate due to tension, underthrusting, and compression (Plummer et al., 2001) ..... 29	29
Figure 2.7	Tectonic map of south and southeast Asia and south China (Polachan et al., 1991) ..... 31	31
Figure 2.8	Seimotectonic provinces in Thailand (Woodward-Clyde, 1998) ..... 33	33
Figure 3.1	Landsat TM5 satellite imagery showing orientation of three major faults – Mae Ping Fault (MPF), Sri Sawat Fault (SSF), and Three Pagodas Fault (TPF) in Western part of Thailand and eastern Part of Myanmar..... 37	37
Figure 3.2	Major faults and plotted epicenters in Changwat Kanchanaburi during 1983 to 1999. The box area shows location of the largest epicenter occurred on April 22, 1983 and its aftershocks ..... 39	39
Figure 3.3	Satellite imagery Landsat TM5 showing the locations of three areas (area A, B, and C), which were studied in detail by aerial photograph interpretation ..... 41	41
Figure 3.4	(a) Part of topographic map (sheet no. 4837 IV) showing topographic features of area A-southern part of the Srinakarind Dam.(b) Aerial photograph showing physiographic feature of area A ..... 44	44
Figure 3.5	(a) Aerial photographic interpretation of rock distribution (form Fig. 3.4(b)) of area A, and (b) Morphotectonic interpretation of the similar area. Symbols are shown in Fig. 3.6 ..... 45	45
Figure 3.6	Legend and symbol, which are used in interpreted rock unit and geomorphologic map, i.e., Fig. 3.5, Fig 3.8, and Fig 3.10..... 46	46
Figure 3.7	(a) Part of topographic map (sheet no. 4837 IV) showing topographic features of area B. (b) Aerial photograph of area B showing morphology. Note that the box area is for Fig. 3.20 ..... 48	48

## LIST OF FIGURES (Continued)

	Page
Figure 3.8 (a) Aerial photographic interpretation of rock distribution (form Fig. 3.7(b)) of area B, and (b) Morphotectonic interpretation of the similar area. Symbols are shown in Fig. 3.6 .....	49
Figure 3.9 (a) Part of topographic map (sheet no. 4837 IV) showing topographic features of area C at Ban Tha Thung Na. (b) Aerial photographic area B showing physiographic feature of area C .....	52
Figure 3.10 (a) Aerial photographic interpretation of rock distribution (form Fig. 3.9(b)) of area C, and (b) Morphotectonic interpretation of the similar area. Symbols are shown in Fig. 3.6 .....	53
Figure 3.11 Geological legend and symbols of geologic map in Fig 3.12 (Modified after Bunopar, 1976).....	55
Figure 3.12 Geological map of the study area and its vicinity showing very deformed and faulted strata of Precambrian to Quaternary ages (after Bunopas, 1976) .....	56
Figure 3.13 Part of topographic map (sheet no. 4837 IV) showing six locations Of field-detailed in study area .....	59
Figure 3.14 Part of station 1 showing talus deposit at the foreground of Khao Nom Nang, view looking N40°E .....	60
Figure 3.15 Close-up view (of Fig. 3.12) showing coarse fragments with high angularity of talus deposit .....	61
Figure 3.16 The Talus deposit right at the down-slope end of station1, view looking N45°E .....	62
Figure 3.17 Close-up view of Fig. 3.14 showing calcareous cement in talus called as "Caliche" .....	62
Figure 3.18 Enlarge aerial photograph of Fig. 3.7 showing a dextrally offset stream (O) and a shutter ridge (S) along the southern segment of SSF. Box indicates detailed survey map in Fig.3.18 .....	63
Figure 3.19 Assemblage of Landforms associated with strike slip faulting (after Vedder and wallace, 1970) .....	63

## LIST OF FIGURES (Continued)

	Page
Figure 3.20	Detail survey map covering offset stream of station 2. Note that the ▲ 1 to ▲ 5 are locations of outcrop exposure in Fig. 3.19 to 3.24 ..... 64
Figure 3.21	Exposure of colluvial deposit at ▲ 1 from Fig. 3.18, view looking N80°W ..... 65
Figure 3.22	Exposure of colluvial deposit at ▲ 2 from Fig. 3.18, view looking S5°E ..... 65
Figure 3.23	Exposure of colluvial deposit at ▲ 3 from Fig. 3.18, view looking S50°W ..... 66
Figure 3.24	Exposure of colluvial deposit at ▲ 4 from Fig. 3.18, view looking S10°E ..... 66
Figure 3.25	The travertine showing characteristic as a vertical wedge penetrating into horizontal gravel bed at ▲ 5 from Fig. 3.18, view looking S10°E... 67
Figure 3.26	A Horizontal gravel bed with somewhat graded bedding at the exposure at ▲ 5 from Fig. 3.18 ..... 67
Figure 3.27	Man-made exposure at Ban Pha Tawan showing sediment deposits on the northwest trench wall (Ban Pha Tawan Trench 1), view looking N50°W ..... 69
Figure 3.28	Road cut exposure showing a major fault whose plane is N60W strike and 35° dip at Ban Namtok Erawan, view looking N65°E..... 71
Figure 3.29	Close -up view of Ban Namtok Erawan showing an offset of surface indicating to reverse fault. .... 71
Figure 4.1	Part of topographic map (sheet no. 4837 IV) of study area showing locations of the excavated trenches ..... 73
Figure 4.2	(a) Photograph of the Kaeng Khaep Trench. It was excavated by back-holes, and trench wall-sides were later cleaned, cured, and brushed by local villager. (b) A top view outline of the Kaeng Khaep Trench showing its dimension and orientation ..... 76
Figure 4.3	Trench log of the west wall in Ban Kaeng Khaep Trench, showing principle stratigraphy and sample location for TL-dating ..... 77

## LIST OF FIGURES (Continued)

	Page
Figure 4.4	Trench log of the east wall in Ban Kaeng Khaep Trench, showing principle stratigraphy and sample location for TL-dating ..... 78
Figure 4.5	White veins of calcite cut into weathered Triassic mudstone bedrocks, west wall- side of the Ban Kaeng Kheap Trench ..... 81
Figure 4.6	Very weathered mudstone bedrocks of unit 7, west wall- side of the Ban Kaeng Kheap Trench ..... 81
Figure 4.7	The Triassic mudstone/siltstone of unit 7 was cut by reverse sense of fault (F1) movement ..... 83
Figure 4.8	East wall-side of Kaeng Khaep Trench showing the sharp contact between the Unit 6 and the Unit 7. These two unit were separated by a major fault (F2). This fault is a reverse fault with low-angle dipping (45° to vertical). Note that there is a sharp contact of Triassic mudstone /siltstone of Unit 6 ..... 84
Figure 4.9	The F3 reverse fault cutting into almost vertical beds of weathered Triassic siltstone bedrock of the Unit 7 on the western side wall of the Ban Kaeng Khaep Trench ..... 86
Figure 4.10	Folded beds of Triassic mudstone of the Unit 6 cut by the F8 fault, west-wall side of the Pha Tawan Trench ..... 87
Figure 4.11	The chocolate colluvium in east-wall side of Ban Pha tawan Trench, was cut by the F3 ..... 87
Figure 4.12	The northeast wall side of the Ban Pha Tawan I Trench showing alternating layers of underconsolidated coarse- and fine-grained sediments, interpreted as debris- and wash-facies, respectively. Note that the white-line square grid is about 0.5m long, and colored flags indicate contact boundary between two adjacent units ..... 89
Figure 4.13	Trench-log sketch map of the northwest wall in Ban Pha Tawan I Trench, showing principle stratigraphy and sample location for TL-dating ..... 90



## LIST OF FIGURES (Continued)

	Page
Figure 4.14 Schematic diagrams showing the deposition of colluvium from a two-event reverse fault scarp (McCalpin, 1996).....	91
Figure 4.15 Close-up view of the northwest trench wall, Ban Phatawan I Trench showing stratigraphy and lithology of unconsolidated sediments with colored flags marked at the contact boundary between two adjacent units. Noted that from the top soil layer to the bottom layer is about 1.5 m thick.....	94
Figure 4.16 Stratigraphy of young, unconsolidated sediment deposits on the southeast trenching wall in Ban Pha Tawan II Trench , Showing location of samples for TL-dating in the fine-grained sediment layer .....	95
Figure 4.17 Close-up view of the southeast trench-wall side, Ban Pha Tawan I Trench, showing abundant angular quartzite and feldspar-rich sandstone. The reverse graded beds represent debris flow deposits .....	96
Figure 4.18 The consolidated gravel layer overlying triassic clastic bedrocks with a sharp contact and showing 2 samples for TL dating, Ban Pha Tawan II Trench. The step like feature (A) and colluvial wedge (B) interpreted to be cause by faulting, view looking N40°W .....	98
Figure 4.19 Panoramic view of the Ban Pha Tawan II Trench (continue Fig. 4.17) showing unconsolidated gravel layer lying over deformed bedrock .....	98
Figure 4.20 Close-up view looking N40°W showing a colluvium wedge and uplift of gravel bed .....	100
Figure 4.21 Close-up view of figure 4.17 showing well-defined colluvium wedge due to earthquake faulting .....	100
Figure 4.22 Close-up view of figure 4.17 showing a colluvium wedge and location of sample for TL dating .....	101
Figure 4.23 Close-up view of figure 4.17 showing highly angular clasts (fragments of quartzite) with a colluvium wedge .....	101

## LIST OF FIGURES (Continued)

	Page
Figure 5.1 Energy band model showing the mechanism of the TL process (after Aitken 1978) .....	104
Figure 5.2 Schematic representation of the parameters of a TL curve (after Marfunin, 1979) .....	104
Figure 5.3 Events that can be dated by TL method (after Singhvi and Wagner 1986) .....	106
Figure 5.4 Weighting the sample as part of sample preparation for annual dose determination. (Mr. Krit Won-In, right, is to scale) .....	109
Figure 5.5 Samples are cleaned and washed with taping water after etching with HF (Mr. Rutchut Nutthee is to scale) .....	109
Figure 5.6 Frantz's isodynamic magnetrometer was applied to separate dark-colored minerals from light-colored less magnetic ones .....	110
Figure 5.7 Gamma-ray spectrometer (bottom right) for determination of uranium, thorium, and potassium contents .....	110
Figure 5.8 Diagram of apparatus for thermoluminescence measurement. (after Aitken, 1985) .....	113
Figure 5.9 Common TL apparatus (the Kyokko 2500 TLD) with a photomultiplier (an instrument with Rutchut is left hand and the monitor (TV on the right) for showing TL signals .....	115
Figure 5.10 The TL glow curve of natural sample no KK5; 3 curve as (a), (b), (c), TL Signal at different amplification: (a) equal to 4 times of (b), and (b) equal to 4.5 times of (c). Each sample was treated in 3 times [(i), (ii), (iii)]. The intensity of natural samples ( $I_{nat}$ ) was evaluated from TL glow peaks at 350°C are 194, 174, and 146, respectively. The average intensity of natural sample [Avr.( $I_{nat}$ )] is 171.....	117
Figure 5.11 The TL glow curve of H+29 Gy The intensity of H+29 Gy samples ( $I_{H+29Gy}$ ) were evaluated from TL glow peak at 350°C are 40, 35, and 35, respectively .....	118

## LIST OF FIGURES (Continued)

	Page
Figure 5.12 The TL glow curve of H+99 Gy The intensity of H+99 Gy samples ( $I_{H+99Gy}$ ) were evaluated from TL glow peak at 350°C are 100, 96, and 95, respectively .....	119
Figure 5.13 The TL glow curve of H+229 Gy The intensity of H+229 Gy samples ( $I_{H+299Gy}$ ) were evaluated from TL glow peak at 350°C are 190, 199, and 188, respectively .....	120
Figure 5.13 The TL glow curve of N+309 Gy The intensity of N+309 Gy samples ( $I_{N+309Gy}$ ) were evaluated from TL glow peak at 350°C are 360, 382, and 279, respectively .....	121
Figure 5.15 The growth curve of sample no. KK5 showing evaluation of paleodose.	122
Figure 5.16 The glow curve of sample KK2 showing difference of natural sample compare with natural samples which were bleach by sunlight at 1, 2, 4, 8 and 16 hr .....	125
Figure 5.17 The glow curve of sample KK5 showing difference of natural sample compare with natural samples which were bleach by sunlight at 1, 2, 4, 8 and 16 hr .....	126
Figure 5.18 The glow curve of sample PT5 showing difference of natural sample compare with natural samples which were bleach by sunlight at 1, 2, 4, 8 and 16 hr .....	127
Figure 5.19 Thermoluminescence remaining after bleaching by expose to sunlight for various time of sample no. KK2. Exposure of samples to 8 hr of sunlight removes all of the light-bleachable.....	128
Figure 5.20 Thermoluminescence remaining after bleaching by expose to sunlight for various time of sample no. KK5. ....	129
Figure 5.21 Thermoluminescence remaining after bleaching by expose to sunlight for various time of sample no. PT5. ....	130
Figure 5.22 The glow curve of sample no. KK5 showing comparison of natural sample and same sample at 8 hr sunlight bleaching .....	131

## LIST OF FIGURES (Continued)

	Page
Figure 5.23	The growth curve of sample no. KK9 showing evaluation of $D(l_0)$ .....133
Figure 5.24	Age of dated samples of the west wall in Ban Kaeng Khaep Trench .....136
Figure 5.25	Age of dated samples of the east wall in Ban Kaeng Khaep Trench .....137
Figure 5.26	Age of dated samples in northwest wall of Ban Pha Tawan Thrench .....139
Figure 6.1	Schematic of oblique slip movement of southern segment of SSF. Note that AB and AD represent apparent lateral-slip components, AD and BC represent apparent vertical components, and AC is a resultant component with the oblique slip movement .....141
Figure 6.2	Arial photograph showing the erosional bench in study area. A-A' is a line of cross section through Khao Wang Masang Mt. in Fig. 6.3 .....143
Figure 6.3	A cross-section along the A-A' line in Fig. 6.2 showing 4 steps of erosional benches in Khao Wang Masang Mt. ....143
Figure 6.4	Schematic showing step of fault movement which produce the erosional bench (Hamblin, 1976) .....144
Figure 6.5	Cross section of part of the Wasath Fault in California, USA, showing wedge-like layer of colluvial sediments (darker colors; Unit 2) interpreted as a result of earthquake faulting (Forman et al., 1991). Numbers of ITL indicate TL dates and the others indicate $^{14}\text{C}$ dates of samples .....145
Figure 6.6	Schematic showing event of earthquakes and their ages; considered by stratigraphy and TL age dating result of Ban Kaeng Khaep Thench, Ban Pha Tawan I Trench and Ban Pha Tawan II Trench .....147
Figure 6.7	Surface rupture length (SRL, in km) as s function of movement magnitude (M) for 77 earthquakes in the historic data set of Wells and Coppersmith (1994). Equatio at bottom lists regression of M on log SRL for all fault types. Note that in part (b) there is a little difference between the relationships for the three fault types. (from Wells and Coppersmith, 1994) .....150

## LIST OF FIGURES (Continued)

	Page
Figure A.1.1 Graph showing the relationship of various magnitudes to moment magnitude. Relation for $m_{bl,g}$ is from Atkinson and Boore (1987). For $M_S$ and $M_L$ the relation come from fitting a quadratic to the data compiled by Ekstrom (1987) and Hanks and Boore (1984), respectively. [From Boore and Joyner (1994); reprinted with permission of the Applied Technology Concil.] .....	172
Figure A.1.2 Example of the calculation of the Richter magnitude ( $M_L$ ) of a local earthquake (Bolt, 1999) .....	173
Figure B.1.1 TL glow curves of sample nos. KK1, KK2, and KK3. ....	176
Figure B.1.2 TL glow curves of sample nos. KK4 and KK5.....	177
Figure B.1.3 TL glow curves of sample nos. KK6 and KK7.....	178
Figure B.1.4 TL glow curves of sample nos. PT1, PT2, and PT3 .....	179
Figure B.1.5 TL glow curves of sample nos. PT4, PT5, and PT6 .....	180
Figure B.1.6 TL glow curves of sample nos. PT7, PT8, and PT9 .....	181
Figure B.1.7 TL glow curves of sample nos. PT10 and PT11 .....	182
Figure B.2.1 TL growth curves of sample nos. KK1 and KK2 ... ..	184
Figure B.2.2 TL growth curves of sample nos. KK3 and KK4 ... ..	185
Figure B.2.3 TL growth curves of sample nos. KK5 and KK6 ... ..	186
Figure B.2.4 TL growth curves of sample nos. KK7 .....	187
Figure B.2.5 TL growth curves of sample nos. PT1 and PT2.....	188
Figure B.2.6 TL growth curves of sample nos. PT3 and PT4.....	189
Figure B.2.7 TL growth curves of sample nos. PT5 and PT6.....	190
Figure B.2.8 TL growth curves of sample nos. PT7 and PT8.....	191
Figure B.2.9 TL growth curves of sample nos. PT9 and PT10.....	192
Figure B.2.10 TL growth curves of sample nos. PT11 .....	193
Figure B.3.1 Plateau curve of sample nos. KK1 and KK2 .....	195
Figure B.3.2 Plateau curve of sample nos. KK3 and KK4 .....	196
Figure B.3.3 Plateau curve of sample nos. KK5 and KK6 .....	197

## LIST OF FIGURES (Continued)

	Page
Figure B.3.4 Plateau curve of sample nos. KK7 .....	198
Figure B.3.5 Plateau curve of sample nos. PT1 and PT2 .....	199
Figure B.3.6 Plateau curve of sample nos. PT3 and PT4 .....	200
Figure B.3.7 Plateau curve of sample nos. PT5 and PT6 .....	201
Figure B.3.8 Plateau curve of sample nos. PT7 and PT8 .....	202
Figure B.3.9 Plateau curve of sample nos. PT9 and PT10 .....	203
Figure B.3.10 Plateau curve of sample nos. PT11 .....	204



สถาบันวิทยบริการ  
จุฬาลงกรณ์มหาวิทยาลัย

# CHAPTER I

## INTRODUCTION

### 1.1 Background and Research Concept

#### 1.1.1 Earthquakes in the World and Thailand

Historically, earthquakes have caused the world's most tragic disasters. No other single natural phenomenon has caused loss of life as great as the 800,000 people killed in the Chinese earthquake of 1556 (Yeats et al., 1997). According to Meteorological Department (2000), report of major worldwide earthquake epicenters and their damages during January 1990 to November 2000, there are 106 major earthquakes with magnitudes of 4.9 to 7.9 on the Richter's scale. Fourteen times of these events brought severe damages, which lose life more than 1,000 persons in each time. Not only large volume of assets and budgets were used for revival of those countries, but also financial losses from even moderate earthquake have become significant drains on national economics. The magnitude 6.7 Northridge-California earthquake of 1994, for example, resulted in damages that exceeded 20 billion dollars, despite a relatively low loss of life (Yeats et al., 1997).

Many countries, where earthquakes have frequently and high potentially occurred, has been seriously studied in order to prevent and avoid their consequent damages. Therefore, the knowledge and technique concern with the study of earthquakes were developed and grown fast in the past few decades. The paleoseismology, one major discipline of this study, also developed.

However, Thailand may not realize to the loss caused by earthquakes yet. Perhaps, in the present time of concern, there is no sufficient large earthquake to produce strong damage. Nevertheless, from historic data, there were many major historical earthquakes felt in Thailand (Nutalaya et al., 1985 and Nutalaya, 1992). In Thailand, the first seismogram was installed in Chiangmai in 1963 and detect many earthquakes since 1963 till present (Nutalaya, 1992). However, most of them are microseismic and low magnitude. Although several seismicities are strong and human-

beings could feel, those earthquakes occurred in quite remote areas with low population density, or in areas with prevailing low-cost wooden building which may not be susceptible to earthquake action and whose failures have no severe economical consequences, particularly those along the Thailand border.

However, we should not abandon the data as explained above because detected seismic distribution from seismograph can confirm us whether or not seismicities still actives in Thailand. Although large earthquakes do not take place in the present time, how do we convince they not occur like in the past. Consequently, we should study about them for avoid and decrease losses and damages.

Furthermore, Bangkok, the capital city of Thailand with a population over eight million and lots of building, is situated on a large and extremely flat alluvial plain, commonly known as the "*Lower Central plain*" of Thailand. The uppermost soil layer is a soft silty marine clay, usually referred to as "*soft Bangkok clay*", which is about 10 to 18 m thick in the Bangkok metropolitan area (Warnichai et al., 2000). The clay has the ability to amplify earthquake ground motion. Therefore, earthquake damage may occur more than our expectation. A well-known example is the 1985 Michoacan earthquake, with a large magnitude ( $M_s=8.1$ ) on the coast of Mexico, caused considerable destruction and loss of life in Mexico City, 350 km from the epicentral location. Much of the destruction was due to significant amplification of earthquake ground motions by thick surficial deposits in the downtown area of Mexico City (Seed et al., 1987). The surficial geologic setting in Bangkok also appears qualitatively similar to the setting of Mexico City, and hence Bangkok, by analogy, appears to be susceptible to the same type of soil amplification of ground motions. According to Warnichai et al. (2000) it is evident that the soil profile underlying Bangkok has the ability to amplify earthquake ground motions about 3 to 6 times for extremely low intensity input motions and about 3 to 4 times for relatively stronger input motions. In addition, Warnichai et al. (2000) concluded that Bangkok, though located at a remote distance from seismic, and is still at risk of strong earthquake ground motions. Such risk is essentially caused by three major factors: the ability of regional seismic sources to generate large earthquakes, the low attenuation rate of ground motions in this region, and the ability of thick



unconsolidated surficial deposits in Bangkok to considerably amplify earthquake ground motions.

### 1.1.2 Earthquakes and Active Faults

Most of earthquakes in Thailand occur from fault movements, especially active faults or potentially active faults. Many authors define the term active fault in different ways:

Willis (1923) defined two classes of faults: active and dead. "An active fault is one on which a slip is likely to occur. A dead fault is one on which no movement may be expected"

Bonilla (1969) defined an active fault as "..... one that has moved in the recent past and may move in the near future". The term "recent past" includes the current hour and extends back to an infinite time that many geologists would take to include at least the Holocene Epoch (about 10,000 years ago) and the term "near future" is used to include the length of time on the order of the useful life of engineering structure or the time span considered in long range plans for the future". Some of criteria to define fault as active: (a) the occurrence of earthquakes that can be relate to the fault with reasonable assurance; (b) one or more episode of surface ruptures (including tectonic creep) or acute bending in the recent past as define above; (c) instrumental evidence of elastic and inelastic strain; and (d) structure coupling to another fault.

Cluff and Bolt (1969) defined that "A fault should be considered active if it has displaced recent alluvium or other recently formed deposits, whose surface effects have not been modified to an appreciable extent by erosion, which has earthquakes located in the near vicinity and whose recurrence of movement is expected.

Wentworth et al. (1970) claimed that "a fault is active if it can undergo movement from time to time in immediate geologic future".

Wesson et al (1972 and 1975) suggested that "active faults are characterized by at least one or more of the following features: (a) historic earthquakes with or without surface fault displacement; (b) ephemeral physiographic feature such as

sag ponds, offset stream, and linear ridges that suggest recent fault displacement; and (c) offset Holocene and Pleistocene deposits and geomorphic features”.

Wesson et al. (1975) expressed that “if a fault has been active over a considerable length of time (millions of years) and has been historical active or show evidence of movement in the geologically recent past, it will most likely sustain movement in the future”.

Keller (1979) also emphasized that “there is no real agreement on what away constitute an active fault. However, many geologists would label a fault “active” if it can be demonstrated that there has been movement during the last 11,000 years (Holocene time). Whereas fault accompanying recorded earthquakes certainly are active, it is often very difficult to prove the activity of fault unrelated to such easily measured phenomena”.

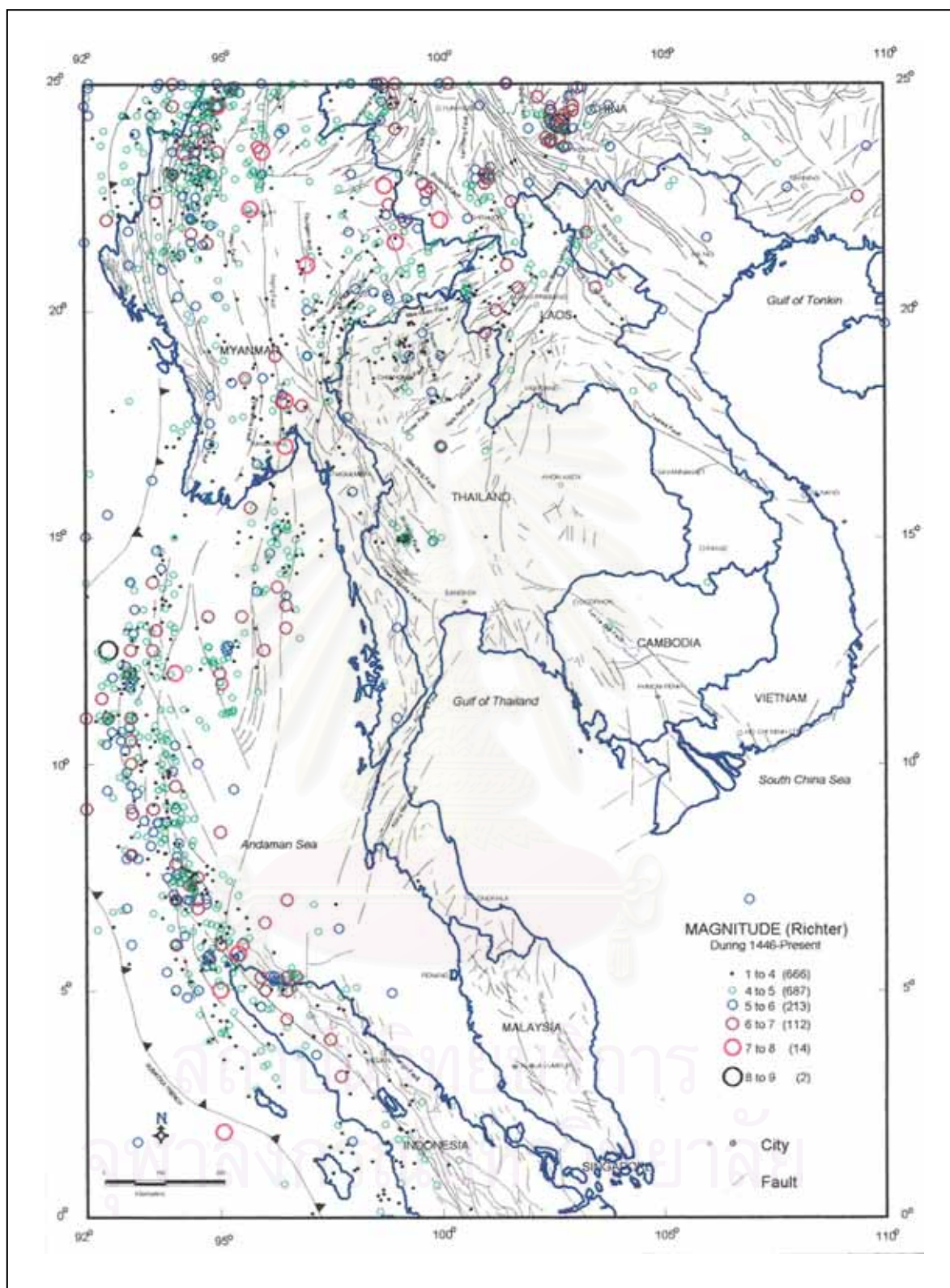
Wallace (1981) defined that “active faults are those faults that are considered likely to undergo renewed movement within a period of concern to humans.”

Wallace (1981) mentioned that the active fault that has moved and produced earthquakes in the recent past (Holocene epoch), and are considered likely to undergo renewed movement within a period of concern to humans. These faults should be studied in detail for define distinctly to be potentially active fault or dead fault, and specify age and magnitude of movement in the past, up to find basis for plan and abate possible calamity cause earthquake in the future.

There are many diversified definitions of active fault according to various authors’ principle and concept as above. However, the definition of Bonilla (1969) was considered to use for meaning of active fault throughout all chapters.

### 1.1.3 Changwat Kanchanaburi and Sri Sawat Fault

Changwat Kanchanaburi is located in the western part of Thailand and there are many earthquakes occurring at various magnitudes for decades (Fig 1.1). Several major faults are recognized in Kanchanaburi area (Won-In, 2000). Among these faults, the NW-trending Three Pagodas (TPF) and Sri Sawat Faults (SSF) seem to be the most important faults, cutting through several strata of different lithologies and ages.



### YOUNG FAULT MOVEMENTS ALONG THE SOUTHERN SEGMENT OF SRI SAWAT FAULT



MR. RUTCHUT NUTTHEE  
DEPARTMENT OF GEOLOGY  
FACULTY OF SCIENCE  
CHULALONGKORN UNIVERSITY

Figure 1.1 Index map of Thailand and neighboring countries showing epicentral distribution since 1456 to 2000 (Charusiri et al., 2001).

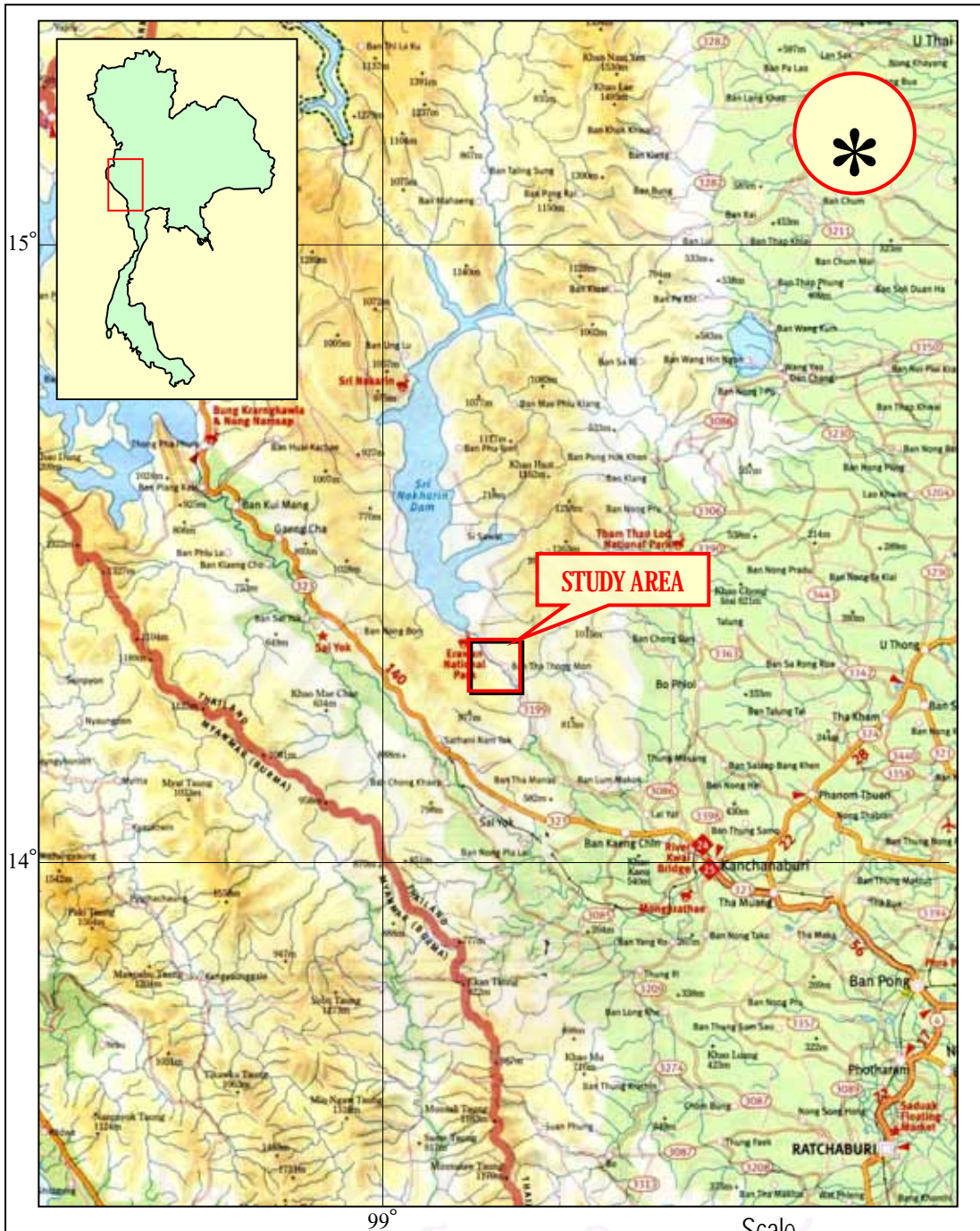
This perhaps makes the geological structure and morphology of the concerned area more intricate.

In April of 1983, there has been series of earthquakes located in the upper reaches of Srinagarind reservoir, the main shock on April 22, 1983 was 5.9  $M_L$ . The earthquakes are regarded closely related to SSF. This fault is the NW-SE trending oblique strike-slip fault with the total length of about 380 km, and can be traced from southeastern Myanmar into western Thailand. The fault is located between Three Pagodas fault and Mae Ping fault (MPF).

At present, there are several potential active faults in Thailand, but there are only few studies on these faults, especially detailed studies of them. This research mainly focuses particularly in detail to the study of a southern segment of the SSF. A study area (Fig 1.2) was located at the south of the Srinakarind Dam, covers about 90 square kilometers. It is about 170 kilometers northwestward from Bangkok. This area shows sharply lineaments and morphology-related fault movements (morphotectonics) (e.g. triangular facet, offset stream, shutter ridge and erosional bench). The fault was expected by the author that it is not old age and still be active fault. Beside, from the geologic map of Changwat Suphun Buri scales 1:250,000 (Bunopas, 1976) (Sec. 3.4), this fault cuts through at least four major rock formations indicates that this is the important fault in this area.

## 1.2 Objectives

The purpose of this research is to clarify the paleoearthquakes along the southern segment of the Sri-Sawat fault (SSF). Recent knowledges and techniques of paleoseismology are used for investigating interesting faults and their paleoearthquakes. Results of this research is to recognize the southern segment of the SSF, to identify each paleoearthquakes, to recognize their behavior, to estimate magnitudes and ages of paleoearthquakes, and to prove that this fault is an active fault, or not. For studying and planing to protect the damage by earthquake in the future.



**LEGEND**

- International Boundary
- Road
- River/Stream
- Province
- Town/District



**YOUNG FAULT MOVEMENTS ALONG THE SOUTHERN SEGMENT OF SRI SAWAT FAULT**



MR. RUTCHUT NUTTHEE  
 DEPARTMENT OF GEOLOGY  
 FACULTY OF SCIENCE  
 CHULALONGKORN UNIVERSITY

Figure 1.2 Route map of western Thailand showing location of main roads, major towns/districts, and the study area (at southern end of Srinagarind Dam).

The main objectives of this research are

1. to identify paleoearthquake evidences along the southern segment of the SSF
2. to determine the ages of fault movement in the study area, and
3. to estimate the magnitude and slip-rate of these events.

## 1.3 Methodology

Methodology of this research is divided into four parts (Fig 1.3) including:

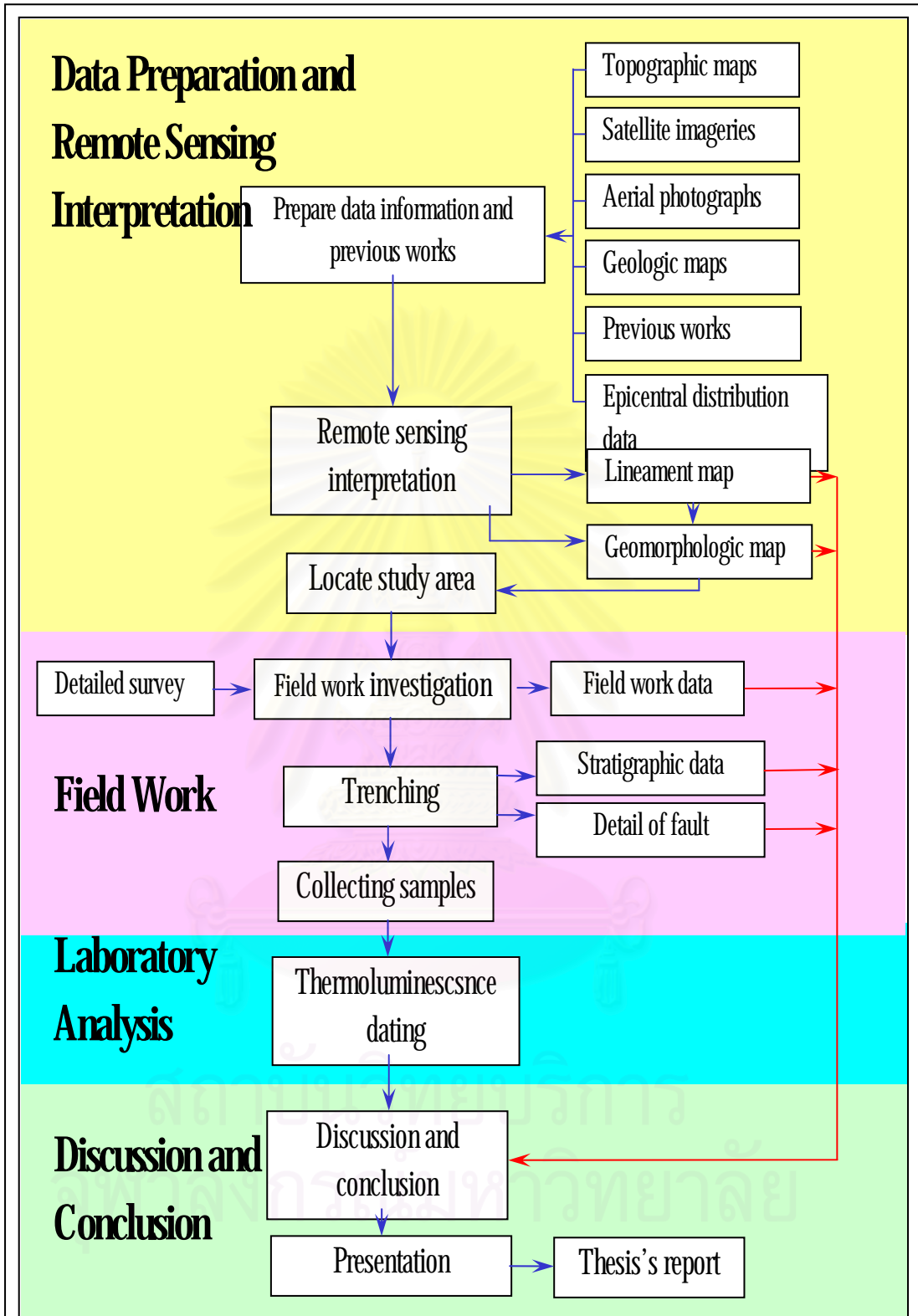
- 1) data preparation and locate study area,
- 2) field work investigation,
- 3) laboratory analysis, and
- 4) analysis, discussion and conclusion.

### 1.3.1 Data Preparation and Locating Study Area

The first part starts from preparing information e.g. literature reviews, preparation of satellite imageries, aerial photographs, topographic and geologic maps of the interested areas, and epicentral distribution data.

Interpretation of remote sensing satellite imagery (JERS and LANDSAT TM5) and epicentral distribution data were used to investigate and locate major faults in western Thailand. These faults including the Mae Ping Fault, Sri Sawat Fault, and Three Pagodas Fault are shown on lineament map. Especially, the Sri Sawat fault was separated into segments for define characteristics of each segment.

The aerial photographic interpretation was used for detailed study in southern segment of Sri Sawat fault. The geomorphologic map was created by the interpretation compared with topographic and geologic maps. Geomorphic mapping emphasizes morphotectonics which helps to indicate fault traces, the approximate size and timing of paleoearthquakes, and relationship of faultings with young sedimentary deposits. These led to locate the area under study.



**YOUNG FAULT MOVEMENTS ALONG THE SOUTHERN SEGMENT OF SRI SAWAT FAULT**



MR. RUTCHUT NUTTHEE  
 DEPARTMENT OF GEOLOGY  
 FACULTY OF SCIENCE  
 CHULALONGKORN UNIVERSITY

Figure 1.3 Flow chart showing the methodology applied in this study.

### 1.3.2 Field Work Investigation

This part commences after selecting the study area, and consists of field investigation, surveying in the interested area, and trenching.

Field investigation is acted for studying geology and geomorphology of the study area, and checking result from remote sensing interpretation. This step emphasizes the geology or geomorphology related to fault movement in the field, and select appreciate area for trenching.

Surveying is for determining fault movements. This also includes to identify offset streams, which effected from fault movements, and to study appearance of lateral fault movement and distance of fault movement.

Excavation of trenches (Sec. 2.1.4.2) leads to the detailed study of subsurface fault and collecting samples for dating age of fault movements. Trench locations are selected and excavated in areas dominated by young sediments. It should not be sited until the geomorphic relations in the area of investigation are thoroughly understood.

### 1.3.3 Laboratory Analysis

The most important of this part is dating of colluvial sediments related to faulting by using thermoluminescence (TL-) dating technique.

### 1.3.4 Discussion and Conclusion

All of results were complied and analyzed in the final part to prove the deformation from faulting, identification of paleoearthquakes, behavior of fault movement, ages and magnitudes of faulting and possibility of active fault.

## 1.4 Selected Literature Reviews and Previous Works

Klaipongpan et al. (1986) studied seismicity of Srinagarind Dam in April of 1983. Series of earthquakes located in upper reaches of the reservoir, were reported around the confluence of Kwaie Yai River, Huai Mae Phlu and Hai Kha Khaeng. This epicentral area is about 60 km north of dam site. The main shock on April 22, 1983 was 5.9  $M_L$  while the largest foreshock and aftershock were both 5.3  $M_L$ . The effect of these events

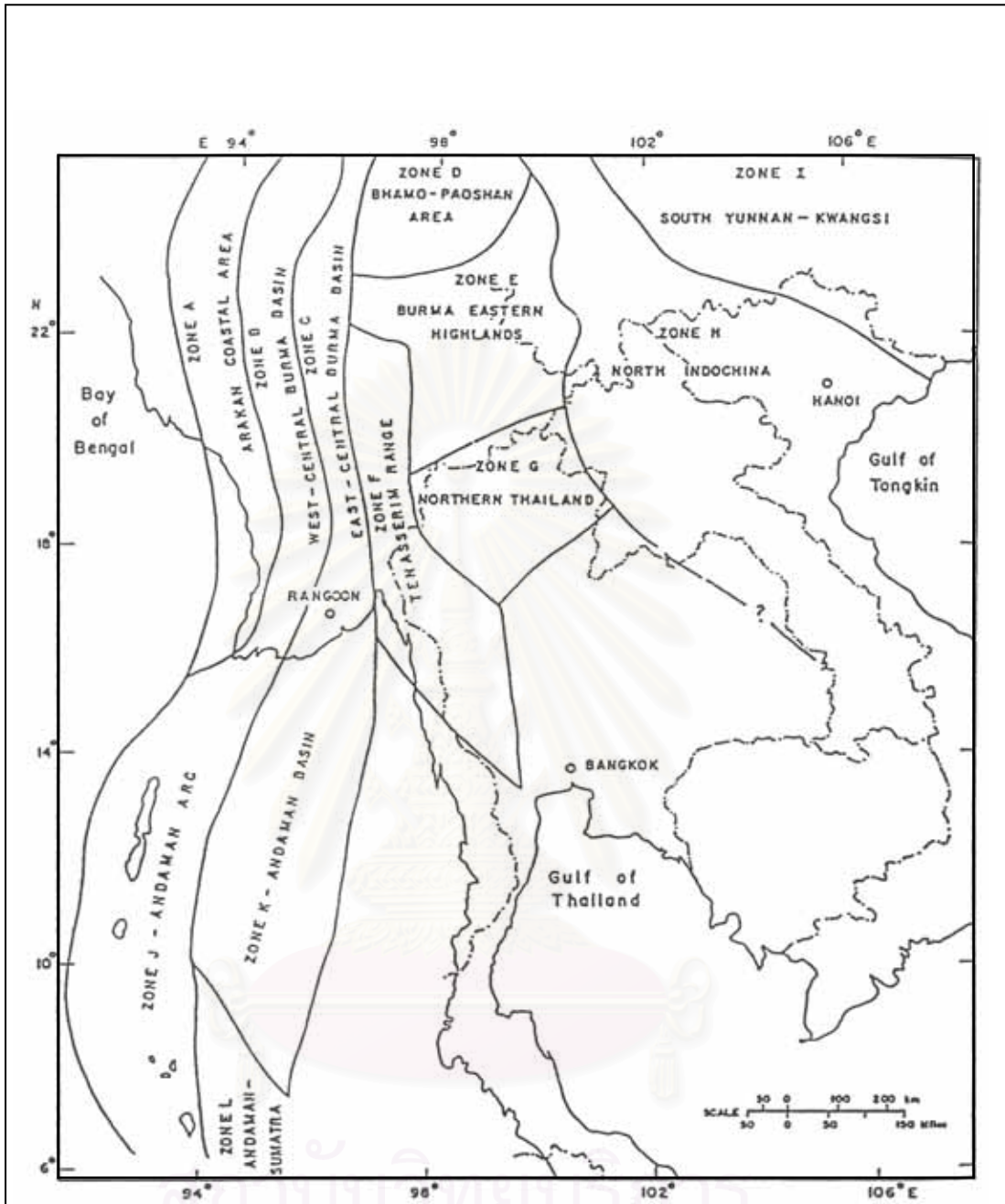


as reported by residents around the reservoir are including of a probable seiche in the epicentral area, such as; the strong shaking of trees, loud rumbling and booming noise, rockfalls, and small scale landslides. In addition, the surface ruptures and sinkhole collapses were also reported just to the south of Huai Mae Phlu. This rupture is very straight and crosscuts existing topography and stream drainages. Such feature trends approximately N75-80°W and is about 4 km, long. They concluded that these seismicity could be reflected from “Reservoir Triggered Seismicity” (RTS). Because the Srinagarind reservoir is sufficiently large and deep to be considered a likely candidate for RTS. The b-value for both foreshocks and aftershocks of the Srinagarind events are closely to unity. Moreover the foreshock b-value is greater than the aftershock b-value which is comparable to the RTS events. And, the pattern of shock of the Srinagarind events is closely corresponded to Mogi’s model type 2, which indicates the non-uniform distribution of the external stress of the region.

Keller (1987) studied active tectonics by uses of surficial earth processes. The evaluation of landforms, soils, and deposits formed by active tectonics is providing basic data necessary for long-term earthquake prediction, seismic-hazard evaluation, and probabilistic seismic-risk assessment.

Investigation of active tectonics based on geomorphic techniques varies from regional reconnaissance work to detailed, site-specific, process-response study. Such approach involves study of faulted Holocene (less than 10,000-yr-old) deposits. Keller (op. cit.) showed that geomorphic indices and faulted landforms (such as offset streams, alluvium fans, marine terraces, river terraces, and glacial moraines: and change in fault-scarp morphology with time) are useful in regional evaluation to identify relative tectonic activity and sites where rates of active-tectonic processes may be evaluated.

Nutalaya (1987) identified twelve seismotectonic source zones (fig 1.4) of the region bound by latitude 5° to 25°N and longitude 90° to 110°E (covering Thailand, Indochina, part of Burma, and China), based on tectonic features and seismicity.



**YOUNG FAULT MOVEMENTS ALONG THE SOUTHERN SEGMENT OF SRI SAWAT FAULT**



MR. RUTCHUT NUTTHEE  
 DEPARTMENT OF GEOLOGY  
 FACULTY OF SCIENCE  
 CHULALONGKORN UNIVERSITY

Figure 1.4 Seismic source zones of Myanmar-Thailand-Indochina (Nutalaya, 1987)

According to this paper, Western Thailand (including the interested area) and east-central Myanmar were designated as zone F; Tenasserim Range (see Fig 1.5).

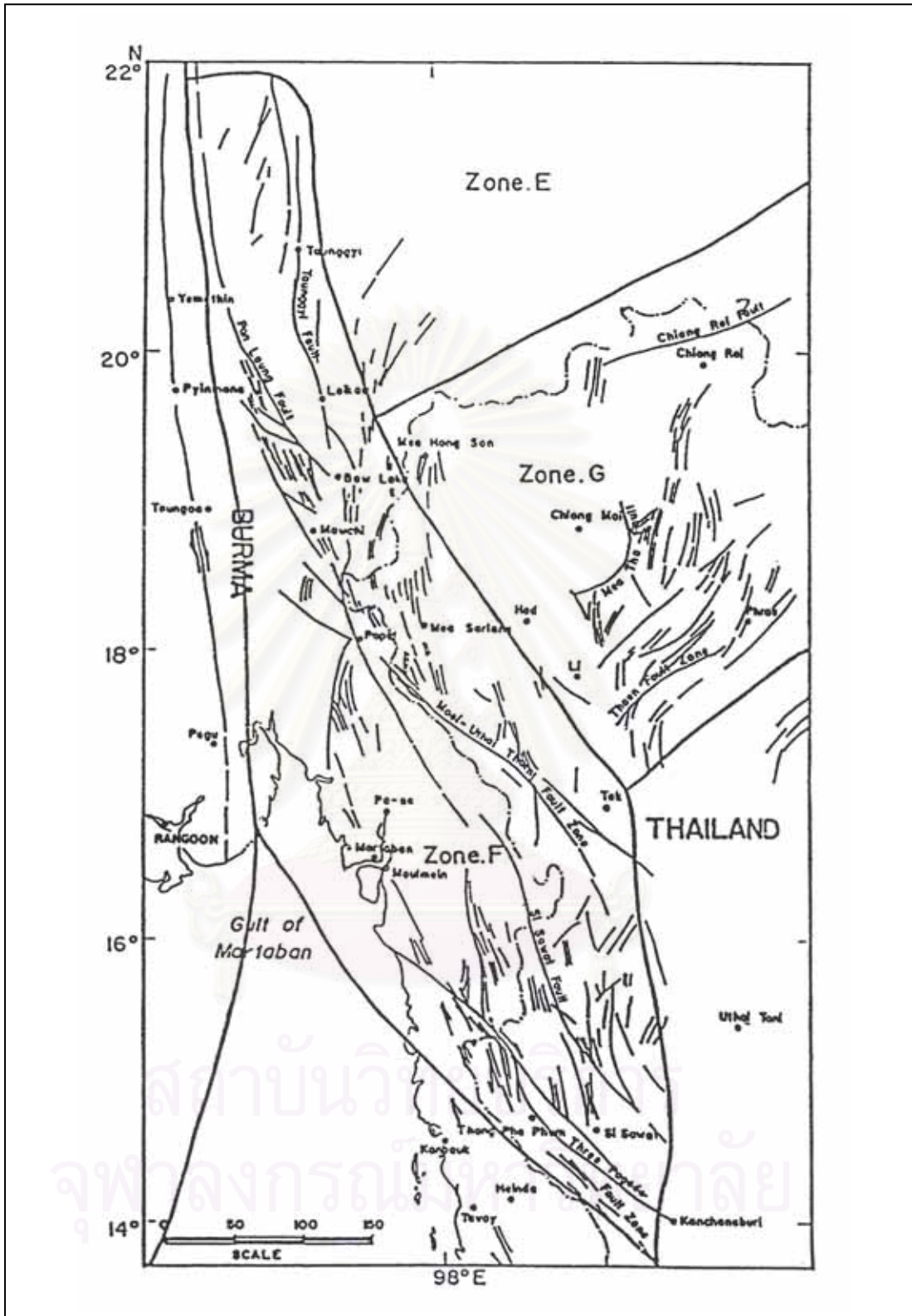
This zone is characterized by the N-trending faults in the Kachin-Tenasserim ranges of Burma and southward extending NW-trending faults in the western ranges of Thailand. Major faults in this area are the Taunggyi Fault, Pan Laung Fault, Moei-Uthai Thani Fault zone, Si Sawat and Three Pagodas Faults. The seismicity associated with these faults is not very high, but a number of events occurred along these faults proved to be very destructive.

Portions of the Pan Laung and Taunggyi faults are traceable via the Tenasserim range into western Thailand and the direction bends toward NE-SE. There are three major faults in western Thailand, more or less parallel to each other, namely Moei Uthai Thani Fault zone, Si Sawat Fault and Three Pagodas Fault. The upper one, the Moei Uthai Thani Fault zone, is characterized by narrow and complex fault zones of normal, thrust and strike-slip nature. The horizontal displacement gives a left-lateral separation.

The two lower faults, Si Sawat and Three Pagodas faults control the Kwaie Yai and Kwaie Noi rivers, which flow southeastward towards the Gulf of Thailand. Nutalaya and Rau (1984) suggested that they indicate right-lateral movement. The movement along these faults is probably related to the movement along the Sagaing Fault of Burma in the Late Cenozoic.

Wallace (1987) studied active faults, paleoseismology, and earthquake hazards in the western United States. Studies of prehistoric earthquakes (paleoseismology) show that average recurrence intervals for large displacements and related earthquakes on most active faults in the western United States are generally longer than 1,000 years; for many the average recurrence is greater than 10,000 years. Only on the San Andreas fault and its major branches are average recurrence intervals as 10-200 years. In some localized areas of western Nevada rates are higher. Probabilistic expressions of the likelihood of future behavior of active faults are needed.

Forman et al. (1991) reported thermoluminescence dating of fault-scarp derived colluvium to decipher the timing of paleoearthquakes on Weber segment of the Wasatch



**YOUNG FAULT MOVEMENTS ALONG THE SOUTHERN SEGMENT OF SRI SAWAT FAULT**



MR. RUTCHUT NUTTHEE  
 DEPARTMENT OF GEOLOGY  
 FACULTY OF SCIENCE  
 CHULALONGKORN UNIVERSITY

Figure 1.5 Seismotectonic map of parts of Myanmar and Thailand showing distribution of major fault (modified after Nutalaya, 1986).

fault zone, North Central Utah. Two trenches was excavated across fault scarps is characterized by stack of three colluvial wedges, deposited in response to three separate faulting events, the oldest of which buried a soil developed on a middle Holocene debris flow. Thermoluminescence age estimates by the partial and total bleach methods and the regeneration method on fine-grained colluvium from the trenches agree within 1 sigma and are concordant with the radiocarbon chronology. A synthesis of the TL and  $^{14}\text{C}$  age estimates indicate that these three faulting events occurred sometime between 4500 and 3500, between 3200 and 2500, and between 1400 and 1000 years ago.

Ding and Lai (1997) studied neotectonic fault activity in Hong Kong by using evidence from seismic events and thermoluminescence dating of fault gouge.

Hong Kong lies within a major NE-trending fault zone that has been reactivated during several tectonic episodes since the Paleozoic. Three main fault sets are recognized in Hong Kong: a dominant NE-trending set, an ENE-varying to E-trending set and a subordinate NW-trending set. Over the last 1000 years, within a distance of 350 km of Hong Kong, there have been about 40 earthquakes with magnitudes of over 4.75, and 11 had magnitudes of over 6.0. Microseismic events in the last ten years are diffuse but may be associated with a major NE-trending fault and a fault intersection. Thermoluminescence dates of fault gouge suggest that there have been three episodes of recent fault activity in Hong Kong; these occurred at approximately at 100,000, 190,000 and 270,000 year BP. TL dating of alluvial sediments also indicates fault activity in the Late Pleistocene.

Kosuwan et al. (1998) investigated neotectonics of Mae Chan Fault in Mae Chan District, Chiang Mai Province. Interpretation of remote sensing satellite imagery (Landsat TM5) and aerial photos indicate the E-W surface rupture, which consists of major faults and minor faults. Morphotectonics, such as offset stream, sag pond, fault scarp, offset ridge and terrace, indicate that the fault is left-lateral strike-slip movement, dipping north about  $45^\circ$ . Four trenches were excavated for detailed study. Sediments and fault gouges in trenches, and fault gouges on outcrop of fault exposure in vicinity, are dated

by  $^{14}\text{C}$  for sediments with organic matter, and TL for fault gouges and sediments without organic matter. This study concluded that the Mae Chan Fault has potential for future earthquake or to be active fault. Fault movements give rise to earthquakes of about 92000, 67000, 48000, 25000, and 1600 years ago. The 1600 years ago event probably caused earthquake magnitude greater than 7 Richter's scale.

Hongjaisee (1999) studies major faults and seismic hazard in northern Thailand. The methods of seismic hazard analysis fall into two types including deterministic and probabilistic analysis. The deterministic analysis is divided into four steps as Landsat and map analysis, geological investigation, trenching, and earthquake and fault hazard analysis. The probabilistic seismic hazard analysis is based on Cornell (1968). The Poisson model was used to analyze probability of exceedance during the period of interest and return period. At 37 percent probability of exceedance, the ground acceleration values in western Thailand are about 100 gals. High acceleration values which are restricted to Thailand-Myanmar border, are in the range of 120 to 150 gals. Acceleration values are very low in northern and southern Thailand.

For the probability of exceedance of 10 percent, which corresponds to an expose time of 100 year, the peak ground acceleration (PGA) values at Phrae, Prayao, Chiang Rai, Chiang Mai are approximately 0.08g. The PGA values at Mae Hong Son, Lamphun, Lampang, and Nan are about 0.04g. For the large dams in northern Thailand, the Mae Kuang dam has a high potential hazard and the Sirikit Dam has a low potential hazard.

Personius and Mahan (2000) reported paleoearthquake recurrence on the East Paradise fault zone, New Mexico. Mapping of two exposures of the fault zone allowed them to measure a total vertical offset of 2.75 m across middle Pliocene fluvial and eolian deposits and to estimate individual surface-faulting events of about 1, 0.5, and 1.25 m. These measurements and several thermoluminescence ages allow them to calculate a long-term average slip rate of  $0.01 \pm 0.001$  mm/yr and date two surface-faulting events to  $208 \pm 25$  ka and  $75 \pm 7$  ka. These data yield an average recurrence interval of  $90 \pm 10$  ka. Offsets of 0.5-1.25 m and a fault length of 13-20 km indicate that

surface-rupturing paleoearthquakes on the East Paradise fault zone had probable  $M_s$  or  $M_w$  magnitudes of 6.8-7.0.

Zilberman et al. (2000) investigated the changes in Holocene Paleoseismic activity in the Hula pull-apart basin, Dead Sea Rift, northern Israel. Paleoseismic analysis of the Azaz fault segment of the Dead Sea fault indicates that this region was subjected to intermittent periods of strong seismicity and quiescence during the latest Pleistocene and the Holocene. Two trenches excavated across a 15-20 m high fault scarp near Kefar Szold expose fluvial and colluvial sequence showing clear evidence of recent tectonics. Optically stimulated luminescence dating of the lower fluvial sequence shows that its age ranges between 12 ka at the base to 6 ka at the top, while the middle part of the overlying colluvium is ca. 4.8 ka. The relation between the lower fluvial units and the fault indicates that at least two large-scale earthquakes occurred in the Early Holocene. During this seismically active period, no coarse colluvial sediments were deposited along the fault trace and thus the region must have had low tectonic relief. The clear contact with the overlying coarse colluvium reflects a Middle Holocene rapid change to the present high, steep relief.



สถาบันวิทยบริการ  
จุฬาลงกรณ์มหาวิทยาลัย

## CHAPTER II

# PALEOSEISMOLOGY AND OTHER RELATED TECTONICS STUDIES

## 2.1 Introduction to Paleoseismology

### 2.1.1 Definition

Paleoseismology is the study of prehistoric earthquakes (Solonenko, 1973; Wallace, 1981), especially their locations, timing, and sizes. Whereas seismologists work with data recorded by instruments during earthquakes, paleoseismologist interpret geologic evidence created during individual paleoearthquakes (McCalpin, 1996). Paleoseismology differs from more general studies of slow to rapid crustal movements during late Cenozoic (e.g., neotectonics) in its focus on the almost instantaneous deformation of landforms and sediments during earthquakes (Allen, 1986).

Paleoearthquakes are *prehistoric* by definition, but does “prehistoric” mean the time before oral records, or the time before contemporaneous written accounts, or the time before written accounts with some quantitative observations of earthquakes? The latter definition is the closest to what paleoseismologists commonly consider prehistoric. This broad definition of “prehistoric” somewhat ameliorates the problems caused by poorly defined and varying times of transition from oral to written history around the globe; for example, from about 3000 BC for China and parts of the Middle East to later than AD 1700 for New Zealand and northwestern America (McCalpin, 1996).

### 2.1.2 Relation of Paleoseismology and Other Neotectonic Studies

Paleoseismology is an interdisciplinary field of research and borrows many concepts from seismology, structural geology, and tectonics. However, paleoseismic methodology and techniques are derived primarily from Quaternary geology and related disciplines, such as geomorphology, soil mechanics,



sedimentology, archaeology, paleoecology, photogrammetry, radioisotope dating, or pedology (soil science) (see also McCalpin, 1996). Most paleoseismic field studies require extensive training or experience in Quaternary geology, itself a highly interdisciplinary field. Thus, it should be no surprise that many significant advances in paleoseismology have been made by geomorphologists and other Quaternary geoscientists and specialists, working at the interface between tectonics and seismology. Paleoseismology is a particularly successful example of applied Quaternary geology (Wallace, 1986).

Paleoearthquake is a subdiscipline within the much broader field of *neotectonics* and *active tectonics*. Neotectonics, or the study of crustal movements during the late Cenozoic (Belousov, 1980; Vita-Finzi, 1986, p.14; Mörner and Adams, 1989). Active tectonics includes many of these types of crustal movements, but is limited in its time frame to studies of “tectonic movements that are expected to occur within a future time span of concern to society” (Wallace, 1986; Weldon, 1991).

The driving force behind most paleoseismic studies is society's need to assess the probability and severity of future earthquakes (Wallace, 1986; Reiter, 1995). The past few decades have spared the most highly industrialized countries from the effects of devastating earthquake, but there is little doubt that earthquakes damaging enough to affect the world economy seriously may occur in cities such as Los Angeles or Tokyo at any time (Wesnousky et al., 1984; Nishenko, 1989; Working Group on California Earthquake Probabilities, 1995).

Paleoseismology supplements historic and instrumental records of seismicity by characterizing and dating large prehistoric earthquakes (Crone and Omdahl, 1987; Vittori et al., 1991). In most countries, useful seismicity records extend back only a few centuries (Gutenberg and Richter, 1954; Stover and Coffman, 1993) and many active fault zones have no historic record of large earthquakes. For example, studies of prehistoric faulting along the Wasatch fault zone in the western United States (Machette et al., 1992) show that the average recurrence interval between large earthquakes is probably three times longer than the period of historic settlement (145 years). In some other regions, both close to near to and far from plate boundaries, paleoseismic studies suggest that earthquake hazard estimates based on short historic

records may actually overestimate the likelihood of future earthquakes, due to the recent occurrence of large earthquakes on faults with long average recurrence times (Lajoie, 1986; Crone et al., 1992; Adams et al., 1991). On a fault that has slipped for millions of years, even a 3,000-year record covers only a fraction of a percent of the history of the fault. Much of the seismic history of most faults is accessible only through the techniques of paleoseismology (McCalpin, 1996).

### 2.1.3 Application of Paleoseismic Data to Seismic Hazard Assessment and Neotectonics Research

Paleoseismic data can be used in research of neotectonic investigations and can provide relatively short-term geologic data that complements longer term geological, geophysical, and seismological data on regional fault behavior and deformation style (e.g., Wesnousky et al., 1984; Wesnousky, 1986). However, most paleoseismic studies to date have been undertaken to provide input for *seismic hazard assessments*; SHAs (Reiter, 1990).

Beginning in the 1960s, the government regulations in several industrialized countries mandated SHAs for construction of new critical facilities (nuclear and other power plants, dams, and schools). A key element of a SHA is seismic source characterization, i.e., the assignment of magnitude and recurrence rate of large, potentially damaging earthquakes that could be generated by active faults near a site. A SHA is required to describe the largest earthquake that could occur within each identified seismic source zone.

However, paleoseismic data by themselves cannot be fully integrated into more research-oriented neotectonic studies unless they can be explained by general models of fault behavior, and understood in the context of present-day tectonic environment and stress field (Schwartz and Coppersmith, 1986). To contribute to the expanding field of neotectonic research, paleoseismic data must be synthesized with other data on historical seismicity moment rate, geodetic strain rates and stress fields to create a seismotectonic synthesis

Paleoseismology is mainly concerned with how the estimate paleoearthquake magnitude and recurrence from field measurements of displacement

and earthquake age. To describe the important seismotectonic concepts of fault segmentation, fault behavior models, earthquake recurrence models, and then applied to SHAs and integrated into larger studies of neotectonics.

## 2.1.4 Field Techniques in Paleoseismology

The methods fall into two broad categories, depending on whether paleoseismic features are landforms (sec. 2.1.4.1) or have stratigraphic expression and controls (sec. 2.1.4.2).

### 2.1.4.1. Mapping Paleoseismic Landforms

The first, and often-fruitful approach to paleoseismic reconstruction should be careful mapping of Quaternary landforms and deposits in the zone of deformation. Basic geomorphic techniques include locating paleoseismic features with remotely sensed imagery and making detailed topographic maps of paleoseismic landform. Geomorphic mapping helps indicate where fault traces are result of single versus multiple events, the approximate size and timing of paleoearthquakes, and locates detail of investigated area. Active fault traces are the easiest such features to map, and they are expressed at the surface as linear belts of landforms across which vertical relief is evident (i.e., dip-slip faults) or where terrain elements are shifted laterally (i.e., strike-slip faults). Fault traces or narrow folds are usually identified by examination of aerial photograph, low-altitude aerial reconnaissance, or field inspection.

### 2.1.4.2. Mapping Paleoseismic Stratigraphy

The stratigraphic expression of paleoearthquakes can range from displaced strata and angular unconformities to clastic dikes and soft sediment deformation. Such stratigraphic evidence may or may not be accompanied by geomorphic evidence of paleoseismicity. Early paleoseismic investigations concentrated on geomorphic evidence because natural vertical exposures in fault zones are rare. In the absence of such exposures, however, early paleoseismic investigators were faced with the choice of (1) relying only on geomorphic data for the paleoseismic analysis, (2) drilling boreholes or collecting geophysical data, or (3) excavating artificial

trench exposures across deformation zones. The development of modern paleoseismology owes much to developments in the latter two of these fields.

Excavation of trenches has become a major element of paleoseismic studies in most countries. Trenching techniques have expanded to address problems of paleoearthquake faulting, folding, ground failure, and faulting-induced sedimentation. Trenches across faults are typically sited to optimize data on either paleoearthquake displacement or paleooccurrence (Sieh, 1981).

#### 2.1.4.3. Geophysical Techniques in Paleoseismology

Geophysical methods are useful in paleoseismology in three ways (1) for characterizing the subsurface geology in mapped fault zones, (2) for detecting buried faults that have no surface expression, and (3) for characterizing deformation features on the bottoms of lakes and oceans. Paleoseismology requires geophysical systems and approaches with high spatial resolution and the ability to distinguish between unconsolidated deposits with very similar material properties. Depth penetration of more than 10 m is usually not required, because the data of interest often lie only a few meters below the surface.

## 2.2 Causes of Earthquake

The occurrence of earthquake can be divided into 2 categories; i.e., artificial and natural earthquakes. Artificial earthquake means that the earthquakes were produced by human activity such as; nuclear explosion, reservoir induced seismicity, and etc. Natural earthquake was occurred by natural activity such as; fault movements, volcanoes, landslides, cave collapses, etc.

Earthquakes most commonly occur when rocks break and move abruptly along a fault (Levin, 1990). It can be explained by the elastic rebound theory proposed by Reid (1911). When fault ruptures, elastic energy stored in rocks is released, partly as heat and partly as elastic waves. These waves are what human-beings called "the earthquake".

However, not all earthquake events are necessarily associated with elastic rebound. With increasing pressure because of burial under 20 or 30 kilometers of

overburden, most rocks deform plastically and are unable to rebound. The elastic rebound theory in its original form would, therefore, be applicable only to earthquakes with extremely shallow foci (Leet et al., 1982)

Deep earthquakes may result from sporadic slippage in rocks simultaneously undergoing plastic deformation. Beyond a depth of about 700 km, however, failure occurs by creep, and earthquakes do not occur (Levin, 1990).

## 2.3 Earthquake and Plate Tectonics Theory

In the first half of the twentieth century, earthquakes recording at seismological observatories allowed remote earthquakes to be detected and mapped uniformly, thence the long-term pattern of global seismicity was resolved. In addition, both the geologic fieldwork and evidence from the recorded seismic-wave patterns indicated that the type of faulting seen at the surface, such as strike-slip or dip-slip displacement, occurred in definite regional patterns. Thus the worldwide distribution of both earthquakes and their fault mechanisms was not random, but rather systematic. The time was ripe for the emergence of fresh overall synthesis of this global information.

One of the great attractions of the concept is plate tectonics, which can explain the distribution of earthquakes and the rock motion associated with them. The concept of plate tectonics is that the earth's surface is divided into a few giant plates. Plates are rigid slabs of rock, thousands of kilometers wide and 70 to 125 (or more) kilometers thick, that move across the earth's surface. Because the plates include continents and sea floors on their upper surfaces, the plate-tectonics concept means that the continents and sea floors are moving. The plates, therefore, change not only position but also size and shape.

Earthquakes occur commonly at the edges of plates but only occasionally in the middle of a plate. Therefore, edges of plates were constructed more clearly by seismic zone. The close correspondence between plate edges and earthquake belts can be seen by comparing the map of earthquake distribution (Fig. 2.1) with the plate map (Fig. 2.2). The most intense tectonic activity takes place at the plate margins or plate boundaries. There are three types of plate boundaries (Fig. 2.3).

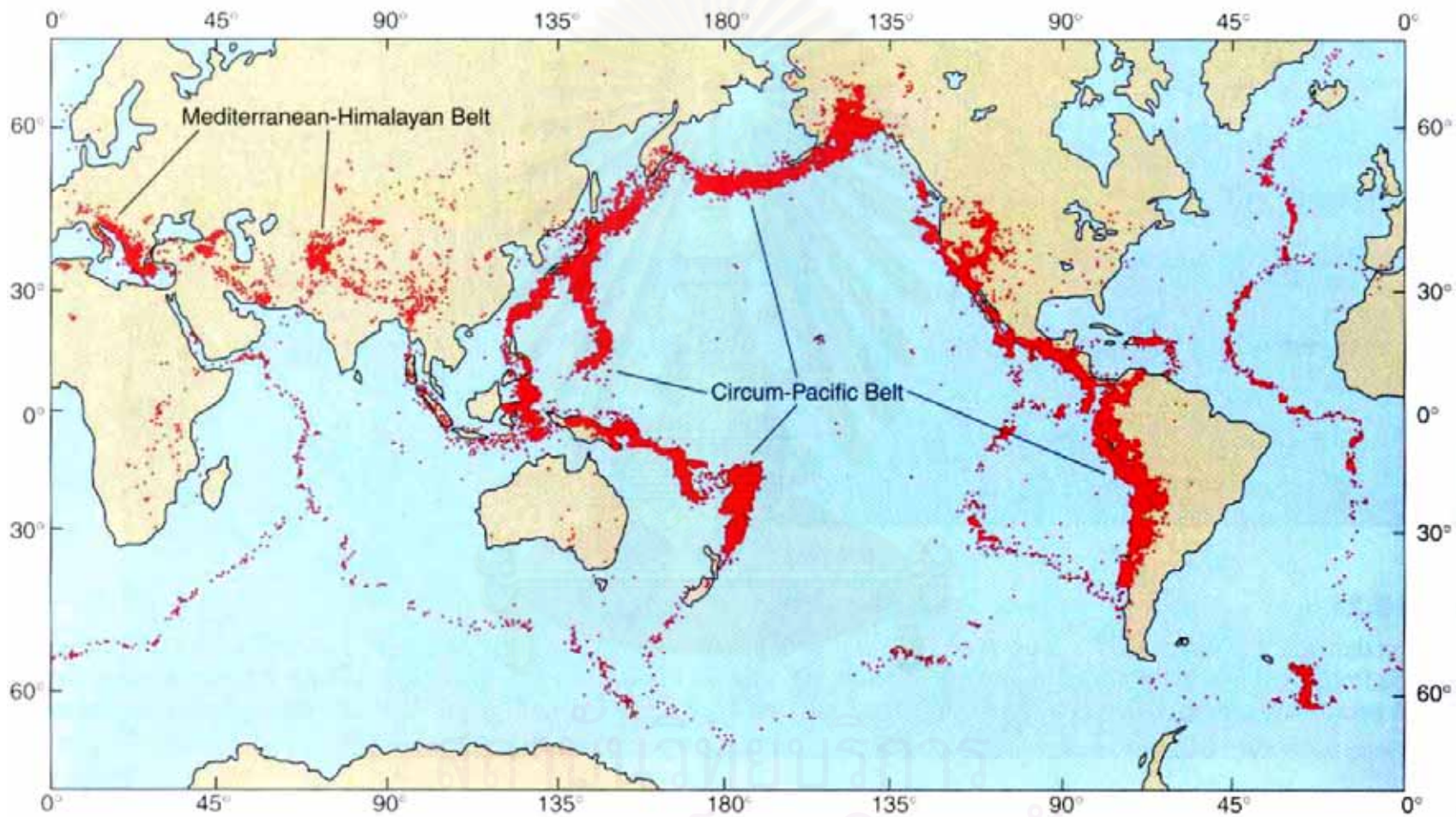


Figure 2.1 World distribution of earthquakes recorded over a six-year period with focal depths between 0 and 700 kilometers, showing major earthquake belts (labeled) (Plummer et al., 2001).

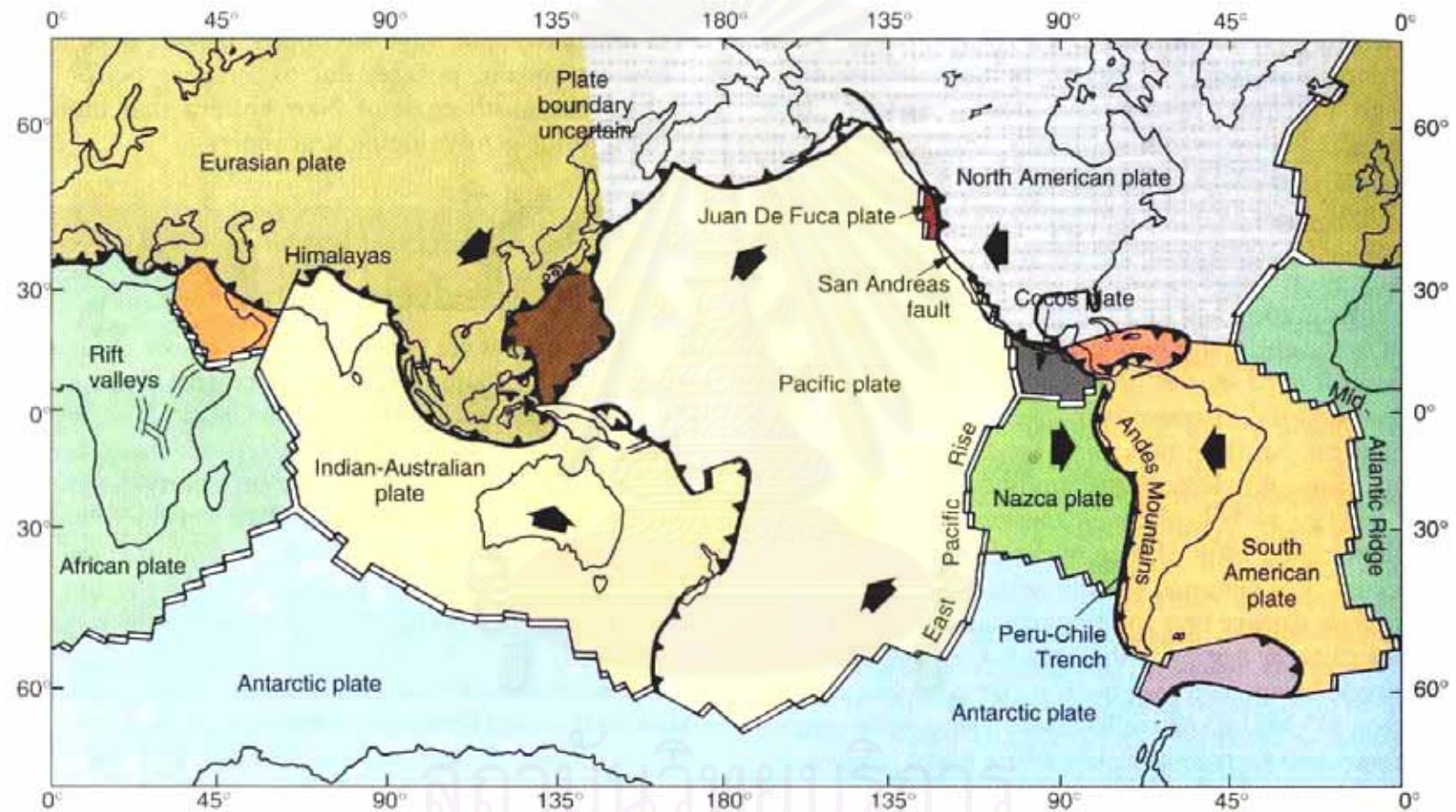


Figure 2.2 Major plates of the world in the theory of plate tectonics. Compare the locations of plate boundaries with earthquake locations shown in figure 2.1. Double lines show diverging plate boundaries, single lines show transform boundaries. Heavy lines with triangles show converging boundaries; triangles point down subduction zone (Plummer et al., 2001).

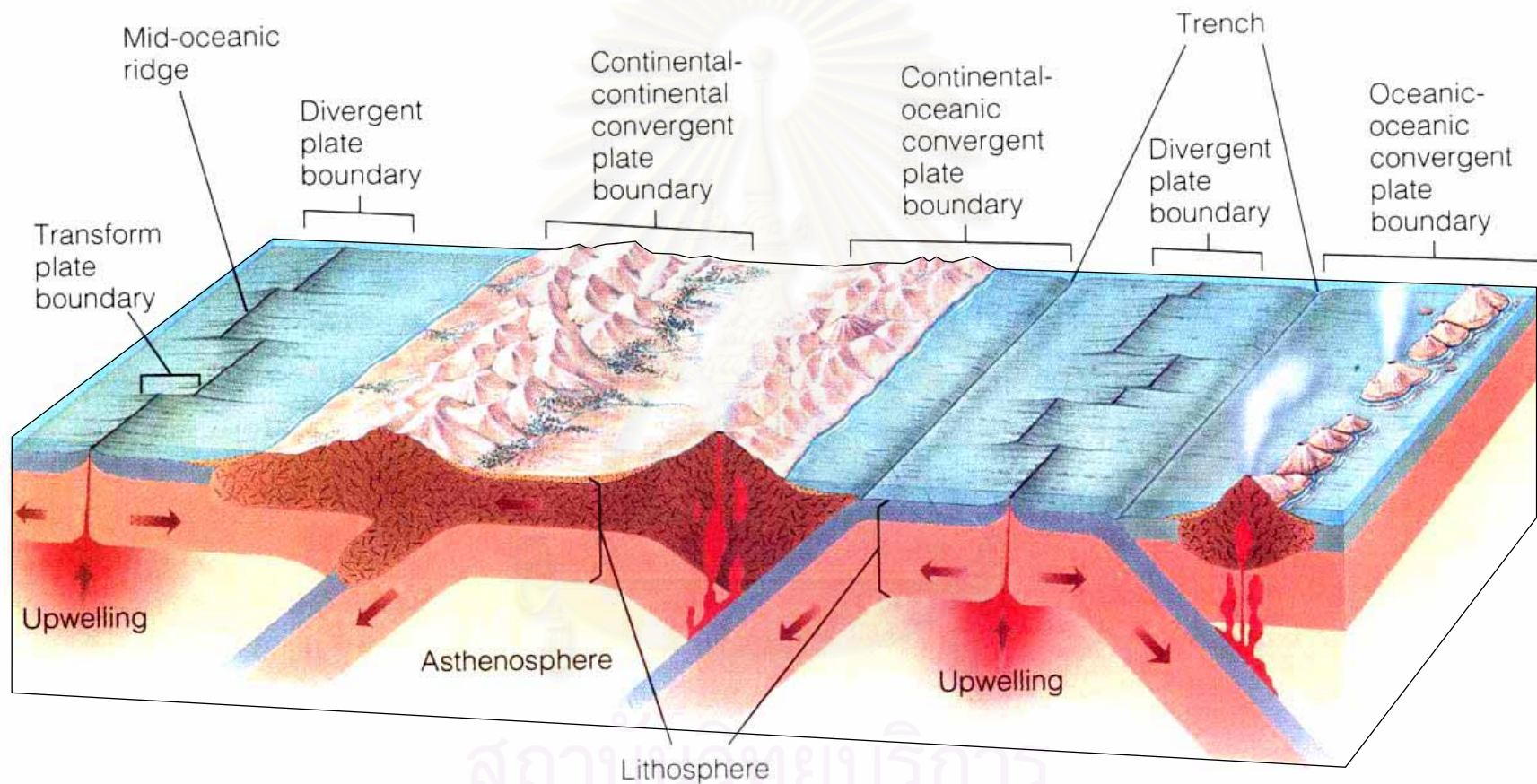


Figure 2.3 An idealized cross-section illustrating the relationship between the lithosphere and the underlying asthenosphere and the three principal types of plate boundaries: divergent, convergent, and transform (Plummer et al., 2001).



### 2.3.1 Divergent Boundaries

At a divergent boundary, where plates move away from each other, earthquakes are shallow and restricted to a narrow band. A divergent boundary on the sea floor is marked by the crest of the mid-oceanic ridge and the rift valley that is often (but not always) found on the ridge crest (Fig. 2.4a). A divergent boundary within a continent is usually also marked by rift valley, shallow focus earthquakes, and normal fault (Fig. 2.4b).

### 2.3.2 Transform Fault Boundaries

Earthquakes occur along transform boundaries are shallow (Fig. 2.5). The resulting earthquakes occur when plates move pasting each other. There, strike-slip fault takes place. These transform faults occur in both continental and oceanic lithospheres. The San Andreas fault in California is a large transform boundary between the North America and Pacific plates, which are sliding pasting each other at the rate of several centimeters per year (Reiter, 1990).

### 2.3.3 Convergent Boundaries

A convergent plate boundary is a type associating plate movement where two plates move toward one another. This boundary has two features: (i) subduction of one plate beneath another plate, and (ii) collision of plates (Fig. 2.6). The subducting plate is melted and the resultant molten magma rises to form volcanoes at the surface. As the subduction proceeds and one plate slides beneath the other, earthquakes are generated at the interface and in the adjacent portions of the interacting plates. The dipping zones of earthquakes are called Benioff or Wadati-Benioff zones. The Benioff zones may extend as deep as 700 kilometers in some subduction zones (Reiter, 1990). The interaction between continental plates normally results in collision rather than subduction. The Himalayas are the result of the collision of the India and Eurasia plates. In a collision setting, earthquakes occur over a wide zone, more than a thousand kilometers wide in several regions. Concentrations of intermediate earthquakes are interspersed among shallow earthquakes, unlike the

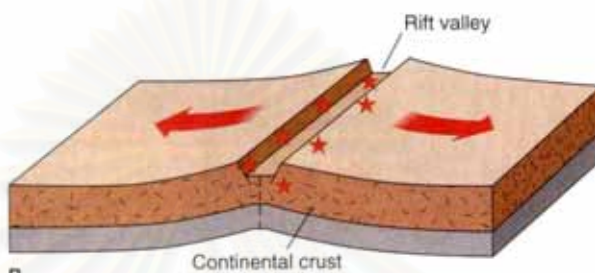
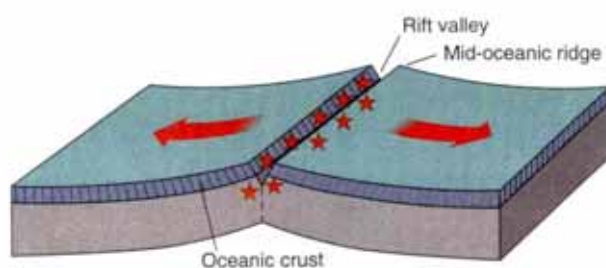


Figure 2.4 Divergent plate boundaries. (A) On the ocean floor. (B) On a continent. Each boundary is marked by a rift valley and narrow band of shallow-focus earthquakes (shown as stars). Depth of rift valleys is exaggerated (Plummer et al., 2001).

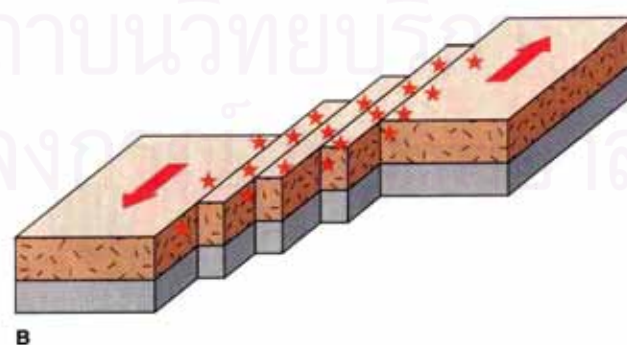
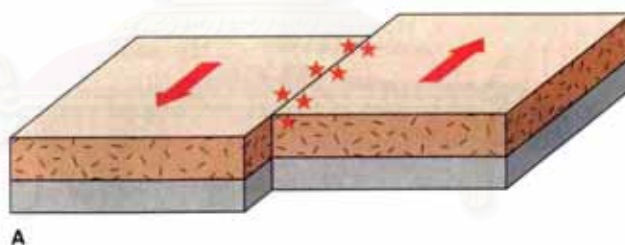
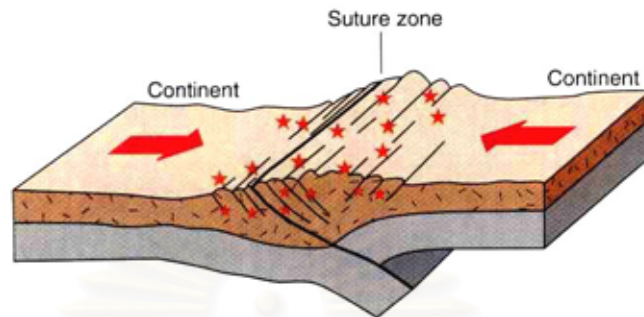
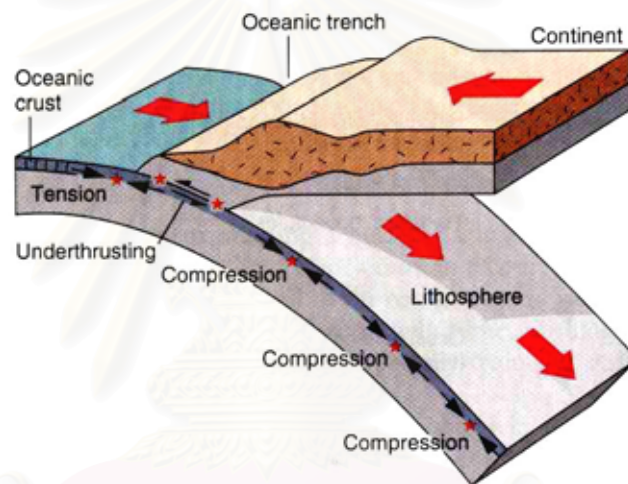


Figure 2.5 Transform boundaries. (A) Narrow band of shallow-focus earthquakes shown as stars along single fault. (B) Broad band of earthquakes along a system of parallel faults (Plummer et al., 2001).



A



B

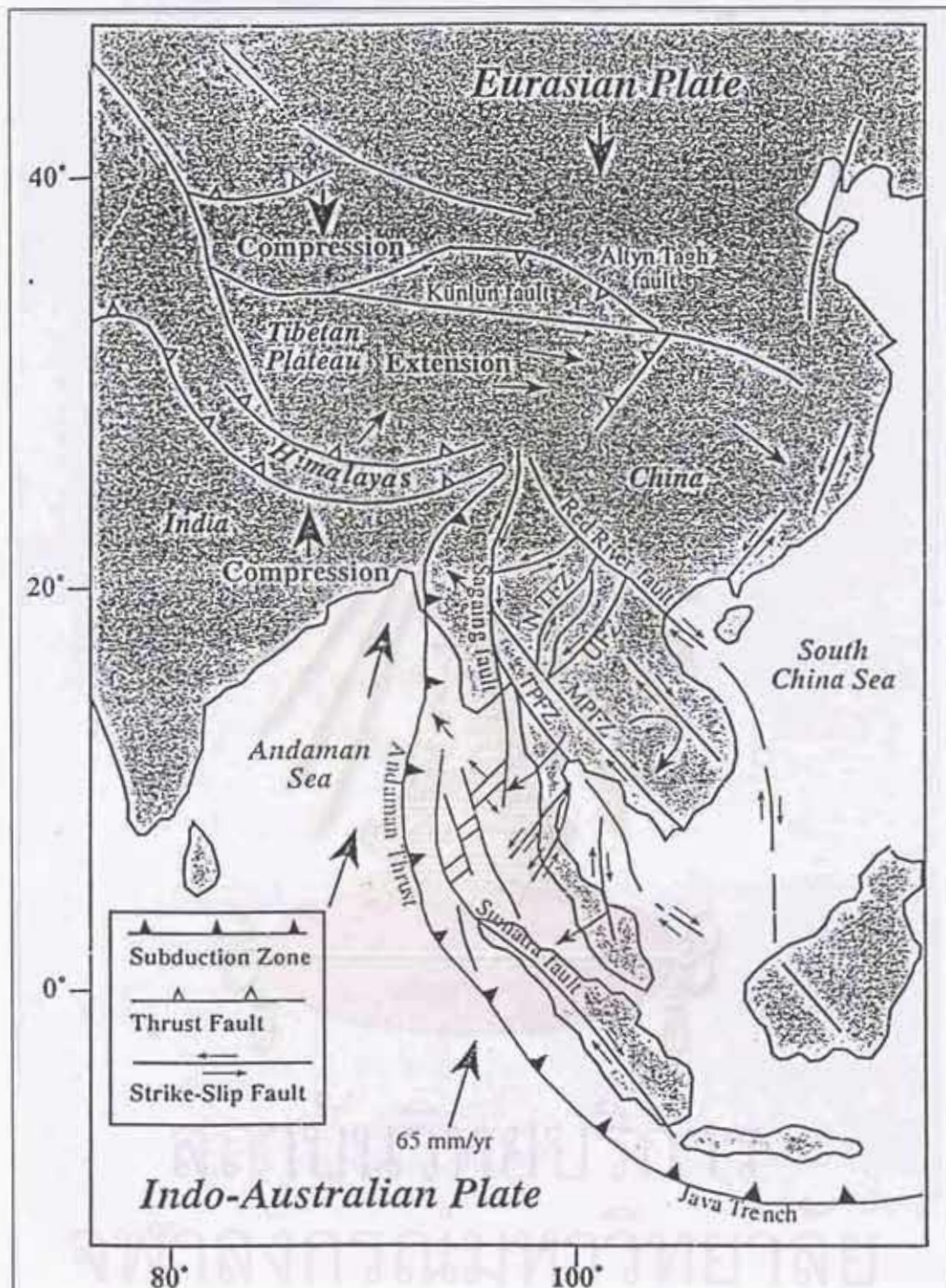
Figure 2.6 (A) A convergent boundary marked by the collision of two continents. A very broad zone of shallow-focus earthquakes occurs along a complex system of faults. (B) A convergent boundary with ocean floor subducting plate due to tension, underthrusting, and compression (Plummer et al., 2001).

increasingly deep earthquakes of the Benioff zones in subduction zone settings. Continental convergence earthquakes, therefore, can be very large (Rieter, 1990).

## 2.4 Seismotectonic Setting

The contemporary tectonic framework of Southeast Asia is a consequence of the interaction between the Indo-Australian, Eurasian, Philippine, and West Pacific plates. The Eurasian thrust, Sunda arc, and Philippine trench to the west, south, and east, respectively (Fig. 2.7) are good examples. Australia is moving northward (along a vector of  $010^\circ$  to  $020^\circ$ ), towards southeast Asia, with a convergence rate of  $67.5 \pm 2.5$  mm/yr. Deformation across these plate margins is diffuse. Partitioning of oblique convergence along the Andaman and Sumatra-Java margins gives rise to broad, complex zones of deformation involving both subduction and transform faulting (Malod and Kemal, 1996), the most notable of the latter being the Sumatra and Sagaing fault (Fig. 2.7). Persistent deformation within the Eurasian plate is illustrated by the number of seismogenic faults in this region (Molnar and Deng, 1984).

Thailand occupies an intraplate setting within the Eurasian plate (Fig. 2.7). The present tectonic stress regime in Thailand is one of transtension, with opening along north-south faults and right- and left-lateral slips on northwest- and northeast-striking faults, respectively (Polachan et al., 1991; Packham, 1993). This regime of transtensional faulting was initiated sometime between the late Cretaceous and early Tertiary (McCabe et al., 1988; Polachan et al., 1991). The Cenozoic tectonics of Thailand and southeast Asia as a whole, are a consequence of collision of India with Eurasia. Collision began about 50 Ma (Middle Eocene) and has resulted in 2,000 to 3,000 km of shortening across the Himalayan orogen (Peltzer and Tapponnier, 1988). As India drove into the southern margin of Eurasia, Indochina was rotated clockwise about  $25^\circ$  and extruded to the southeast by approximately 800 km along the Red River, Mae Ping (Papun-Wang Chao), and Three Pagodas fault zones (Fig. 2.8) during the first 20 to 30 million years of collision (Peltzer and Tapponnier, 1988). Extension migrated northwards onto the Altyn Tagh fault (figure 2.8) as collision progressed. Rotation of Indochina continued, reversing the sense of motion of the Red River, Mae Ping, and Three Pagodas faults from left-lateral to right-lateral (Allen et al., 1984; Peltzer and



MPFZ: Mae Ping fault zone; NTFZ: Northern Thailand fault zone;  
 TPFZ: Three Pagodas Fault zone; UFZ: Uttaradit fault zone

**YOUNG FAULT MOVEMENT ALONG THE SOUTHERN SEGMENT OF SRI SAWAT FAULT**



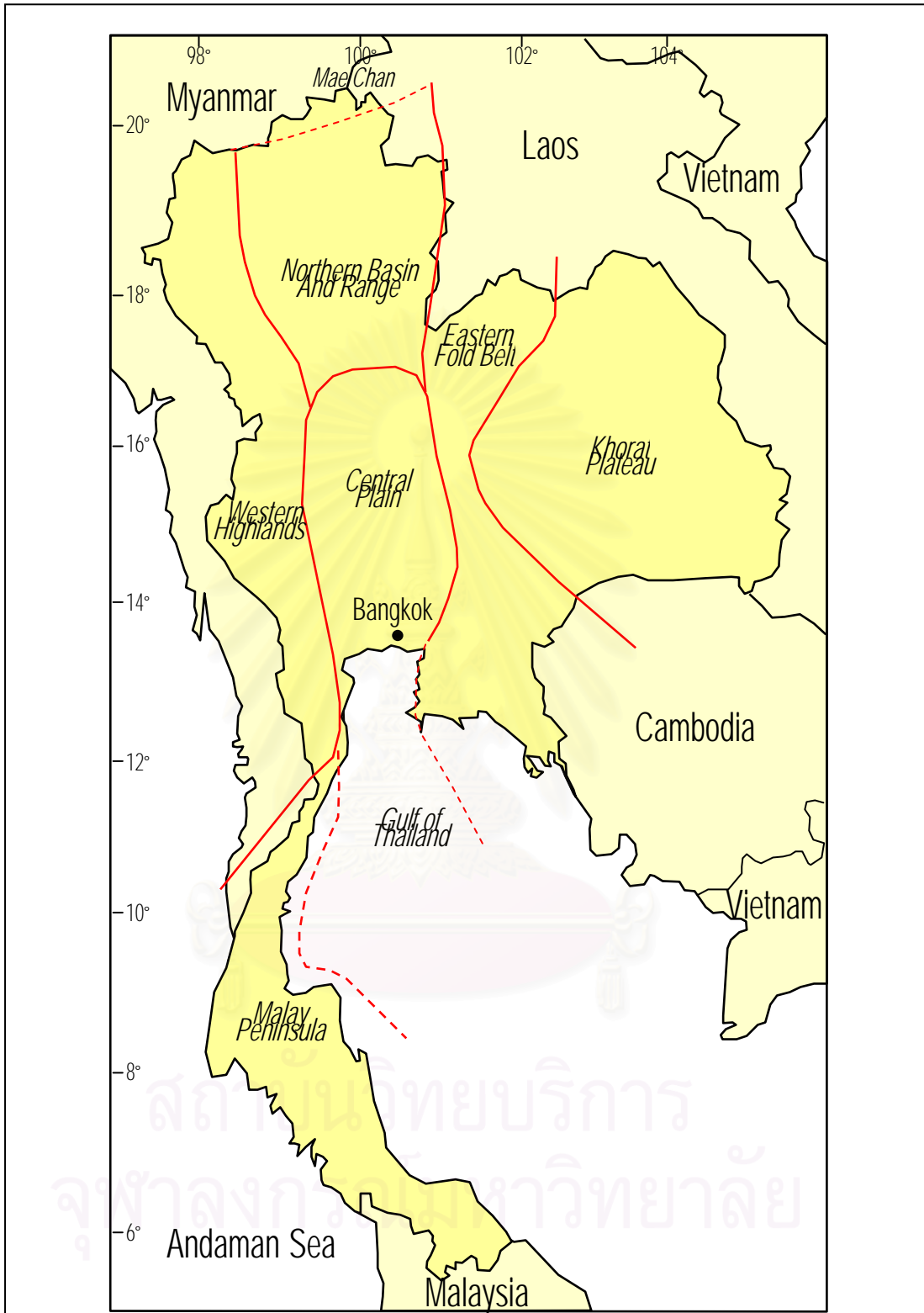
MR. RUTCHUT NUTTHEE  
 DEPARTMENT OF GEOLOGY  
 FACULTY OF SCIENCE  
 CHULALONGKORN UNIVERSITY

Figure 2.7 Tectonic map of south and southeast Asia and south China (Polachan et al., 1991)

Tapponnier, 1988). Differential slip between the strike-slip faults, created a transtensional regime that resulted in the opening of Tertiary basins in southeast Asia (Ducrocq et al., 1992).

Tertiary basins of Thailand are grabens or half grabens, typically bounded by N-trending normal faults (Polachan et al., 1991; Lorenzetti et al., 1994). The location and geometry of the basins are controlled by the north-south structural grain in pre-Triassic rocks and pre-existing northwest-trending, strike-slip faults (O'Leary and Hill, 1989). Basin evolution throughout Thailand follows a roughly similar sequence of events. The main phase of strike-slip tectonism, resulting in rapid extension, with widespread fluvial sedimentation (Oligocene-Early Miocene), was followed by lacustrine sedimentation as basins became increasingly isolated (Early-Middle Miocene). Lacustrine sedimentation ended, and there was an influx of coarse terrigenous clastics suggesting a period of rapid, localized uplift (Middle-Late Miocene). Finally, following a brief period of basin inversion that resulted in a widely recognized Late Miocene unconformity, fluvial sedimentation, generally coarsening upward, resumed (Late Miocene-Recent) (Polachan et al., 1991; Remus et al., 1993; Alderson et al., 1994). The climax of extensional tectonism is marked by the eruption of late Tertiary and Early to Middle Quaternary alkaline basalts (Hoke and Campbell, 1995). Paleomagnetic data, showing localized rotations during the Tertiary, indicates that the opening of these basins appears to have been fairly complex (McCabe et al., 1988, 1993; Richter et al., 1993). The total amount of extension across the region is unknown. However, Olinstad et al. (1989) estimated about 50 km of Cenozoic extension at the northern end of the Gulf of Thailand. In addition, thickness of basin-fill sediments is poorly constrained and geometry of the basin-bounding faults are not well known. Many of the basins, however, are bounded by linear escarpments that display a number of geomorphic features suggesting that they may still be active structures (Siribhakdi, 1986).

Thiramongkol (1983) divided Thailand into seven physiographic provinces that also roughly represent differences in the underlying geologic structure. Almost all of western Thailand, including the study area, lies within the 'West Continental Highland' province (Fig 2.8). This province is primarily an upland region comprising deformed plutonic, metavolcanic and metasedimentary sequences. The mountains attain altitudes



**YOUNG FAULT MOVEMENTS ALONG THE SOUTHERN SEGMENT OF SRI SAWAT FAULT**



MR. RUTCHUT NUTTHEE  
 DEPARTMENT OF GEOLOGY  
 FACULTY OF SCIENCE  
 CHULALONGKORN UNIVERSITY

Figure 2.8 Seismotectonic province in thailand (modified after Woodwarc Clyde, 1986).

of greater than 1,000 m and, although they are extensively dissected, contain peneplain remnants at various elevations across the region.

Nutalaya et al. (1985) first defined a series of seismotectonic provinces for Thailand. The majority of Thailand falls into one zone, Zone F (Tenasserim Range), defined primarily on the distribution of historic earthquake epicenters. Subsequent authors (e.g. Hinthong, 1991; Lukkunaprasit, 1993; Suwanlert, 1992) have all adopted the seismotectonic provinces of Nutalaya et al. (1985) without significant alteration. Charusiri et al. (2002a,b), however, by incorporating geologic data, have attempted to better define the seismotectonic provinces in Thailand.

Incorporating geologic, heat flow, and fault activity data, Woodward-Clyde (1998) have modified the seismotectonic zones of Nutalaya et al. (1985) to represent the seismotectonic character of Thailand (Fig. 2.8). Most of western Thailand falls within the Western Highlands province. This is a region of dissected uplands, comprising deformed and metamorphosed Paleozoic bedrock: part of the Sibumasu block of Richter and Fuller (1996) or the Shan-Thai block of Bunopas and Vella (1992). The structural grain of this region trends approximately N to NE (or S to SE) and is traversed by a series of NW to N-NW-striking Cenozoic strike-slip faults (Fig. 2.7). These faults, including the Mae ping and Three Pagodas fault systems, are part of the Andaman Sae-Sagaing fault transform system (Lacassin et al., 1997; Maung, 1987). Contemporary seismicity is diffusely distributed, low level, does not appear to be associated with currently mapped faults, and is probably confined to the upper 10 to 20 km of the crust. Focal mechanisms indicate that the Western Highlands is currently undergoing north-south maximum compression (Woodward-Clyde, 1998). Heat flow is presently low ( $<40 \text{ m W/m}^2$ ) and has been since the initiation of rifting in the early Tertiary (Thienprasert and Raksaskulwong, 1984; Raksaskulwong and Thienprasert, 1991). The Western-Highlands has fewer Tertiary basins than the neighboring Northern Basin and Range, and Central Basin provinces (Polachan and Sattayarak, 1989; Polachan et al., 1991).



## CHAPTER III

### GEOLOGICAL CONSIDERATION OF THE SRI SAWAT FAULT

#### 3.1 Studies of the Sri Sawat Fault in Thailand

The Sri Sawat Fault (SSF) is one of the important faults in western Thailand, which controls geological structure of this region. The Khwae Yai River mainly follows SSF. The fault is located between upper Mae Ping fault and lower Three Pagodas fault (Fig. 3.1). A few authors mentioned SSF in several ways as follow.

Nutalaya and Rau (1984) suggested that the SSF has the right-lateral movement. Such movement along SSF is probably related to the movement along the Sagaing Fault in Myanmar during the Late Cenozoic.

Siribhakdi (1987) considered that the southern end of the NNW-trending SSF running along the Khwae Yai River and seems to join the NW-trending Three Pagodas Fault (TPF). The earthquakes of April 15 and 22, 1983 are closely related to this fault but no fault plane solution has been done. His field works in western Thailand on a collective structural synthesis indicate that the Three Pagodas Fault is not a regular wrench faulting but rather shows a thick skin tectonic behavior, but the SSF seems to be an east-dipping thrust. All these two faults and their structural elements indicate a compression force from the southwest direction. He also concluded that the tectonic force might have been originated from spreading ridges and subduction zone in the Andaman Sea.

Lineament interpretation from Landsat imagery by Aramprayoon (1981) shows that the lineament features between the Three Pagodas and the Moei-Uthai Thani Fault (or the Mae Ping Fault) exhibit a broad Z-shape fault system. The appearance of this feature supports the left-lateral movement along then two faults. Thus the Z-shape fault system is triggered by extensional tectonics.

Shrestha (1987) identified the active fault traces along the TPF. He grouped a southern segment of the SSF as a part of TPF. However, he did not show any detailed description of this fault. Additionally, he shows an average slip rate of 0.73 mm per year and a stress drop of 10.6 bars. These parameters were computed by using empirical relations established between earthquake magnitude and seismic source parameters.

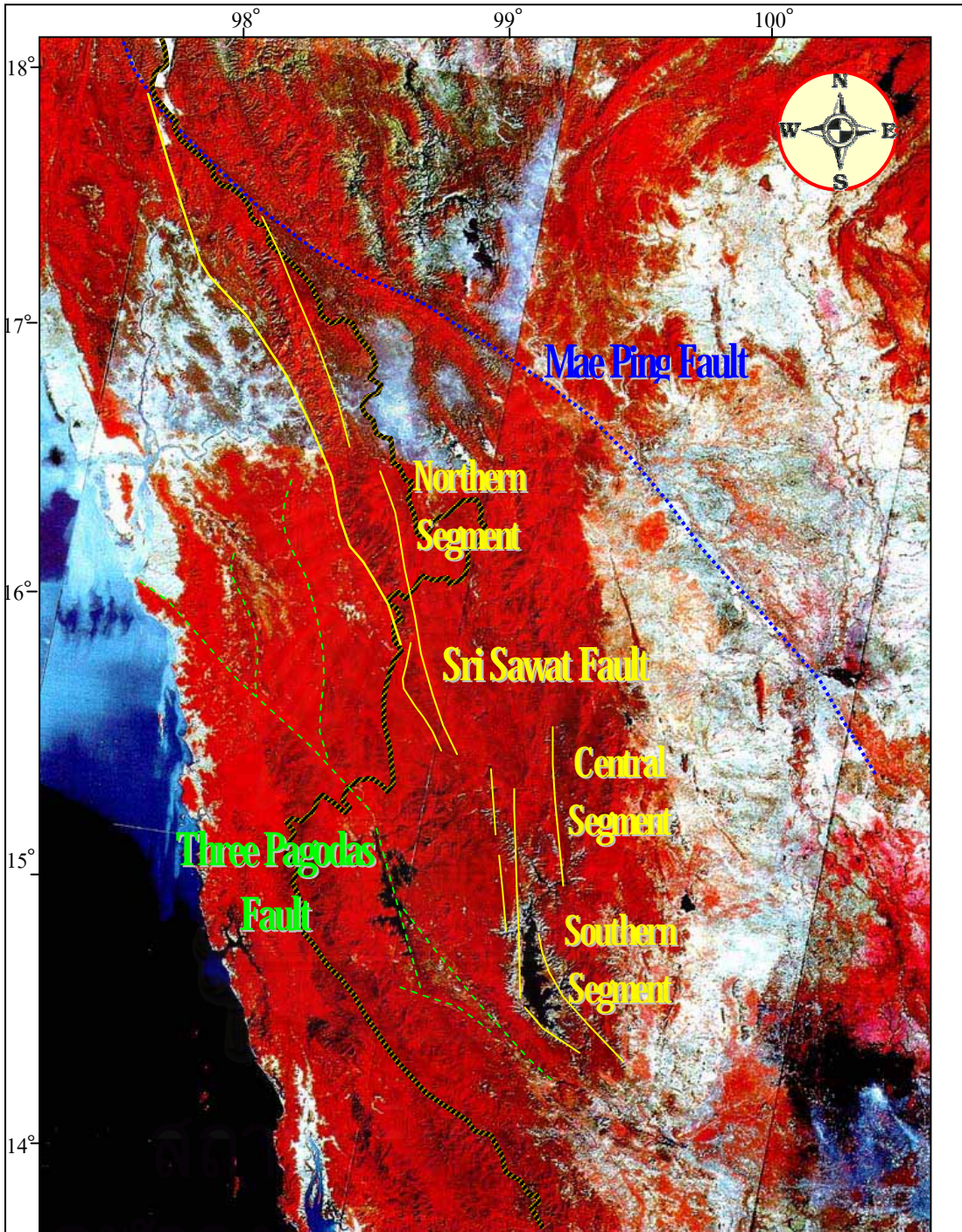
Chuaviroj (1991) reviewed geotectonics of Thailand and mentioned several major faults in Thailand. In his note, the roughly N-trending Sri Sawat Fault (SSF) Zone with the curvilinear pattern at both ends, consists of several fault sets, but mostly is situated between the Mae Ping and Three Pagodas Fault Zones. The SSF commences from Amphoe Srisawat to the northern part of Amphoe Bo Phoi, Kanchanaburi Province.

Hinthong (1991a) mentioned that the Sri Sawat Fault splits out from the Pan Laung Fault in Myanmar and runs in a NW direction in western Thailand. The fault cuts through Paleozoic to Mesozoic rocks and may continue to lower Central Plain to Bangkok. Its history is left lateral strike-slip fault in early Tertiary. Later, the fault changed its movement from left to right in Quaternary period as a result of collision of Indian with Asian continent during 45-51 million years ago to present.

Nutalaya (1992) mentioned that the SSF occupies the Khwae Yai and Mae Klong River channels and extends northwesterly into Myanmar. The total length is more than 500 km. Several hundred earthquakes were reported along this fault, the largest of which occurred on April 22, 1983 with magnitude of 5.9  $M_L$ . All earthquakes were of shallow depths. The focal plane solution of the April 22, 1983 earthquake shows a right lateral strike slip along this fault.

### 3.2 Segmentation of the Sri Sawat Fault

The satellite imagery Landsat TM5 scale 1:1,000,000 cover northern, western and central part of Thailand, and some Eastern part of Myanmar, was applied to interpret to locate three major faults (Fig. 3.1) in western Thailand into the Mae Ping Fault (MPF), Sri Sawat Fault (SSF), and Three Pagodas Fault (TPF). The Mae Ping and Three



**Legend**

- ⋯⋯⋯ Mae Ping Fault
- Sri Sawat Fault
- - - Three Pagodas Fault
- International Boundary

0 25 50 75 km

(provided by National Research Council of Thailand)

**YOUNG FAULTING ALONG THE SOUTHERN SEGMENT OF SRI SAWAT FAULT**



MR. RUTCHUT NUTTHEE  
DEPARTMENT OF GEOLOGY  
FACULTY OF SCIENCE  
CHULALONGKORN UNIVERSITY

Figure 3.1 Landsat TM5 satellite imagery showing orientation of three major faults – Mae Ping Fault (MPF), Sri Sawat Fault (SSF), and Three Pagodas Fault (TPF) in western part of Thailand and eastern part of Myanmar

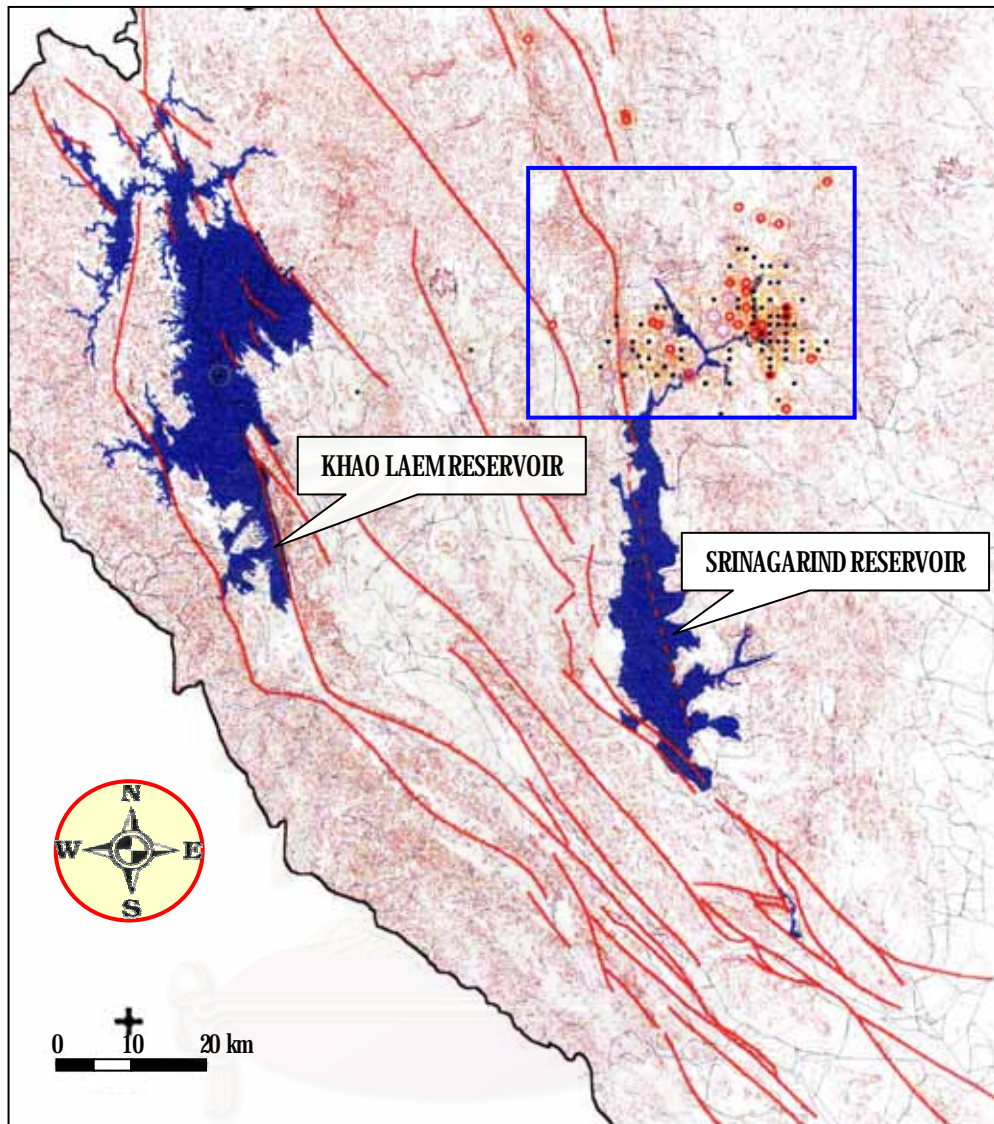
Pagodas Faults lie in the NW-direction, while the SSF seems to be the NNW-trending. The SSF are considered especially and separated into three segments namely northern, central, and southern segments, base on geologic (bounded by Quaternary basins, and geomorphic indicators such as mountain range, triangular facet) and geometric such as change in fault orientation or gap in faulting (see more detail in McCalpin, 1996). The detailed descriptions of individual fault segments are shown below.

### 3.2.1 Northern Segment of the Sri Sawat Fault

Northern segment is the uppermost part of Sri Sawat Fault. It can be clearly traced in a NNW direction. The north end of this segment seems to join with the upper MPF in Myanmar. However, it can be separated from the MPF by difference in their orientations. Sharp lineaments indicate the morphology of mountain range with west-facing triangular facet along the fault segment. Total length of the segment is about 255 km. Most of them are, however, in Myanmar. The average orientation of the northern segment is about N25°W. This segment can be subdivided into 4 fault traces (Fig. 3.1), base on gap in faulting. All of them lay in the same direction. The uppermost fault is the longest trace about 195 km. The upper-east fault is about 95 km long. Both of these fault segments situate in eastern part of Myanmar. The lower-west fault is about 50 km long running from Thai-Myanmar border near Khao Mamaung Sam Mun and run along west of Khao Kaphrieo Dang. The lower-east is about 110 km long from eastern part of Myanmar passing Thai-Myanmar border to Ban Thi La Ku.

### 3.2.2 Central Segment of the Sri Sawat Fault

Central segment located in north of the Srinagarind Reservoir. Unlike the northern segment, the central segment orients in the N-S direction. This segment shows sharp lineaments along the mountain rang with sets of west-dipping triangular facets along the fault. Total length of segment is about 110 km. The large earthquakes of magnitude 5.6 and 5.8 on April 15 and 12, 1983, respectively (Fig. 3.2), occurred around this area. The central segment can be subdivided into 3 fault traces. The western fault is about 55 km long, running from Ban Thi Laku passing Khao Huai Plu to the western reach of Srinagarind Reservoir. The middle fault is the longest trace with about 85 length



**Magnitude (Richter)**

- 5 to 6
- 4 to 5
- 3 to 4
- 1 to 3

[provide by Suwith Kosuwan, DMR, (personal contact)]

**YOUNG FAULTING ALONG THE SOUTHERN SEGMENT OF SRI SAWAT FAULT**



MR. RUTCHUT NUTTHEE  
DEPARTMENT OF GEOLOGY  
FACULTY OF SCIENCE  
CHULALONGKORN UNIVERSITY

Figure 3.2 Major faults and plotted epicenters in Changwat Kanchanaburi during 1983 to 1999. The box note that the largest epicenter occurred on April 22, 1983 and its aftershocks.

of km, running from Khao Ong lang passing Khao Ong Kha to flank with western rim of the Srinagarind Dam. The last segment is the eastern fault is about 65 km, running from Khao Nam Dip along the Huai Kha Khaeng through Ban Taling Sung to upper reach of the reservoir.

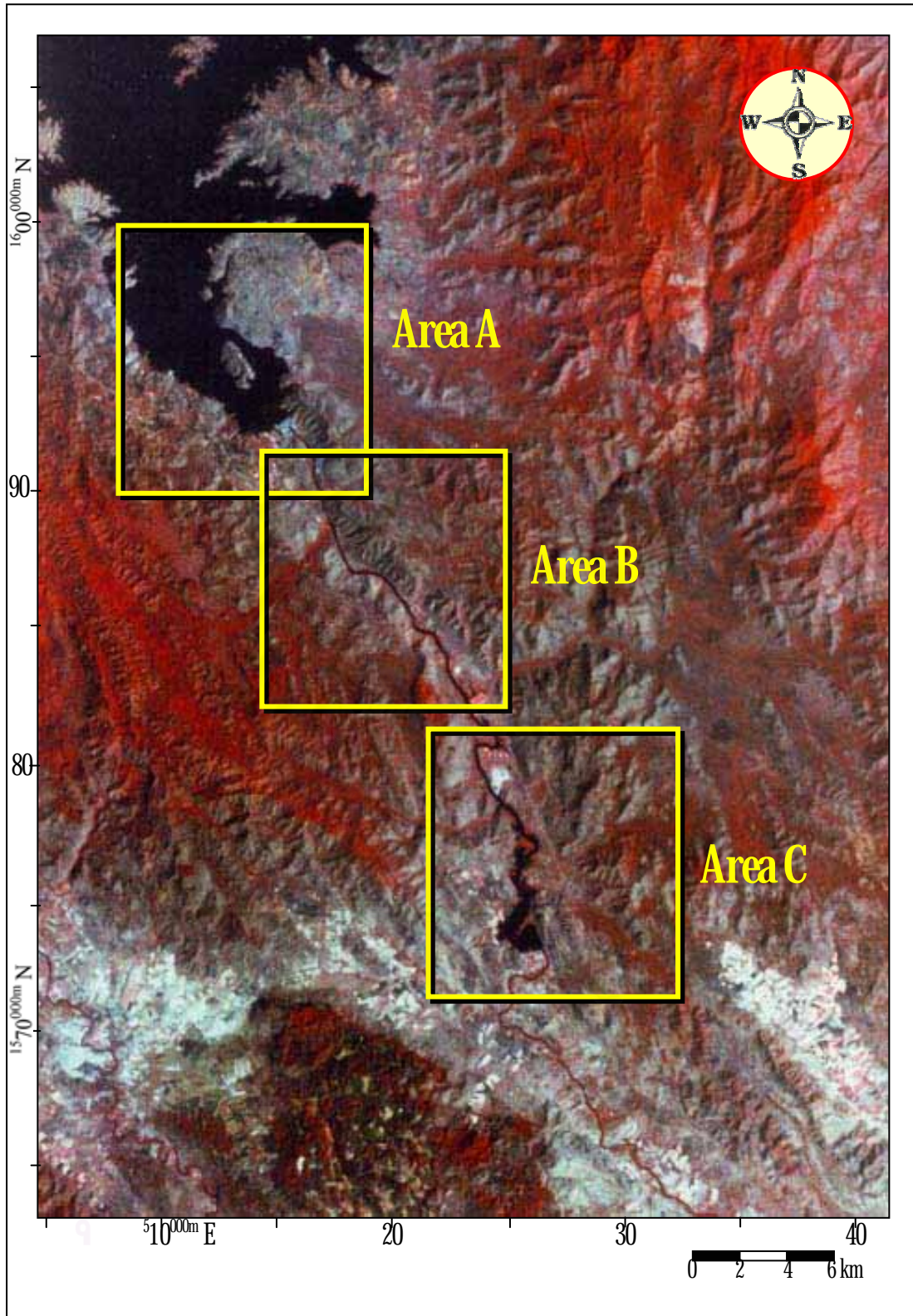
### 3.2.3 Southern Segment of the Sri Sawat Fault

Southern segment is the lowermost part located south of the Srinagarind Dam. The average orientation is about  $N40^{\circ}W$ . This segment can be subdivided into 2 fault traces. The eastern fault is about 75 km long running from Ban Phu Toei through Amphor Sri Sawat to Tumbon Thung Masang. The western fault is about 12 km long, passing Ban Tap Tao to Ban Sadong. It is the most interested fault, because it shows several morphotectonic features very clear, and young sedimentary deposits cut by the fault.

### 3.3.1 Locating the Study Area

The application of the satellite-borne images allows to locate and pinpoint the study area. The central segment (see section 3.2.2) is important on the basis of present-day seismicity as shown by a swarm of epicenters. However, disappearance of clearly-defined morphotectonic features causes inattractiveness of the central segment. The northern segment displays much better-define tectonic morphology But, it is near Thai-Myanmar border. Furthermore, its remoteness makes difficulty to access and the area quite dangerous. This conclusion is also applied to the northern segment. The southern segment located south of the Srinagarind Dam. The area in the southern segment is of interest due to the fact that it shows very clear fault traces with abundant morphotectonics features, such as triangular facets, offset streams, and young sedimentary deposits that indicate young faulting. In addition, this area is near the dam, so it is easy to access. Additionally, road-cut and constructions provide many well-preserved exposures.

Three interested areas (area A, B, and C) (Fig. 3.3) in the southern segment have been defined in the south of the Srinagarind Reservoir for detailed study using



**YOUNG FAULTING ALONG THE SOUTHERN SEGMENT OF SRI SAWAT FAULT**



MR. RUTCHUT NUTTHEE  
 DEPARTMENT OF GEOLOGY  
 FACULTY OF SCIENCE  
 CHULALONGKORN UNIVERSITY

Figure 3.2 Satellite imagery Landsat TM5 showing the locations of three areas (area A, B, and C), which were studied in detail by aerial photograph interpretation.

aerial photographic interpretation (Fig. 3.2) and field survey. The geomorphotectonic map was created using this current interpretation combined with previous geologic map.

### 3.3.1 Area A; Srinagarind Dam

The area A, about 100 square kilometers, covers the Srinagarind Dam site (Fig. 3.3). General topography is highland with a range of mountain and a major river (Khwaie Yai River) (Figs. 3.4a and b). Several intermittent streams are observed along mountain slopes, running vertically to the Khwaie Yai River and the main streams i.e., Huai Chak, Huai Tha Rabo, Huai Song Khlong, and Haui Kaeng Riang. General land level is about 200 m to 800 m above the mean sea level (MSL) to the top of mountain. The Khwaie Yai River, is 50-100 m wide, meanders from a flat plain in the northwest to a narrow gorge in the southeast of area A. It has a gentle stream profile with average 65 m above mean sea level.

The lithology in this area was separated into 3 mappable units (Fig 3.5a) based upon field and aerial photographic interpretation. They are quartzite, limestone, and young Cenozoic sediments, all of which align in the northwest-southeast direction.

Quartzite (Qz), was observed about 7 % on this area. It is identified by intermediate tone with fine texture and specific drainage pattern (Fig 3.4b). The drainage pattern develops mostly on steep slopes with sharp ridges. It displays more wide-spaced, less ramified, short straight, and V-shape gullies. The wide-spaced texture indicates homogeneous hard rock with uniform resistance to erosion, such as intrusive or massive metamorphics (von Bandat, 1962). This rock unit was classified as the oldest rock type, by Bunopas (1976) and Chantaramee et al. (1981), in this area.

Limestone (Ls)- the most abundant rock type, occupies about 65 % on this area. It shows light tone with coarse texture, sinkhole pattern, and karst topography (Fig. 3.4b). Two ages of limestone were reported-one in the northeast being of Ordovician and the other in the southwest being of Permian.

Young Cenozoic sediment deposits are found about 28 % as long and narrow belts in many places within toes of the mountain slopes and rims of the Khwaie



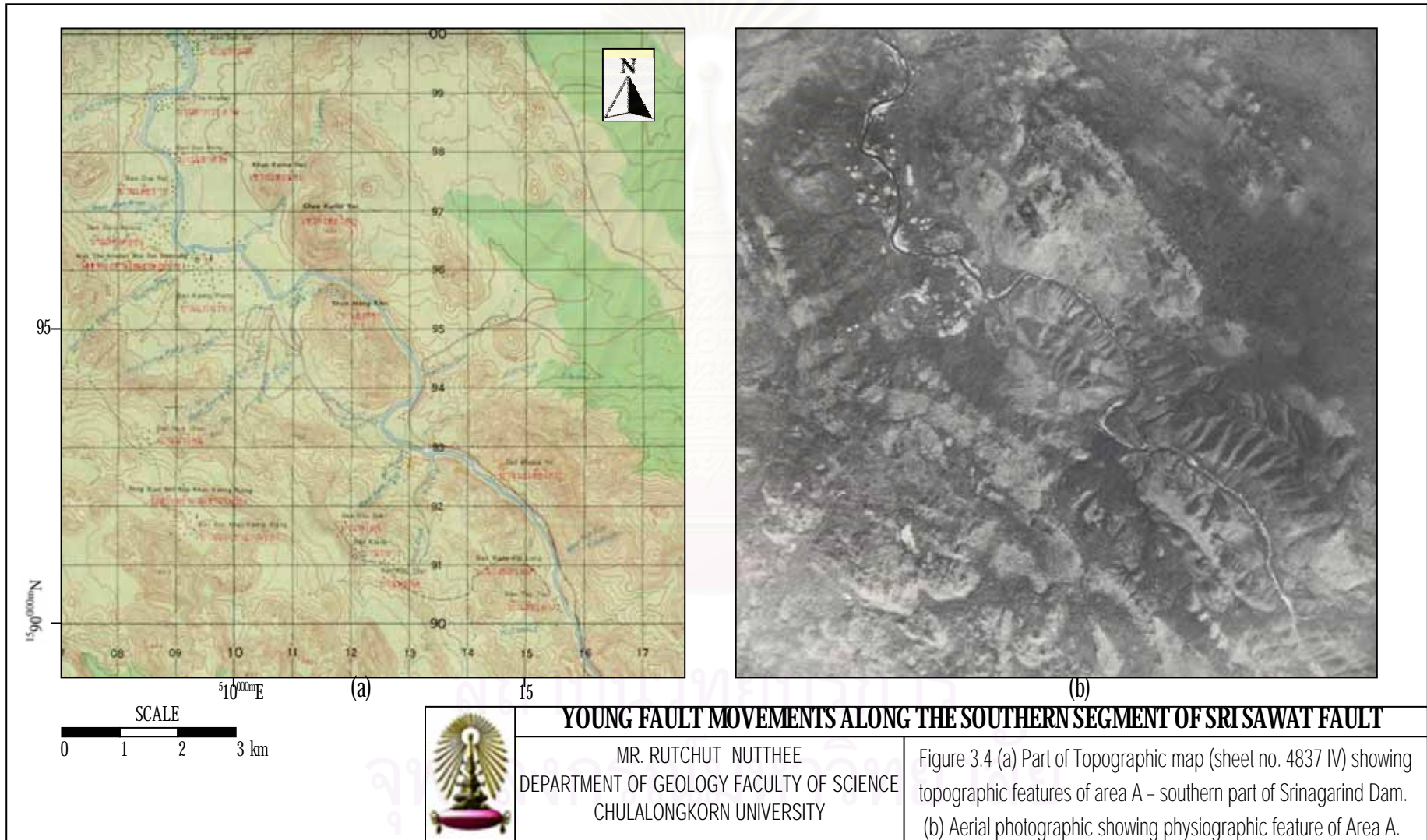
Yai River. It comprises of colluvial, terrace, and river deposits. The colluvial deposits (Dc) usually were found on the toe of mountain slope. River deposits (Dr) compose of flood plains and sandbars. The flood plains mostly appear in northeast of this area. The sandbars, which are observed by white tone with very fine texture, deposited on near or rims of the river. One terrace deposit (Dt) was recognized at toe slope of limestone units, southeast of area and west of Khwae Yai River (Fig. 3.5a). It shows 3 steps at attitudes of 270, 400, and 440 m MSL. This terrace may be controlled by young tectonics activity in this area.

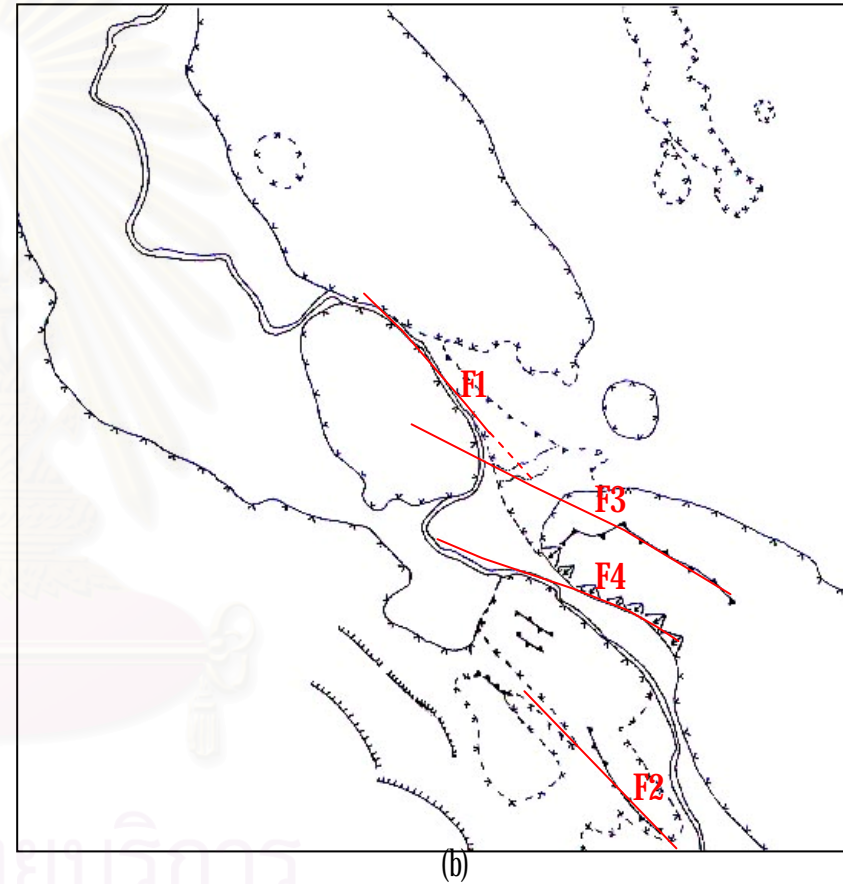
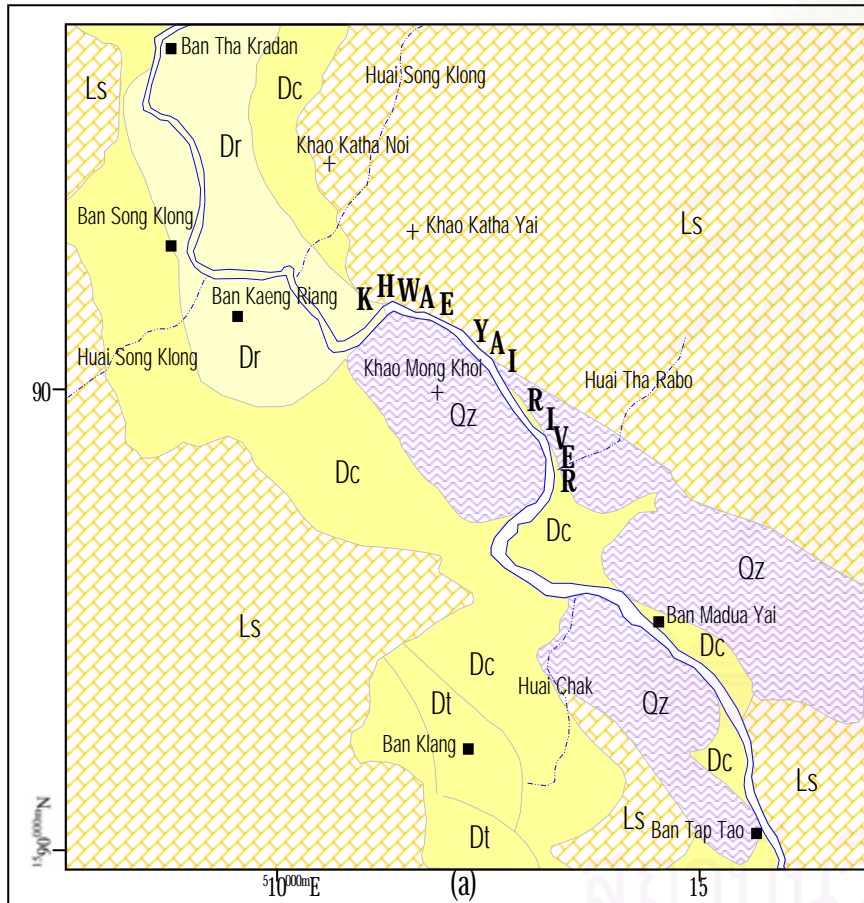
Several fault traces are observed in this area (Fig. 3.5b). They are divided into two major groups-one in  $N40^{\circ}W$ , and the other in  $N70^{\circ}W$ . The  $N40^{\circ}W$ -trending group consists of 2 separated fault traces. The F1 fault in the northern part running from eastern toe slope of Khao Mong Khoi through Khwae Yai River to Huai Tha Rabo. The fault is about 3 km long with a set of east-facing triangular facets and two offset streams along this fault. The F2 fault in the southern part running from Huai Chak to Ban Tap Tao with the total length of 2.5 km in this mapped area. It is the same fault (major fault) extending to in Area B. The total length of the fault is about 12 km.

The  $N70^{\circ}W$ -trending fault group consists of 2 subparallel fault traces. The upper fault trace (F3) is about 5 km long, running from limestone mountain (Khao Mong Khoi) southeastward to the mountain that located in east of Ban Madua Yai. The lower one (F4) is about 5 km long, running from Huai Nam Mut to Ban Madua Yai. It is traceable from toe slopes of quartzite mountain into limestone unit. There is the set of triangular facets on quartzite mountain shows along this fault trace.

### 3.3.2 Area B; Ban Kaeng Khaep

The area B is about 100 square kilometers. This area is located southeast of area A along the Khwae Yai River. General topography is highlands, similar area A. The Khwae Yai River runs through a steep-valley narrow gorge in southeastward direction (Figs. 3.6a and b). The famous large waterfall, Erawan Waterfall, is on the scarp of limestone, northwest of area and west of Khwae Yai River (Fig. 3.7a). The 7-tiered Erawan Waterfall is widely regarded as being one of Thailand's loveliest cascades.





**YOUNG FAULT MOVEMENTS ALONG THE SOUTHERN SEGMENT OF SRI SAWAT FAULT**

MR. RUTCHUT NUTTHEE  
DEPARTMENT OF GEOLOGY FACULTY OF SCIENCE  
CHULALONGKORN UNIVERSITY

Figure 3.5 (a) Aerial photographic interpretation of rock distribution (from Fig. 3.4 (b)) of area A, and (b) Morphotectonic interpretation of the similar area. Symbols are shown in Fig. 3.6.

## LEGEND

Dr	River deposits	Ss	Clastic rock
Dt	Terrace deposits	Ls	Limestone
Dc	Colluvial deposits	Qz	Quartzite
■	Village		
+	Top of mountain		

## SYMBOL

F	Fault line	TTTTTT TTTTTT	Miner scarp, terrace
■■■■	Fault scarp	▲▲▲	Ridge
▽▽▽	Concave break of slope	▽	Sharp valley
▽▽▽	Concave change of slope	▲	Triangular facet
▲▲▲	Convex break of slope	~~~~~	Stream, river
▲▲▲	Convex change of slope		

(Modified after McCalpin, 1996 and Denmek, 1972)

### YOUNG FAULT MOVEMENTS ALONG THE SOUTHERN SEGMENT OF SRI SAWAT FAULT



MR. RUTCHUT NUTTHEE  
DEPARTMENT OF GEOLOGY  
FACULTY OF SCIENCE  
CHULALONGKORN UNIVERSITY

Figure 3.6 Legends and symbols, which are used in interpreted rock unit and geomorphologic map, i.e., Fig 3.5, Fig 3.8, and Fig 3.10.

Base on the aerial photographic interpretation, the mapable unit can be grouped into 4 units (Fig. 3.7b) including quartzite, limestone, clastic rock, and young Cenozoic sediment deposits, as shown below.

Quartzite appears about 12 % on the area. The intermediate tone with fine textures and wide-spaced drainage patterns are the feature of this rock type; similar to that of area A. It was observed as a mountain range with northwest direction, in the middle portion of the study area (Fig. 3.7b)

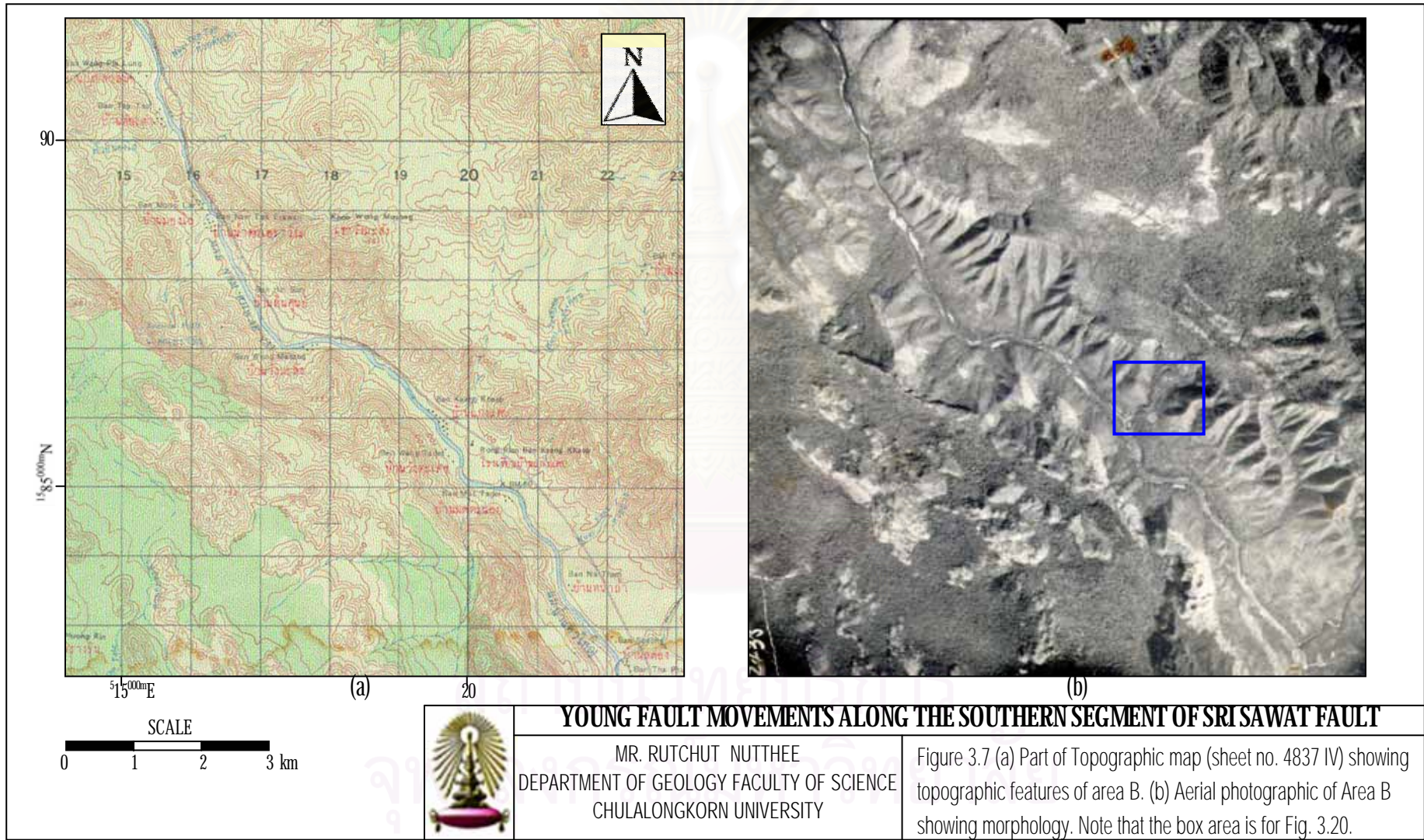
Limestone was found about 65 % from feature as light tone with coarse textures, prominent sinkhole patterns, and karst topography.

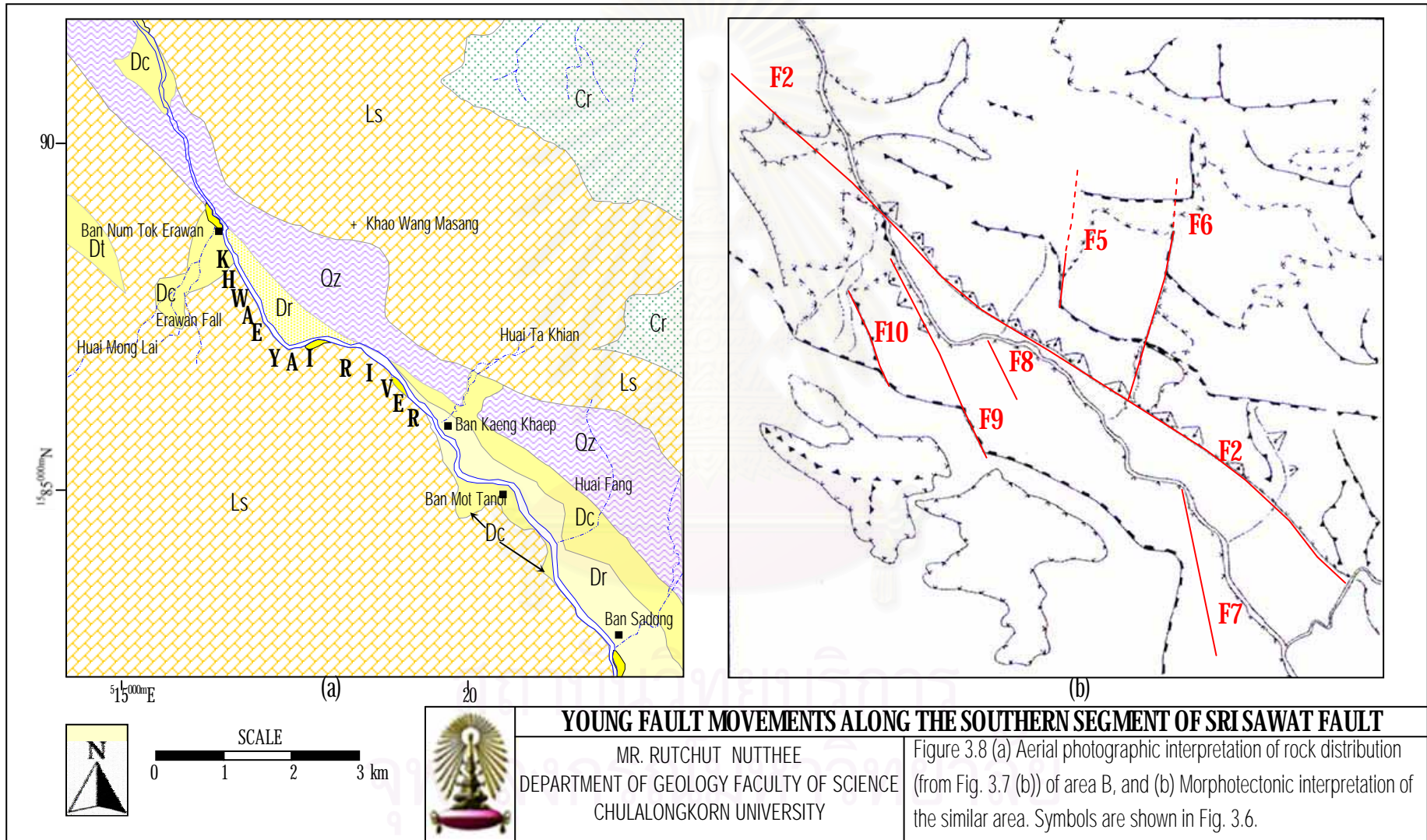
Clastic rock (15 %) displays dark tone with coarse textures and medium-spaced drainage patterns. It is observed in the east and northeast parts of the investigated area. It was observed as the mountain northeastern part of the area.

Young sediment deposits are found about 8 %, composes of colluvial, terrace, and river. It comprises of colluvial, river, and terrace deposits. The colluvial deposits were observed well at foot slopes of the mountain, especially east of the Khwae Yai River along the main fault (F2). The flood plains mostly deposit in southeast of this area, and sandbars on rims of the river. The terrace deposit shows 1 steps of deposit, which extends from area A, is about 320 m (above MSL) at foot slopes of limestone units, northeast of area and west of Khwae Yai River. Most of Triassic rock unit, which proposed by Bunopas (1976), in this area was covered by these young sediment deposits.

Several faults can be easily traced using aerial photographic interpretation in this area (Fig. 3.7b). They are divided into 3 major groups, namely those of  $N50^{\circ}W$ ,  $N5^{\circ}E$  and  $N25^{\circ}W$ . The  $N50^{\circ}W$  trending group consists of only one fault (F2). However, it is the most essential and longest fault (about 12 km). It shows very clear tectonic morphology, such as sets of triangular facets, offset streams, shutter ridges, and young sedimentary deposits, along the fault trace. The offset stream indicates right-lateral fault movement.

The  $N5^{\circ}E$  trending fault group consists of 2 fault traces. Both are located in the east of the Khwae Yai River. The eastern fault trace (F5) is about 3 km long, running northeastward from Ban Kaeng Khaep. It cuts and pushes off the fault scarp on





limestone unit. The upper one (F6) is slightly shorter about 2 km long, running northeastward near Khao Wang Masang. It seems cutting and pushing off the fault scarp on quartzite unit in the southern end of the trace and limestone unit in the northern part of the fault. Both of the offsets show right-lateral fault movement.

The N25°W trending fault group consists of 5 fault traces (F7-10). All of them forming the en echelon pattern are found on the western side of the Khwae Yai River with the length ranging from 700 m (F8) to 2.2 km (F9). They seem to cut into and push off the fault scarp on the limestone unit. The offset of scarp also indicates right-lateral fault movement. Set of 3 triangular facets is observed along F9. The fault belonging to this group in the easternmost part is F7. This fault is likely to meet the Khwae Yai River at Ban Na Tham. The F7 is about 1.5 km long and is found to act as the boundary between Permian limestone and Cenozoic deposit.

### 3.3.3 Area C; Ban Tha Thung Na

This area is about 100 square kilometers, covering Tha Thung Na Reservoir (Fig. 3.3). General topography is characterized by highlands with ranges of mountain including Khao Mo Thao, Kho Wang Kula, Khao Chong Sadao, and Khao Phu Phrao, and the major river, Khwae Yai River (Fig. 3.8a). Attitudes of the area surveyed range from 200 m MSL to 600 m in the top of mountain.

In this area, limestone is the most abundant rock type (Fig. 3.9a), cover about 60% of the investigated area. It was shown by light tone with coarse textures, karst topography, and sinkhole patterns (Fig. 3.8b); similar the area A and B.

Clastic rock (about 15%) cover this area. It is manifested by medium to dark tone with coarse texture and medium-spaced drainage pattern. It was observed at Khao Pu Prao, middle part of the surveyed area; east of the Khwae Yai River and the southwestern part of the area.

Young Cenozoic sediment deposits (about 12%) comprises of colluvial, terrace, and river deposit; like the area A and B. The river deposit, which composes of the flood plains and sandbars, is found mostly on this area. The flood plain mostly observed in the north and southern part of this area along the Khwae Yai River. The sandbars are found as white tone with very fine texture along rims of the river. The



colluvial deposits were found on the toe of mountain slope at north and southwestern part of the area along the F11 and F14, respectively. The terrace deposit was observed on foot slope of limestone units, east of the Khwae Yai River and north of Huai Phu Prao. The terrace form two elevated levels – as the lower level at the attitude of 200 m above MSL and the other as the higher level at the altitude of 350 m above MSL.

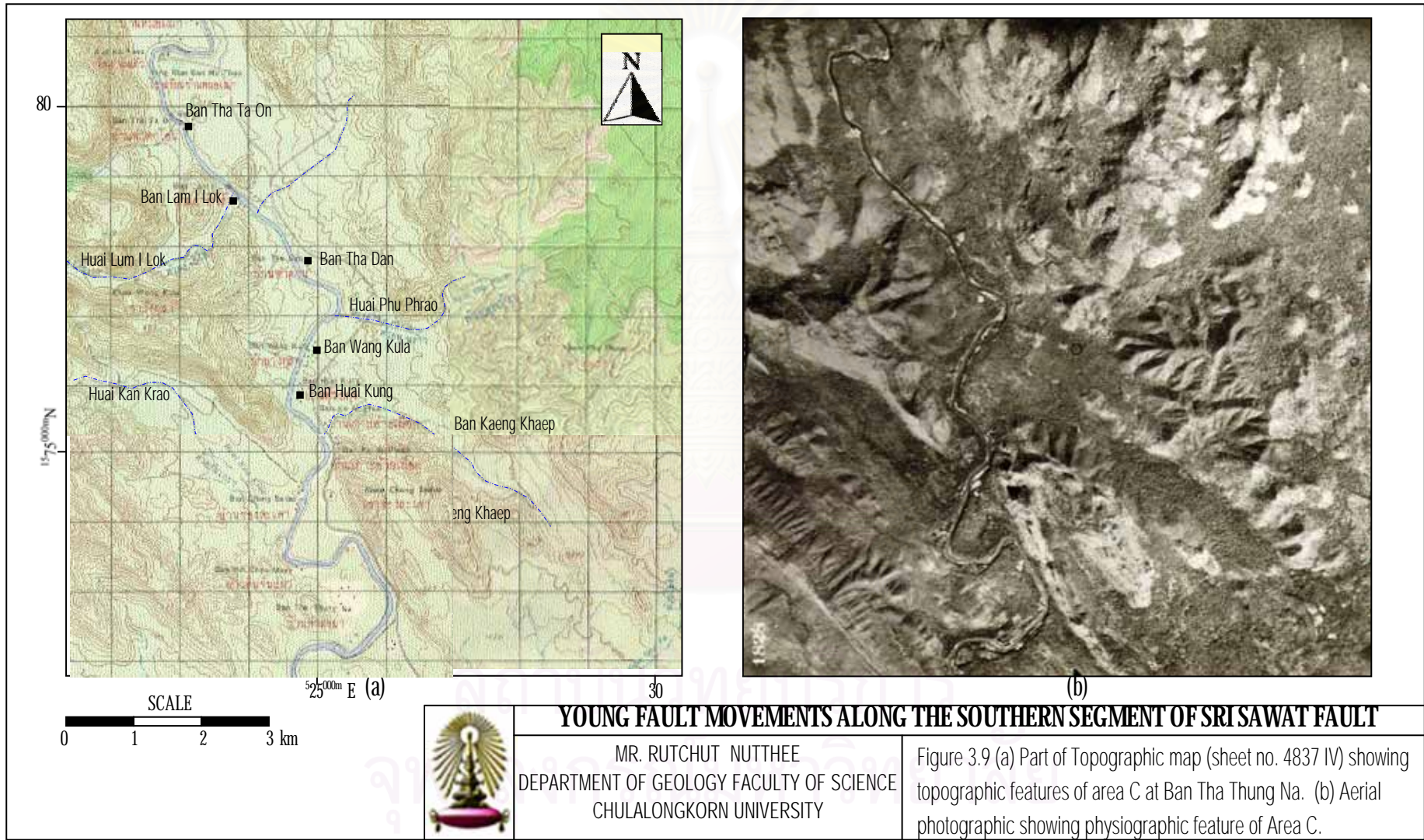
Several fault traces were found in this sub-study area (Fig. 3.9b). They are divided into 4 major trends including N35°W, N10°E, N75°W, and E-W trending. The N35°W trending fault consists of 5 fault traces (F11-15). The easternmost fault (F11) is observed in the east of Khwae Yai River. It is about 8 km long and extends from Ban Mo Thoa through Huai Phu Phrao to west facing of Khao Phu Phrao. It is well observed on Landsat TM5 imagery (Fig. 3.3), but not a clear fault trace on aerial photographs. This perhaps due to sediment covers. The northwestern fault (F12) is about 1.5 km long in the west of Khwae Yai River near Ban Tha Ta On. The east-facing fault scarp observed in the limestone unit, is related with this fault. The southern fault (F13) is about 3 km long. The fault scarp is observed in limestone unit along this fault. The two almost parallel fault (F14 and 15) is located in the southwestern part of the study area. The F14 was traced in the clastic rock unit, and F15 occurred between the clastic rock unit and the limestone unit. These two faults follow the mountain range system and 2 sets of triangular facets was observed along the fault traces.

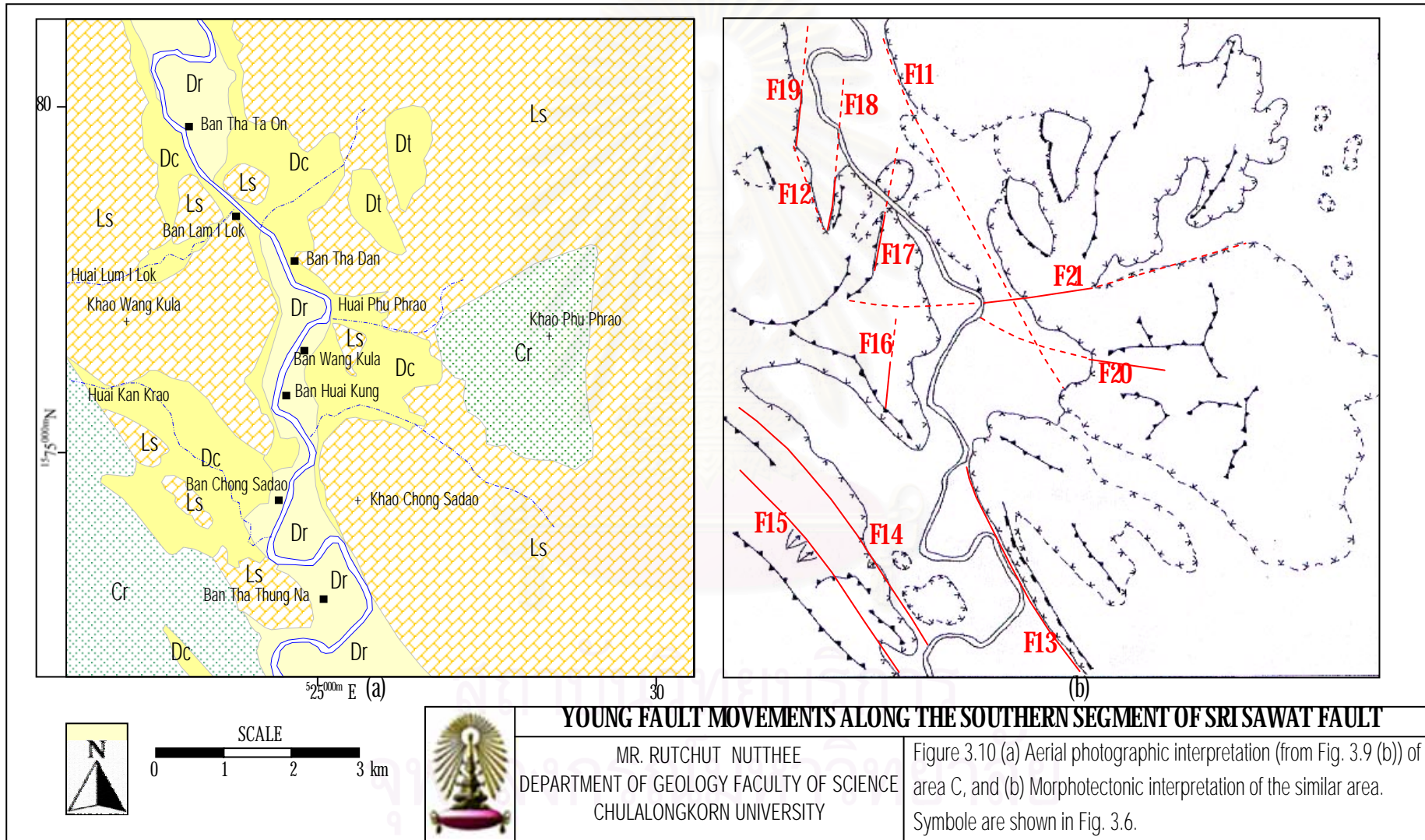
The N10°E-trending fault group consists of 4 fault traces (F16-19), in the western part of area. Each fault is about 1-2 km long. The lineaments show fault trace, but they do not show clearly-defined tectonic morphology.

The N75°W-trending group is observed as one fault (F20) in this area. It is about 3 km long and western portion is ended at Huai Phu Phrao. The fault cuts the clastic rock unit and develops two deeply SW-facing triangular facets.

The E-trending group is found as one fault (F21). It is about 5 km long and passes Ban Tha Dan to the eastern side of Khao Wang Kula. The fault shows fault scarps in east part of this fault. In the west part, the fault cannot be clearly traced, and perhaps covered by young Cenozoic sediments.

According to aerial photographic interpretation, the major fault (F2) in area B is the most interesting fault. Because, it is the longest fault showing very clear and





prominent fault-trace with well-defined morphotectonic features along the fault such as; sets of triangular facets, offset streams, shutter ridges, and young sediment deposits along the fault boundary. The faults in area A and C are shorter and some faults are not clear. However, it is noteworthy that the surface of area A is extensively covered by water of Srinagarind Reservoir (Fig. 3.3).

### 3.4 General Geology of the Study Area.

Geology of the entire study area and its vicinity has been studied by Electric Power Development Co., Ltd. (1973). Much work concerned about engineering foundation and construction of the Srinagarind Dam. Therefore, main part of those studies were emphasized to lithology, geologic structure, and engineering rock properties for dam construction. The systematic geological investigation was performed by Bunopas (1976) as a geologic map; Changwat Suphan Buri (ND47-7) Sheet; scale 1:250,000. Additionally, Chantaramee et al. (1981) studied general geology and distribution of rock units, and stratigraphy in areas of the Tha Thung Na Reservoir and some part of the Srinagarind Reservoir.

#### 3.4.1 Geological Setting

According to Bunopas (1976) (Fig. 3.10), the rocks in the study area can be grouped stratigraphically into four main rock units including Chao Nen Quartzite (E), Thung Song Group (O), Sai Yok Limestone (Ps), and Chong Khap Formation (Tr).

##### Chao Nen Quartzite (E)

The oldest rock unit in the study area is the Chao Nen Quartzite which was designated for the rocks occurring in Cambrian by Bunopas (1976). In regional, this rock unit include massive ortho-quartzite, bedded sandstone of brown to greenish colors, and calcareous shale. In the study area, it displays white massive ortho-quartzite (see Fig. 3.26; right of photograph). The thickness of this unit is about ----m. Its regional trend is in the NW direction following major regional structure. The major fault (F2) appears as a fault contact between this unit and the younger units including

## GEOLOGICAL LEGEND AND SYMBOL

### LEGEND

Q	Recent flood plain alluvials, sands, silts and swamps.		RECENT
Q1	Old alluvial fan, colluvial and old flood plain deposit of high and low terrace.		PLEISTOCENE
Mz	Mainly red sandstones, shales and basal conglomerates.	KHAENG RABOET SANDSTONE	? JURASSIC
T̄	Mainly shale with Doanella and Halobia sandstone and interbedded limestone.	CHONG KHAP FORMATION	TRIASSIC
Pt	Red sandstone with quartz sandstone; Thickly beded.	THA MADUA SANDSTONE	PERMIAN
Ps	Massive and beded limestones containing fusulines brachiopods, pelecypods and bryozoans.	SAI YOK LIMESTONE	
Pm	Brown, calcareous sandstone containing brachiopods, pelecypods, bryozoans and corals.	KHAO MUANG KRUT SANDSTONE	
DC	Pebbly mudstone, grey sandstone and dark grey shale, also red shale.	KHAENG KRACHAN FORMATION	CARBONIFEROUS-DEVONIAN
SD	Quartzite, phyllite, tuffaceous sandstone, limestone bands, brownish shale and chert beds.	BO PHLOI FORMATION KANCHANABURI FORMATION	DEVONIAN-SILURIAN
O	Banded, argillaceous limestone, argillite, quartzite and cephalopods.	THUNG SONG GROUP	ORDOVICIAN
CO	Banded, white, sugary marbles; in part dolomitized; also quartz mica schist.	U-THONG MARBLES	ORDOVICIAN- ? CAMBRAIN
C	Massive ortho-quartzite, bedded sandstone of brown to greenish colors, and calcareous shale.	CHAO NEN QUARTZITE	CAMBRIAN
PC	Metamorphic complexes; augen gneiss, granite gneiss, biotite schist, calc-silicate rocks and marbles.	THABSILA GNEISS	PRECAMBRIAN
gr	Granite, granodiorite, diorite and quartz feldspathic dikes.	IGNEOUS ROCKS	MESOZOIC

### SYMBOL

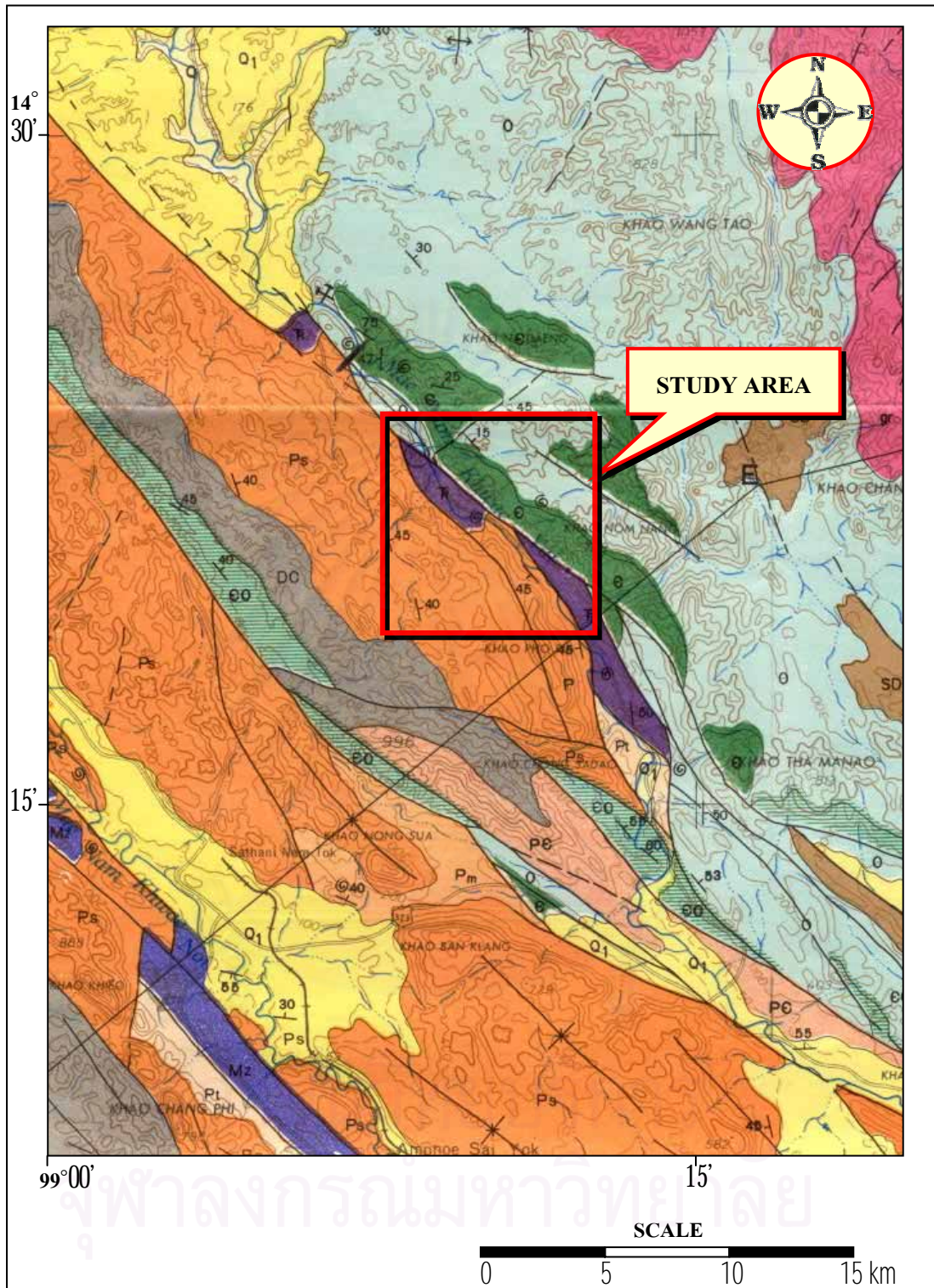
	Contact		Strike and dip		Overtured		Fossil Locality
	Anticline		Syncline		(Inferred)		Mine, or Quarry
	Fault		Thrust fault		(Inferred)		
	Thrust fault		(Inferred)		(Inferred)		

### YOUNG FAULT MOVEMENTS ALONG THE SOUTHERN SEGMENT OF SRI SAWAT FAULT



MR. RUTCHUT NUTTHEE  
DEPARTMENT OF GEOLOGY  
FACULTY OF SCIENCE  
CHULALONGKORN UNIVERSITY

Figure 3.11 Geological legends and symbols of geologic map in Fig. 3.12 (modified after Bunopas, 1976)



**YOUNG FAULT MOVEMENTS ALONG THE SOUTHERN SEGMENT OF SRI SAWAT FAULT**



MR. RUTCHUT NUTTHEE  
DEPARTMENT OF GEOLOGY  
FACULTY OF SCIENCE  
CHULALONGKORN UNIVERSITY

Figure 3.12 Geological map of the study area and its vicinity showing very deformed and faulted strata of Precambrian to Quaternary ages (after Bunopas, 1976).

Ordovician limestone, Permian limestone and Triassic mudstone. The regional strike is in N55°W to N75°W and the average dip is variously about 25° to 75°E.

### Thung Song Group (O)

The name Thung Song Group (Javanaphet, 1969) has been officially applied to all Ordovician limestones in Thailand. This unit was observed mostly in northeastern part of the area. In regional, most of the rocks belonging to Ordovician age are mainly banded argillaceous limestone, argillite, quartzite and cephalopods.

### Sai Yok Limestone (P)

The name Ratburi Limestone (Brown et al., 1951) and Ratburi Group (Javanaphet, 1969) have been applied throughout Thailand from limestones and associated classic rocks of Permian age. Permian rocks in Kanchanaburi can be divided into 3 types as Khao Muang Khrut sandstones, Sai Yok Formation and Tha Madua sandstones (Bunopas, 1976). In regional, Sai Yok Formation consists of massive and bedded limestone containing fusulines, brachiopods, pelecypods and bryozoans. This unit appears in southern part of area. The strike is about N20°W to N40°W and the average dip is about 45°W in western part of the unit and 40° to 45°E in eastern part.

### Chong Khap Formation (Tr)

The name Chong Khap Formation was designated for the rocks occurring in Triassic by Bunopas (1976). Regionally, the formation consists of mainly shale with *Doanella* and *Halobia*; sandstone and interbedded limestone. At Ban Chong Khap and Ban Tha Thong Mon, *Posidonia* (bivalve fossil), *Halobia* and *Doanella* were identified as middle Triassic in age (Bunopas, 1981). This rock unit appears between Chao Nen Quartzite and Sai Yok Limestone in the middle and southeast of the area (Fig. 3.10). The regional trend is in the NW direction with average thickness is about ---.

## 3.4.2 Structural Setting

### Faulting

Several faults in this study area and vicinity have been discovered and mostly they are in the NW-SE direction concurring with topographic feature of this area (Chantaramee et. al., 1981; Won-In, 2000; Fig. 3.10). Regionally, major faults in the area are not much intricate, except changing of fault direction. The change of fault directions

is within the range of 30 from the main strike (N50°W). Therefore, faults seem lie in the same direction, suggesting that they may have occurred in the same tectonics event. Three kinds of faults are observed viz. strike-slip faults (with oblique components), reverse fault, and normal faults. The first category seems to be much more abundant.

### Folding

In Kanchanaburi area, mostly fold axes are the NW-SE trending (Bunopas, 1976; Siribhakdi et. al., 1976; Sripongpan and Kojedee, 1987; Kemlek et al., 1989). Fold structures can be recognized in several rocks with many tectonic characters such as synclinal and anticlinal folds (Bunopas, 1976; and Chantaramee et. al., 1981). However, difference of form and attitude of fold depend on characteristic and thickness of rocks. Common attitudes of fold axes normally follow by the NW direction of major faults (Chantaramee et. al., 1981).

## 3.5 Detailed Geological Investigation

Detailed field investigation is the best way for studying characteristics of faults. The features, which are related to faults have been provided by remote sensing interpretation, and was studied, checked and compared in the field. In this current study six stations were selected for fault investigation (Fig. 3.11)

### 3.5.1 Station 1

<u>Map name</u>	Ban Kaeng Riang	<u>Map sheet</u>	4837 IV
<u>Location</u>	km-stone 42+000	<u>Grid reference</u>	052045 E 158565 N

This station was found as outcrop beside the main road no. 323. It is covered by talus deposits (Fig. 3.12). The talus is poorly sorted and comprises mainly coarse gravels with reddish brown color (Fig. 3.13). Fragment consists of quartzite and weathered feldspar rich sandstone 3-5 cm in diameter, high angularity. The essential sizes of matrix are fine gravel to fine sand. Clay and silt usually absent on surface, but increase in volume toward the lower part. The poor sorting indicates to rapidly mass movements. Large volume of sediment deposit and very coarse grained fragment reflect a transition of tectonic activity. High angularity reflects talus deposit adjacent to



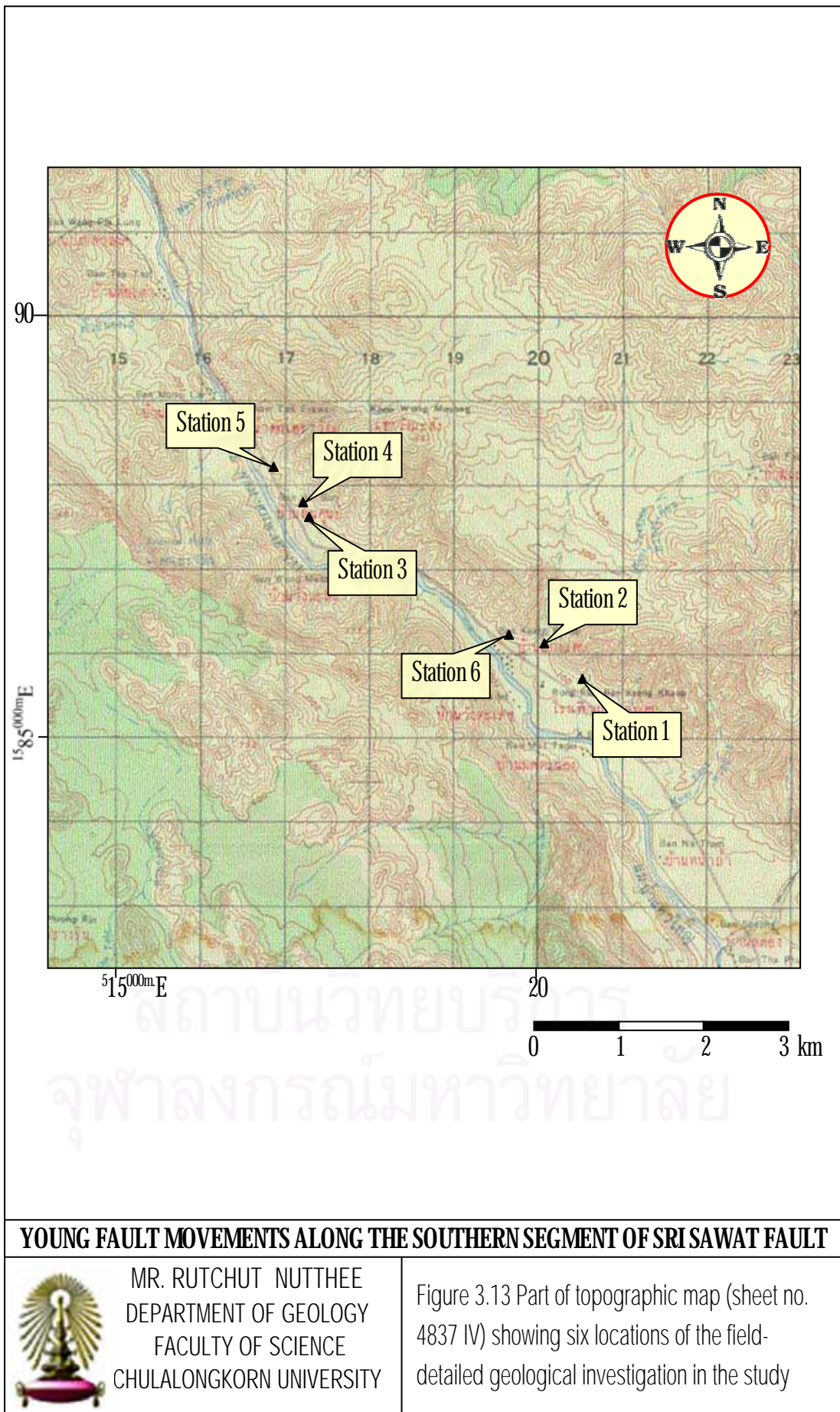




Figure 3.14 Part of station 1 showing talus deposit at the foreground of Khao Nom Nang, view looking N40°E.



Figure 3.15 Close-up view (of Fig. 3.14) showing coarse fragments with high angularity of talus deposit.

fault activity. Toward the toe of the slope (near the road), the deposit was partly cemented by calcareous substance, usually called as “*caliche*” (Figs. 3.16 and 3.17).

### 3.5.2 Station 2

<u>Map name</u>	Ban Kaeng Riang	<u>Map sheet</u>	4837 IV
<u>Location</u>	km-stone 42+400	<u>Grid reference</u>	052005 E 158615 N

According to remote sensing interpretation, offset stream and shutter ridge (Fig. 3.18) were found in this area. Offset stream indicates lateral fault movement and shear sense. It was obstructed by shutter ridge. This pattern consists with general lateral slip fault model of Vedder and Wallace (1970) (Fig. 3.19).

Surveying was used to see clearly view of fault movement and measure fault displacement. Offset stream shown 2 lines of fault displacement are 124 m in the upper line, and 54 m in the lower line (Fig. 3.20).

This station was covered by colluvial deposits (Fig. 3.21-3.24). The colluvium lie on the Triassic mudstone call as “Chong Kheap formation” (Bunopas, 1976). It is poorly sorted and mainly coarse gravel. Fragment consist of 40% pebble, 50% cobble and 5% granule, compose of quartzite, sandstone, mudstone and travertine. The composition of matrix consist of coarse sand to clay about 10%. Somewhere, colluvium was cemented by calcareous substance. Near the shutter ridge (Fig.3.20), travertine layer (fig 3.25) with vertical-wedge characteristics and slickensides penetrates into horizontal gravel bed of Quaternary age (Fig. 3.26). This suggests that the travertine is relatively younger than the gravel bed. The slickensides developed in travertine implied the fault activity occurring in Quaternary.



Figure 3.16 The Talus deposit right at the down-slope end of station1, view looking N45°E.



Figure 3.17 Close-up view of Fig. 3.16 showing calcareous cement in talus called as "Caliche"

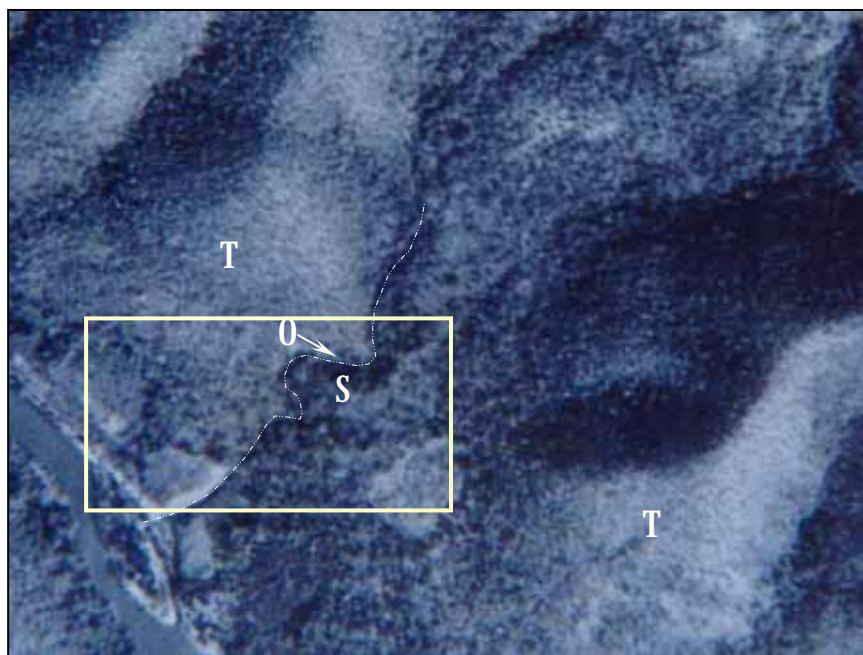


Figure 3.18 Enlarge aerial photograph of Fig. 3.7 showing a dextrally offset stream (O), a shutter ridge (S), and triangular facet (T) along the major fault. Box indicates detailed survey map in Fig.3.20.

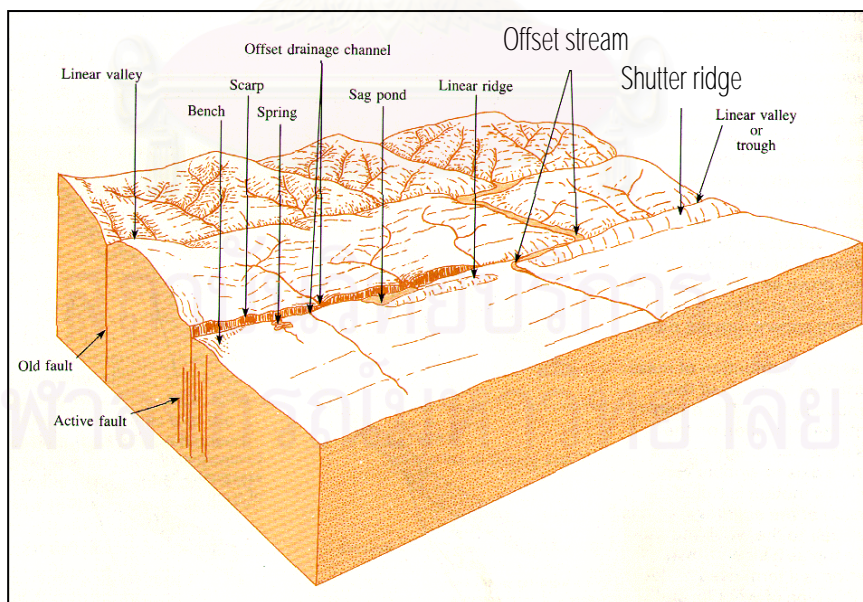


Figure 3.19 Assemblage of Landforms associated with strike slip faulting (after Vedder and Wallace, 1970)

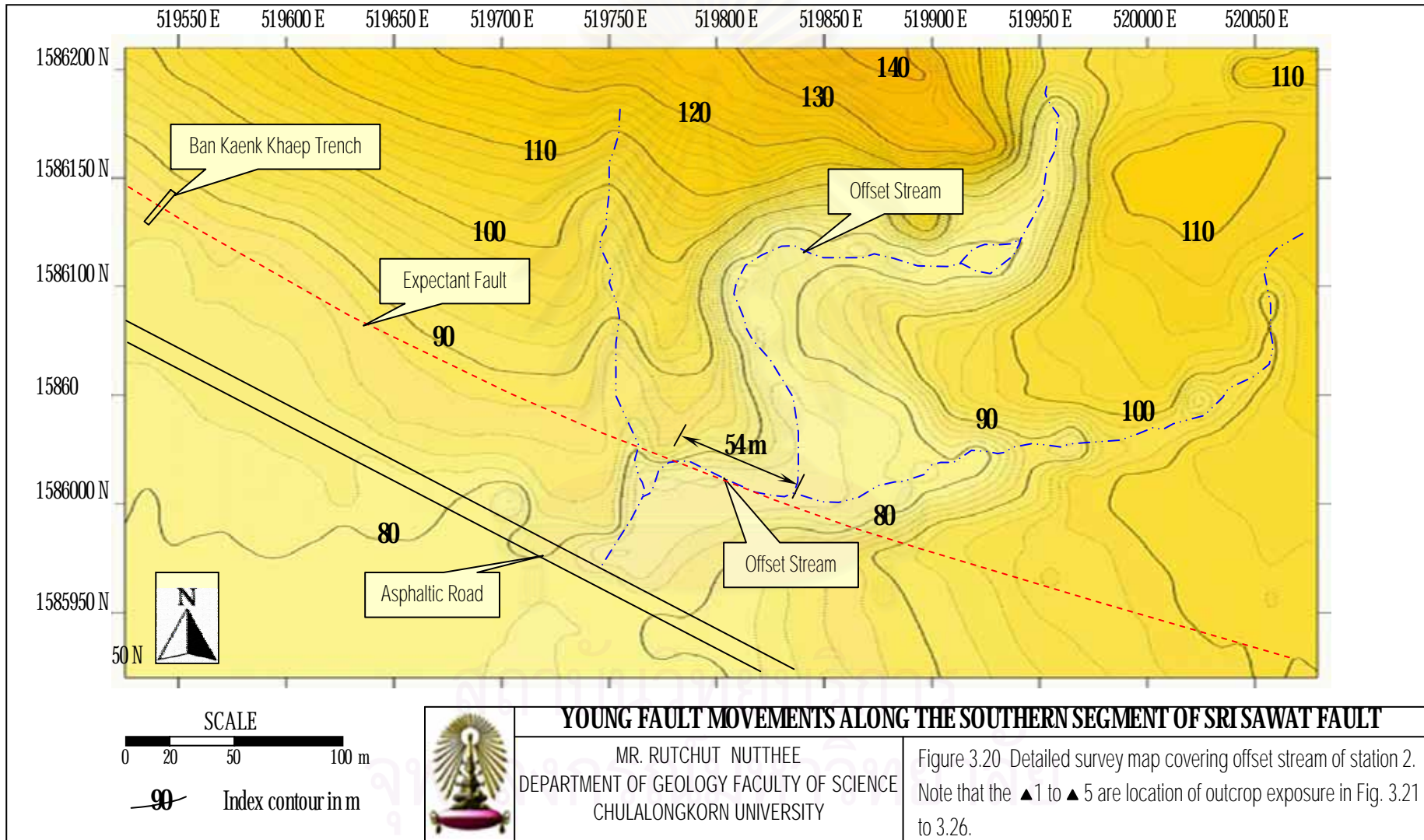




Figure 3.21 Exposure of colluvial deposit at ▲ 1 from Fig. 3.20, view looking S80°W.



Figure 3.22 Exposure of colluvial deposit at ▲ 2 from Fig. 3.20, view looking S5°E.



Figure 3.23 Exposure of colluvial deposit at ▲ 3 from Fig. 3.20, view looking N50°W.



Figure 3.24 Exposure of colluvial deposit at ▲ 4 from Fig. 3.20, view looking S10°E.





Figure 3.25 The travertine showing characteristic as a vertical wedge penetrating into horizontal gravel bed at ▲ 5 from Fig. 3.20, view looking S10°E.



Figure 3.26 A Horizontal gravel bed with somewhat graded bedding at the exposure at ▲ 5 from Fig. 3.20.

### 3.5.3 Station 3

Map name Ban Kaeng Riang      Map sheet 4837 IV  
Location km-stone 45+700      Grid reference 051725 E 158775 N

The outcrop in this station was exposed by village digging out the upper soil for home-construction. Two pit-walls are interested; the northwest wall (Fig. 3.28) shows clear 8 layers of colluvium, i.e., coarse grained layers interbedded fine grained layers, with sharp contacts. The other is the southeast wall located opposite to the northwest wall, no clear bedding difference from the opposite one. It contains poorly-sorted coarse gravel and is supported by a silty-clayey matrix with coarse gravel lenses.

In this study we apply two names for the NW and SE walls as Ban Pha Tawan trench I and II walls, respectively. The detailed study was described in section 4.4.

### 3.5.4 Station 4

Map name Ban Kaeng Riang      Map sheet 4837 IV  
Location km-stone 45+800      Grid reference 051715 E 158775 N

This outcrop was exposed by villagers like that of the station 3. It shows the young river gravel bed overlying the Triassic mudstone. Gravel bed is poorly sorted, and coarse gravel is supported by sity-clayey matrix. It was covered and graditional contacted by dark gray topsoil (A-horizon) and sharp contact with lower bedrock.

The contact between gravel beds and bedrocks shows an uplift nature of river gravel bed. The appearance of gravel wedge may indicate an effect of recent tectonic activity.

This site is about 200 m northeastward from station 3. It was defined as Ban Pha Tawan trench 2. The detailed description is shown in section 4.5.



Figure 3.27 Man-made exposure at Ban Pha Tawan showing sediment deposits on the northwest trench wall (Ban Pha Tawan I Trench), view looking N50°W.

สถาบันวิทยบริการ  
จุฬาลงกรณ์มหาวิทยาลัย

### 3.5.5 Station 5

Map name Ban Kaeng Riang      Map sheet      4837 IV

Location      km-stone 47+000      Grid reference      051665 E 158860 N

This outcrop is road-cut exposure. It shows lithology change by faulting. The fault cuts and shows sharp contact between Triassic mudstone on right hand and Cambrian quartzite on left (Fig. 3.26).

This fault may be main fault in this area, and lies in N60°W trending. Its appearance is 15 m long, dipping east 35°. Top surface shows fault scarp about 1 m high, indicate reverse faulting (Fig. 3.27).

### 3.5.6 Station 6

Map name Ban Kaeng Riang      Map sheet      4837 IV

Location      km-stone 48+800      Grid reference      0519604 E

This station was selected for trenching excavation due to its location is near the offset stream (Fig. 3.18), which is comparatively with fault displacement. Its location is on the young sediment deposit. Trench was excavated cross fault tract perpendicularly for detail studied of fault. This trench is defined as Ban Kaeng Khaep Trench (the detail in section 4.3).

สถาบันวิทยบริการ  
จุฬาลงกรณ์มหาวิทยาลัย



Figure 3.28 Road cut exposure showing a major fault whose plane is N60W strike and 35° dip at Ban Namtok Erawan, view looking N65°E.



Figure 3.29 Close –up view of Ban Namtok Erawan showing an offset of surface indicating to reverse fault.

## CHAPTER IV

### PALEOSEISMIC STUDY BY USING TRENCHING TECHNIQUES

#### 4.1 Location of Trenches

Three trench sites namely Ban Kaeng Khaep, Ban Pha Tawan I, and Ban Pha Tawan II (Fig. 4.1), were selected for detailed studies of fault and trench logging. Ban Kaeng Khaep Trench was excavated on young sediment deposit cross fault trace perpendicularly, near the offset stream (mentioned in sec. 3.5.6). Ban Pha Tawan I and II trenches are abandoned quarry excavated through Triassic clastics by villagers for road/building construction. Although two trenches at Ban Pha Tawan did not cut cross fault trace, they show colluvial deposit closely related to fault movement.

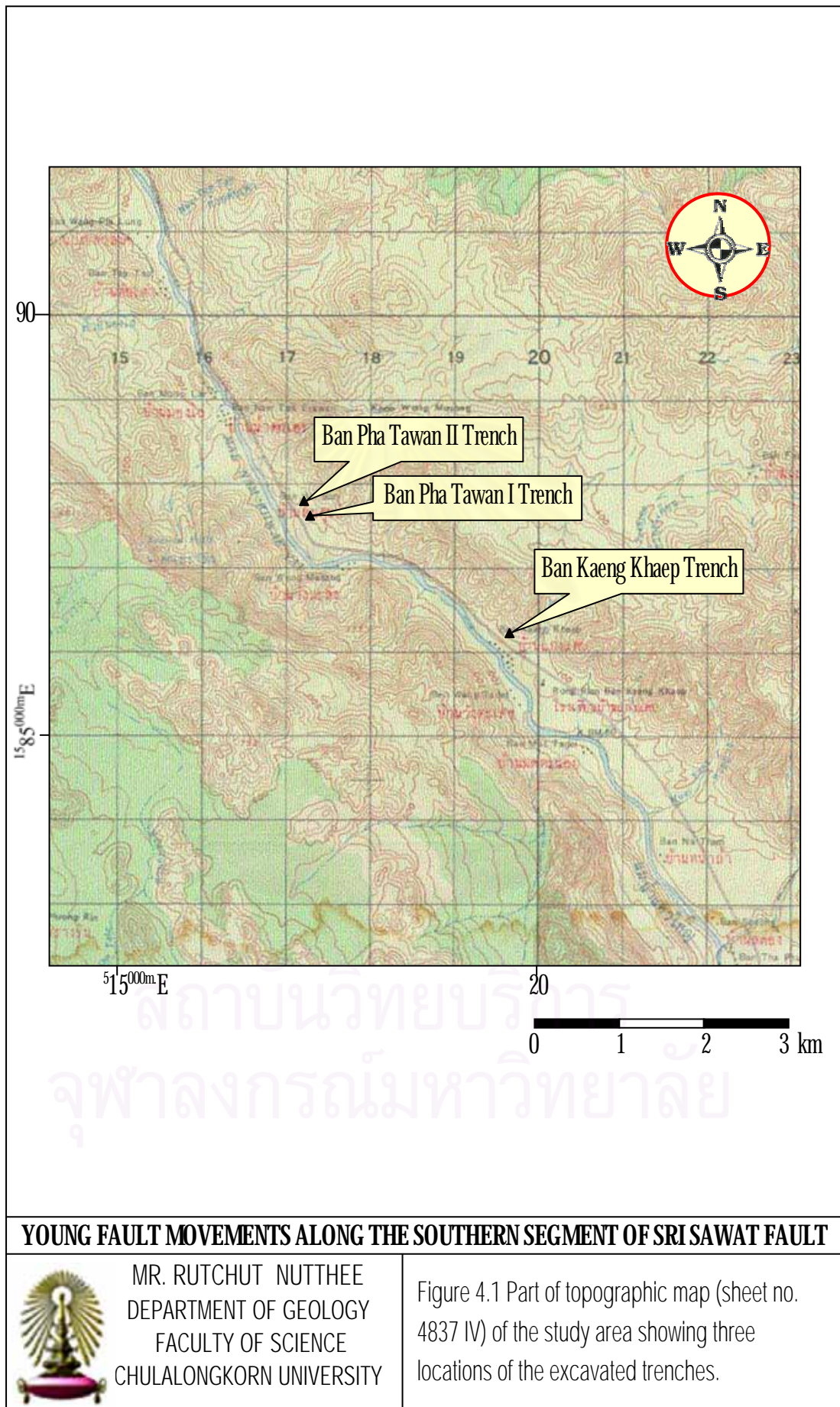
The techniques, such as trench wall cleaning, curing and brushing, were used to locate and enhance stratigraphy, faults, fractures, and features related faulting in trench. Each trench was gridded with 50 cm square grids and logged on graph papers for detail. Detailed logging shows a geologic interpretation of the structural and stratigraphic relations exposed in the trench. After logging, representative samples were collected for age determination of faulting.

#### 4.2 Sample Collection for Thermoluminescence (TL-) Dating

In this study, all of the samples, which were determined age, are sediments regarded as colluvium. In this case, the samples must be much stringent to precautions against exposure to light. Procedure of sample collection in this study follows that described by Aitken (1985), shown below.

Quantity. For thermoluminescence measurement, two samples for each level of the same unit are desirable, preferably not close together; each was collected between ½ to 1 kg for radioactive analysis (e.g., a lump about 10 cm across from each level). The radioactive analysis samples does not need to kept dark, nor does it to be sealed for water content measurement

Context. Most samples were taken from the *middle part* of a thick (i.e., ½ m or more) layer. However, in the case of thin layers it can be checked by radioactive



measurements whether neighboring layers have differing radioactivities, and to some extent allowance can be made by calculation. Of course, if the sample is within 0.2 m of the ground surface, the situation is not good and the accuracy attainable is severely limited (Aitken, 1985).

Treatment. *It is absolutely vital that there be no exposure to direct sunlight;* exposure to daylight or fluorescent light was minimal (i.e., not more than about 10 min). If there is a need to examine the samples, this should be done with a bulb light or with a torch. Exposure to sunlight is likely to make the TL data erroneously too recent (Aitken, 1985).

Therefore:

1. Scrape off at least 1 cm of the already exposed surface; this is done in order to get deeper than where the light has penetrated. Shade from direct sunlight. If the surface is too hard for scraping, make a mark on the exposed face.

2. Still shading, collect the sample in an opaque or semi-opaque container; straightway put the container in a black plastic bag or other light-tight container.

3. Because it is necessary to get information about water content, the container used should be moisture-tight (e.g., tins tightly sealed with tape, or two tightly sealed thin plastic bags-as in the case of pottery). Sometimes measurement of the water content can be made by the site excavator on a separate comparable sample; this is highly preferable and, of course, the need for watertight sealing is then eliminated.

The water content can be calculated by Eq. 4.1

$$\text{Wt.} = \frac{\text{Ww} - \text{Wd}}{\text{Wd}} \times 100 \dots \dots \dots (4.1)$$

where Wt. = Water content (%)

Ww = Weight of wet soil (g)

Wd = Weight of dry soil (g)



### 4.3 Ban Kaeng Khaep Trench

Kang Khaep trench was selected and excavated for stratigraphic log and detailed study of the southern segment of the Sri Sawat fault. Trench location is near the offset stream, at grid reference 1586148N 05196604E on 1:50,000 sheet 4837IV (Ban Kaeng Riang) of the topographic map. It was long about 20 m, 2 m wide, and as deep as 4 m, covers and cross perpendicular to the fault trace (Fig. 4.2).

#### 4.3.1 Mapping Units and Description

The mappable units exposed in a trench (Figs. 4.3 and 4.4) was divided into 8 units (as show below) and the summary of lithology is shown on Table 4.1.

##### Unit 1 Topsoil or disturbed soil

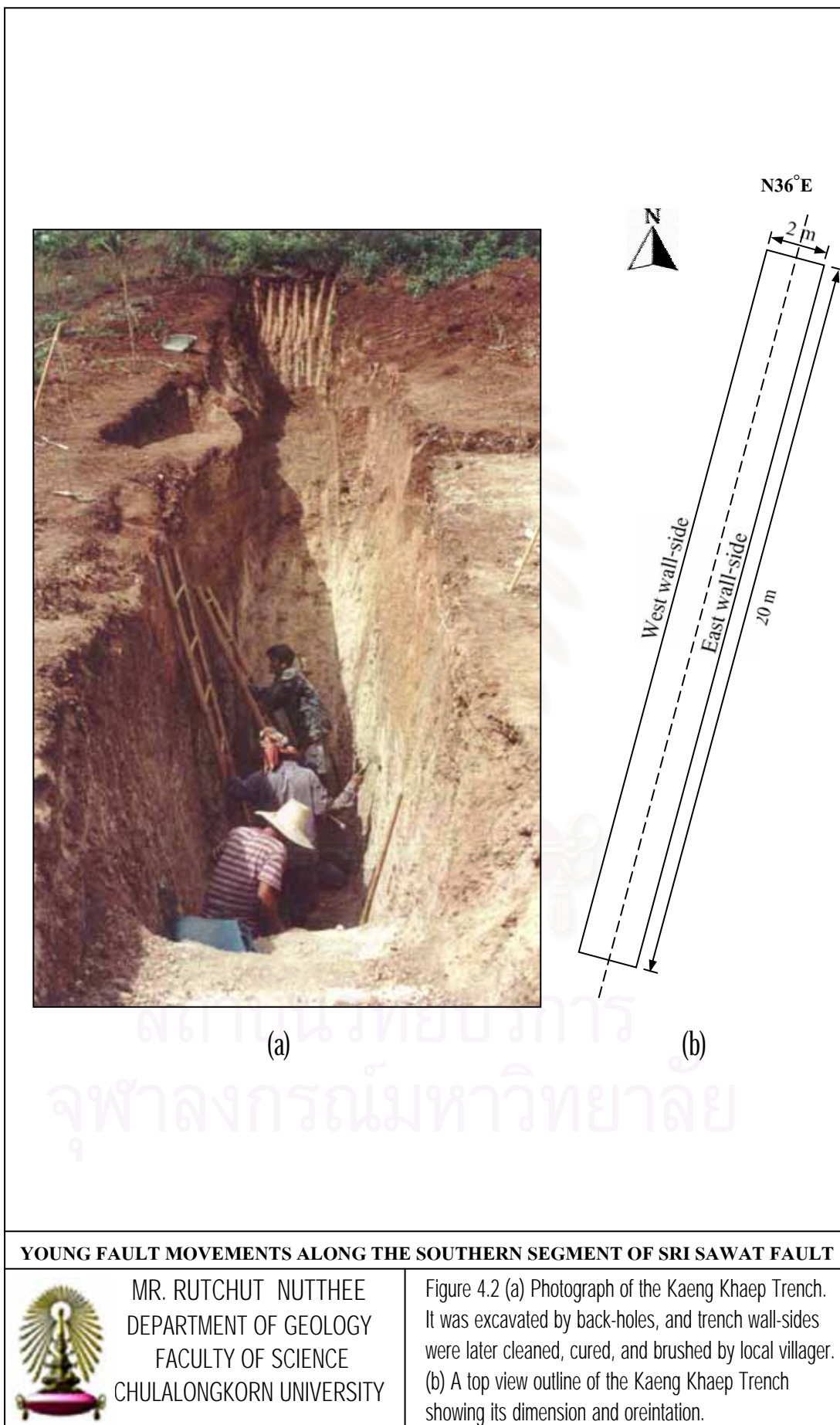
This unit is the topsoil layer with thickness varying from 6 to 40 cm and averaging 20 cm. It is poorly sorted and mainly gravels about 70%, yellowish brown. Rock fragments are sparsely distributed and mainly are quartzite and mudstone, both with high angularity. Due to the unit lies at the topmost, it is easily disturbed by human and agricultural activities.

##### Unit 2 Chocolate brown colluvium

This unit is the colluvium composed mainly of coarse gravel about 85% and sand (plus silt and minor) about 15%. The colluvium is chocolate brown in color, with thickness varying from 5 to 55 cm and averaging 40 cm. Most fragments are angular quartzite and feldspar-rich sandstone (av. 1-5 cm in diameter). The fragments are supported by brown silty-clayey matrix. This unit is interpreted as the youngest colluvial layer in the trench.

##### Unit 3 Red Colluvium

This colluvium is different from the overlying chocolate brown colluvium (Unit 2) by lithology and color. It is poorly sorted and mainly comprises coarse to medium gravels. Fragments include quartzite and feldspar-rich sandstone with high angularity and 1-3 cm diameter. The matrix consists of mostly fine sand and silt, and is orangish red. The shape of the red colluvium varies considerably from 5 to 16 cm. Such



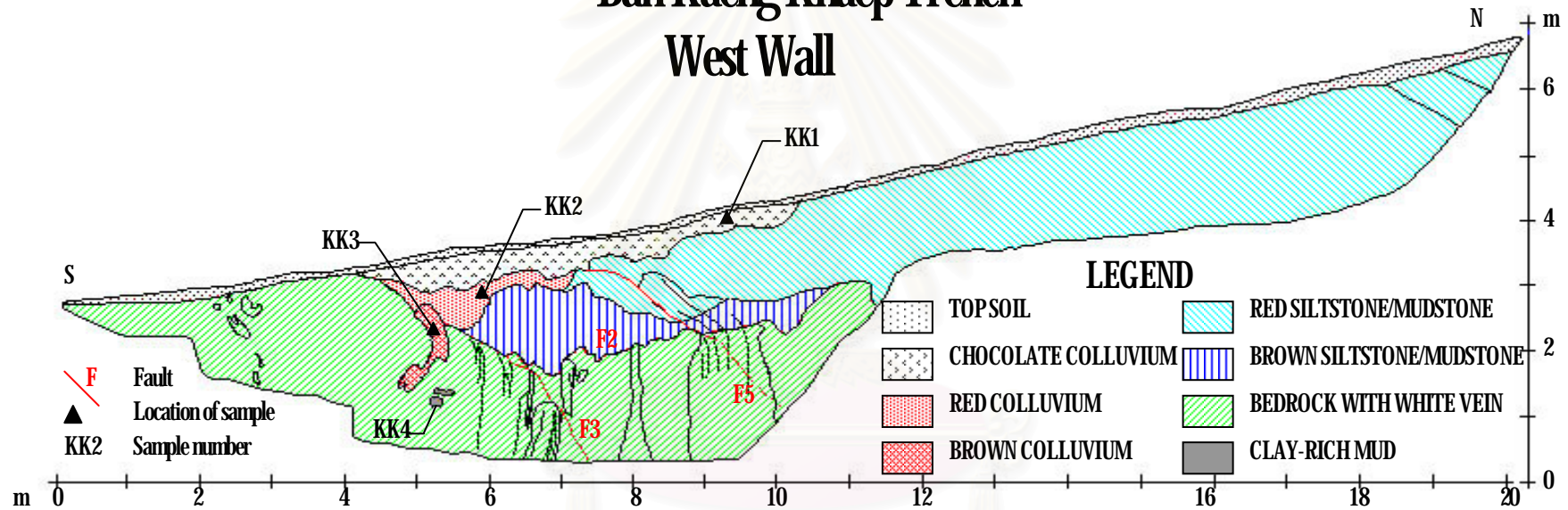
**YOUNG FAULT MOVEMENTS ALONG THE SOUTHERN SEGMENT OF SRI SAWAT FAULT**



MR. RUTCHUT NUTTHEE  
DEPARTMENT OF GEOLOGY  
FACULTY OF SCIENCE  
CHULALONGKORN UNIVERSITY

Figure 4.2 (a) Photograph of the Kaeng Khaep Trench. It was excavated by back-holes, and trench wall-sides were later cleaned, cured, and brushed by local villager. (b) A top view outline of the Kaeng Khaep Trench showing its dimension and orientation.

# Ban Kaeng Khaep Trench West Wall



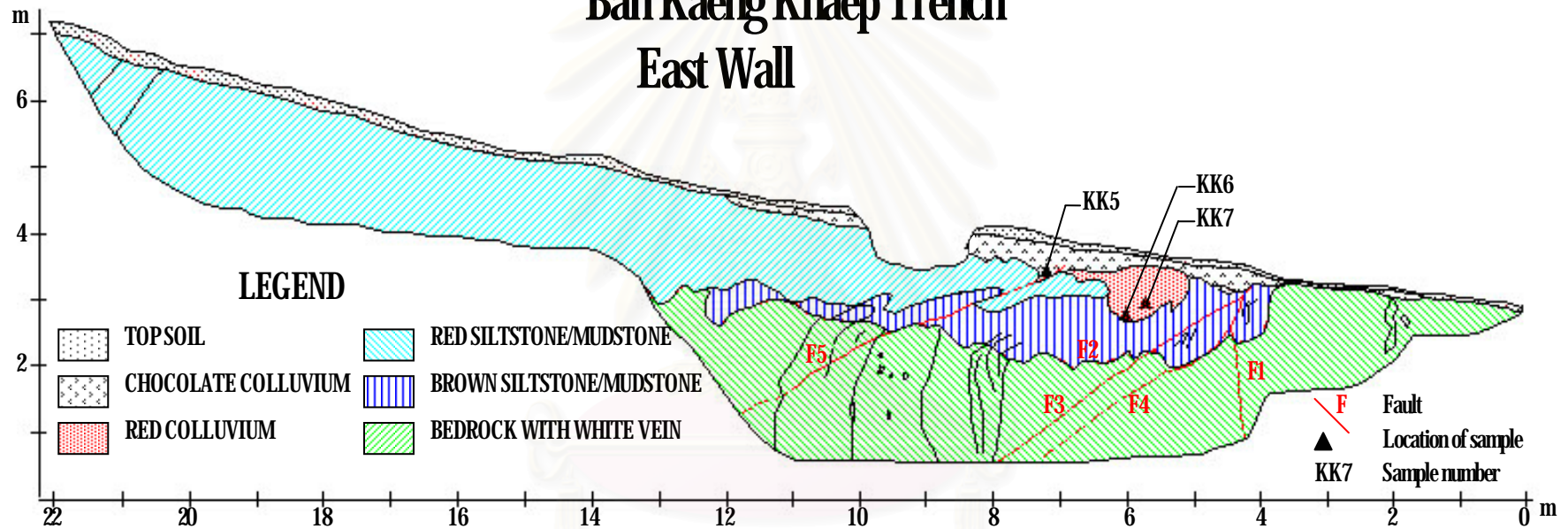
## YOUNG FAULTING ALONG THE SOUTHERN SEGMENT OF SRI SAWAT FAULT



MR. RUTCHUT NUTHEE  
DEPARTMENT OF GEOLOGY FACULTY OF SCIENCE  
CHULALONGKORN UNIVERSITY

Figure 4.3 Trench log of the west wall in Ban Kaeng Khaep Trench, showing principle stratigraphy and sample location for TL-dating.

## Ban Kaeng Khaep Trench East Wall



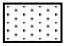
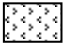




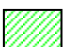

### YOUNG FAULTING ALONG THE SOUTHERN SEGMENT OF SRI SAWAT FAULT



MR. RUTCHUT NUTTHEE  
DEPARTMENT OF GEOLOGY FACULTY OF SCIENCE  
CHULALONGKORN UNIVERSITY

Figure 4.4 Trench log of the east wall in Ban Kaeng Khaep Trench, showing principle stratigraphy and sample location for TL-dating.

Table 4.1 Summary of the description of mapped under for both side wall of the Kaeng Khaep Trench

Unit Legend	Description	Thickness (cm.)	
		Range	Average
 (1) Disturbed soil	Top soil; dark yellowish brown, poorly sorted, gravel containing up to 70% quartzite and mudstone, angularity	6-40	20
 (2) Colluvium unit	Chocolate colluvium; chocolate brown, poorly sorted, gravel containing up to 85% quartzite and feldspar-rich sandstone, angularity	0-55	40
	 (3) Red colluvium; orangish red, poorly sorted, gravel containing up to 80% quartzite and feldspar-rich sandstone, angularity	0-60	30
	 (4) Brown colluvium; brown, poorly sorted, gravel containing up to 65% quartzite and mudstone, Subroundness, irregular shape	20-50 <sup>*1</sup>	30 <sup>*1</sup>
 (5) Displaced bedrock unit	Red interbedded siltstone/mudstone, orangish red, without white vein, strongly weathered	0-201	150
	 (6) Brown interbedded siltstone/mudstone yellowish, brown, without white veins, moderately weathered	15-130	70
 (7) Bed rock unit	Bed rock with white veins; brown to dark brown and white, interbeded siltstone/ mudstone, white veins and veinlets effervescent with dilute HCl	136-206 cm	160 cm
	 (8) Black mud; dark brown to black, lens-shapes, clay-rich	0-25 Lenses and ball	20 <sup>*2</sup>

\*1 thickness measured in horizontal level

\*2 diameter (maximum thickness)

the morphology together with a sharp contact with the underlying unit lead us to regard; the red colluvium as a colluvium wedge.

#### Unit 4 Brown Colluvium

This unit is poorly sorted and mainly coarse sand to gravel. Fragment are essentially very weathered, yellowish brown, subrounded mudstone with diameter ranging from 0.1-1.0 cm. The matrix consists of silt and clay.

Due to the similarity in texture and lithology to the underlying unit, it is possibly derived from the bedrock by residual weathering. This brown layer unit is regarded as the oldest colluvial unit in the trench.

#### Unit 5 Red interbedded siltstone/mudstone

This unit is strongly weathered mudstone interbedded with siltstone. It is the uppermost bedrock with the average thickness of 150 cm, and shows orangish red to red color probably from oxidation process. The unit regarded as the youngest bed rock unit.

#### Unit 6 Brown interbedded siltstone/mudstone

Beneath the Unit 5 is the brown mudstone interbedded with siltstone. The unit varies in thickness from 15 to 130 cm and averaging about 70 cm. Its textures and lithologies are similar to those of the Unit 5. The unit is characterized by brown to deep brown colors due to less weathering process.

#### Unit 7 Bedrock with white veins/veinlets

This unit is represented by brown to dark brown mudstone interbedded with yellowish brown siltstone layer which bears almost similar textures and mineral constituents to the two overlying layers. The thickness of the Unit 7 expose varies from 136 to 206 cm with the average of 160 cm. However, the most striking feature is the presence of abundant veins. This veins are mainly calcite showing effervescent with weak HCl acid (Figs. 4.5 and 4.6). These veins and veinlets disappear in the overlying Units 5 and 6. These calcite veins/veinlets vary in thickness about 0.5 to 12 cm. It is



Figure 4.5 White veins of calcite cut into weathered Triassic mudstone bedrocks, west wall- side of the Ban Kaeng Kheap Trench.



Figure 4.6 Very weathered mudstone bedrocks of unit 7, west wall- side of the Ban Kaeng Kheap Trench.

considered that Unit 7 is separated by the overlying Unit 6, either by a fault contact or erosional surface (see details in section 4.3.2).

### Unit 8 Clay-rich mud

The Unit 8 is located within the Unit 7. The Unit 8 is only observed at the west side of trenching wall, and is characterized by very fine-grained, black sediments with somewhat high plasticity. Its size varies from silt to clay, the latter is more common. Its shape of this unit is almost ovoid to round, its diameter range from 25 cm for the longer axis to cm for shorter axis. The unit is interpreted to be an excavation due to animals as their dwellings.

## 4.3.2 Fault Description

In the Kaeng Khaep Trench, 5 faults are recognized, as shown below.

F1. This fault was found in eastern trenching walls (Fig. 4.4). The fault cut bedrocks with white veins (Unit 7) and its attitude dip almost vertical on the eastern wall-side (Fig. 4.7). It is regarded as the oldest fault and was cut by the F2 fault. The F1 fault shows the movement in the reverse sense.

F2. This fault was inferred in both trenching walls (Figs. 4.3 and 4.4) in a contact zone between brown interbedded siltstone/mudstone layer (Unit 6) and bedrocks with white veins (Unit 7). Abundant veins and veinlets are common in Unit 7, but they disappear in Unit 6. So the contact zone was interpreted into two ways;

(1) Erosional surface – this type common occurred in the contact zone. Nevertheless, in this case, two rock unit below (Unit 7) and above (Unit 6) the contact zone are the same lithology and show no difference to one another. Only the presence of calcite veins/veinlets in Unit 7 is conspicuous. Moreover, in the case of erosional surface, the lower contact zone of mudstone Unit 7 should be more weathered because of prevailing weathering process. Therefore the contact zone by erosional surface is less supported.

(2) Fault contact - this type is also common occurred in the contact zone. The abrupt disappearance of white veins/veinlets above the contact zone provide good support for the fault contact. The other striking feature is grooves cause by movements





Figure 4.7 The Triassic mudstone/siltstone of unit 7 was cut by reverse sense of fault (F1) movement.

สถาบันวิทยบริการ  
จุฬาลงกรณ์มหาวิทยาลัย



Figure 4.8 East wall-side of Kaeng Khaep Trench showing the sharp contact between the Unit 6 and the Unit 7. These two unit were separated by a major fault (F2). This fault is a reverse fault with low-angle dipping ( $45^\circ$  to vertical). Note that there is a sharp contact of Triassic mudstone /siltstone of Unit 6

of the overlying Unit 6. However, the evidences that indicate fault contact are not clearly. So, the other trenches should be dug to prove this fault in three dimensions.

F3. This fault was observed in both trenching walls. It cut bedrocks with white veins (Unit 7) (Figs. 4.9 and 4.10) and the chocolate brown colluvium (Unit 2). It strikes in and dips about  $45^\circ$ .

F4. This fault was observed only in the eastern wall-side (Fig. 4.4). This fault dips about  $45^\circ$  to and cuts in bedrocks with white veins of Unit 7.

F5. This fault is regarded as the youngest fault and was observed in both of two trenching walls. It cuts in the weathered fine clastic bedrocks with white veins (Unit7). It continues to cut the chocolate colluvium (Unit 2) (Fig. 4.11). Its dip is about  $45^\circ$ . The fault has a reverse sense of movement.

### 4.3.3 Location of Collected Samples

Seven samples were collected in the Kaeng Khaep Trench for age determination by thermoluminescence dating. All of them were collected in the colluvium or sediment units. Four samples were collected in the western wall of trench (Fig. 4.3), while three samples were collected in the eastern wall (Fig. 4.4).

Sample nos. KK1 and KK5 were collected in the chocolate colluvium (Unit 2) on western and eastern wall, respectively.

Sample nos. KK2, KK6, and KK4 were collected in the red colluvium (Unit 3), the first one were collected on western wall and the rests were collected on eastern wall.

Sample no. KK3 and KK4 were collected in the brown sediment (Unit 4) on western wall.

## 4.4 Ban Pha Tawan I Trench

The Ban Pha Tawan I Trench was dug by local villagers for road and building construction. Its location is about 300 m southwest from toe slopes of a nearest triangular facet along southern segment of Sri Sawat Fault, at grid reference 15587752N 0517257E (Fig. 4.1) on 1 : 50,000 sheet 4837 IV (Ban Kaeng Riang) of topographic map.

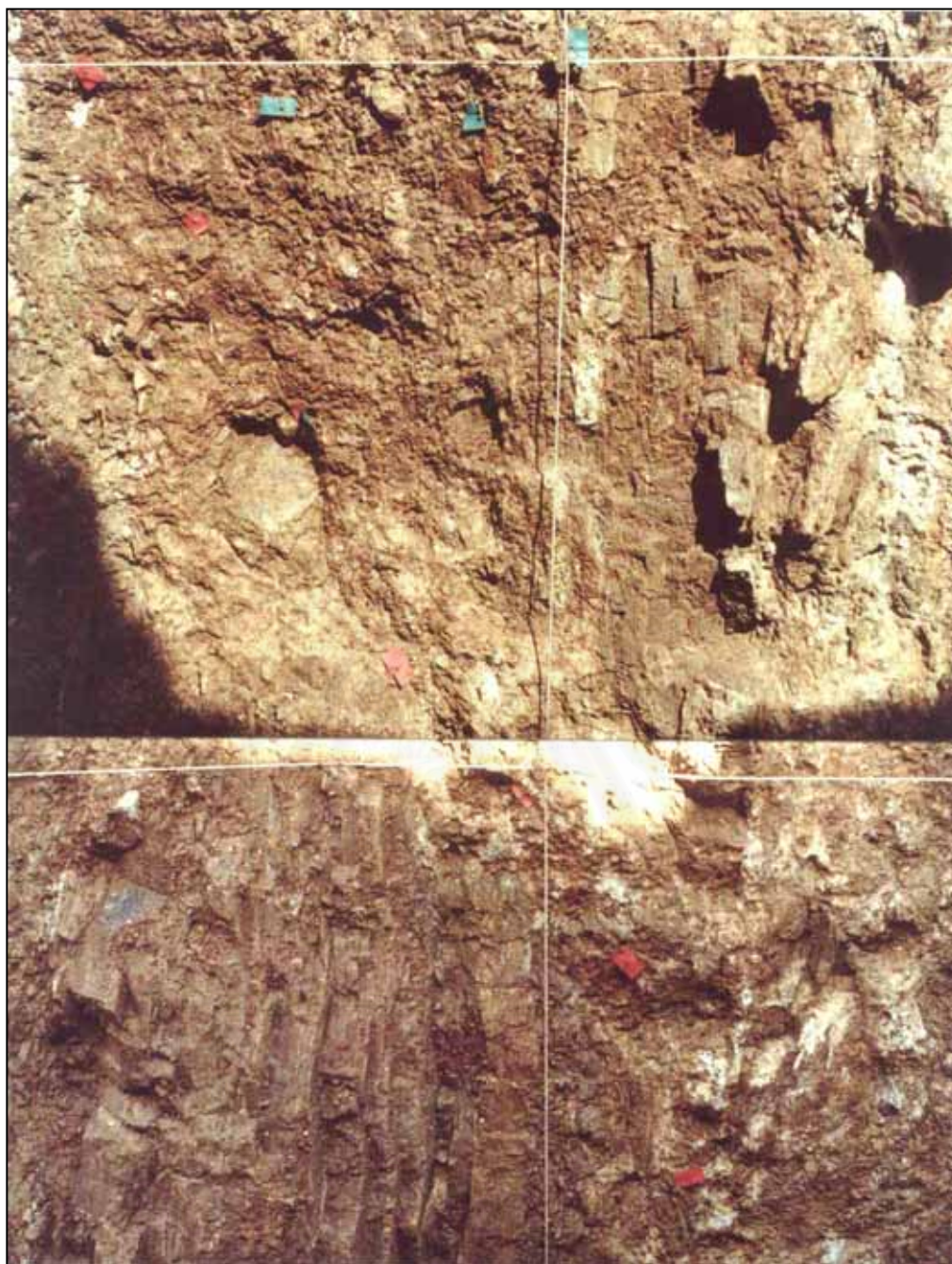


Figure 4.9 The F3 reverse fault cutting into almost vertical beds of weathered Triassic siltstone bedrock of the Unit 7 on the western side wall of the Ban Kaeng Khaep Trench



Figure 4.10 Folded beds of Triassic mudstone of the Unit 6 cut by the F8 fault, west-wall side of the Pha Tawan Trench.



Figure 4.11 The chocolate colluvium in east-wall side of the Pha Tawan Trench, was cut by the F3.

Two trench walls were northwest and southeast walls. The northwest trench wall is about 8 m long and 4 m height. There are 8 easily recognizable horizontal sediment layers of colluvium with coarse and fine-grained interbeds. These colluvium layers are considered to represent times of fault-related earthquakes tranquility and these deposited near foots of tectonically active slope (Fig. 4.12). The deposit adjacent to fault scarp is commonly divided into *debris and wash facies* (Wallace, 1977; Nelson, 1987). The coarse-grained colluviums are poorly sorted and compose chiefly of boulder- to pebble-size clasts of mainly high-angularity quartzite and feldspar-rich sandstone. These two colluviums are rapidly deposited primarily by gravity-controlled process. Blocks and clasts can be released from the exposed fault free face during activity period by falling and slumping (see Fig 4.13). These were called "*debris facies*". The fine-grained layer comprises largely medium - fine sand to clay, deposited relatively slowly by surface wash processes, called "*wash facies*". They are inferred to have occurred during the periods of slope stability between faulting events.

In this area, the interbedded sequence of coarse- and fine-grained sediments which displayed almost similar thickness of layer shows cycles of tectonic activity controlling sequence of fault movements. On the other hand, the gravity deposits such as those occurring in caves and at cliffs may give rise to structureless beds of poorly-sorted fragments. However the repeated sequences as those occurred by earthquake/tectonic activities are rare.

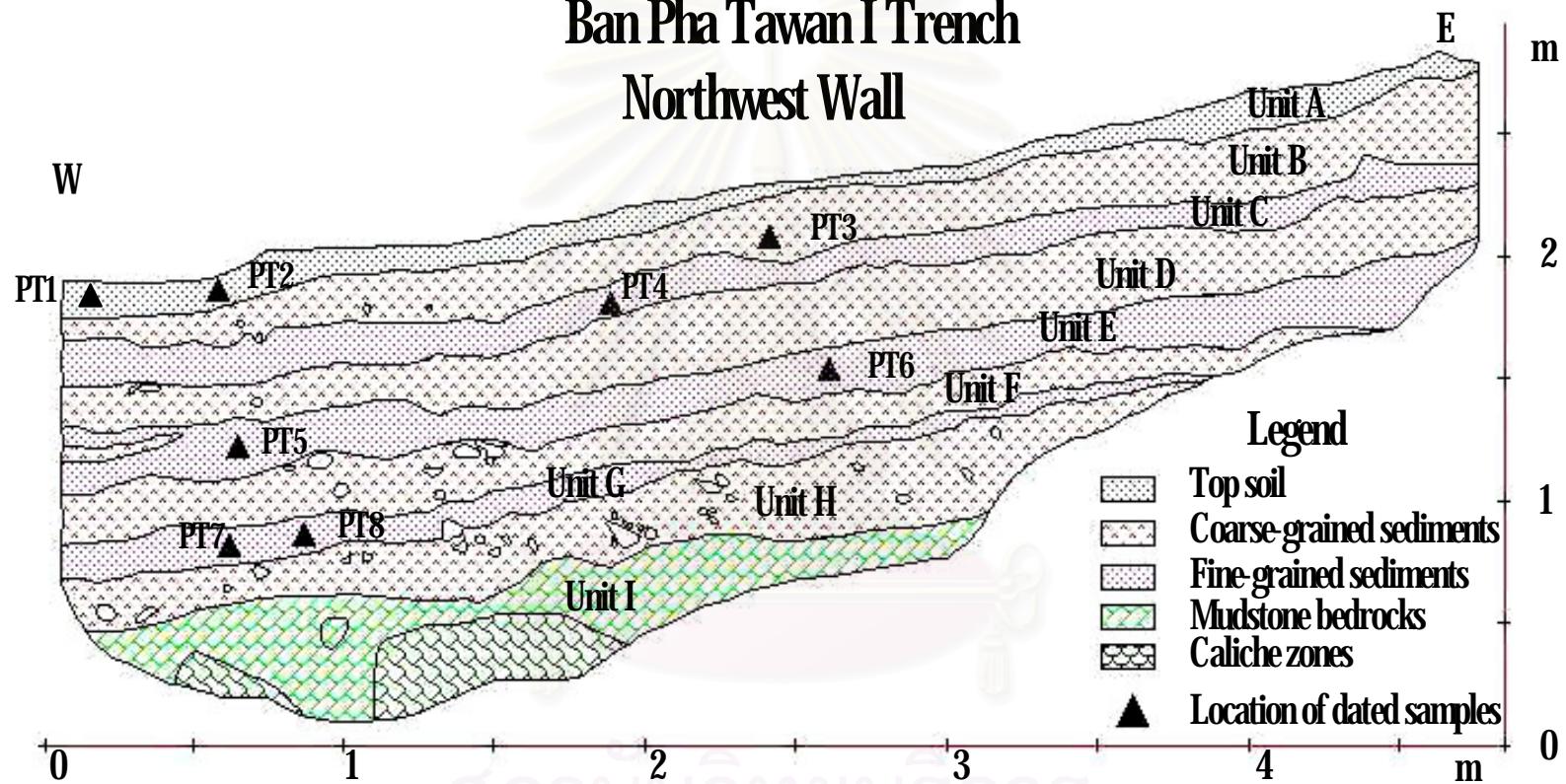
It is therefore interpreted that eight young unconsolidated sediment layers of alternated coarse- (debris) and fine- (wash) facies may represent 4 faulting-triggering earthquake events.

The southeast wall-side is opposite about 15 m from the northwest wall side. The southeast wall-side is about 10 m long and 3 m height. It shows not clear bedding as compared to other wall-side.



Figure 4.12 The northeast wall side of the Ban Pha Tawan I Trench showing alternating layers of underconsolidated coarse- and fine-grained sediments, interpreted as debris- and wash-facies, respectively. Note that the white-line square grid is about 0.5m long, and colored flags indicate contact boundary between two adjacent units.

## Ban Pha Tawan I Trench Northwest Wall



### YOUNG FAULTING ALONG THE SOUTHERN SEGMENT OF SRI SAWAT FAULT



MR. RUTCHUT NUTHEE  
DEPARTMENT OF GEOLOGY FACULTY OF SCIENCE  
CHULALONGKORN UNIVERSITY

Figure 4.13 Trench-log sketch map of the northwest wall in Ban Pha Tawan I Trench, showing principle stratigraphy and sample location for TL-dating.



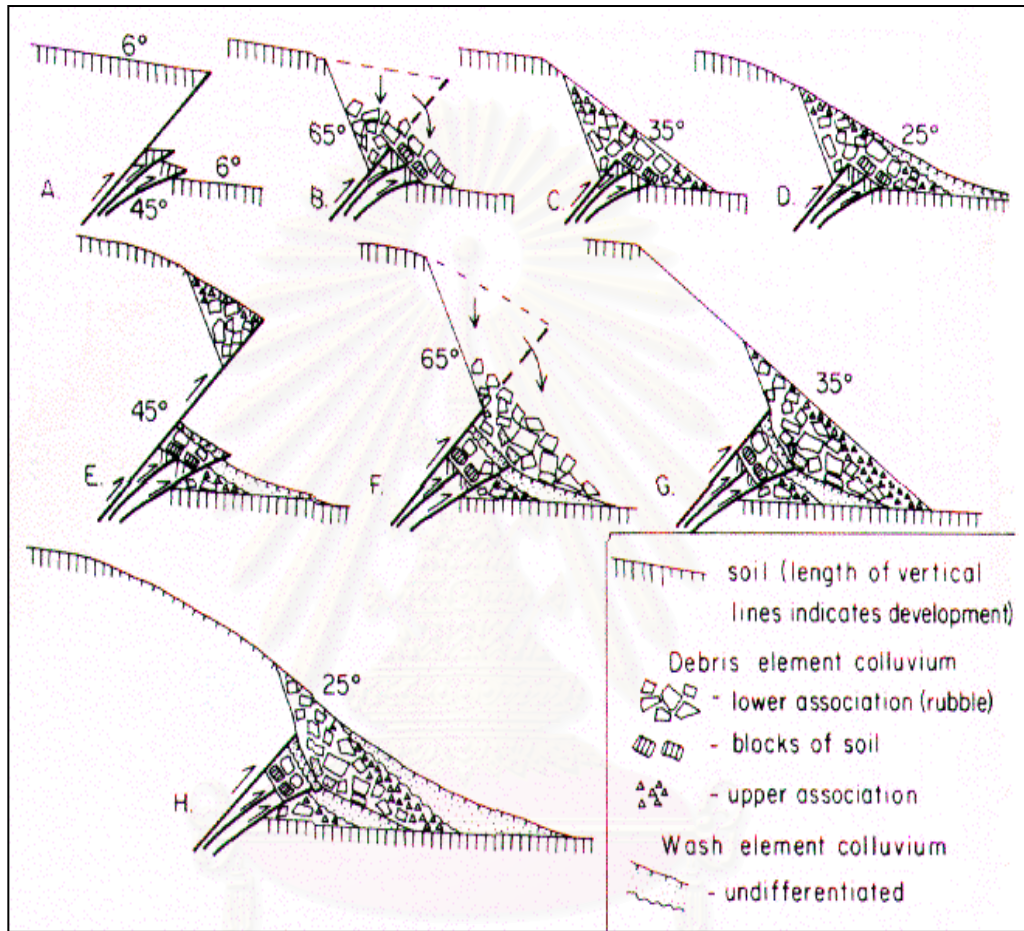


Figure 4.14 Schematic diagrams showing the deposition of colluvium from a two-event reverse fault scarp (McCalpin, 21996)

จุฬาลงกรณ์มหาวิทยาลัย

## 4.4.1 Mapping Unit and Description

### 4.4.1.1 Northwest Trench Wall

The mappable units exposed in the northwest wall of the Ban Pha Tawan I Trench (Fig 4.13) can be defined into 9 units as shown below.

**Unit A** (topsoil). This unit is the top sediment layer in this wall. It is well-sorted, mainly fine sand to clay, dark brownish grey, and 15 to 20 cm thick. It is loosely compacted and has rather high moisture and organic matter.

**Unit B.** This unit is coarse-grained brownish red colluvium with thickness of 30-40 cm. It is poorly sorted and comprises mainly coarse to medium gravels about 70%. Gravels are mostly quartzite and vary in diameter from 0.5 to 3 cm. The Unit B shows a sharp contact with overlying and underlying layers.

**Unit C.** This unit is fine-grained brownish red colluvium with thickness 15-25 cm. It is moderately sorted and composed of mainly fine sand to clay. Clasts contain fine gravels of quartzite and weathered feldspar-rich sandstone is about 40% and 60% of matrix are consist mostly of medium sand of silt. Clast varies from 0.5 to 1 cm in diameter and have high angularity.

**Unit D.** This unit is 30-50 cm thick, coarse-grained brownish red colluvium. It is poorly sorted and mainly contains coarse gravels about 80% (quartzite and weathered feldspar-rich sandstone). Clasts are 1-5 cm in diameter, and show high angularity. The matrix composes of silt and clay.

**Unit E.** This unit is 25-30 cm thick, fine-grained brownish red colluvium. The Unit E is moderately sorted and comprises mainly silt to clay. Clasts consist mainly of fine gravel about 20% (of quartzite and weathered feldspar-rich sandstone). Clasts range from 0.5 to 1 cm in diameter and have high angularity.

**Unit F.** This unit is 25-30 cm thick, coarse-grained brown colluvium. The Unit F is poorly sorted and consist of coarse gravels about 85% (quartzite and weathered feldspar-rich sandstone). The clasts are 3-7 cm in diameter and possess high angularity. The matrix is composed essentially of silt and clay.

**Unit G.** This unit represents the older unconsolidated sediment layer, and is 10-25 cm thick, fine-grained brownish red colluvium. It is moderately sorted and

comprise mainly silt to clay. Clasts are mainly fine gravels about 40% (quartzite and weathered feldspar rich sandstone). Clasts is about 0.5-1 cm in diameter and has high angularity.

**Unit H.** This unit is 20-50 cm thick, coarse-grained brown colluvium. The Unit H is poorly sorted and consists mainly of coarse gravels about 85%. Gravels are mainly quartzite and weathered feldspar-rich sandstone. The clasts are about 5-8 cm in diameter and have high angularity. The matrix is composed mainly of silt and clay.

**Unit I.** This unit is a bedrock. It is yellow mudstone with moderately to highly weathered process. Some parts were cemented by carbonate substance called as “caliche”.

The close-up photograph shows lithology and stratigraphy of sediment units is shown in Fig. 4.15.

#### 4.4.1.2 Southeast Trench Wall

The southeast trench wall is about 10 m long, and 3 m height. Sediments deposited in this area are principally brownish red colluvium (Fig. 4.16). The colluvium show not clear bedding differences to the northwest trench wall (Fig 4.17). The colluvium is poorly sorted and comprises mainly coarse gravels, and about 50% of clasts are quartzite and feldspar rich sandstone, and are 1-7 cm in diameter with high angularity. The matrix is composed of loosely compacted red clay and silt. The reverse graded beds in few units (Fig. 4.17) may represent debris flow deposits which are herein considered to have formed by down slope rapid mass movement by surface to have water during earthquake events.

#### 4.4.2 Location of Collected Samples

Eleven samples were collected from Ban Pha Tawan I Trench for age determination by thermoluminescence dating. All of them were collected in colluvial unit. The 9 samples were collected in northwest wall of trench (Fig. 4.13), while 2 samples were collected in southeast wall (Fig. 4.16).

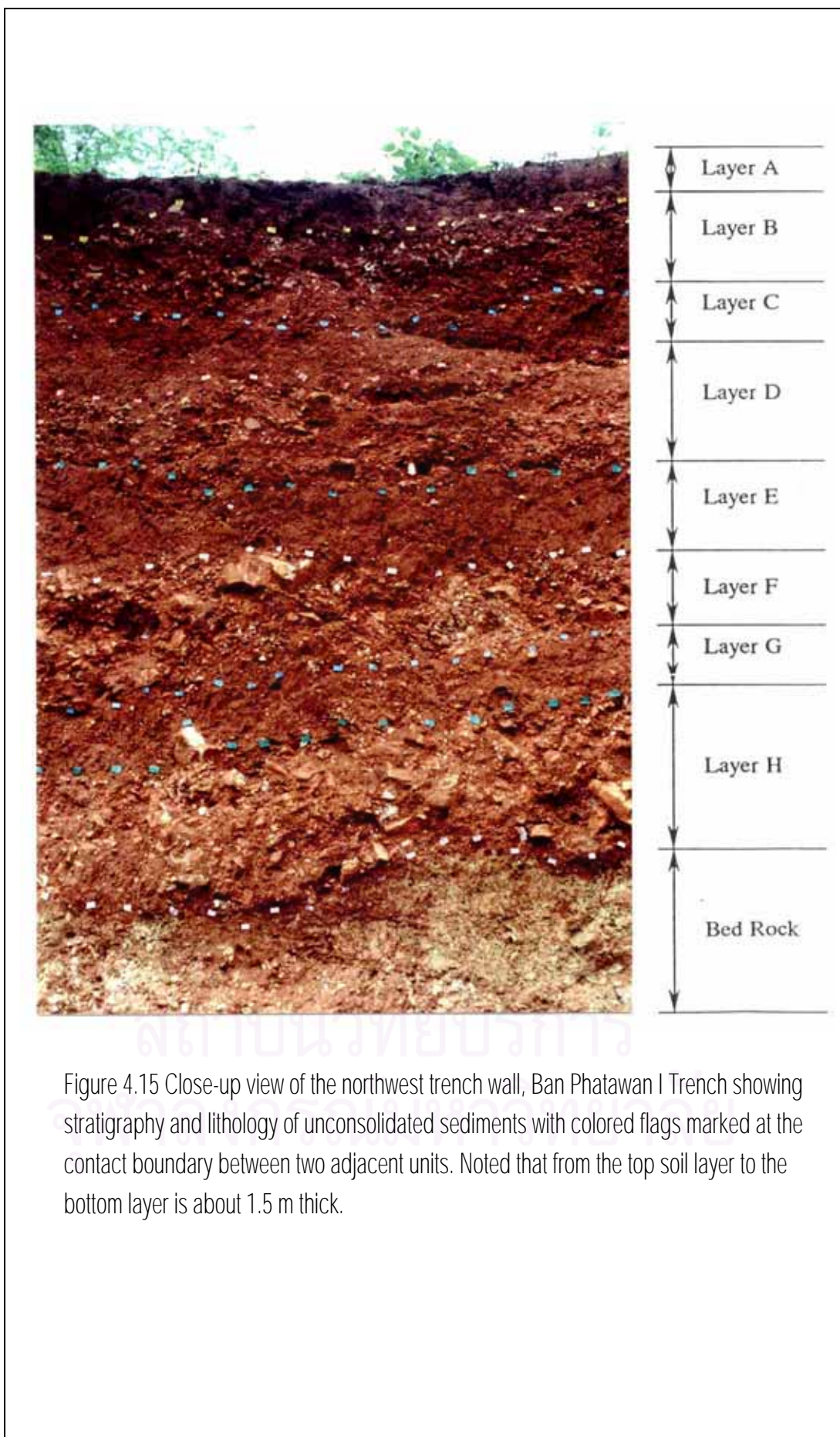


Figure 4.15 Close-up view of the northwest trench wall, Ban Phatawan I Trench showing stratigraphy and lithology of unconsolidated sediments with colored flags marked at the contact boundary between two adjacent units. Noted that from the top soil layer to the bottom layer is about 1.5 m thick.



Figure 4.16 Stratigraphy of young, unconsolidated sediment deposits on the southeast trenching wall in Ban Pha Tawan II Trench , Showing location of samples for TL-dating in the fine-grained sediment layer.

สถาบันวิทยบริการ  
จุฬาลงกรณ์มหาวิทยาลัย



Figure 4.17 Close-up view of the southeast trench-wall side, Ban Pha Tawan I Trench, showing abundant angular quartzite and feldspar-rich sandstone. The reverse graded beds represent debris flow deposits.

## The Northwest Trench Wall

Sample nos. PT1 and PT2 were collected from the topsoil of the Unit A.

Sample no. PT3 was collected from the coarse-sediments of the Unit B.

Sample no. PT4 was collected from the fine-sediments of the Unit C.

Sample nos. PT5 and PT6 were collected from the fine-sediments of the Unit E.

Sample nos. PT7 and PT8 were collected from the fine-sediments of the Unit G.

## The Southeast Trench Wall

Two sample, nos. PT9 and PT10, were collected from the coarse-sediments in colluvium sediments in the southeast trench wall of the Ban Pha Tawan I Trench (Fig. 4.16).

## 4.5 Ban Pha Tawan II Trench

Ban Pha Tawan II Trench was dug by villagers for road and building construction (Figs. 4.18 and 4.19). It is situated at about 200 m northwest from Ban Pha Tawan I Trench, at grid reference 158775N 051715E on 1 : 50,000 sheet 4837 IV (Ban Kaeng Riang) of topographic map.

### 4.5.1 Mapping Unit and Description

The mappable unit exposed in northwest wall was defined into 3 units as shown below.

**Unit A.** This unit is the top layer in this area. The unit is 10-15 cm thick, dark grey to black soil. It is poorly sorted and comprises mainly coarse gravels about 50%. Clasts are mostly coarse gravels of very angular quartzite. Clast diameter is about 1-5 cm. The matrix comprises of silt and clay. It is covered by many trees on surface. There is graditional contact with coarse-grained colluvium (Unit B).

**Unit B.** This unit is orangish red coarse-grained colluvium, with thickness ranging 0.5-3.0 m. It is poorly sorted and consists mainly of coarse gravels about 85%. Gravels are mostly highly angular quartzite about 3-15 cm in diameter. Matrix are mainly orangish red silt and clay. The Unit B is covered and shows a graditional contact with the dark grey topsoil and a sharp contact with the underlying bedrocks.

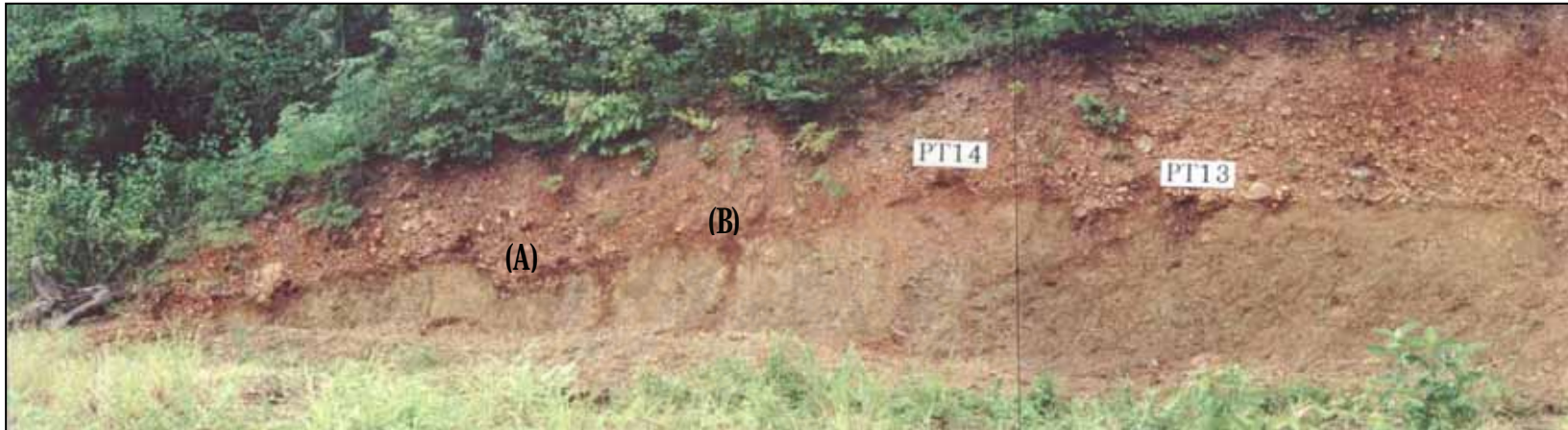


Figure 4.18 The consolidated gravel layer overlying triassic clastic bedrocks with a sharp contact and showing 2 samples for TL dating , Ban Pha Tawan II Trench. The step like feature (A) and colluvial wedge (B) interpreted to be cause by faulting, view looking N40°W.



Figure 4.19 Panoramic view of the Ban Pha Tawan II Trench (continue Fig. 4.18) showing unconsolidated gravel layer lying over deformed bedrock.



**Unit C.** This unit is bedrock of Triassic (by Bunopas, 1976). The unit is brown mudstone with interbedded yellow siltstone. This unit exposes about 0.5-3.5 m thick. The structure in this unit is tight folds. In some part, the folds change abruptly in attitude due to faulting. Furthermore, the contact between gravel bed with bedrock shows a colluvial wedges and step-like uplifts of the gravel bed (Figs. 4.19 to 4.23), possibly indicating to the effect of earthquake-related tectonic activity.

#### 4.5.2 Location of Collected Sample

Only one sample, sample no. PT 11, was collected in the coarse-grained colluvium layer (Unit B) (Fig. 4.18).





Figure 4.20 Close-up view looking N40°W showing a colluvium wedge and uplift of gravel bed.



Figure 4.21 Close-up view of figure 4.17 showing well-defined colluvium wedge due to earthquake faulting.

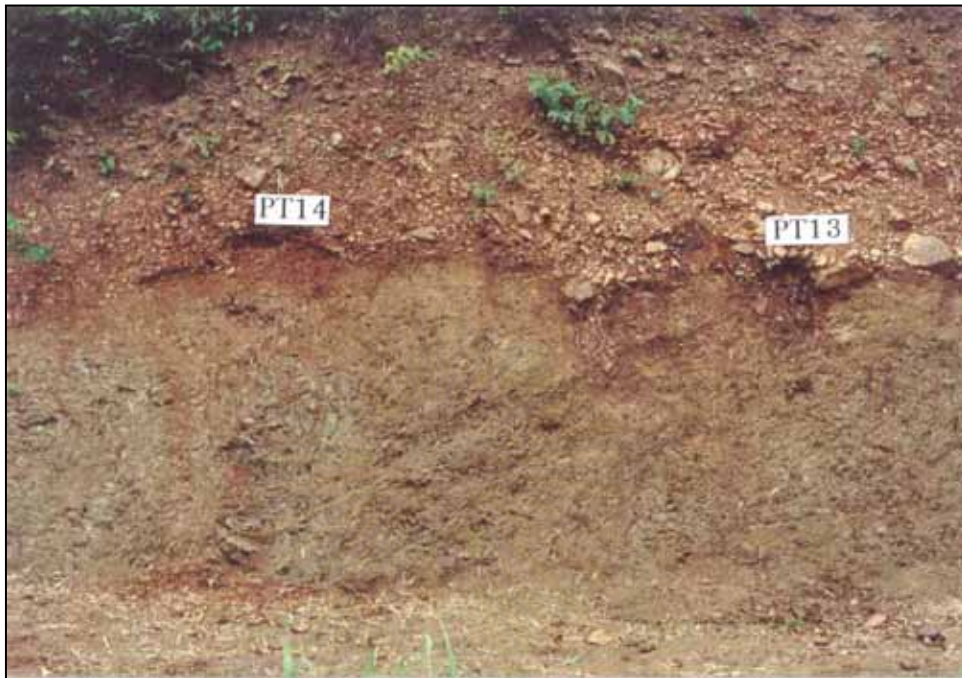


Figure 4.22 Close-up view of figure 4.17 showing a colluvium wedge and location of sample for TL dating.



Figure 4.23 Close-up view of figure 4.17 showing highly angular clasts (fragments of quartzite) with a colluvium wedge.

## CHAPTER V

### AGE DETERMINATION BY THERMOLUMINESCENCE DATING

The age determination is an important approach in paleoseismology which is one kind of geological science concerning the time during Quaternary period. Many methods are applied for determining age in Quaternary period, such as; radiocharbon ( $^{14}\text{C}$  AMS), thermoluminescence (TL), radiogenic isotope (K-Ar, Ar-Ar, U-series), cosmogenic nuclide ( $^{10}\text{Be}$ ,  $^{26}\text{Al}$ ,  $^{36}\text{Cl}$ ,  $^3\text{He}$ ), fission track, electron spin resonance (ESR), dendrochronology, lichenometry, soil-profile development, scarp morphology datings etc. However, each method has the different limitation and accuracy to determine age of samples in different time span. The TL dating was used in this research, because no organic matter was observed in trenches, and this is an appropriate method for determining ages of materials ranging the excavated from 200 to 2,000,000 years (Charusiri et al., 2001). In the contrast,  $^{14}\text{C}$  dating can only dated organic matters or substances that contain carbon. And, it can be use only for any sample with an age less than 5,000 years B.P. (Charusiri et al., 2544). However, for past earthquake events, there are several authors applied results of TL-dating data in comparison with other methods. A good example is that of Forman et al. (1991) which the TL dates were applied along with the  $^{14}\text{C}$  dates for the best estimates for correlative paleoseismological events. In addition, more recently Reneau et al. (1996) studied and determined ages of buried soils by TL (48 to 61 ka) and  $^{14}\text{C}$  analysis (50 to > 58 ka). Their age results show relatively similar in and agree very well with ESR dating results (45 to 72 ka) done by Toyoda et al. (1995) who determined ages of soil in the same region.

#### 5.1 The Thermoluminescence Process

Thermoluminescence (TL) is the thermally stimulated emission of light in addition to incandescence (Singhvi and Wagner, 1986). It is a phenomenon induced by ionizing radiation and is exhibited to varying degrees by ionic crystals (e.g. silicate, calcium carbonate, and sodium chloride). The basic process of the production of

thermoluminescence is best understood in terms of band theory of solids and comprises the following steps (Fig. 5.1).

(i) Irradiation by ionizing radiation produces an avalanche of free charges (electrons and holes). Most of these free charges recombine instantaneously giving either a prompt luminescence and/or they expend their energy in “heating” the crystal lattice. A small fraction (about a hundredth or a thousandth or less) is able to diffuse from valance band into conduction band, and in doing so gets trapped at various lattice defects (electron trap; T) such as; ion vacancies, impurities, etc. Mobile holes move towards to luminescence trap (L).

(ii) Trapping of an electron at a forbidden energy level (T) and a mobile hole can form a luminescence center.

(iii) However, an appropriate stimulation by way of heating (or optically by an UV lamp or laser) can cause electron was released from electron trap and recombine with mobile holes at an appropriate center (termed a luminescence center), and if so, visible light is emitted in the process of recombining.

In a crystal, there could be a multitude of traps and recombination centers and these could be probed sequentially by heating the sample at a fixed rate and observing the stimulated luminescence intensity. The experimental curve representing the relationship of TL vs. temperature is called a glow curve (Fig. 5.2), and comprises one or more glow peaks.

## 5.2 Thermoluminescence Dating

### 5.2.1 The Age Equation

TL-dating is, in effect, a radiation microdosimetry of natural settings, and the requirement is to measure the radiation dose provided by natural radioactivity ( $^{238}\text{U}$ ,  $^{232}\text{Th}$  and  $^{40}\text{K}$ ) to minerals. Natural ubiquitous minerals such as quartz, feldspars, zircons, have good TL properties which enable them to record irradiation received by them, and of preserving this record through geologic time. Natural radioactivity constitutes a source of constant radiation to these minerals. In a first approximation, the dose rate can

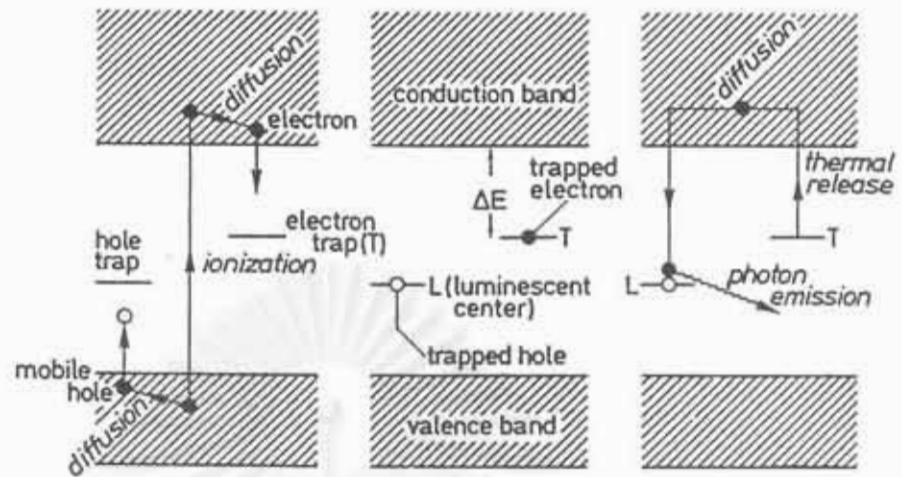


Figure 5.1 Energy band model showing the mechanism of the TL process  
(after Aitken 1978)

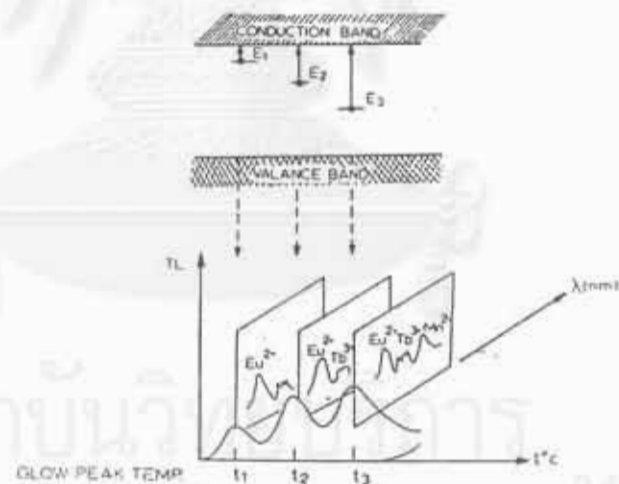


Figure 5.2 Schematic representation of the parameters of a TL curve  
(after Marfunin, 1979)

be assumed constant through time (though substantial deviations can occur) (Aitken, 1967; Singhvi and Wagner, 1986).

The TL age equation in its simplest form is:

$$\text{Age (years)} = \frac{\text{Total accumulated irradiation dose (Gy)}}{\text{Irradiation dose per year (Gy/year)}} \quad (\text{Eq.5.1})$$

- Total accumulated irradiation dose, or irradiation dose received by natural radioactivity and of preserving this record through geologic time, is called *paleodose* (PD). Paleodose is the measurement the intensity of the luminescence from the sample and related luminescence intensity of irradiation dose is calculated by irradiating the sample. The dose is given in gray (1 Gy = 100 rad). One gray corresponds to one joule of absorbed energy per kg of matter.

- Irradiation dose per year, or dose rate is called *annual dose* (AD), is calculated from the chemical data of radiogenic elements (U, Th, K) and cosmic ray evaluation (sec. 5.4.2).

## 5.2.2 Events Dated by Thermoluminescence

In thermoluminescence dating, it is assumed that initially (viz. the time of formation or the last heating to above 500°C) none of the sufficiently “deep” traps in the sample were occupied by electron (Daniels et al, 1990). Basically, there are three types of events that may be dated by the TL method (Singhvi and Wagner, 1986; Figs. 5.3 a, b and c):

(i) The most recent *thermal event* would have caused sufficient heating (>500°C) to induce a complete detrapping of all the charges (i.e. removal of geological TL). Subsequent burial within the context results in a re-induction of TL that continues until excavation and laboratory heating. Samples in this category are archaeological pottery (Fleming, 1979), sediments baked by lava flows (Huxtable et al., 1978), fault gouge heated by fault movements (Ding and Lai, 1997), burnt stones and flints (Aitken and Wintle, 1977; and Valladas, 1978), and fusion crust of meteorites dating the time of meteorite fall (Singhvi and Wagner, 1986). In all these case the heating event (which is dated) ensures a total emptying of geological TL.

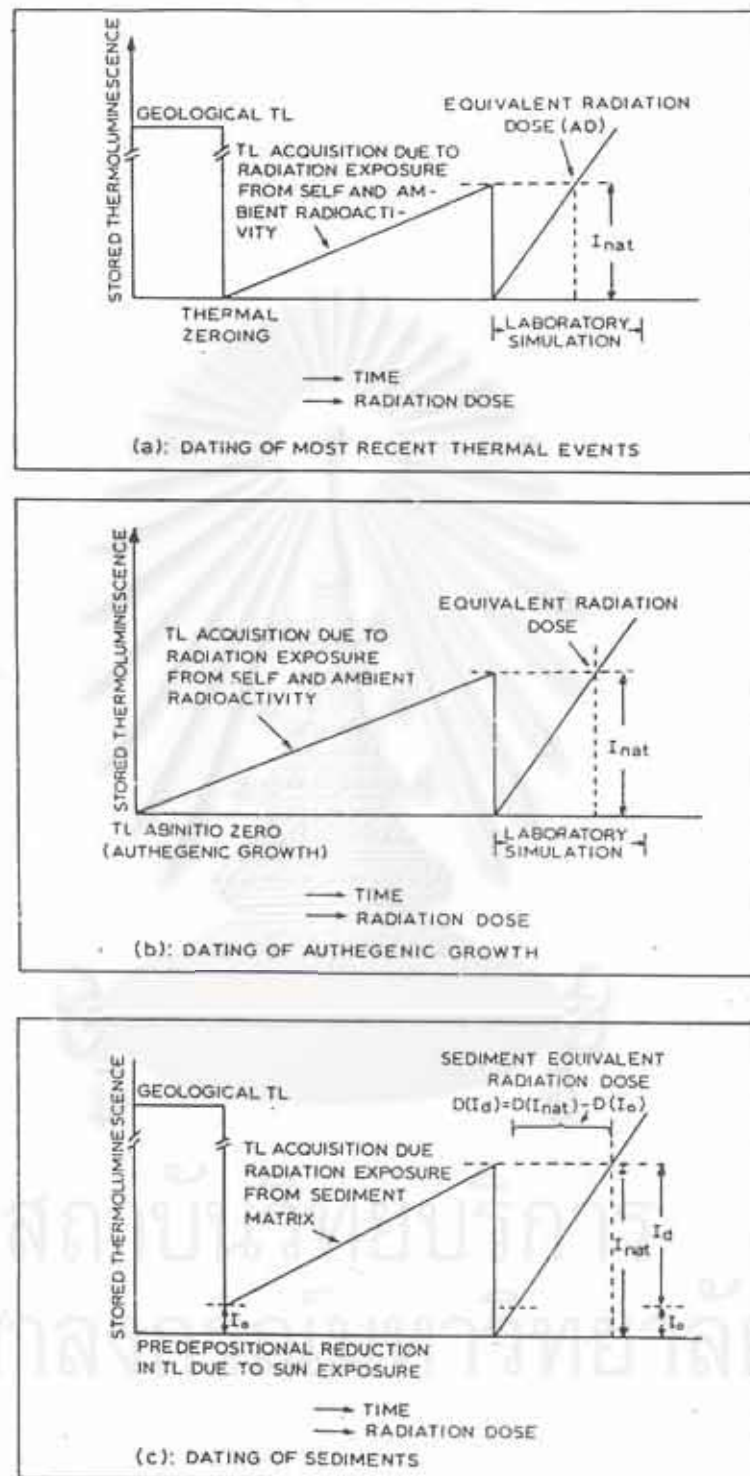


Figure 5.3 Events that can be dated by TL method (after Singhvi and Wagner 1986)



(ii) With *crystallization* it is the event of crystallization that is dated and TL is *ab initio* zero. A good example is the formation of travertine in caves (Wintle, 1978) or *in-Situ* precipitation of gypsum (Nambi, 1983). Another case of *ab initio* zero TL is the impact glasses formed by meteorite impact (Sengupta et al., 1984; and Sutton, 1984).

(iii) The event of most recent *sun bleaching*, when sediments are exposed to the sun immediately prior to deposition. The first suggestion that sunlight would reset the TL of sediments appears to have come from Shelkopyas and Morozov (1965) in the former USSR. However, This work did not become known outside the USSR until after Wintle and Huntley (1979,1982) had recognized the possibility and develop practical methods for its use (Prescott and Robertson, 1997). This provides the age of burial which is discussed in detail in section 5.5.2.

### 5.3 Sample Preparation

All samples for TL-dating method in this study were collected from fault-related colluvial sediments following the method described in section 4.2. In the current study, the samples for TL dating were prepared following the method described by Takashima and Watanabe (1994). All the sample preparation was made at the laboratory of Department of Geology, Faculty of Science, Chulalongkorn University and Central Laboratory of Akita University.

#### 5.3.1 Crushing and Sieving

The samples, which were collected from outcrops, were dried in the dark at room temperature. Each sample was shattered using a rubber-hammer, and sieved to pass through a 20 mesh; the coarser fractions were removed. The samples of 300-400 g was separated to keep in plastic container (Fig. 5.4) for annual dose determination (sec. 5.4.2). A remained part of the 20 mesh sample was re-crushed to obtain 60-200 mesh grains. This part was kept in beakers for purify quartz grains.

### 5.3.2 Sample Cleaning and Purification

The samples from sec 5.3.1, which were kept in beaker for purify quartz grains, were washed with water (Fig. 5.5) about 10 times for removing organic matters, some mica minerals, and clay particles. The carbonates were dissolved with 18% HCl, and washed with water again, then baked in an oven at about 40-50°C for 24 hours. HF was then used to dissolve the plagioclase and outer layers of quartz grains to a depth sufficient for the core remaining to have a negligible component of alpha particle dosage. The sample was placed in 26% HF for 30 minute, thoroughly rinsed and placed in 18% HCl is about 20 minute, and wash with water again (Fig. 5.5), then baked in an oven at about 40-50°C for 24 hours. The dried sample was then separated to remove out dark minerals (e.g. zircon, garnet, and metallic minerals) by using an isodynamic separator (Frantz isodynamic magnetrometer; Fig. 5.6). As a result, the sample supposed to contain pure quartz (more than 98%) can be used to determined age by TL-dating.

## 5.4 Sample Treatment

### 5.4.1 Water Content Determination

The water content is highly preferable, if it were measured in situ. If not, it can be measured in laboratory, however, the sample should be kept carefully in moisture-tight container. The water content can be calculated by Eq. 4.1. The results of water contents for individual samples are displayed in Table 5.1.

### 5.4.2 Annual Dose Determination

Annual dose was determined by calculation of natural radioactive content in prepared sample in sec. 5.3.1. Chemical analyses were performed by gamma ray spectrometry (Fig. 5.7) at Akita University, Japan. The detector employed was a 76Ø x 76 mm NaI(Tl) scintillator connected to a multichannel analyzer (Takashima and Watanabe, 1994). Standard employed were NBS samples for U and Th, and a K<sub>2</sub>CO<sub>3</sub> chemical reagent for K. The estimated standard errors were less than 10% for U and Th, and less than 3% for K using the fixed count error calculation method. Annual doses were calculated by the equation derived from Bell (1979) and Aitken (1985).



Figure 5.4 Weighting the sample as part of sample preparation for annual dose determination.  
(Mr. Krit Won-In, right, is to scale)



Figure 5.5 Samples are cleaned and washed with tapping water after etching with HF (Mr. Rutchut Nutthee is to scale)



Figure 5.6 Frantz's isodynamic magnetrometer was applied to separate dark-colored minerals from light-colored less magnetic ones.



Figure 5.7 Gamma-ray spectrometer (bottom right) for determination of uranium, thorium, and potassium contents.

$$AD = \frac{(0.1148U + 0.0514Th + 0.02069K)}{(1 + 0.14 \text{ Wt.})} + \frac{(0.1462U + 0.0286Th + 0.6893K)B + 0.15\dots}{(1 + 1.25 \text{ Wt.})} \quad (\text{Eq. 5.2})$$

where U = concentration of uranium in ppm,  
 Th = concentration of uranium in ppm,  
 K = concentration of potassium oxide (%),  
 B = beta dose attenuation in quartz grains, and  
 Wt. = Water content (%/100)

Results of U, Th, and K analyses and calculated annual dose are shown in table 5.1.

### 5.4.3 Reset Existing TL Signals to Zero and Artificial Irradiation

The simplest approach to the evaluation of paleodose is by the straightforward procedure of measuring the natural thermoluminescence from a natural sample (N) and comparing it with the artificial thermoluminescence from the same samples that know certain dosage (artificial irradiate sample). The artificial irradiate sample was heated in 320°C and 1 hour-duration which were enough to reset existing TL signals (Takashima et al., 1989). The heated samples were exposed to artificial irradiation from the radioisotope gamma ray source, which can control the certain dosages. In this study, the dosages applied are 29Gy, 99Gy, and 299Gy. All samples were irradiated at Akita University Hospital. Irradiation intensity of heated sample with additive doses are assigned herein as H+γ (e.g. H+29Gy, H+99Gy, and H+299Gy), and those of natural samples with additive doses are designated as N+γ, herein as N+309Gy.

### 5.4.4 Measurement of Thermoluminescence

There are some geological minerals from which the TL is bright enough to be seen with the naked eye, but in dating we are dealing with light levels lower by many orders of magnitudes. As indicated above, it was the development of the photomultiplier that made TL dating a practical possibility. The common process of TL apparatus was shown in Fig 5.8. Here, TL emission was measured by using the Kyokko 2500TLD

Table 5.1 Results of water content, natural radioactive content (U, Th, K<sub>2</sub>O) and annual dose for TL dating samples from Ban Kaeng Khaep and Ban Pha Tawan I and II Trench.

Ban Kaeng Khaep Trench

Sample No.	Water content	U (ppm)	Th (ppm)	K <sub>2</sub> O (%)	Annual Dose (mGy/y)
KK1 <sup>a</sup>	13.834	1.048	13.387	3.416	3.441
KK2	12.593	1.468	11.702	2.422	2.768
KK3	11.945	1.491	10.480	2.149	2.522
KK4	13.743	1.397	11.425	2.292	2.602
KK5	10.991	1.332	13.182	3.266	3.512
KK6	11.107	0.988	10.328	2.529	2.714
KK7	10.393	1.631	13.153	2.256	2.851

Ban Pha Tawan I Trench

Sample No.	Water content	U (ppm)	Th (ppm)	K <sub>2</sub> O (%)	Annual Dose (mGy/y)
PT1 <sup>b</sup>	11.018	2.089	15.628	2.096	2.968
PT2	15.155	1.933	13.175	1.661	2.327
PT3	7.515	1.891	15.361	2.048	3.010
PT4	7.528	2.088	15.139	2.037	3.028
PT5	8.334	1.900	14.898	1.939	2.867
PT6	12.160	2.155	14.735	1.845	2.700
PT7	9.263	2.062	17.060	2.104	3.132
PT8	9.765	1.937	15.318	1.846	2.780
PT9	4.582	1.589	15.222	2.921	3.740
PT10	10.852	2.027	15.689	2.547	3.297

Ban Pha Tawan II Trench

Sample No.	Water content	U (ppm)	Th (ppm)	K <sub>2</sub> O (%)	Annual Dose (mGy/y)
PT11	11.677	1.469	18.717	3.047	3.702

<sup>a</sup>KK1 = Number of samples that collected from Ban Kaeng Khaep Trench

<sup>b</sup>PT1 = Number of samples that collected from Ban Pha Tawan Trench

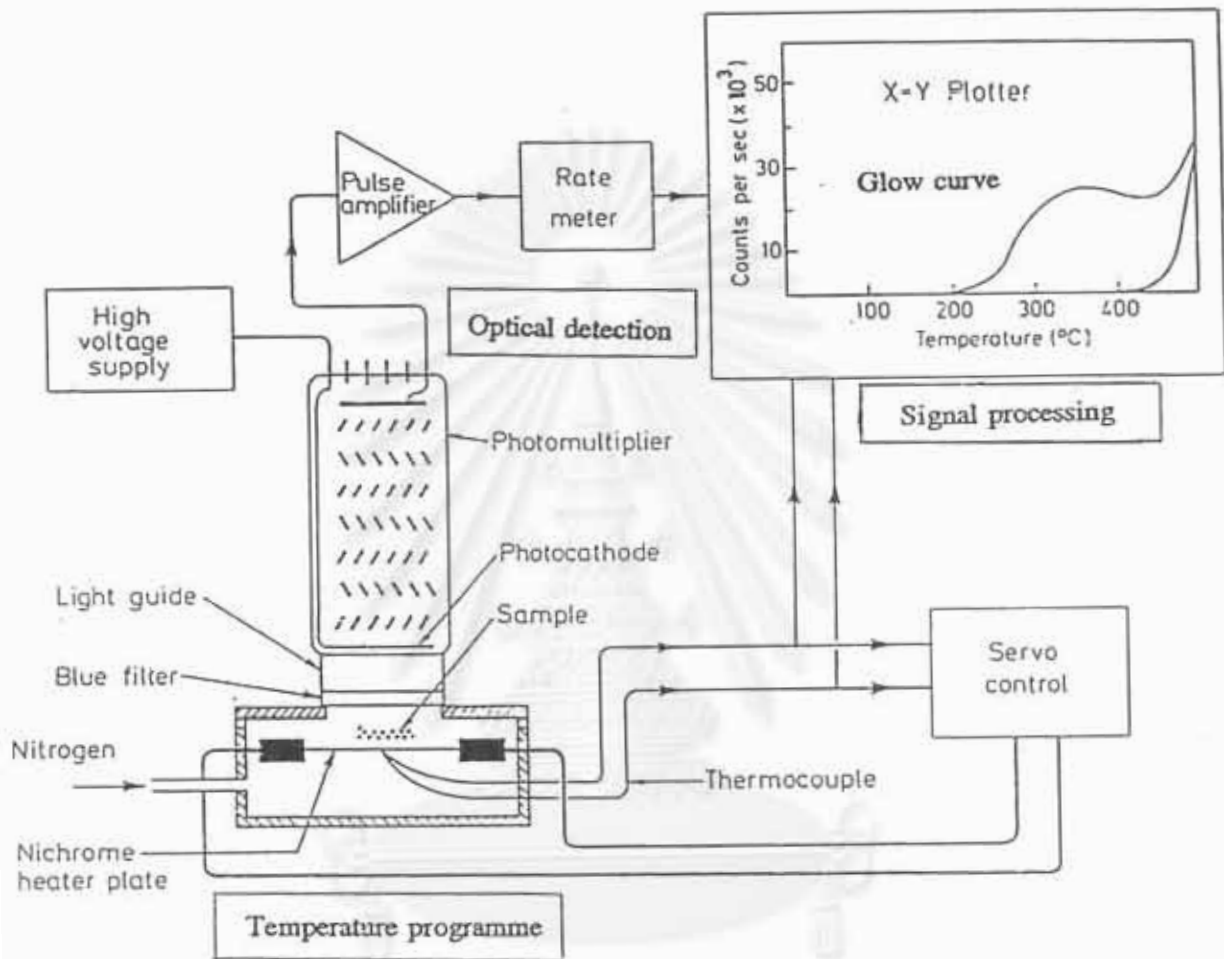


Figure 5.8 Diagram of apparatus for thermoluminescence measurement.

(after Aitken, 1985)

dosimeter (Fig. 5.9) at Akita University, Japan. The samples are heated on a molybdenum disk under nitrogen to 500°C with a heating rate of 200°C/min.

The light emission is amplified and measured by the photomultiplier (Fig. 5.8), and recorded simultaneously with the temperature of the sample. The term “glow curve” is given to plot of emitted light versus temperature (Fig. 5.10). The peak of each curve is between 300-450°C is assumed to be proportional to the accumulated paleodose in Eq. (5.1) (Daniels et al., 1953; Geyh and Schleicher, 1990).

## 5.5 Calculation of Thermoluminescence Age

### 5.5.1 Evaluation of Paleodose

There are several methods applied for estimating paleodose of sediments. Generally, three common methods were used for paleodose estimation, i.e., the *partial bleach* (Wintle and Huntley 1979), the *total bleach* (Singhvi et al., 1982); [Aitken, 1985 called “*additive-dose method*”], and the *regeneration* (Wintle and Proszynska, 1982) method (Aitken, 1986; Singhvi and Wagner, 1986; Geyh and Schleicher, 1990; and Forman et al. 1991). In this study, the evaluation of paleodose method was used following the method of Takashima and Watanabe (1994), which was modified from the regeneration method by using ratio of intensity of gamma ray irradiated ( $H+\gamma$ ) / natural (N) for plotting the growth curve. For regeneration method, the intensity of irradiated dose sample ( $H+\gamma$ ) is only used for plotting the growth curve.

The glow curve, it is a curve (Fig. 5.10) whose x-axis is temperature (in °C) and y-axis is TL signal (in a.u. (arbitrary unit)). The TL glow curve commenced to increase the temperature of 200°C, until it reached the maximum curve at about 335-370 °C. The TL measurement was done in a natural sample (N), an additive dose heated sample ( $H+\gamma$ ), and an additive dose natural sample ( $N+\gamma$ ) (see Sec. 5.4.3). Each sample was separated into 3 aliquots for 3 runs of treatment. In each run, three curves appear at the same time as (a), (b), and (c) (see Fig. 5.10(i)). In this case, curve (b) is used for standard measurement, so the signal is record base upon this curve. Therefore, curve (b) of each run was chosen and re-plotted on a graph paper for each sample no. They were shown in Appendix B-1.





Figure 5.9 Common TL apparatus (the Kyokko 2500 TLD) with a photomultiplier (an instrument with Rutchut is left hand and the monitor (TV on the right) for showing TL signals

สถาบันวิทยบริการ  
จุฬาลงกรณ์มหาวิทยาลัย

For example, TL glow curves of sample no. KK5 are shown in Figs. 5.10 to 5.14. The TL intensity ( $I$ ) of each sample was determined at a temperature similar to that of the natural sample. So, the TL intensities of sample no. KK5 was determined from the temperature of 350°C. This temperature (350°C) was used for TL intensities of irradiated samples (such as, H+29Gy, H+99Gy, H+299Gy, and N+309Gy) (Figs. 5.11 to 5.13). The TL intensities of sample no. KK5 are measured at about 194 a.u., 179 a.u., and 146 a.u. for natural sample (Fig. 5.10), 40 a.u., 35 a.u., 35 a.u. for H+29Gy (Fig. 5.11), 100 a.u., 99 a.u., 95 a.u. for H+99Gy (Fig. 5.12), 190 a.u., 199 a.u., 188 a.u. for H+299Gy (Fig. 5.13), and 360 a.u., 382 a.u., 279 a.u. for N+309Gy (Fig. 5.14).

In this study, the glow peaks of natural samples correspond mostly to temperature of about 340 to 350°C (see Appendix C-1) and few to that of 360 to 370°C (PT2, PT4, PT8, PT9, and PT10).

The ratio between TL intensities of additive dose preheat sample (H+ $\beta$ ) and average natural intensity [ $(I_{(H+\beta)})/Avr.(I_{nat})$ ] were plotted on graph paper as “TL growth curve” (Fig 5.15). In this figure, the vertical axis was set by ratio of  $(I_{(H+\beta)})/(I_{nat})$ , and the horizontal axis was set by the irradiate dose (Gy) which was added in a preheat sample. If the line was drawn from where the y-intercept = 1 (which mean  $(I_{nat})/(I_{nat})$ ) and to meet the growth curve, then the line drawn straight down to the x-intercept on x-axis. The value on x-intercept point is total accumulated dose of natural sample [ $D(I_{nat})$ ], or paleodose (Fig. 5.14). All of the growth curves were shown in Appendix C-2.

Basically, the age of sample is ratio of PD/AD. However, the correction in dated sediment (see detail in sec. 5.5.2) must be done. Therefore, the age of samples in this step are “*apparent age*”, as were shown in Table 5.2.

## 5.5.2 Correction of Dated Sediments

### 5.5.2.1 Basis of Dating of Sediments

The TL technique directly dates silicate mineral grains in sediment, the age reflecting the time since the sediment grains were last exposed to sunlight (Wintle and Hunley, 1980; Forman et al., 1991). However, The resetting of the TL signal by sunlight is less efficient than by heat (Rodbell et al., 1997). Because sunlight does not completely empty the electron traps that produce TL (Wintle and Huntley, 1980;

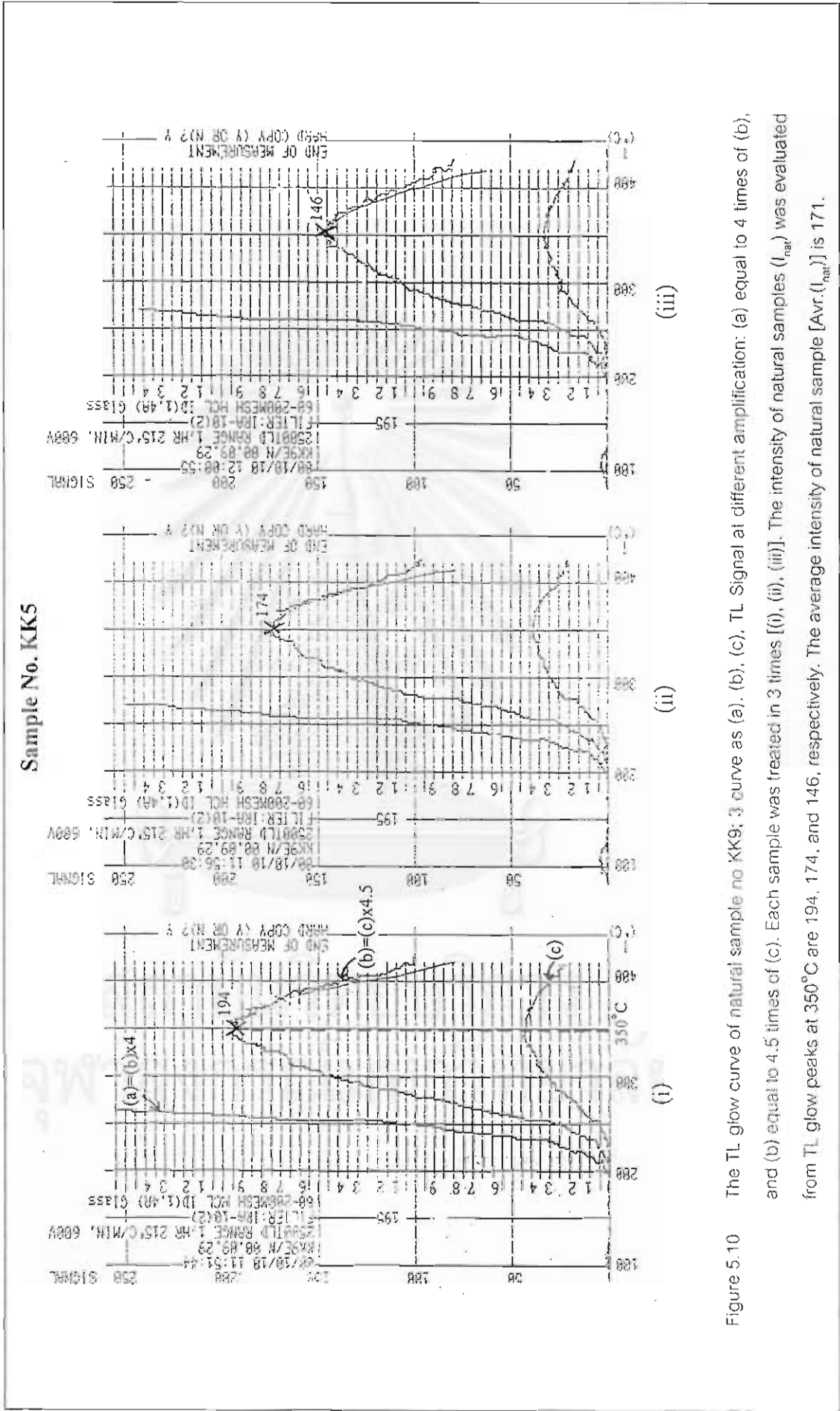


Figure 5.10 The TL glow curve of natural sample no. KK9; 3 curve as (a), (b), (c), TL Signal at different amplification: (a) equal to 4 times of (b), and (b) equal to 4.5 times of (c). Each sample was treated in 3 times [(i), (ii), (iii)]. The intensity of natural samples ( $I_{nat}$ ) was evaluated from TL glow peaks at 350°C are 194, 174, and 146, respectively. The average intensity of natural sample [ $A_{v}(I_{nat})$ ] is 171.

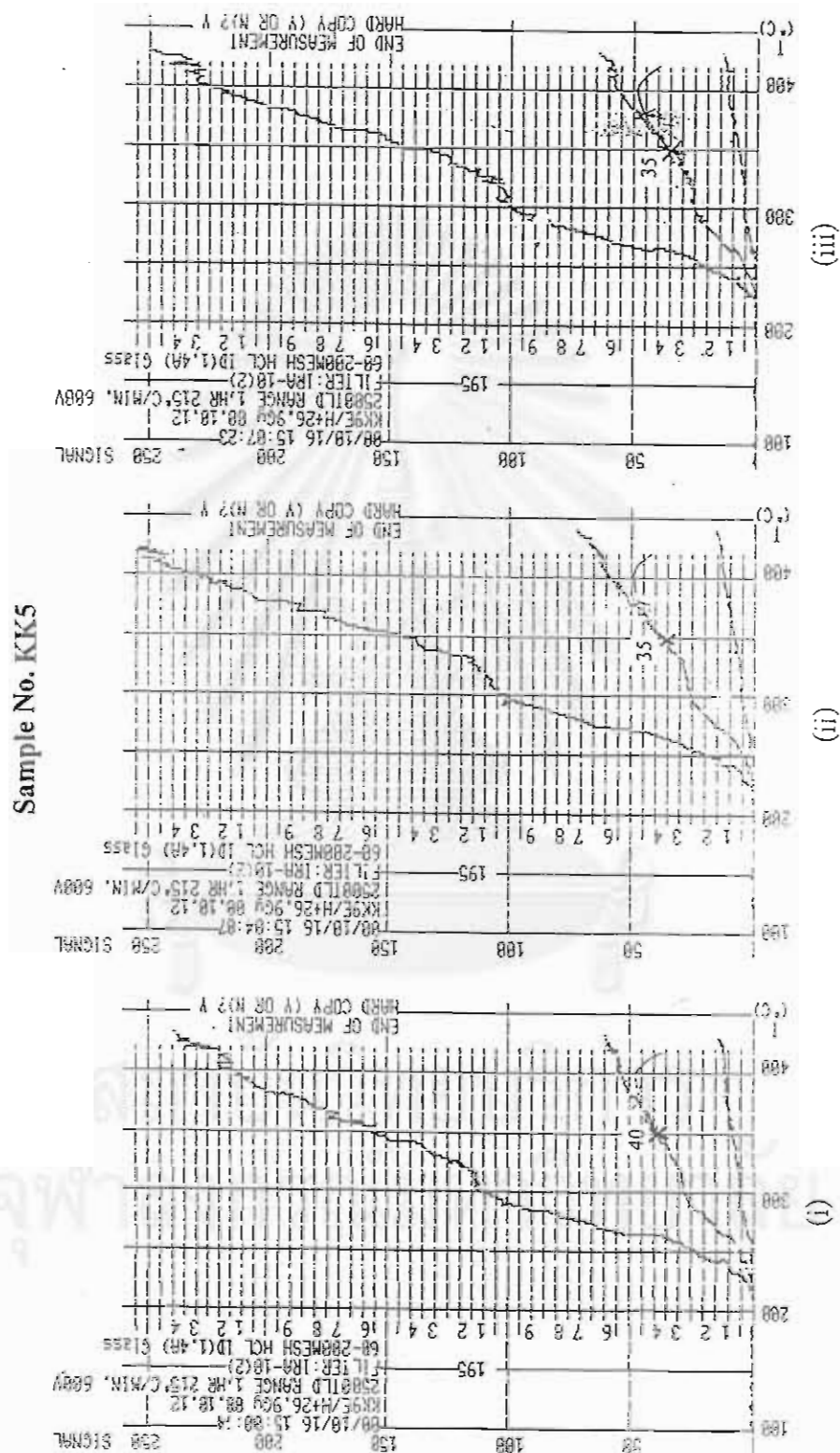


Figure 5.11 The TL glow curve of H+29Gy. The intensity of H+29Gy samples ( $I_{350}^{H+29Gy}$ ) were evaluated from TL glow peak at 350°C are 40, 35, and 35, respectively.

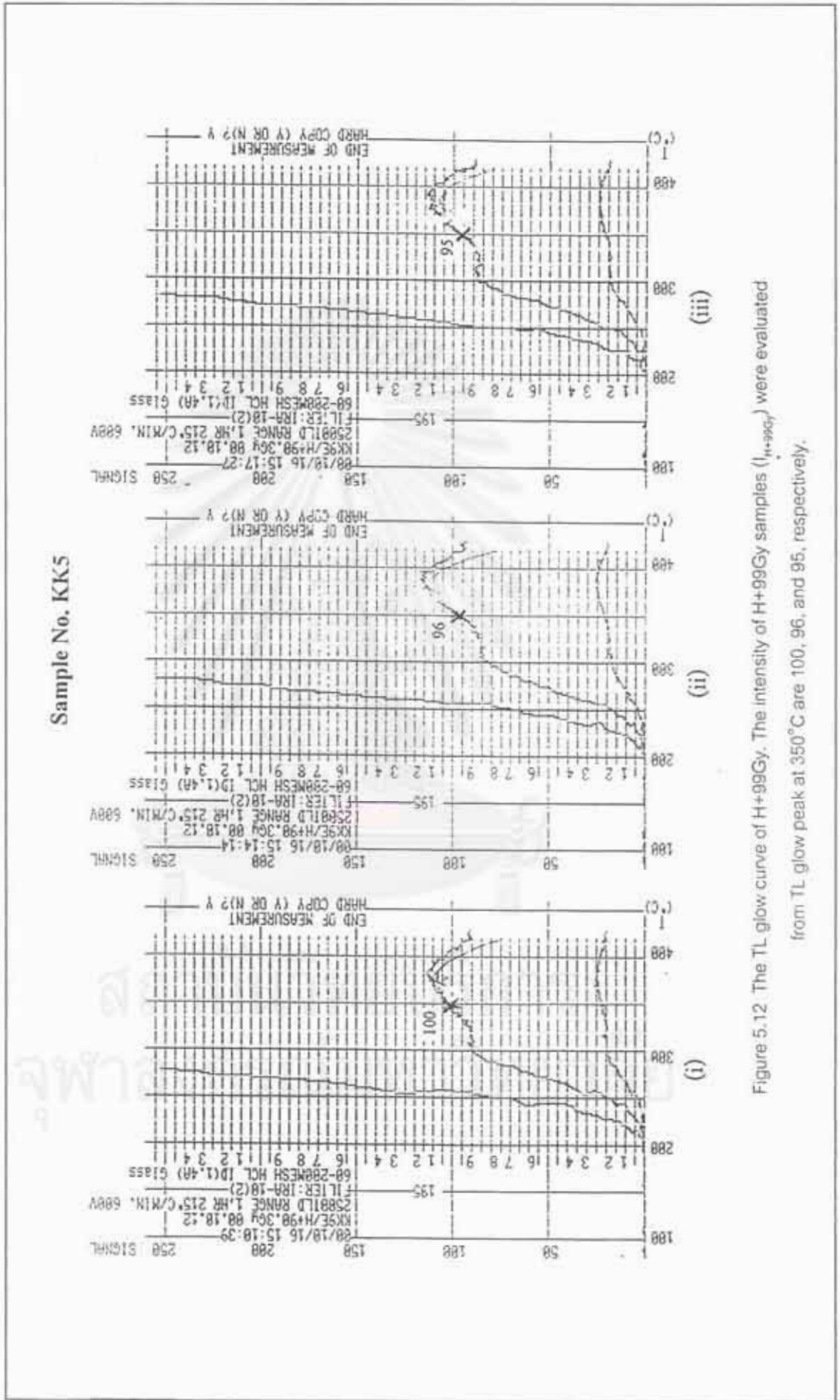
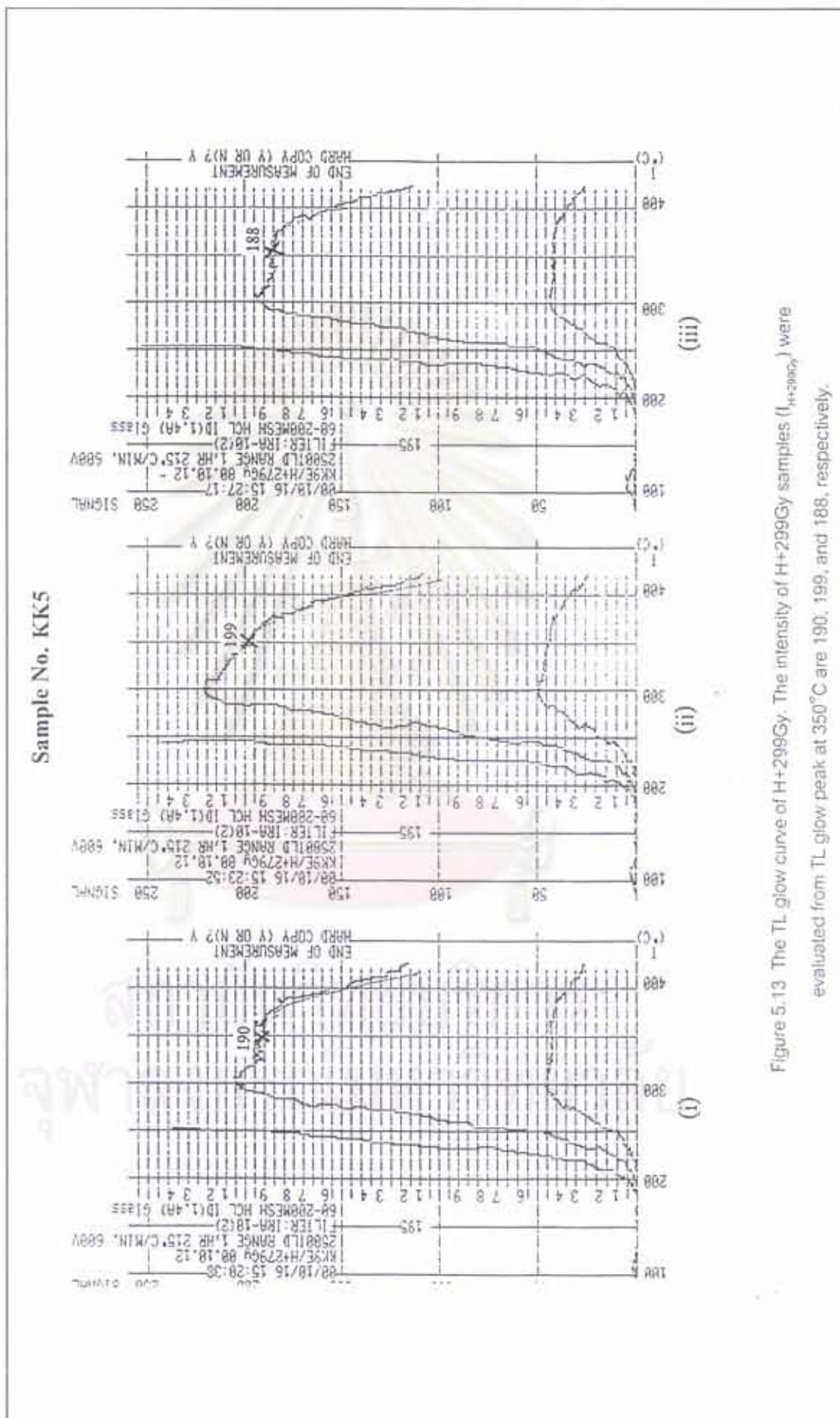


Figure 5.12 The TL glow curve of H+99Gy. The intensity of H+99Gy samples ( $I_{H+99Gy}$ ) were evaluated from TL glow peak at 350°C are 100, 96, and 95, respectively.



Sample No. KK5

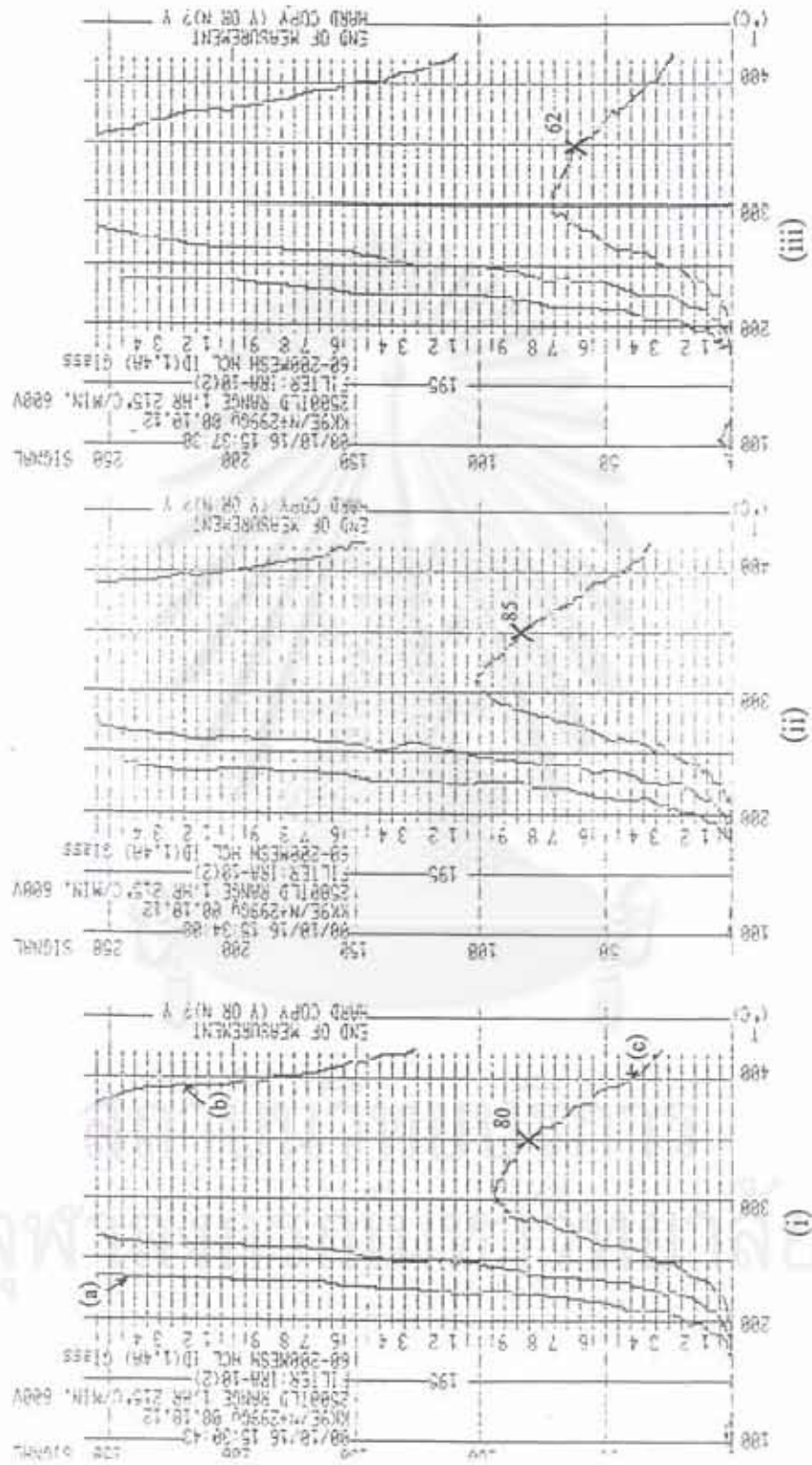


Figure 5.14 The TL glow curve of N+309Gy. The intensity of N+309Gy samples ( $I_{N+309Gy}$ ) were evaluated from TL glow peak at 350 °C are 360, 362, and 279, respectively.

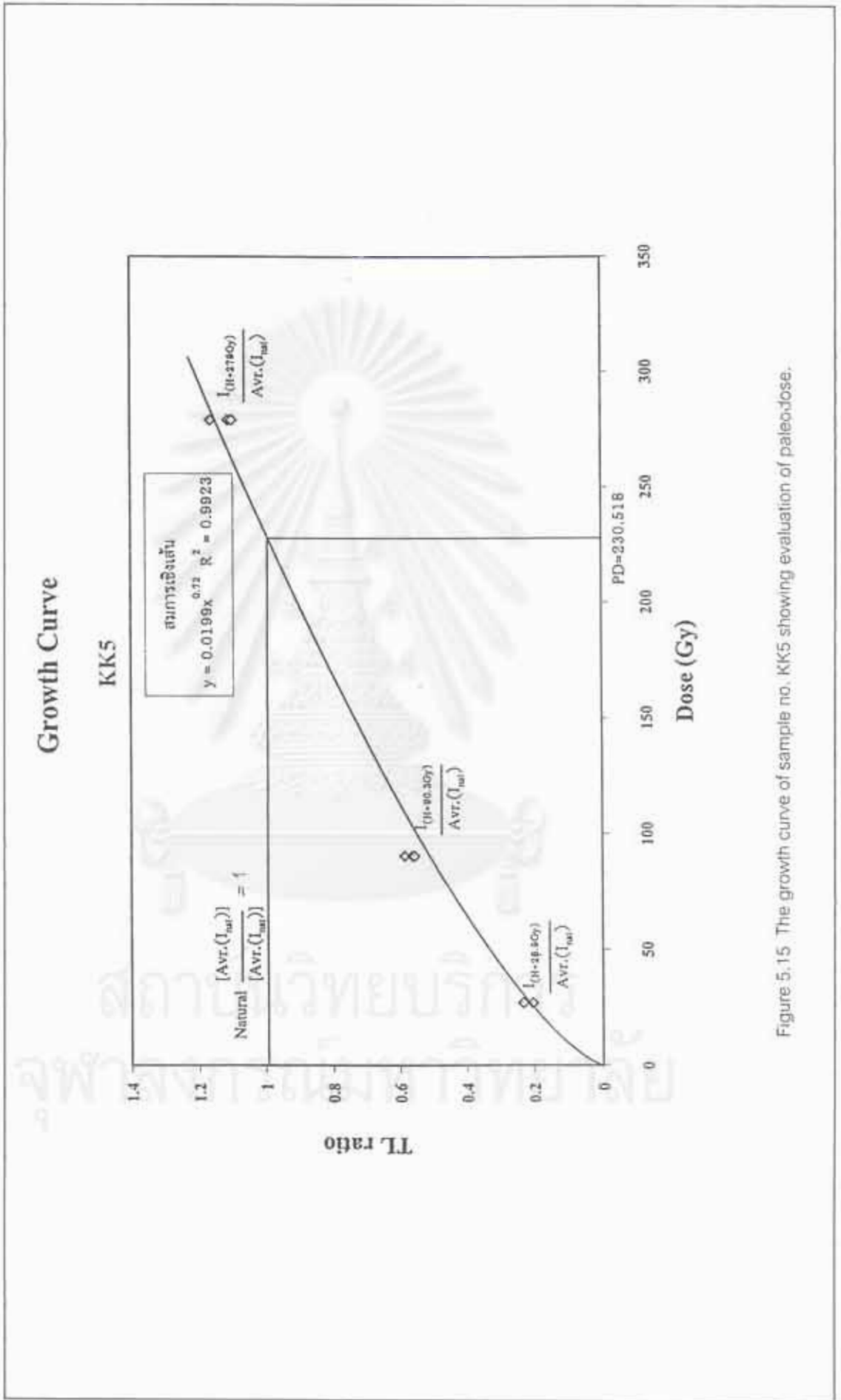


Figure 5.15 The growth curve of sample no. KK5 showing evaluation of paleodose.



Huntley, 1985). The small residual dose must be determined, so that the accumulated dose after deposit can be determined. The basis of the dating sediment (which had no thermal “zeroing”) is summarized briefly below (Fig. 5.3) (Singhvi and Wagner, 1986).

(i) A pre-depositional sun exposure of sediment constituents during weathering and transport causes a drastic reduction (optical bleaching) of geological TL levels to a small residual value ( $I_0$ ).

(ii) On sedimentation, the sample is shielded from sun exposure and reacquisition of TL (over and above  $I_0$ ) is initiated due to radiation exposure from the radioactivity of the sediments.

(iii) A laboratory analysis yields a TL level ( $I_{nat}$ ) from which  $I_0$  should be subtracted to obtain the accrued since sedimentation i.e. ( $I_d$ ).

(iv) The ratio of radiation dose corresponding to  $I_d$ , to the annual dose rate provides the date of the most recent sun exposure.

The sediment TL age equation is :

$$\text{Age (year)} = \frac{D(I_d) [= D(I_{nat}) - D(I_0)]}{\text{Annual Dose}} \dots \dots \dots \text{(Eq. 5.3)}$$

Where  $D(I_{nat})$  = Total accumulated dose or natural paleodose

$D(I_0)$  = Residual TL dose

$D(I_d)$  = Accumulated dose after deposit

Many authors dated sediments and corrected their ages. For example, Forman et al. (1991) determined age of colluvium in the Wasatch fault zone, north central Utah. They concluded that TL age estimate by either the partial bleach, total bleach or regeneration methods are statistically identical and are in agreement with a  $^{14}\text{C}$  analysis.

Forman et al. (1992) determined age of loess in upper Mississippi River Valleys by TL dating for which both the total and partial bleach techniques were applied. The results indicate no systematic or significant (at  $\pm 1\sigma$ ) age differences for both techniques.

Wintle et al. (1993) tested various luminescence methods in northern Natal, South Africa. Fine grain samples were measured using TL and IRSL

method. Total bleach and regeneration methods of analysis were applied. There was agreement among the ages obtained using the IRSL methods and some of the radiocarbon dates, but the TL dates were much older than the others. Suggested explanations lie in the insufficient bleaching of colluvial fine grains. The same techniques were further explored by Wintle et al. (1995) but using 100  $\mu\text{m}$  feldspar grains. In this case, well-bleached samples showed good agreement between TL and IRSL ages.

Moreover, Millard and Maat (1994) applied partial and total bleach analyses of duplicate samples of the Crowley's Ridge in eastern Arkansas, USA. The results yield TL date based on the partial bleach method ( $50.1 \pm 5.0$  ka) that is not significantly different (at  $\pm 1\sigma$ ) than the age based on the total bleach method ( $43.7 \pm 3.9$  ka).

Rodbell et al. (1997) dated loess deposits sample in the Mississippi Valleys. Comparison of TL and available  $^{14}\text{C}$  age estimates for loess suggests that the TL level remaining after exposure to 8 hr of artificial UV light is the appropriate residual TL level for these deposits.

#### 5.5.2.2 Method of Evaluation of the Accumulate Dose $[D(I_0)]$ After Deposit

In this research, three samples were selected (i.e., KK2, KK5, and PT5) to expose to 1, 2, 4, 8, and 16 hr of sunlight. The glow curves of these samples display decreasing TL remaining after bleaching (Figs. 5.16 to 5.18).

The curves of these samples were (re-)plotted between TL remaining after bleaching at 330, 350, 370°C with bleaching time (Figs. 5.19 to 5.21). These show decreasing TL remaining after bleaching as exponential type, while bleaching time is increase. At 8 hr, the curve is stable (not increasingly continue). It indicates that this TL remaining cannot be erased by sunlight, although bleaching times increase. Therefore, 8 hr of sunlight is optimum bleaching time for evaluated residual TL Dose  $[D(I_0)]$ .

In this study, all of sample was exposed to 8 hr of sunlight. The glow curve of sample with 8 hr bleaching was drawn and compared with the same natural sample, as shown in Fig 5.22. Intensity of 8-hr bleaching sample ( $I_0$ ) at the

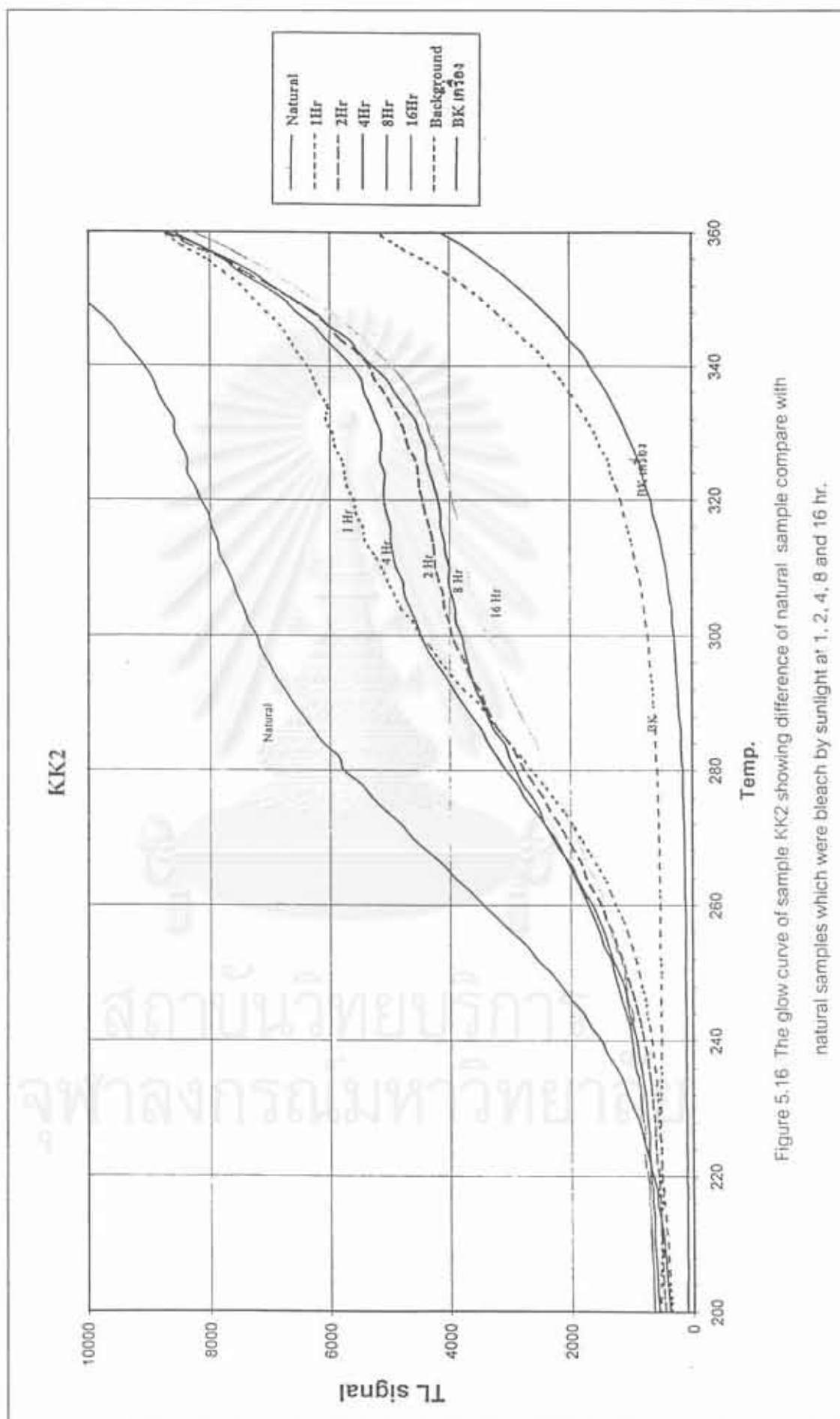


Figure 5.16 The glow curve of sample KK2 showing difference of natural sample compare with natural samples which were bleach by sunlight at 1, 2, 4, 8 and 16 hr.

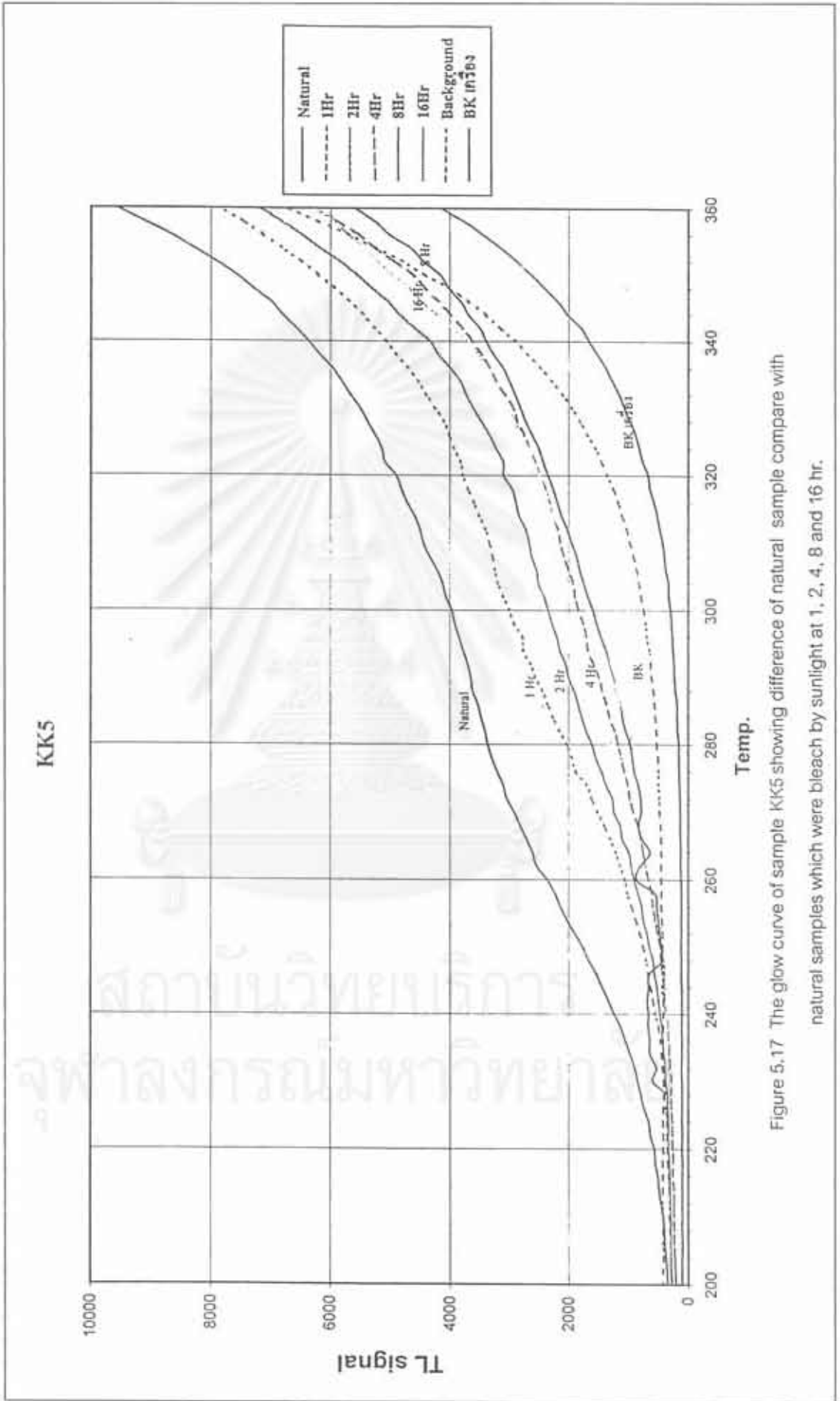


Figure 5.17 The glow curve of sample KKS showing difference of natural sample compare with natural samples which were bleached by sunlight at 1, 2, 4, 8 and 16 hr.

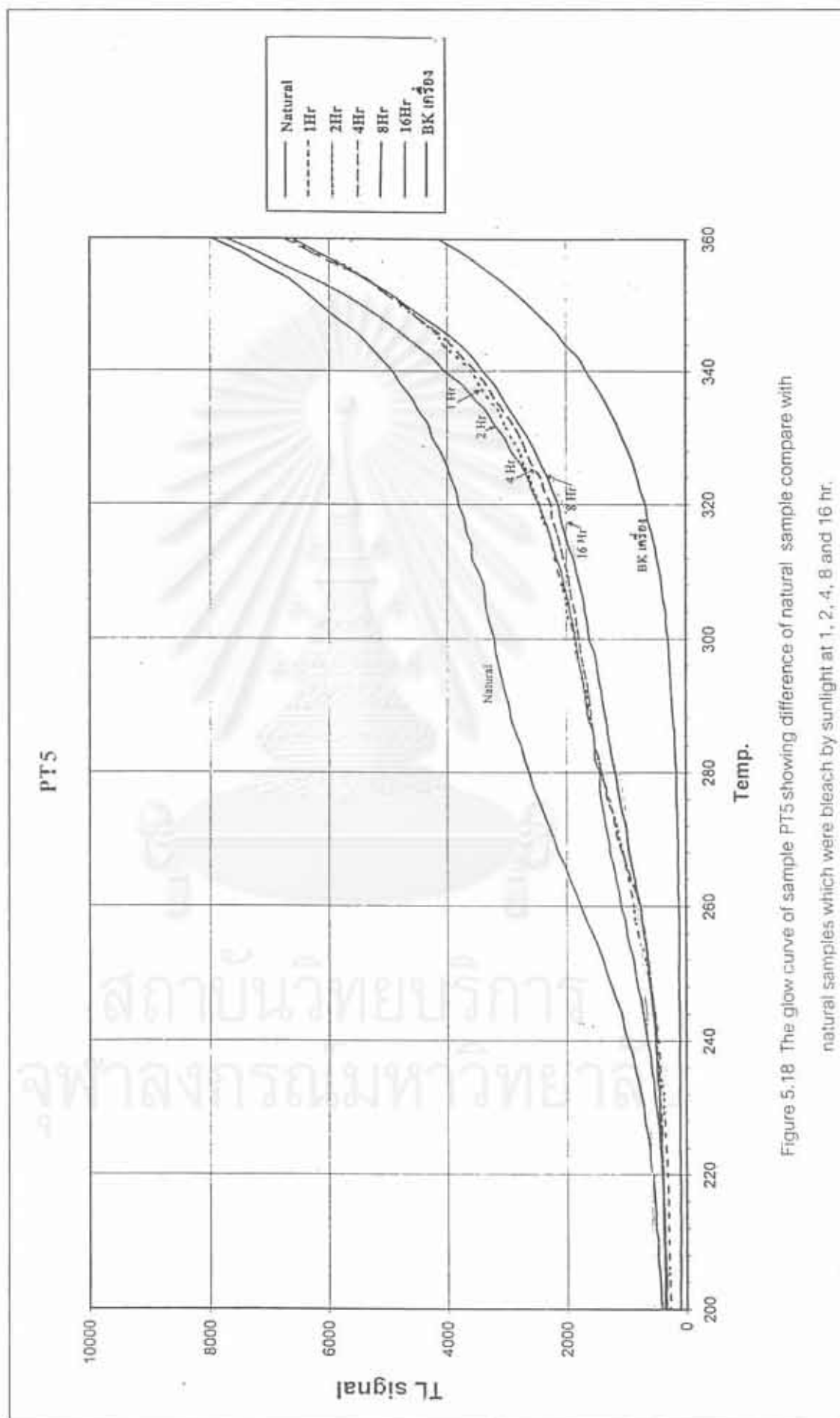


Figure 5.18 The glow curve of sample PTS showing difference of natural sample compare with natural samples which were bleach by sunlight at 1, 2, 4, 8 and 16 hr.

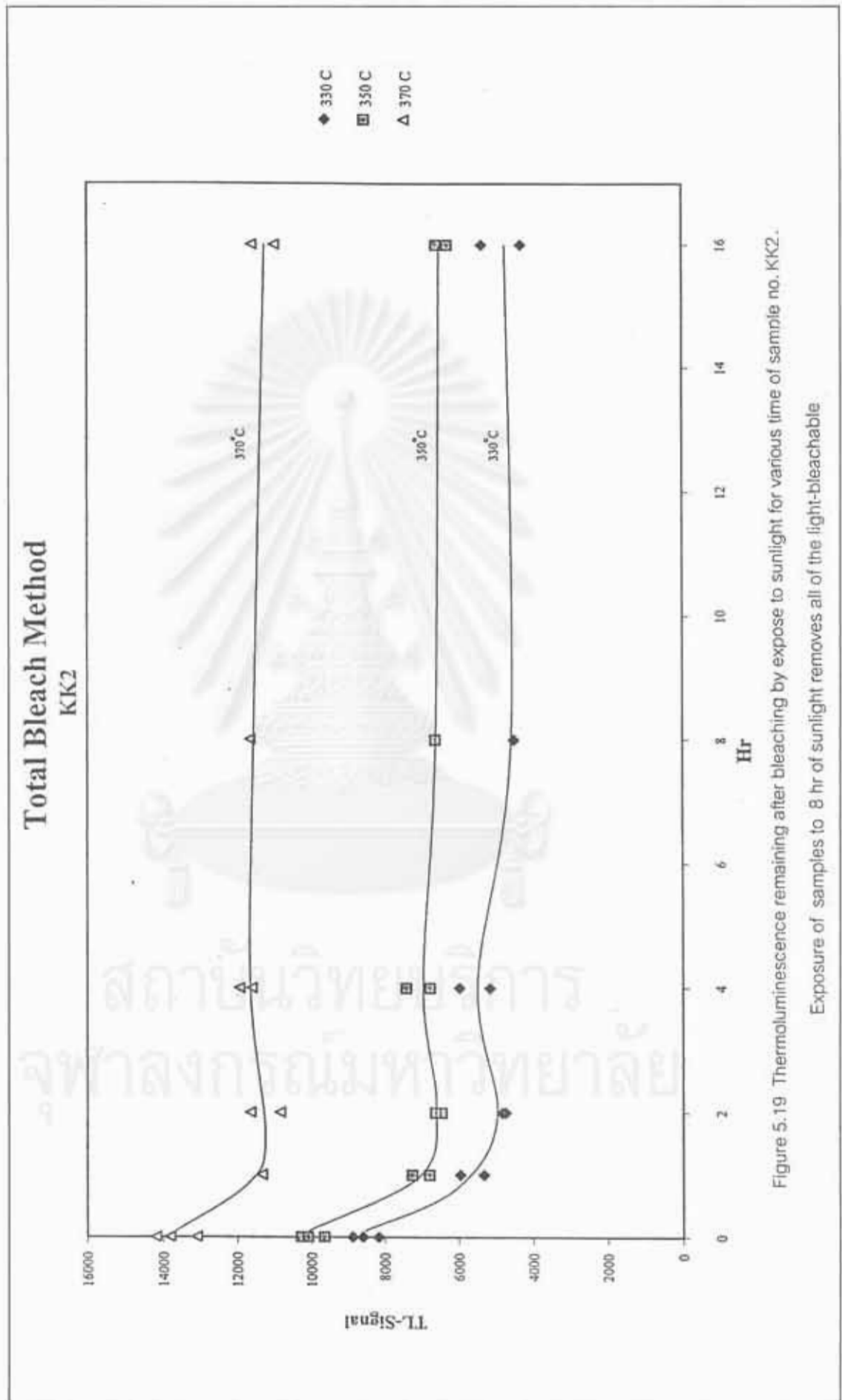


Figure 5.19 Thermoluminescence remaining after bleaching by expose to sunlight for various time of sample no. KK2.

Exposure of samples to 8 hr of sunlight removes all of the light-bleachable

## Total Bleach Method KK5

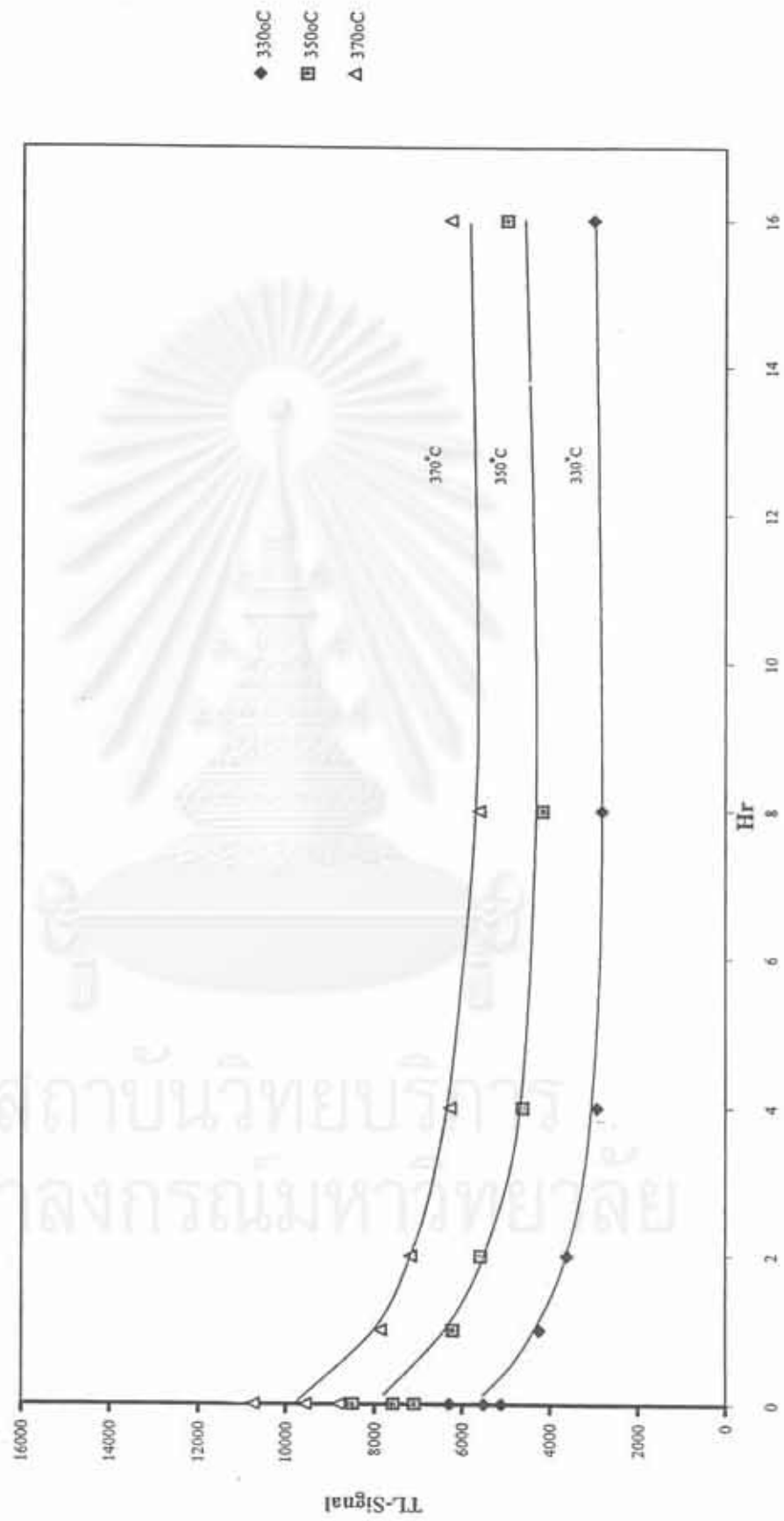


Figure 5.20 Thermoluminescence remaining after bleaching by expose to sunlight for various time of sample no. KK5.

## Total Bleach Method PT5

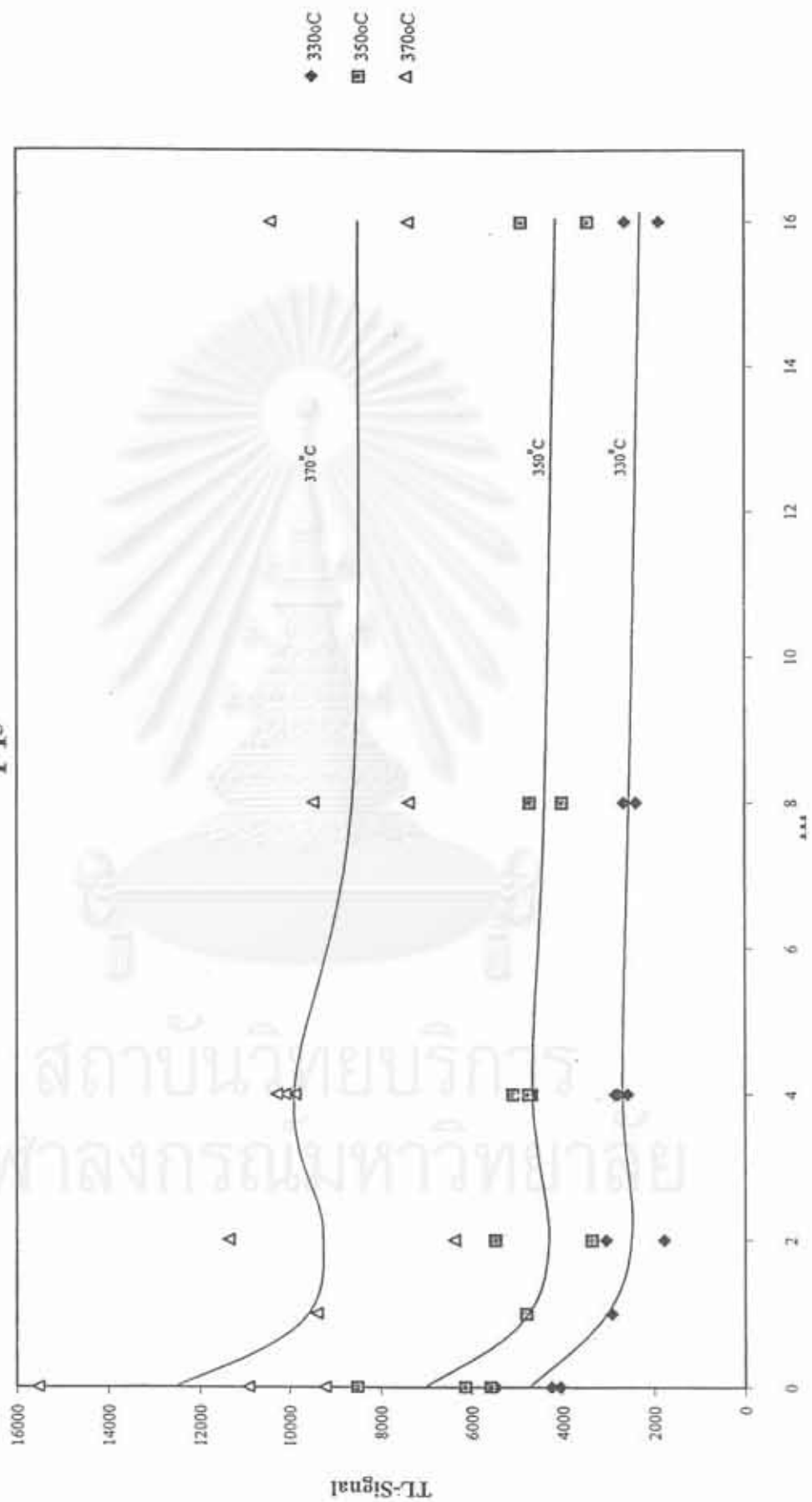


Figure 5.21 Thermoluminescence remaining after bleaching by expose to sunlight for various time of sample no. PT5.



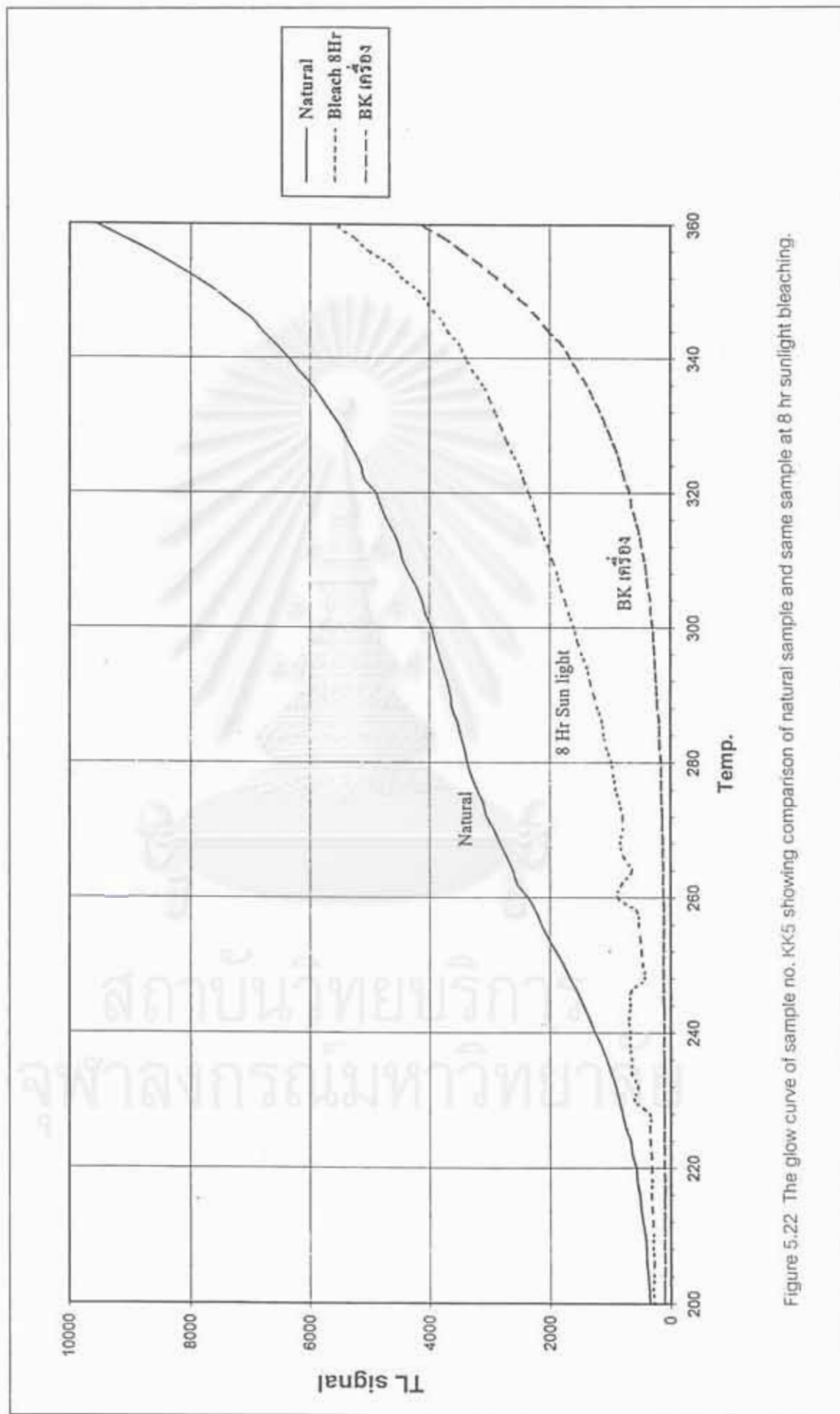


Figure 5.22 The glow curve of sample no. KK5 showing comparison of natural sample and same sample at 8 hr sunlight bleaching.

chosen temperature in sec. 5.5.1 was divided by average intensity of natural sample  $[Avr.(I_{nat})]$ .

The ratio of  $I_o / Avr.(I_{nat})$  was plotted on the y-axis of the growth curve. Then, the line was drawn from the ratio of  $I_o / Avr.(I_{nat})$  on y-axis to meet the growth curve, and drawn straight down to the x-intercept on x-axis. The value in x-intercept point is the residual TL Dose  $D(I_o)$  (Fig. 5.23). Then, the accumulated dose after deposit  $D(I_d)$  was computed by the  $D(I_{nat})$ , or paleodose, was minus by  $D(I_o)$ . However,  $D(I_{nat})$ ,  $D(I_o)$ , and  $D(I_d)$  were shown in Table 5.2.

## 5.6 Stability of Thermoluminescence Record; The Plateau Test

The thermal stability of the natural TL emission is checked by plotting the ratio of TL signal value on glow curve between natural sample and additive dose natural sample (TL value<sub>nat</sub>/TL value<sub>(N+β)</sub>). The plateau curves of all samples were shown in Appendix C-3. The plateau curves mostly display plateau starting at 225°C to 275°C. However, they do not represent well plateau, cause the curve to increase above the plateau value at higher temperatures, indicated that the samples were poorly TL resetting to zero by heated or exposed to sunlight, that is, the deeper trap would still contain electrons accumulated during geologic times (Aitken, 1985). This confirms that the resetting of the TL signal by sunlight to zero not complete. Then the correction of dated samples has to be used (see section 5.5.2).

## 5.7 Thermoluminescence Age Estimate

The TL age estimate after correction of sedimentary sample or the "*corrected age*", was calculated from Eq. 5.3 (see Sec. 5.5.2.1).

Errors in TL dating result derives mainly from sample preparation and TL measuring apparatus (av. 10%), (Takashima, personal communication), as well as standard deviation (SD) from measured values of ratio  $H+\gamma / N$  on growth curve. So equation for dating errors is described as

$$\text{Error} = \sqrt{(\text{SD})^2 + (0.10)^2} \dots\dots\dots (\text{Eq. 5.4})$$

The TL age of seven samples from Ban Kaeng Khaep Trench (location of samples were shown in Figs. 5.24 and 5.25), ten samples from Ban Pha Tawan I Trench

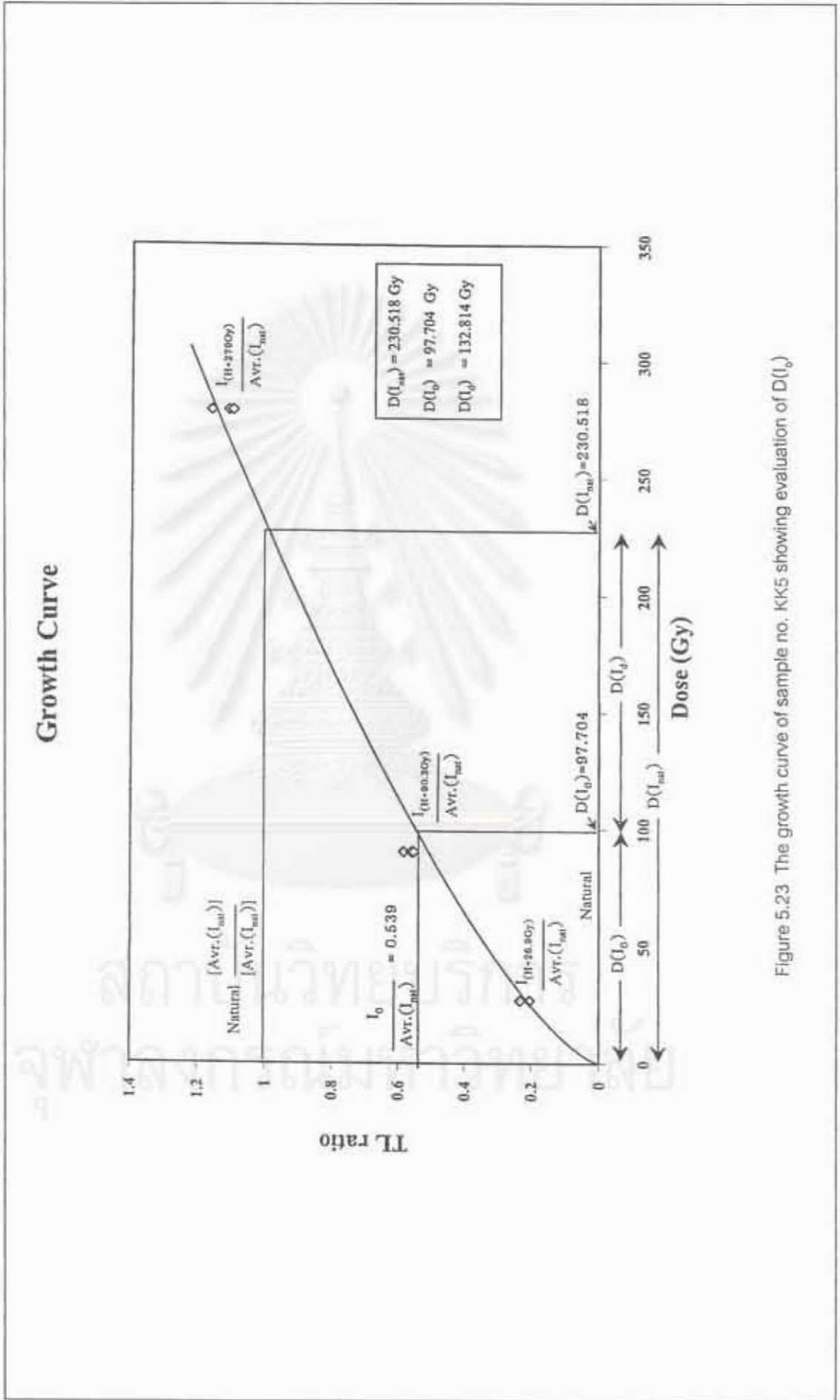


Figure 5.23 The growth curve of sample no. KK5 showing evaluation of  $D(I_0)$

(location of samples were shown in Fig. 5.26), and one samples from Ban Pha Tawan II Trench, were estimated from the applied regeneration method by Takashima and Watanabe (1990) with 8 hr bleaching by sunlight were displayed in Table 5.2.

## 5.8 Thermoluminescence Age of Sedimentary Unit

### 5.8.1 Dates of Ban Kaeng Khaep Trench (Figs. 5.24 and 5.25)

As shown in Figs. 5.24 and 5.25, this trench consists of three sedimentary units from top to bottom as chocolate brown colluvium, red colluvium, and brown sediment. Interpretation of TL age results is shown below.

**Chocolate colluvium.** The corrected ages of this unit from sample no. KK1 in the west trenching wall and KK5 in the east trenching wall are  $30.010 \pm 4.22$  and  $37.445 \pm 4.11$  ka, respectively. So, the age of this unit is about  $30.010 \pm 4.22$  to  $37.445 \pm 4.11$  ka.

**Red colluvium.** The corrected ages of this unit as determined from sample no. KK2 in the west trenching wall, and KK6 and KK7 in the east trenching wall are  $80.424 \pm 13.09$ ,  $77.048 \pm 11.25$ , and  $273.727 \pm 50.32$  ka, respectively. The date of sample KK7 is much old and probably regarded fictitious when compared with those of the KK2 and KK6 in the same unit. Beside, this unit shows loosely compacted sediment which indicates to young deposit; that is the 273.727 ka is too old for this unit. However, analytical error may occur on this sample that was described detail in section 5.9, and see Fig. C.2.4 in Appendix C. This unit is inferred that the age of this unit might be  $77.048 \pm 11.25$  to  $80.424 \pm 13.09$  ka.

**Brown sediment.** This unit was found only in the west wall. The corrected age of this unit was determined from sample no. KK3 is  $36.005 \pm 5.81$  ka. The date is younger than that of the upper unit. Perhaps this sediment is the catacomb of insects, as ants and termites. It was disturbed by bioturbation. The other corrected age is from sample no. KK4 which is  $34.261 \pm 6.03$  ka. This sample was collected from black mud ball that penetrates in bedrock with white vein. The date is younger than that of the upper unit. This unit may be replaced from bioturbation because it looks like animal's cavity.

Table 5.2 Age estimates for samples from Ban Kaeng Khaep and Ban Pha Tawan I and II Trench.

Ban Kaeng Khaep Trench

Sample No.	Ann. Dose (mGy/y)	$D(I_{nat})^a$ (Gy)	Apparent Age <sup>b</sup> (Ka)	$D(I_0)^c$ (Gy)	$D(I_d)^d$ (Gy)	Corrected Age <sup>e</sup> (Ka)
KK1	3.441	159.836	46.444 ± 6.53	56.557	103.279	30.010 ± 4.22
KK2	2.768	467.281	168.841 ± 27.48	244.701	222.581	80.424 ± 13.09
KK3	2.522	211.309	83.798 ± 13.51	120.517	90.792	36.005 ± 5.81
KK4	2.602	126.614	48.668 ± 9.40	37.480	89.134	34.261 ± 6.03
KK5	3.512	209.371	59.618 ± 6.55	77.868	131.503	37.445 ± 4.11
KK6	2.714	571.035	210.409 ± 30.73	361.931	209.104	77.048 ± 11.25
KK7	2.851	1085.718	380.758 ± 70.00	305.195	780.523	273.727 ± 50.32

Ban Pha Tawan I Trench

Sample No.	Ann. Dose (mGy/y)	$D(I_{nat})$ (Gy)	Apparent Age (Ka)	$D(I_0)$ (Gy)	$D(I_d)$ (Gy)	Corrected Age (Ka)
PT1	2.968	88.850	29.934 ± 4.32	59.776	29.074	9.795 ± 1.41
PT2	2.327	19.526	8.390 ± 1.08	19.016	0.510	0.219 ± 0.03
PT3	3.010	100.321	33.332 ± 4.57	83.013	17.308	5.751 ± 0.79
PT4	3.028	95.254	31.459 ± 3.76	67.430	27.823	9.189 ± 1.10
KK5	2.867	183.094	63.870 ± 9.64	91.228	91.866	32.046 ± 4.90
KK6	2.700	184.296	68.264 ± 9.61	85.333	98.963	36.656 ± 5.16
KK7	3.132	230.380	73.547 ± 11.87	130.696	99.684	31.823 ± 5.14
KK8	2.780	242.814	87.349 ± 12.26	105.684	137.130	49.331 ± 6.93
KK9	3.740	302.423	80.862 ± 10.40	187.076	115.347	30.842 ± 3.97
KK10	3.297	229.808	69.706 ± 9.94	163.782	66.026	20.027 ± 2.85

Ban Pha Tawan II Trench

Sample No.	Ann. Dose (mGy/y)	$D(I_{nat})$ (Gy)	Apparent Age (Ka)	$D(I_0)$ (Gy)	$D(I_d)$ (Gy)	Corrected Age (Ka)
PT1	3.702	405.394	109.499 ± 13.40	296.266	109.129	29.476 ± 3.61

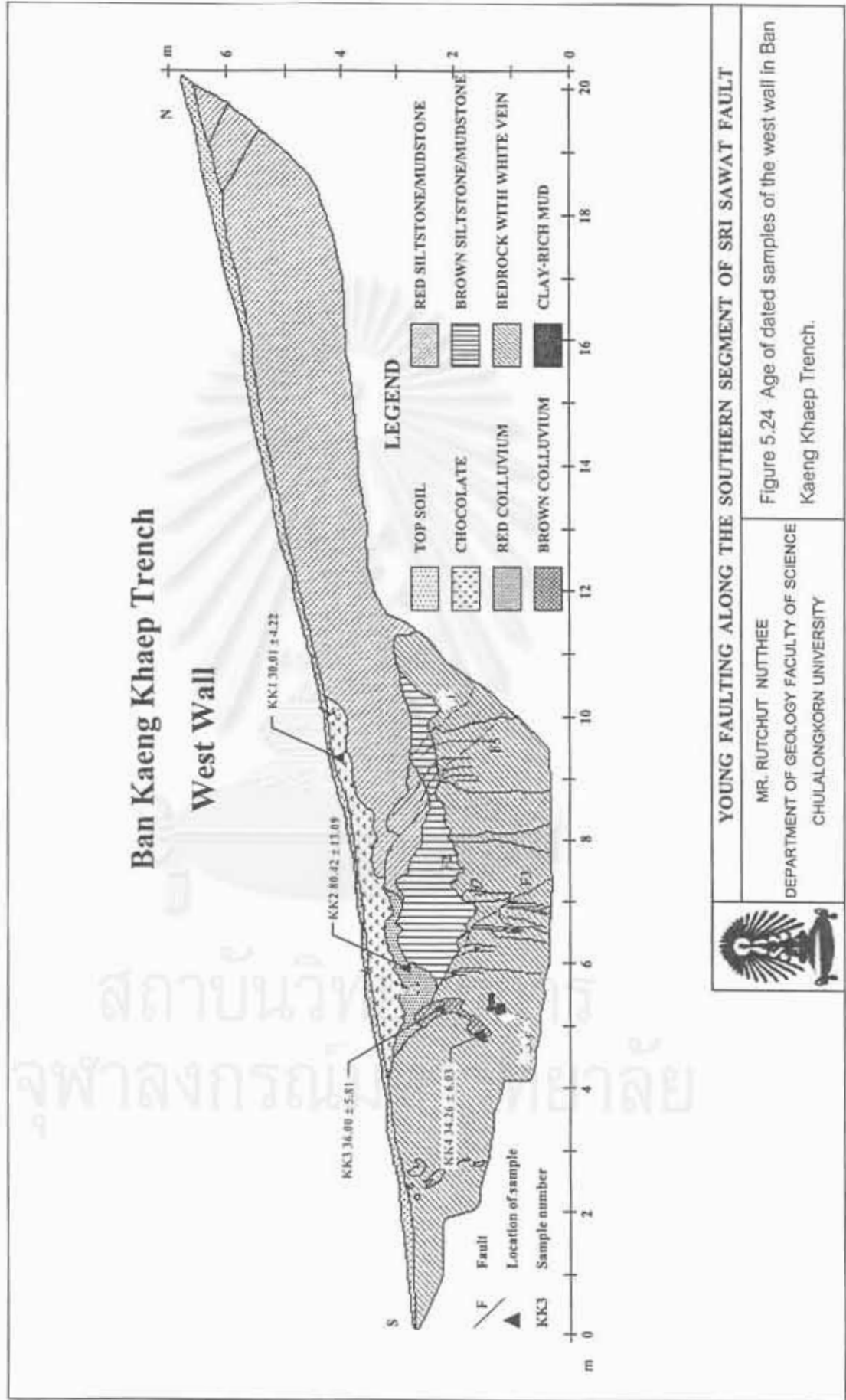
<sup>a</sup> $D(I_{nat})$  = Total accumulated dose or natural dose

<sup>b</sup>Apparent age = TL age estimate before the correction of sedimentary samples

<sup>c</sup> $D(I_0)$  = Residual TL dose

<sup>d</sup> $D(I_d)$  = Accumulated dose after deposit

<sup>e</sup>Corrected age = TL age estimate after the correction of sedimentary samples

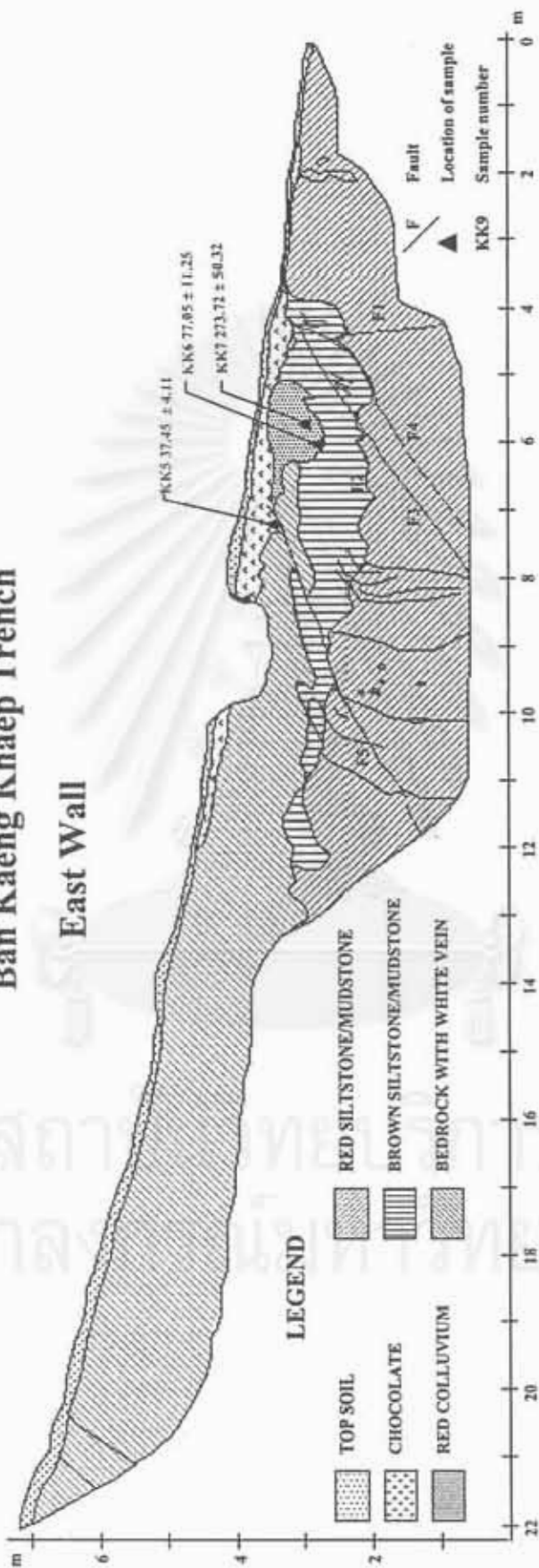


**YOUNG FAULTING ALONG THE SOUTHERN SEGMENT OF SRI SAWAT FAULT**  
 MR. RUTCHUT NUTTHEE  
 DEPARTMENT OF GEOLOGY FACULTY OF SCIENCE  
 CHULALONGKORN UNIVERSITY

Figure 5.24 Age of dated samples of the west wall in Ban Kaeng Khaep Trench.

# Ban Kaeng Khaep Trench

## East Wall



YOUNG FAULTING ALONG THE SOUTHERN SEGMENT OF SRI SAWAT FAULT

MR. RUTCHUT NUTTHEE

DEPARTMENT OF GEOLOGY FACULTY OF SCIENCE  
CHULALONGKORN UNIVERSITY

Figure 2.25 Age of dated samples of the east wall in Ban Kaeng Khaep Trench.

## 5.8.2 Dates of Ban Pha Tawan I Trench (Fig. 5.26)

### Northwest Trenching Wall

**Layer A.** This unit is a topsoil layer. It contains fine-grained sediment. The corrected ages determined from sample nos. PT1 and PT2 are  $9.795 \pm 1.41$  and  $0.219 \pm 0.03$  ka, respectively.

**Layer B.** This unit is coarse-grained colluvium. The collected age determined from sample no. PT3 is  $5.751 \pm 0.79$  ka.

**Layer C.** This unit is fine-grained colluvium. The collected age was determined from sample no. PT4. The date of this layer is about  $9.189 \pm 1.10$  ka.

**Layer E.** This unit is fine-grained colluvium. The collected ages were determined from sample no. PT5 and PT6. The age of this layer is about  $32.046 \pm 4.90$  to  $36.656 \pm 5.16$  ka.

**Layer G;** This unit is fine-grained colluvium. The collected ages were determined from sample no. PT7 and PT8. The age of this layer is about  $31.823 \pm 5.14$  to  $49.331 \pm 6.93$  ka. The  $31.823 \pm 5.14$  ka of sample PT7 is younger age than upper units, that is analytical error may occur on this sample (see detail in section 5.9, and see Fig. C.2.8 in Appendix C).

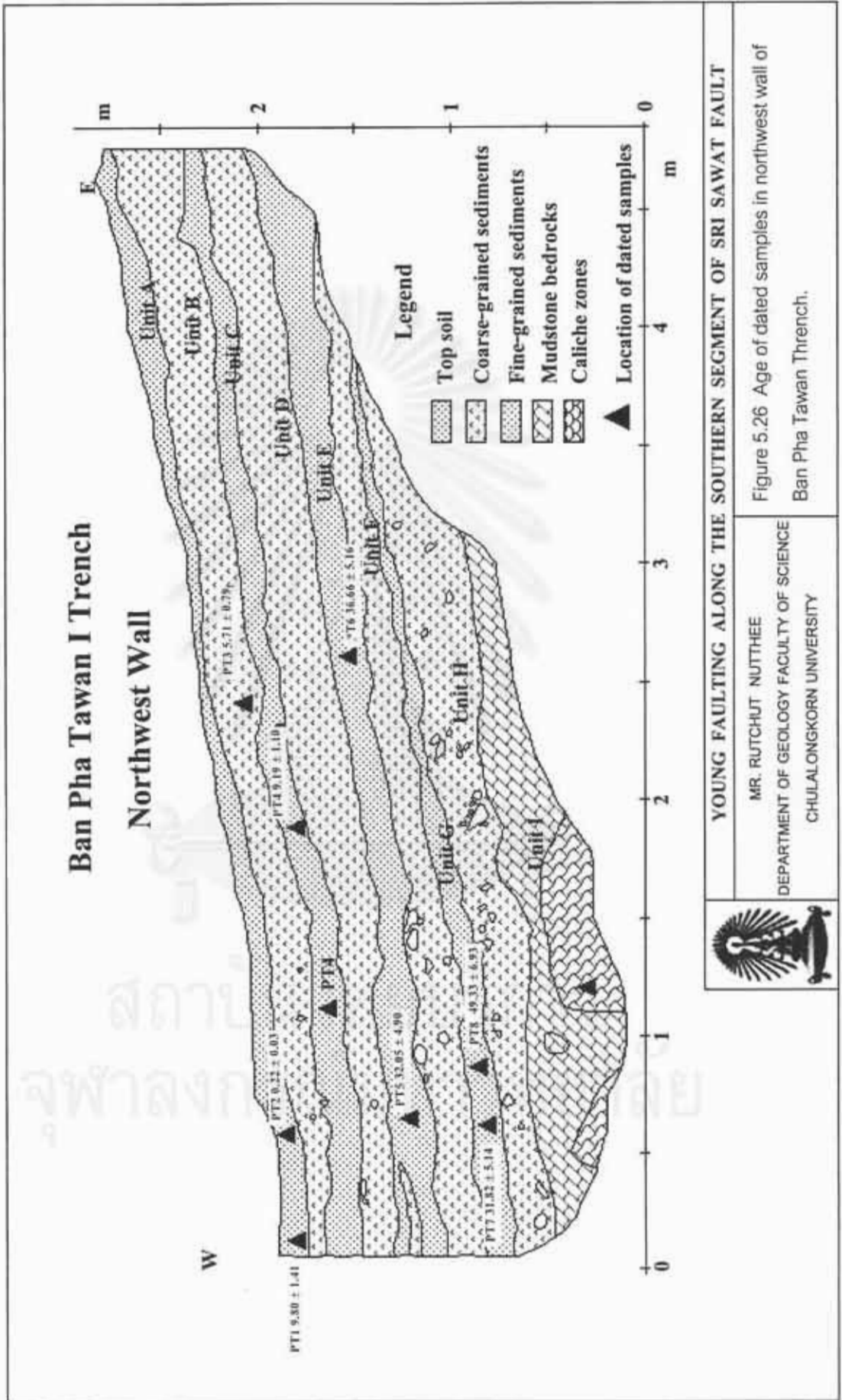
Southeast Trenching Wall (locations of collected sample were shown in Fig 4.15)

The sediment in this area is coarse-grained colluvium. It shows structureless feature. The corrected age of this unit was determined from sample nos. PT9 and PT10. The date of this colluvium is about  $20.027 \pm 2.85$  to  $30.842 \pm 2.85$  ka.

## 5.8.3 Dates of Ban Pha Tawan II Trench (location of collected sample were shown in Fig 4.17)

The sediment in this area is coarse-grained colluvium. The corrected age of this unit was determined from sample no. PT11. The age of this colluvium is about  $29.476 \pm 3.61$  ka.





YOUNG FAULTING ALONG THE SOUTHERN SEGMENT OF SRI SAWAT FAULT

MR. RUTCHUT NUTTHEE  
DEPARTMENT OF GEOLOGY FACULTY OF SCIENCE  
CHULALONGKORN UNIVERSITY

Figure 5.26 Age of dated samples in northwest wall of Ban Pha Tawan Trench.

## 5.9 Suggestion of TL Dating Results

1) In paleodose evaluation such as those of some dated samples (i.e. KK2, KK6, KK7, PT6 and PT11: see Appendix C-2), no values of irradiated samples are close to 1 on the growth curve. So, uncertainties may happen on the paleodose evaluation. Therefore to avoid this situation, before irradiation of the natural sample, intensity measurement of individual natural samples are significantly required. Moreover, the heated samples should be irradiated in several dosages for the betterment of growth curve. Analytical error occurred on some samples; not occurred on all of dated samples. However, most ages of dated samples are in acceptable range, although analytical error was occurred.

2) The number of samples corrected in each unit are small and age of some samples is not good sequence because of analytical error and bioturbation. Therefore, number of samples should be more than this for more reliable data of individual units.

3) In the correction of age determination, the samples were bleached by 8 hr sunlight to reset TL signals. However, it is possible that the dated colluvial sediments may have not been exposed to the long period of sunlight. This give rise to the "overbleaching" of TL signals. Then the  $I_0$  is large amount than it was, and the paleodose becom smaller. Consequently, "overbleaching" produces TL-age underestimation (Berger, 1984; Huntley, 1985; Rodbell et al., 1997), and results in younger age than the true age.

4) The TL age estimate should be confirmed by comparison with other dating methods such as  $^{14}\text{C}$  or ESR dating, for the best results.

## CHAPTER VI

### DISCUSSION AND CONCLUSION

In this chapter, all available information and results obtained from the previous chapters are used for discussing behavior of faults, sequence of fault movement, ages of fault movement, and estimation of slip rate and earthquake magnitude of the Sri Sawat Fault (SSF).

#### 6.1 Behavior of Ancient Movement

The aerial photograph interpretation in the study area supports that the southern segment of SSF is estimated to be as long as 11 km with the N50°W trend. The support for this part of the SSF is displayed by sharp lineaments, young sedimentation and several clear morphotectonic features. Well-defined fault scarps, sets of triangular facets, offset streams and shutter-ridges, advocate the youthfulness of the fault.

The offset streams along the 11 km-long of southern SSF indicate that this fault shows right-lateral displacement and the distance of offset stream measured by our detailed survey is about 54 m. Furthermore, the offset of soils and pediments observed from the recent road-cut exposures strongly indicates the local reverse faulting of the SSF (Fig. 3.28). In addition, the fault in Ban Kaeng Khaep Trench, which shows a contact between bedrock without white vein (Unit 6) and bedrock with white vein (Unit 7), is reverse faulting. Consequently, this fault is regarded as the oblique slip fault shown as a block diagram in Fig. 6.1.

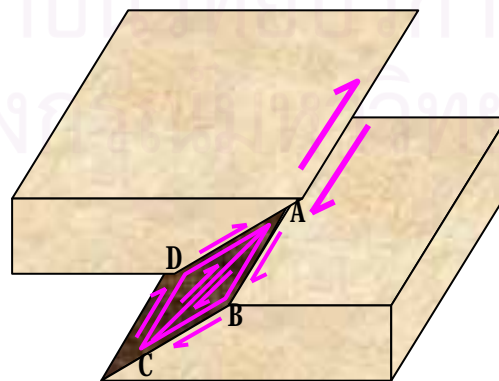


Figure 6.1 Schematic of oblique slip movement of southern segment of SSF. Note that AB and AD represent apparent lateral-slip components, AD and BC represent apparent vertical components, and AC is a resultant component with the oblique slip movement.

As the 1.2 m of vertical movement is less significant comparing with 54-m of horizontal movement, therefore the right-lateral strike-slip movement is the major component of this oblique-slip fault movement.

## 6.2 Sequence of Fault Movements

The colluvial deposition in Ban Pha Tawan Trench<sup>1</sup> shows stratigraphy of eight alternated sedimentary layers of colluviums with coarse- and fine-grained interbeds. Poor sorting and highly angular fragments (or talus) suggesting rapid deposition provide good evidence for “debris facies”. On the contrary, fine-grained layer composed mostly silty sand to clay suggest low-energy and slow deposition by surface wash processes. They were inferred to occur during the periods of slope stability between the faulting events. Therefore, these eight coarse- and fine-grained colluvium layers are inferred to represent four episodes of past faulting earthquake.

The aerial interpretation of the southern segment of SSF shows the escarpment comprises a series of triangular faceted spurs (Fig. 3.5) interrupted by several benches (Figs. 6.2 and 6.3) and erosional pediment remnants (Fenton et al., 1997). Hamblin (1976) has shown that such features were the result of episodic fault movement. These facets were formed during periods of fault movement and the benches may have formed during periods of tectonic stability, erosion and fault scarp retreat (Fig. 6.4). The erosional benches along this fault, especially around Khao Wang Masang Mt., show 3 steps of benches support multiple episodes of fault movement in the past.

Nevertheless, the occurrence of four-step erosional benches at Khao Wang Masang Mt. may be older than what was indicated as a young movement. So, they may not correspond with that of the colluvial layers due to the ages of bench are probably older than the ages of colluvium layers in station 3.

## 6.3 Constraint on Earthquake Events

In this current study, all TL-dated samples were collected from fault-related colluviums on trenching walls, i.e., Ban Kaeng Khaep Trench, Ban Pha Tawan I Trench, and Ban Pha Tawan II Trench.



Figure 6.2 Aerial photograph showing the erosional bench in study area. A-A' is a line of cross section through Khao Wang Masang Mt. in Fig. 6.3.

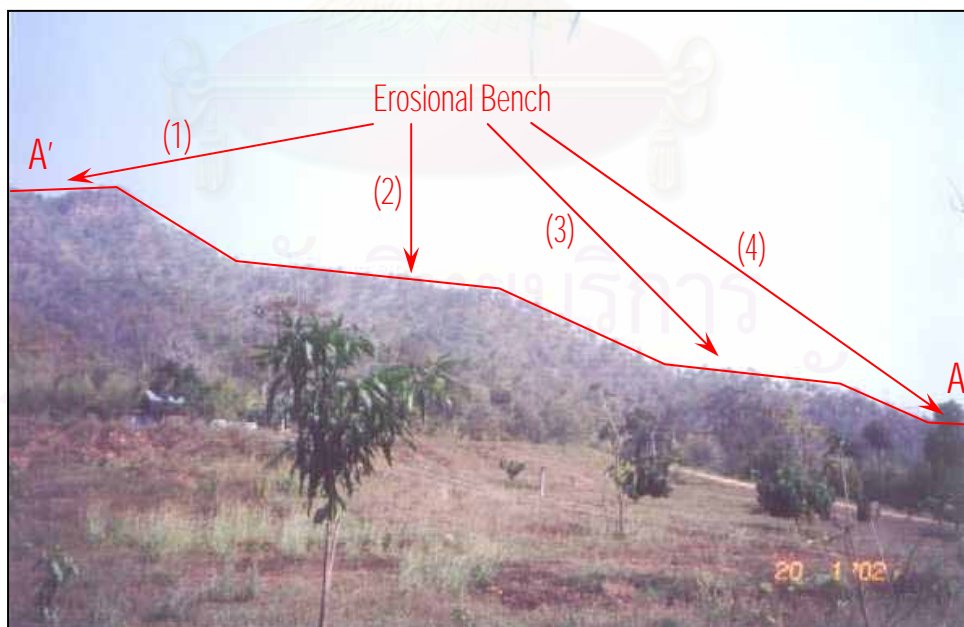


Figure 6.3 A cross-section along the A-A' line in Fig. 6.2 showing 4 steps of erosional benches in Khao Wang Masang Mt.

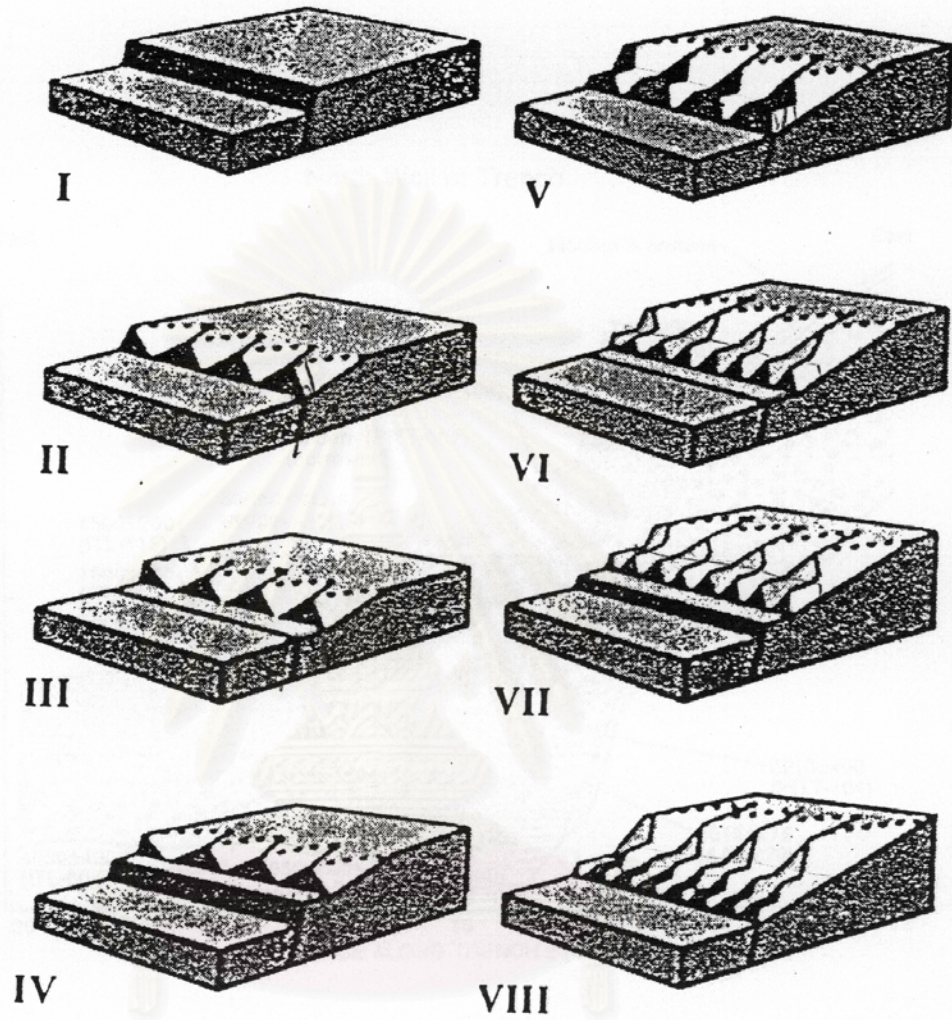


Figure 6.4 Schematic showing step of fault movement which produce the erosional bench (Hamblin, 1976)

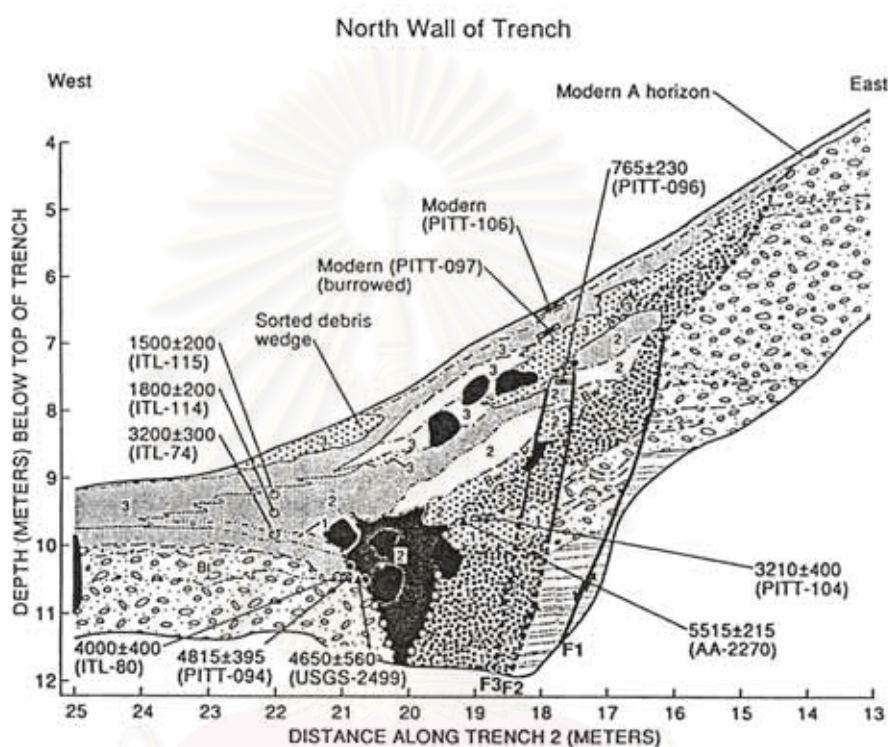


Figure 6.5 Cross section of part of the Wasath Fault in California, USA, showing wedge-like layer of colluvial sediments (darker colors; Unit 2) interpreted as a result of earthquake faulting (Forman et al., 1991). Numbers of ITL indicate TL dates and the others indicate  $^{14}\text{C}$  dates of samples.

สถาบันวิทยบริการ  
จุฬาลงกรณ์มหาวิทยาลัย

At Ban Kaeng Khaep Trench, two sedimentary units were considered for ages of faulting are red colluvium and chocolate colluvium. The red colluvium shows wedge-shaped body deposited following faulting event. Similar situation occurred for the colluvium wedges deposited in trenches excavated across fault scarps on the Weber Segment of the Wasatch Fault Zone by Forman et al. (1991) (Fig. 6.5). The dates of fault-related red colluvium wedge which are the oldest dates, therefore, indicate the first earthquake faulting may have occurred immediately prior to deposition of the red colluvium. We consider that the age of this faulting might be little older than that of red colluvium more than 80.4 ka B.P. The occurrence of coarse-grained gravels in unit H at Ban Pha Tawan Trench (Fig. 6.6) supports this fault activity. No sample was collected for TL age activity in this unit.

After red-colluvial deposition, the fault may have re-activated during 36.0-77.1 ka B.P. as evidenced by the appearance of the chocolate coarse-fragment colluvium deposited over the red colluvium. This chocolate colluvium with 30.2-36.8 ka date corresponds to the unit E with 32.1-36.7 ka date in Ban Pha Tawan I Trench. The second faulting may have occurred before deposition of the chocolate colluvium and the Unit E but after deposition of red colluvium. This faulting is responsible for the deposition of coarse-grained gravels (Unit F) without any confirmation of TL dating. So, the second faulting should have occurred between 36.7-49.3 ka B.P.

Moreover, we found that the wedge-shaped body in chocolate colluvium layer (Fig. 4.11), which corresponding to Unit E in Ban Pha Tawan I Trench, were cut by fault. So, this subsequent faulting may have occurred after deposition of the chocolate colluvium (and the Unit E) but before that of 9.2 ka of Unit C. The third faulting may have caused deposition of the undated Unit D. However, the sediment of Unit D is regarded equivalent to the gravel layer on southeast trenching wall in Ban Pha Tawan I Trench with the dates of 20.0-30.8 ka. Moreover, The presence of the 29.5 ka of gravel layer in Ban Pha Tawan II Trench provides a good support for this earthquake event. So, the third earthquake faulting may have taken place between 29.5-30.0 ka B.P.

The debris sediments of Unit B, which probably occurred by earthquake activity, deposited during 5.8 ka B.P. So, the latest (fourth) earthquake may have triggered (after the Unit C but before the Unit B) during 5.8 and 9.2 ka B.P.



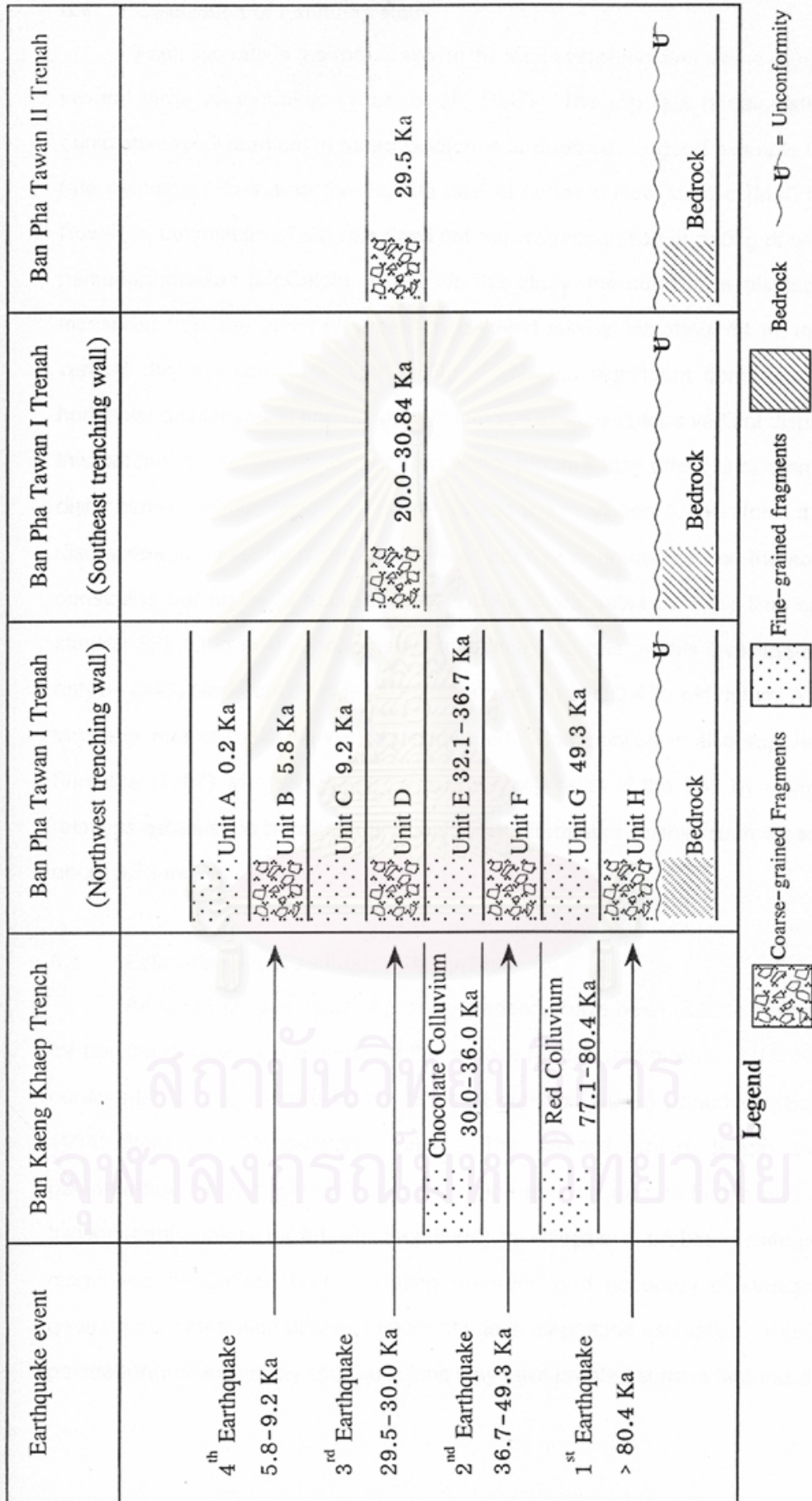


Figure 6.6 Schematic showing event of earthquakes and their ages; considered by stratigraphy and TL age dating result of Ban Kaeng Khaep Trench, Ban Pha Tawan I Trench and Ban Pha Tawan II Trench.

## 6.4 Calculation of Fault Slip Rate

Fault slip rate is the rate of slip on the fault averaging over a time period involving several large earthquakes (Yeast et al., 1997). The slip rate is calculated from the cumulative displacement of dated landforms or deposits. A good example for such slip rate calculation is that of the Pajarito fault of northern New Mexico (McCalpin, 1995). However, calculation of slip rate does not require recognition or dating of any individual paleoearthquakes (McCalpin, 1996). In this study, the cumulative displacement was measured from the offset of stream by detailed survey; viz about 54 m, due to 1.2-m vertical displacement in station 5 (Fig. 3.27) less significant comparing with 54-m horizontal displacement and no another location to shows better vertical displacement in this present study. In addition, the erosional process may effect to decrement of fault displacement which exposed on ground surface in station 5, therefore, it is not true displacement. Small numbers of paleoearthquakes characterized on the southern SSF constrains our ability to access the variability of slip rates over the time span for the studied SSF. Due to Holocene geologic setting, slip rate on this investigated fault can only be calculated from cumulative displacement on the 80.4 ka-old datum. A mean long-term slip rate of 0.672 mm/yr was computed. Confirmation is also supported that of Shrestha (1987) who estimated the average slip rates of the SSF by using empirical relations established between earthquake magnitude and seismic source parameters at about 0.73 mm/yr.

## 6.5 Estimating Paleearthquake Magnitude

Although various types of primary evidence have been used to infer magnitudes for paleoearthquakes, the length of the surface rupture and maximum displacement on continental fault traces are by far the most commonly used parameter (Bonilla et al., 1984; Wells and Coppersmith, 1994). The inferred rupture length and slip for paleoearthquakes are compared to worldwide data on rupture length and slip during historic earthquakes (of known magnitude) to estimate a probable paleoearthquake magnitude (McCalpin, 1996). Dating precision and accuracy of stratigraphic and geomorphic correlation play an important role in magnitude estimation. This is between paleoearthquakes closely spaced in time may have created surface features that appear

to the product of one large paleo earthquake after thousand year (see McCalpin, 1996). Moreover, two sources of uncertainties exist in the SRL method as noted by Bonilla et al. (1984), and Fumal et al. (1993). The first source is from deficiencies in the lengths cited in the historical data set, and the second source is by difficult in accurately measuring the length of prehistoric rupture.

Paleoearthquake magnitudes have traditionally been estimate from primary fault-zone evidence (surface rupture length or displacement), rather than from secondary ground-shaking evidence. The earlier approach was to compare the inferred rupture length (L) or maximum displacement (D) from a paleoearthquake with the corresponding measurements from historic earthquakes of known magnitude.

Surface rupture length method of paleomagnitude estimate involves estimating the length of prehistoric surface rupture, and comparing its length to the surface rupture lengths (SRLs) of historic earthquakes of known magnitude. The most recently analyzed historic data set for this comparison is that of Wells and Coppersmith (1994), although similar plots are presented by Slemmons (1982), Bonilla et al. (1984), Heaton et al. (1986), and Khromovskikh (1989). Wells and Coppersmith's regression of surface rupture length on moment magnitude ( $M_w$ ) (see Appendix A) for 77 worldwide earthquakes of all slip type is shown in Fig. 6.7. The historical data range from  $M_w$  5.8 to 8.1. Table 6.1 shows some of Wells and Coppersmith's regression relationship. Although, regression may be made for different styles of faulting (strike-slip, thrust, or normal), Wells and Coppersmith (1994) concluded that the difference were not large.

In this study, the equation for all fault types (Eq. 6.1) was used for estimating a paleoearthquake magnitude of the southern segment of the SSF.

$$M = 5.08 + 1.16 \log(\text{SRL}) \dots \dots \dots (6.1)$$

Where M is Moment magnitude ( $M_w$ )

SRL is Surface rupture length (km)

Base on the Landsat TM5 imagery and aerial photograph interpretation, the length of the studied southern segment of the SSF is about 11 km (see also Fig. 6.7). Therefore, the paleoearthquake magnitude is about 6.29  $M_w$ . To prove this, probable paleoearthquake magnitudes are also calculated from the equation quoted in Table 6.1; and the range of 6.23 to 6.33  $M_w$  are cited.

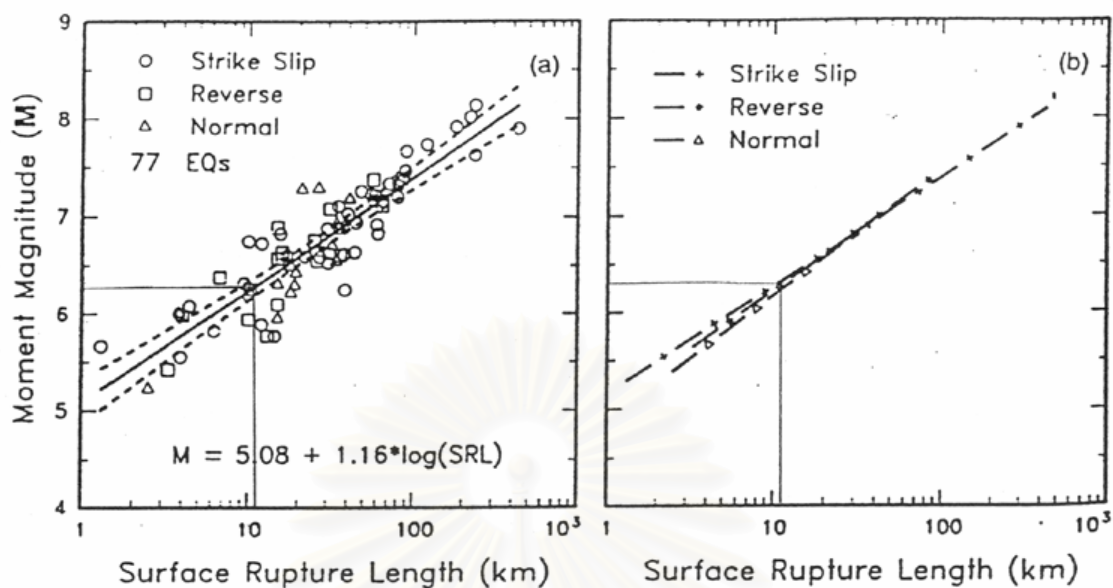


Figure 6.7 Surface rupture length (SRL, in km) as a function of movement magnitude (M) for 77 earthquakes in the historic data set of Wells and Coppersmith (1994). Equation at bottom lists regression of M on log SRL for all fault types. Note that in part (b) there is a little difference between the relationships for the three fault types. (From Wells and Coppersmith, 1994)

Table 6.1 Empirical relationships between moment magnitude (M) and fault parameters (Wells และ Coppersmith, 1994)

Equation	Slip type <sup>2</sup>	Number of events	Coefficients and standard errors		Standard deviation	Correlation Coefficient (r)
			a	b		
$M = a + b \cdot \log(\text{SRL})^1$	SS	43	5.16	1.12	0.28	0.91
	R	19	5.00	1.22	0.28	0.88
	N	15	4.86	1.32	0.34	0.81
	All	77	5.08	1.16	0.28	0.89

<sup>1</sup> SRL, Surface Rupture Length

<sup>2</sup> SS, strike-slip; R, reverse; N, normal; All, all fault types.

## CHAPTER VII

### CONCLUSIONS AND RECOMMENTATION

#### 7.1 Conclusion

Base upon Landsat TM5 imagery and aerial photographic interpretation with detailed field investigation, and TL-dating results, conclusions can be drawn for the southern segment of the Sri Sawat Fault as follows;

1. The southern segment of the SSF is about 11 km long. Behavior of this segment shows oblique strike slip movement with the right lateral and reverse components.

2. Geochronological results together with morphotectonic and structural field analysis point to the four events of past earthquake faulting i.e., the prior 80.4 ka event, the 36.7 to 49.3 ka, the 29.5 to 30.0 ka and 5.8 to 9.2 ka events.

3. The studied southern segment of the SSF is regarded as the active fault because the last faulting event occurred during a period of 11,000 years (Holocene time)

4. The measurement of offset stream and TL age results, allows calculating an average slip rate, based on method described by McCalpin (1996), to be about 0.672 mm/year.

5. The fault length of 11 km indicates the surface rupturing of paleoearthquakes on the southern segment of the SSF, based on method described by Wells and Coppersmith (1994), to be  $M_w$  magnitudes of 6.29.

#### 7.2 Recommendation

This present study is a detailed study of southern segment of SSF which no any other similar works were previously conducted. It demonstrates and measures their activity in terms of historical or prehistorical large earthquakes. The special techniques such as; trenching, detailed surveying, and dating of sample, were used in this study. The study leads to result in terms of fault segmentation, ages of faulting events, average slip rate, and maximum paleo-magnitude.

This study reveals few results, if compare with the similar study in worldwide scale, for example, Porat et al. (1996) determined age of fault-related alluvial fan sediments by luminescence dating in southern Arava Valley, Israel. More than twenty trenches have been

excavated across fault scarp and terrace risers, in both active channels and the alluvial fan. Moreover, in Thailand, Kosuwan et al. (personal contact) studies the neotectonics of Mae Chan Fault. They have been excavated nine trenches and dated sample more than 120 sample by TL and  $^{14}\text{C}$  dating method.

The paleoseismology of the SSF should be more studied in the future for ascertainment of data and information. The good paleoseismic data is necessary for seismic hazard assessments (SHAs) in this area. The age of faulting should be considered and relied on more samples, and other dating methods that will be obtained.

However, the present study indicates, though a low chance, that this fault is considered to be of interest, regarding that large associated earthquakes possibly occur in the future.



สถาบันวิทยบริการ  
จุฬาลงกรณ์มหาวิทยาลัย

## REFERENCES

- Adam, J., Wetmiller, R. J., Hasegawa, H. S. and Drysdale, J. (1991). The first surface faulting from a historic intraplate earthquake in North America. Nature (London) 352: 617-619.
- Aitken, M. J. 1967. Thermoluminescence. Science Jour. 1: 32-38. Cited in Mebus A. Geyh and Helmut Schleicher (eds.), Absolute age determination: Physical and chemical dating methods and their application. Berlin: Springer-Verlag, 1990.
- Aitken, M. J. 1978. Dose rate evaluation. PACT Journal 2:18-33.
- Aitken, M. J. 1985. Thermoluminescence Dating. London: Academic.
- Aitken, M. J. and Wintle, A. G. 1977. TL dating of calcite and burnt flint; the age relation for slices. Archaeometry 19: 100-105.
- Alderson, A., Holmes, N. A. and Murphy, C., 1994. A summary of the biostratigraphy and biofacies for the Tertiary sequence, Gulf of Thailand. In P. Angsuwathana, T. Wongwanich, W. Tansathein, S. Wongsomsak, and J. Tulyatid (eds.), Proceedings of the International Symposium on Stratigraphic Correlation of Southeast Asia, pp. 292-295. Bangkok: International Geological Correlation Project 306.
- Allen, C.R., 1986. Seismological and paleoseismological techniques of research in active tectonics. In R. E. Wallace (chairman), Active Tectonics: Studies in Geophysics, pp. 148-154. Washington, DC: National Academy Press.
- Allen, C. R., Gillespie, A. R., Huan, H., Sieh, K. E., Buchanan, Z. and Chengnan, Z. 1984. Red River and associated faults, Yunnan Province, China: Quaternary geology, slip rates, and seismic hazard. Geological Society of America Bulletin 95: 686-700.
- Aramprayoon, B. 1981. Photolineament and folding map of Thailand, scale 1:1,000,000. Photogeologic Section, Geological Survey Division, Department of Mineral Resources.
- Atkinson, G. M., and Boore, D. M. 1987. On the  $m_N$ , M relation for eastern North American earthquakes. Seismological Research Letters 58: 119-124.
- Bath, M. 1981. Earthquake magnitude; recent research and current trends. Earth Science Reviews 17: 315-398.

- Bell, W. T. 1979. Thermoluminescence dating: Radiation dose-rate data. Archaeometry 21: 243-245.
- Beloussov, V. V. 1980. Geotectonics. Springer-Verlag: Berlin.
- Berger, G. W. 1984. Thermoluminescence dating studies of glacial silts from Ontario. Canadian Journal of Earth Science. 21: 1393-1399.
- Bolt, B. A. 1999. Earthquakes. 4<sup>th</sup> ed. New York: W. H. Freeman and Company.
- Bonilla, M. G. 1969. Surface faulting and related effects. In Earthquake Engineering, pp. 47-74. New Jersey: Prentice-Hall.
- Bonilla, M. G., Mark, R. K., and Lienkaemper, J. J. 1984. Statistical relation among earthquake magnitude, surface rupture length, and surface fault displacement. Bulletin of the Seismological Society of America 74: 2379-2411.
- Boore, D. M., and Joyner, W. B. 1994. Prediction of ground motion in North America. In Proceedings of the ATC-35 Seminar on New Development of earthquake Ground Motion Estimates and Implications for Engineering Design Practice, pp. 6-1 to 6-14. CA: Redwood City.
- Brown, G. F. et al. 1951. Geologic reconnaissance of the mineral deposit of Thailand. United States Geological Survey Bulletin 984: 21.
- Bunopas, S. 1976. Geology of map Changwat Suphan Buri, Sheet ND 47-7, Scale 1:250,000. Report of Investigation, Number 16, Volume 1 and 2. Geologic map and text. Bangkok : Department of mineral Resources.
- Bunopas, S. 1981. Paleogeographic history of western Thailand and adjacent part of southeast Asia: A plate tectonic interpretation. Doctoral dissertation, Graduate School, Victoria University of Wellington.
- Bunopas, S. and Vella, P. 1983. Tectonic and geologic evolution of Thailand: In Proceedings of the Workshop on Stratigraphic Correlation of Thailand and Malaysia, pp. 307-322. September 1983. Haad Yai: Thailand.
- Bunopas, S. and Vella, P. 1992. Geotectonics and geologic evolution of Thailand. In C. Piancharoen (ed.), Proceedings of a National Conference on Geologic Resource of Thailand: Potential for Future Development, pp. 209-228. Supplementary Volume, Department of Mineral Resources, Bangkok: Thailand.



- Chantaramee, S., Thanadpipat, C., Wattanikorn, K., Hararak, M., and Jitapunkul, S. 1981. Tectonic pattern of west and northwest Thailand (in Thai). Unpublished report prepared for National Research Council of Thailand: Bangkok.
- Charusiri, P., Charusiri, B., Hinthong, C., Vivattananon, P. and Daorerk, V. 2002. Some aspects of tectonic activity and its relationship to seismicity in Thailand. Journal of Southeast Asian Earth Sciences. (in prep.)
- Charusiri, P., Daorerk, V., and Kosuwan, S. 2001. Earthquakes not far from us (in Thai). Scientific Journal (March-April): 76-91. (Unpublished Manuscript)
- Charusiri, P., Daorerk, V., Supajanya, T. and Charusiri, B. 2002. Applications of enhanced remote-sensing techniques to geological structures related to earthquakes and earthquake-prone areas in Thailand and neighbouring areas: A preliminary investigation. Journal of Thai Geosciences. (in prep.)
- Charusiri, P., Kosuwan, S., Tuteechin, W., Vejbunthoeng, B., Suwanweerakumthorn, R., and Thanapongsakul, T., 1997. The study of causes of earthquake in Thailand concern with geological structure of southeast Asia by using satellite imagery Landsat TM5 (in Thai). National Research Council of Thailand: Bangkok. (Unpublished Manuscript)
- Chuaviroj, S. 1991. Geotectonic of Thailand (in Thai). Bangkok: Geological Survey Division, Department of Mineral Resources.
- Cluff, L. S., and Bolt, B. A. 1969. Risk from earthquakes in the modern urban environment with special emphasis on the San Francisco Bay Area, urban environmental geology in the San Francisco Bay region. In Association Engineering Geologist Sacramento, pp. 25-64. California: San Francisco Section Special Public.
- Cornell, C. A. 1968. Engineering seismic risk analysis. Bulletin of the Seismological Society of America 58: 1583-1606.
- Crone, A. J., and Omdahl, E. M., (eds.). 1987. Directions in Paleoseismology, Proc. Of Conf. XXXIX United States Geological Survey Open File Report. 87-673: 1-456.
- Crone, A. J., Machette, M. N., and Bowman, J. R. 1992. Geologic investigations of the 1988 Tennant Creek, Australia, earthquakes- implications for paleoseismicity in stable continental regions. United States Geological Survey Bulletin 2032-A: A1-A51.

- Daniels, F., Botd, C. A., and Saunders, D. F. 1990. Thermoluminescence (TL) method. In M. A. Geyh and H. Schleicher (eds.), Absolute age determination: Physical and chemical dating methods and their application, pp. 256-217. Berlin: Springer-Verlag.
- dePolo, C. M., and Slemmons, D. B. 1990. Estimation of earthquake size for seismic hazards. In E. L. Krinitsky and D. B. Slemmons (eds.), Neotectonics in Earthquake Evaluation, Geol. Soc. Am., Rev. Eng. Geol. 8: 1-28.
- Ding, Y.Z., and Lai, K.W. 1997. Neotectonic fault activity in Hong Kong: evidence from seismic events and thermoluminescence dating of fault gouge. Journal of Geological Society 154: 1001-1007.
- Ducrocq, S., Buffetaut, E., Buffetaut-Tong, H., Chaimanee, Y., Jaeger, J. J., Lacassin, R. and Suteethon, V. 1992. Tertiary continental basins of Thailand as a result of strike-slip motions induced by the India-Asia collision. Journal of Southeast Asian Earth Sciences, 7: 260.
- Ekström, G. A., 1987. A broad band method of earthquake analysis. Ph.D. Thesis, Harvard University, Cambridge.
- Electric Power Development Co., Ltd. 1973. Supplementary report for Quae Yai No.1 Project. Tokyo: Japan.
- Fenton, C. H., Charusiri, P., Hinthong, C., Lumjuan, A., and Mangkonkarn, B. 1997. Late Quaternary faulting in northern Thailand. In Prisit Dheeradilok et al. (eds.), Proceedings of the International Conference on Stratigraphy and Tectonic Evolution of Southeast Asia and the South Pacific, pp. 436-452. Bangkok: Department of Mineral Resources.
- Fleming, S. L., 1969. The acquisition of radio thermoluminescence by ancient ceramics. Ph.D. Thesis, University of Oxford.
- Forman, S.L., Bettis, E. A., III, Kemmis, T. J., and Miller, B. B. 1992. Chronologic evidence for multiple periods during the Late Pleistocene in the Missouri and Mississippi River Valleys, U.S.: Implications for the activity of the Laurentide ice sheet. Palaeogeography, Palaeoclimatology, Palaeoecology 20: 71-83.
- Forman, S.L., Nelson, A.R., and McCalpin, J.P. 1991. Thermoluminescence dating of faulting-Scarp-derived colluvium: Deciphering the timing of paleoearthquake on the

- Weber Segment of the Wasatch fault zone, North Central Utah. Journal of Geophysical Research 96: 595-605.
- Fumal, T. E., Pezzopane, S. K., Weldon, R. J., II, and Schwartz, D. P. 1993. A 100-year average recurrence interval for San Andreas fault at Wrightwood, California. Science 259, 199-203.
- Geyh, M. A., and Schleicher, H. (eds.). 1990. Absolute age determination: Physical and chemical dating methods and their application. Berlin: Springer-Verlag.
- Gutenberg, B. 1945. Magnitude determination for deep focus earthquakes. Bulletin of the Seismological Society of America 35: 117-130.
- Gutenberg, B. and Richter, C. F. 1954. Seismicity of the Earth and Associated Phenomena, 2<sup>nd</sup> ed. Princeton, New Jersey: Princeton University Press.
- Hamblin, W. K. 1976. Patterns of displacement along the Wasatch fault. Geology 4: 619-622.
- Hanks, T. C., and Boore, D. M. 1984. Moment-magnitude relations in theory and practice. Journal of Geophysical Research 89: 6229-6235.
- Hanks, T. C., and Kanamori, H. 1979. A moment magnitude scale. Journal of Geophysical Research 84: 2348-2350.
- Heaton, T.H., Tajima, F., and Mori, A. W. 1986. Estimating ground motions using recorded accelerograms. Survey Geophysics. 8:25-83.
- Hinthong, C. 1991a. Plate tectonic and earthquakes. Bangkok; Department of Mineral Resources.
- Hinthong, C., 1991b. Role of tectonic setting in earthquake events in Thailand, In ASEAN-EC Workshop on Geology and Geophysics, pp. 1-37. Jakarta: Indonesia.
- Hoke, L. and Campbell, H. J. 1995. Active mantle melting beneath Thailand. In W. Youngme, C. Buaphan, K. Srisuk, and R. Lertsirivorakul (eds.), Proceedings of the International Conference on Geology, Geotechnology, and Mineral Resources of Indochina, pp. 13-22. Khon Kaen, Thailand: Department of Geotechnology, Khon Kaen University,
- Hongaisee, U. 1999. Major faults and seismic hazard in northern Thailand. Master's Thesis. Department of geological science, Graduate School, Chiang Mai University.
- Huntley, D. J. 1985. On the zeroing of the thermoluminescence of sediments. Physics and Chemistry of Minerals 12: 122-127.

- Huxtable, J., Aitken, M. J., and Bonhomment, N. 1978. Thermoluminescence dating of sediment baked by lavaflows of the Chaîne de Puys. Natural (London) 275: 207-209.
- Javanaphet, J.C. 1976. Geological map of Thailand. Scale 1:1,000,000. Bangkok: Department of Mineral Resources (a map with explanatory note).
- Kanamori, H. 1977. The energy release in great earthquakes. Journal of Geophysical Research 82:2981-2987.
- Kanamori, H. 1983. Mechanism of the 1983 Coalinga earthquake determined from long-period surface waves. In J. H. Bennett, and R. W. Sherburn (eds.), The 1983 Coalinga, California Earthquakes. Spec. Publ.-Calif. Div. Min. Geol. 66: 233-240.
- Keller, E. A. 1979. Environmental geology. 2<sup>nd</sup> ed: Bell and Howell.
- Keller, E.A., 1987. Investigation of active tectonics. Use of Surficial Earth Processes, California: University of California Institute of Technology. 136-147.
- Kemlek, S., and Jeamton, S., and Angkhajan, V. 1989. Geology of Amphoe Thong Pha Phum, Ban I-tong. And Khao Ro Rae, with geological map scale 1:50,000, sheet 4738 III and 4738 IV (in Thai). Bangkok: Department of Mineral Resources.
- Khromovskikh, D. S. 1989. Determination of magnitudes of ancient earthquakes from dimension of observed seismodislocations. Tectonophysics 166: 1-12.
- Klaipongpan, S. Pinrode, J., Chakramanont, V., and Chittrakarn, P. 1986. Geological and seismicity evaluation of Srinagarin Dam, Nonthaburi: Electricity Generating Authority of Thailand: 1-7.
- Kosuwan, S. and Lumchuan, A. 1997. Neotectonics of Mae Chan Fault in Mae Chan District, Chiang Mai Province (in Thai). Bangkok: Department of Mineral Resources. (Unpublished Manuscript)
- Lacassin, R. et al. 1997. Tertiary diachronic extrusion and deformation of western Indochina: Structural and <sup>40</sup>Ar/<sup>39</sup>Ar evidence from NW Thailand. Journal of Geophysical Research 102: 10,013-10,037.
- Lajoie, K. R. (1986). Coastal tectonics. In R. E. Wallace, (chairman), Active Tectonics: Studies in Geophysics, pp. 95-124. Washington, DC: Natl. Acad. Press.
- Leet, L. D., Judson, S., and Kauffman, M. E. 1982. Physical Geology. New Jersey: Prentice hall.
- Levin, H. L. 1990. Contemporary Physical Geology. 3<sup>rd</sup> ed. Florida: Rinehart and Wenston.

- Lorenzetti, E. A., Brennan, P. A., and Hook, S.C. 1994. Structural styles in rift basins: Interpretation methodology and examples from southeast Asia. American Association of Petroleum Geologist Bulletin 78: 1152.
- Lukkunaprasit, P., and Kuhatasanadeekul, N. 1993. Seismic zoning and seismic coefficients for Thailand. In The 1993 Engineering Technology Symposium and Exhibition 267-268.
- Machette, M.N., Personius, S. F. and Nelson, A. R. 1992. Paleoseismology of the Wasatch fault zone: A summary of recent investigations, interpretations, and conclusions. In P.L. Gori, and W. W. Hays (eds.), Assessment of Regional Earthquake Hazards and Risk Along the Wasatch Front, Utah pp. 1500-A: A1-A71. United States Geological Survey Professional Paper.
- Malod, J. A., and Kemal, B. M. 1996. Sumatra margin: Oblique subduction and lateral displacement of the accretionary prism. In R. Hall, and D. J. Blundell (eds.), Tectonic Evolution of Southeast Asia, pp. 19-28. Geological Society Special Publication No. 106. London.
- Marfunin, S.A. 1979. Spectroscopy, luminescence and radiation centres in minerals. Heidelberg: Springer Verlag.
- Maung, H. 1987. Transcurrent movements in the Burma-Andaman Sea region. Geology 15: 911-912.
- McCabe, R., Celaya, M., Cole, J. T., Han, H. -C., Ohnstad, T., Pajitprapapon, V., and Thitipawan, V. 1988. Extension Tectonics: The Neogene opening of the north-south trending basins of central Thailand. Journal of Geophysical Research 93: 11,899-11,910.
- McCabe, R., Harder, S., Cole, J. T., and Lumadyo, E. 1993. The use of paleomagnetic studies in understanding the complex Tertiary Tectonic history of east and southeast Asia. Journal of Southeast Asian Earth Sciences. 8: 257-268.
- McCalpin, J. P. 1995. Frequency distribution of geologically-determined slip rates for normal faults in the western USA. Bulletin of the Seismological Society of America 85, 1867-1872.
- McCalpin, J. P. (ed). 1996. Paleoseismology. San-Diego : Academic Press.

- Meteorological Department. 2000. Report of major worldwide epicenters and their damages during January 1990 to November 2000 (in Thai). Bangkok: Meteorological Department. (Unpublished Manuscript)
- Millard, H. T., Jr., and Maat, P. B. 1994. Thermoluminescence dating procedures in use at the U.S. Geological Survey, Denver, Colorado. United States Geological Survey Open-File Report 94-249.
- Mogi, K. 1962. Study of elastic shocks caused by the fracture of heterogeneous materials and its relation to earthquake phenomena. Bulletin Earthquake Research Institute 40: 125-173.
- Molnar, P., and Deng, Q. 1998. Faulting associate with large earthquakes and the average rate of deformation in central and eastern Asia. Journal of Geophysical Research 89: 6,203-6,227.
- Monroe, J. S., and Wicander, R. 1998. Physical geology: Exploring the earth. 3<sup>rd</sup> ed. Belmont, California: Wadsworth.
- Mörner, N. -A., and Adams, J., (eds.). 1989. Paleoseismicity and neotectonics. Tectonophysics 163 (whole volume).
- Nambi, K. S. V. 1982. ESR and TL dating studies on Quaternary marine-gypsum crystal. PACT Journal 6: 314-321.
- Nelson, A. R. 1987. A facies model of colluvial sedimentation adjacent to a single-event normal fault scarp, Basin and Range province, western United states; Directions in Paleoseismology. United States Geological Survey Open File Report 87-673: 136-145.
- Nishenko, S. P. 1989. Circum-Pacific seismic potential 1989-1999. United States Geological Survey Open File Report 89-86: 1-126.
- Nutalaya, P. 1987. Seismotectonic map of Thailand. In P. Lukunaprasit, K. Chandrangru, S. Poobrasert, and M. Mahasuverachai (eds.), Proceeding of the 1<sup>st</sup> Workshop on Earthquake Engineering and Hazard Mitigation, pp.137-149. November 1986. Bangkok: Chulalongkorn University.
- Nutalaya, P. 1992. Crustal stability and seismic hazards in Thailand. In Proceeding of a National Conference on Geologic Resources of Thailand: Potential for Future Development, pp.s2-1 – s2-20. Bangkok: Thailand.

- Nutalaya, P., and Rau, J. L. 1984. Structure framework of the Chao Phaya Basin. Thailand. In Proceeding of the Symposium on Cenozoic Basins of Thailand: Geology and Resources, October, Chiangmai: Chiangmai University.
- Nutalaya, P., Sodsri, S., and Arnold, E. P. 1985. Series on Seismology Volume II-Thailand: Southeast Asia Association of Seismology and Earthquakes Engineering, 403 p.
- O'Leary, J., and Hill, G. S. 1989. Tertiary basin development in southern central Plains, Thailand. In T. Thanasuthipitak, and P. Ounchanum (eds.), Proceedings of the International Symposium on Intermontane Basin: Geology and Resources, Chiang Mai, Thailand 30 Jan-2 Feb 1989, pp. 254-264. Thailand: Chiang Mai University.
- Olinstad, T., Moriarty, T., Harder, S. and McCabe, R. 1989. Cenozoic rifting in Thailand. EOS, Transaction of the America Geophysics Union: Volume 70.
- Packman, G. H. 1993. Plate tectonics and the development of sedimentary basins of the dextral regime in western southeast Asia. Journal of Southeast Asian Earth Science 8: 497-511.
- Pelzer, G., and Tapponier, P. 1988. Formation and evolution of strike-slip faults, rifts, and basins during the India-Asia collision: an experimental approach. Journal of Geophysical Research 93: 15,085-15,117.
- Personius, S. F. and Mahan, S. A. 2000. Paleoearthquake recurrence on the East Paradise fault zone, metropolitan Albuquerque, New Mexico. Bulletin of the Seismological Society of America 90: 357-369.
- Plummer, C. C., McGeary, D., and Carlson, D. H. 2001. Physical Geology. 8<sup>th</sup> ed. New York: McGraw-Hill.
- Poolachan, S. and Satayarak, N. 1989. Strike-slip tectonics and the development of Tertiary basins in Thailand. In T. Thanasuthipitak, and P. Ounchanum, (eds.), Proceedings of the International Symposium on Intermontane Basin: Geology and Resources, Chiang Mai, Thailand 30 Jan-2 Feb 1989, pp. 243-253. Thailand: Chiang Mai University.
- Poolachan, S., Pradidtan, S., Tongtaow, C., Janmaha, S., Intrawijitr, K., and Sangsuwan, C. 1991. Development of Cenozoic basin in Thailand. Marine and Petroleum Geology 8: 84-97.

- Porat, N., Amit, R., Zilberman, E., and Enzel, Y. 1997. Luminescence dating of fault-related alluvial fan sediments in the southern Arava Valley, Israel. Quaternary Science Reviews (Quaternary Geochronology) 1: 31-53.
- Prescott, J. R., and Robertson, G. B. 1997. Sediment dating by luminescence: A review. Radiation Measurements 27: 893-922.
- Raksasukulwong, M., and Thienprasert, A. 1991. Heat flow studies and geothermal energy development in Thailand. Journal of Thai Geosciences 2: 111-123.
- Reid, H. F. 1911. The elastic rebound theory of earthquakes, Bulletin of the Department of Geology, University of Berkeley 6: 413-444.
- Reiter, L. 1990. Earthquake Hazard Analysis: Issues and Insights. New York: Columbia University Press.
- Remus, D., Wedster, M., and Keawkan, K. 1993. Rift architecture and sedimentology of the Phetchaburi intermontaine basin, central Thailand. Journal of Southeast Asian Earth Science 8: 421-432.
- Reneau, S. L., Gardner, J. N. and Forman, S. L. 1996. New evidence for the age of the youngest eruption in the Valles caldera, New Mexico. Geology 24: 7-10.
- Richter, B., and Fuller, M. 1996. Paleomagnetism of the Sibumasu and Indochina blocks: Implications for the tectonic model. In R. Hall and D. J. Blundell (eds.), Tectonic Evolution of Southeast Asia, pp. 203-224. Geological Society Special Publication No. 106. London.
- Richter, B., Fuller, M., Schmidtke, E., Myint, U. T., Ngwe, U. T., Win, U. M., and Bunopas, S. 1993. Paleomagnetic results from Thailand and Myanmar; Implications for the interpretation of tectonic rotations in southeast Asia. Journal of Southeast Asian Earth Science 8: 247-255.
- Richter, C. F. 1935. An instrumental earthquake magnitude scale. Bulletin of the Seismological Society of America 25: 1-32.
- Rodbell, D. T., Forman, S. L., Pierson, J., and Lynn, W. C. 1997. Stratigraphy and chronology of Mississippi Valley loess in western Tennessee. GSA Bulletin 109: 1134-1148.



- Seed, H. B., Romo, M. P., Sun, J. P., Jaime, A., and Lysmer, J. 1987. Relationships between Soil Conditions and Earthquake Ground Motions in Mexico City in the Earthquake of Sept. 19, 1985. UCB/EERC-87/15. California: University of California.
- Schwartz, D. P. and Coppersmith, K. J. 1986. Seismic hazard; new trend and analysis using geologic data. In Active Tectonics: Study in geophysics, pp.215-230. Washington, DC: National Academy Press.
- Senupta, D., Bhandari, N., Singhvi, A. K., Basilevesky, A. T., and Nazarov, M. 1984. Thermoluminescence of glasses from Lunar Meteor Crater. In F. R. G. Warmes (ed.), IV th Specialist Seminar on TL and ESR Dating (Abstract).
- Shelkplyas, V. N., and Morozov, G. V. 1965. Determination of the relative age of Quaternary deposits of the middle Dnieper by the thermoluminescence method. In Survey of Problems in the Study of the Quaternary Period. Nauka, Moscow. (in Russian, translation of title by JRP)
- Shreatha, P. M. 1987. Investigation of Active Fault in Kanchanaburi Province, Thailand. Master's Thesis. Graduate school, Asian Institute of Technology, Bangkok.
- Sieh, K. E. 1981. 1981. A review of geological evidence for recurrence times for large earthquakes. In D. W. Simson and T. G Richards (eds.), Earthquake prediction: An international review, Maurice Ewing Ser pp.181-207. America Geophysical Union, Washington, DC.
- Singhvi, A.K., and Wagner, G.A. 1986. Thermoluminescence dating and its applications to young sedimentary deposits. In A.J. Hurford, E. Jager, and J.A.M.Ten Cate (eds.), Dating Young Sediments: Proceeding of the Workshop, Beijing, pp. 159-190. Bangkok: CCOP Technical Secretarial.
- Siribhakdi, K. 1987. Seismogenic of Thailand and periphery. In P. Lukunaprasit, K. Chandrangru, S. Poobrasert, and M. Mahasuverachai (eds.), Proceeding of the 1<sup>st</sup> Workshop on Earthquake Engineering and Hazard Mitigation, p.151-158. November 1986. Bangkok: Chulalongkorn University.
- Siribhakdi, K., Salyapongse, S., and Sutheeron, V. 1976. Geological map of Tavoy, scale 1:250,000, sheet ND47-6. Bangkok: Geologic Survey Division, Department of mineral Resources.

- Slemmons, D. B. 1982. Determination of design earthquakes magnitudes for microzonation. In Proc. Third Int. Earthquake Microzon. Conf., Seattle, WA; Earthquake Engineering Research Institute 1: 110-130.
- Solonenko, V. P. 1973. Paleoseismogeology. Izv. Acad. Sci. URRS, Phys. Solid Earth 9: 3-16.
- Sripongpan, P., and Kojedee, T. 1987. Geology of Ban Tha Ma dua, Khao Bo Ngam, Ban Phung and Ban Lin Thin with geological map scale 1:50,000, sheet 4738 IV, 4738 I, 4838 IV and 4838 IV (in Thai). Bangkok: Geologic Survey Division, Department of mineral Resources.
- Stover, C. W. and Coffman, J. L. 1993. Seismicity of the United States, 1568-1989 (revised). United States Geological Survey Professional Paper 1527, 1-418.
- Sutton, S. R. 1984. Thermoluminescence dating study of shock metamorphosed rock from Meteor Crater. Unpublished Doctoral Thesis, Washington.
- Suwanlert, J. 1992. Seismotectonics of Thailand. Seismicity and Focal Mechanism. Individual Studies by Participants at the International Institute of Seismology and Earthquake Engineering 28: 115-129.
- Takashima, I., and Watanabe, K. 1994. Thermoluminescence age determination of lava flow/domes and collapsed materials at Unzen Volcano, SW Japan. Bulletin of Volcanology Society of Japan 1: 1-12.
- Takashima, I., Honda, S., and Naya, H. 1990. TL age of the Hakkoda pyroclastic flow deposits, Aomori Prefecture, Northeast Japan. Journal of Mineralogy, Petrology and Economic Geology 85: 459-468 (in Japanese with English abstract).
- Thienprasert, A. and Raksaskulwong, M. 1984. Heat Flow in northern Thailand: Tectonophysics 103: 217-233.
- Thiramongkol, N. 1983. Reviews of geomorphology of Thailand, In N. Thiramongkol, and V. Pisutha-Arnond (eds.), Proceedings of the First Symposium on Geomorphology and Quaternary Geology of Thailand, pp. 6-23. Bangkok: Department of Geology, Chulalongkorn University.
- Toyoda, S., Goff, F., Ikeda, S., and Ikeya, M. 1995. ESR dating for quartz phenocrysts in the EL Cajete and Battleship Rock Members of the Valles Rhyolite, Valles caldera, New Mexico. Journal of Volcanology and Geothermal Research 67: 29-40.

- Valladas, G. 1978. Thermoluminescence dating of a burnt stone from a prehistoric site. PACT Journal 2/3: 180-184.
- Vita-Finzi, C. 1986. Recent Earth movements-An Introduction to Neotectonics. Orlando, Florida: Academic Press.
- Vittori, E., Labini, S. S., and Serva, L. (1991). Palaeoseismology; review of the state-of-the-art. Tectonophysics 193: 9-32.
- von Bandat, H. F. 1962. Aerogeology. Houston, Texas: Gulf Publishing Company.
- Wallace, R. E. 1977. Profile and ages of young fault scarps, north-central Nevada. Bulletin of the Seismological Society of America 9: 1267-1281.
- Wallace, R. E. 1981. Active faults, paleoseismology and earthquakes hazards in the western United States. In D. W. Simson and T. G Richards (eds.), Earthquake prediction: An international review, Maurice Ewing Ser. Vol.4, pp. 209-216. Am. Geophys. Union, Washington, DC.
- Wallace, R. E., (chairman). 1986. Active Tectonics: Studies in Geophysics. National Academy Science., Washington, DC.
- Wallace, R.E., 1987. Active Fault, Paleoseismology, and Earthquake Hazard in the Western United States pp.209-216. Geological Survey, Menlo Park. California. USA.
- Warnichai, P., Sangaranyakul, C., and Ashford S. A. 2000. Seismic hazard in Bangkok due to long-distance earthquakes. In Proceedings of the 12<sup>th</sup> World Conference on Earthquake Engineering, paper no. 2145, pp.1-8. Auckland: New Zealand.
- Weldon, R. J., III. 1991. Active tectonic studies in the United States, 1987-1990. In U.S. National Report to International Union of Geodesy and Geophysics : 890-906.
- Wells, D. L. and Coppersmith, K. J. 1994. New empirical relationships among magnitude, rupture length, rupture area, and surface displacement. Seismological Society of American Bulletin 84: 974-1002.
- Wenworth, C. M., Ziony, J. S., and Buchman, J. M., 1970. Preliminary geologic environmental map of the Greater Los Angeles area, California: USGS TID - 25363, Reactor Tech (TID - 4500).
- Wesnousky, S. G. (1986). Earthquakes, Quaternary faults, and seismic hazard in California. Journal of Geophysical Research 91: 12,587-12,631.

- Wesnousky, S. G., Schoz, C.H., Shimazaki, K. , and Matsuda, T. 1984. Integration of geological and seismological data for the analysis of seismic hazard; a case study of Japan. Bulletin of the Seismological Society of America 74: 687-708.
- Wesson, R. L., Helly, E. J., Lajoie, K. R. and Wenworth, C. M. 1975. Fault and future earthquakes, in Bocherdt, In R. D., (ed.), Studies for Seismic Zonation of the San Francisco Bay Region, pp. A5-A30. USGS Professional Pap. 941-A.
- Willis, B. 1923. A fault map of California. Bulletin of the Seismological Society of America 13: 1-12.
- von Bandat, H. F. 1962. Aerogeology. Houston, Texas: Gulf Publishing Company.
- Wintle, A. G., and Huntly, D. J. 1979. Thermoluminescence dating of deep sea sediments. Nature 279: 710-712.
- Wintle, A. G., and Huntly, D. J. 1980. Thermoluminescence dating of ocean sediments. Canadian Journal of Earth Science 17: 348-360.
- Wintle, A. G., and Huntly, D. J. 1982. Thermoluminescence dating of sediments. Quaternary Scientific Reviews 1: 31-53.
- Wintle, A. G., Li, S. H., and Botha, G. A. 1993. Luminescence dating of colluvium deposits from Natal, South Africa. South African Journal of Sciences. 89: 77-82.
- Wintle, A. G., Li, S. H., Botha, G. A., and Vogel, J. C. 1995. Evaluation of luminescence-dating procedures applied to late-Holocence colluvium near St Paul's Mission, Natal, South Africa. The Holocene 5: 97-102.
- Won-In, K. 2000. Neotectonic evidence along the Three Pagoda Fault Zone, Changwat Kanchanaburi. Master's Thesis, Department of Geology, Graduate School, Chulalongkorn University.
- Woodward-Clyde Federal Services.1998. Preliminary Seismic Hazard Evaluation of Khao Laem and Srinagarind Dams, Thailand. Unpublished report prepared for Electricity Generating Authority of Thailand: Bangkruay, Nonthaburi.
- Working Group on California Earthquake Probabilities, 1995. Seismic hazards in southern California-Probable earthquakes, 1994-2024. Bulletin of the Seismological Society of America 85: 379-525.
- Yeats R. S., Sieh, K., and Allen C. R. 1997. The geology of earthquakes. Oxford: Oxford University Press.

Zilberman, E., Amit, R., Heimann, A., and Porat, N. 2000. Change in Holocene Paleoseismic activity in Hula pull-apart basin, Dead Sea Rift, northern Israel. Tectonophysics 321: 237-252.

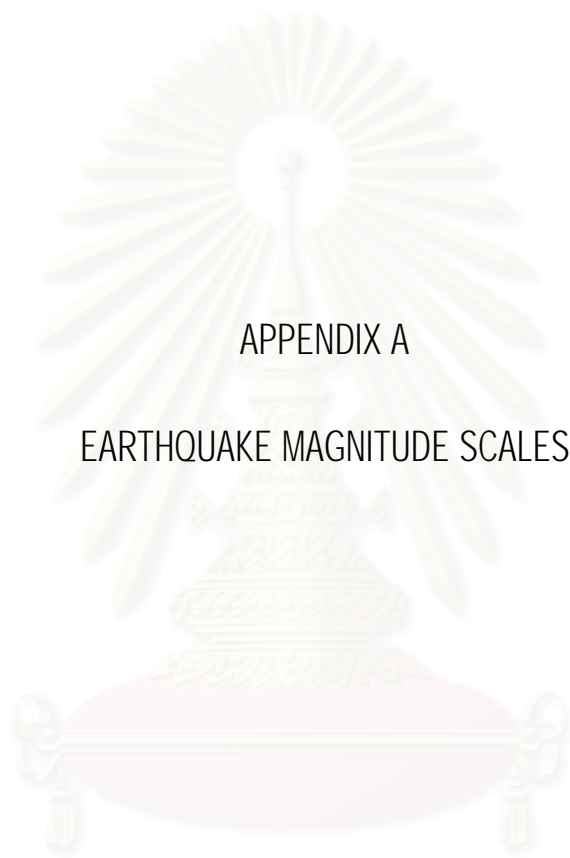


สถาบันวิทยบริการ  
จุฬาลงกรณ์มหาวิทยาลัย



APPENDICES

สถาบันวิทยบริการ  
จุฬาลงกรณ์มหาวิทยาลัย



APPENDIX A

EARTHQUAKE MAGNITUDE SCALES

สถาบันวิทยบริการ  
จุฬาลงกรณ์มหาวิทยาลัย

## APPENDIX A

### EARTHQUAKE MAGNITUDE SCALES

Several magnitude scales are widely used and each is based on measuring of a specific type of seismic wave, in a specified frequency range, with a certain instrument. The scales commonly used in western countries, in chronological order of development (McCalpin, 1996), are: local (or Richter) magnitude ( $M_L$ ), surface-wave magnitude ( $M_S$ ), body-wave magnitude ( $m_b$  for short period,  $m_B$  for long period), and moment magnitude ( $M_W$  or  $M$ ). Reviews of these magnitude scale are given by Bath (1981), Kanamori (1983), and dePolo and Slemmons (1990); their interrelations are shown in Fig. A.1

#### Local (Richter) Magnitude ( $M_L$ )

Richter magnitude was the first widely used instrumental magnitude scale to be applied in USA (McCalpin 1996). Charles Richter developed the first magnitude scale in 1935 (Richter, 1935). Richter's magnitude is the logarithm to the base 10 of the maximum seismic-wave amplitude, in thousandths of a millimeter, recorded on a special type of seismograph (Wood-Anderson seismograph) at a distance of 100 km from the earthquake epicenter. Richter took into account the decrease amplitude with increase distance from the earthquake (increased time between P and S waves) such that a Richter magnitude could be calculated if both the amplitude and the distance were know.

The Richter magnitude scale accurately reflects the amount of seismic energy released by an earthquake up to about  $M_L$  6.5. but for increasingly larger earthquakes, the Richter scale progressively underestimate the actual energy release. He scale has been said to "saturate" above  $M_L$  6.5, from a combination of instrument characteristics and reliance on measuring only a single, short-period peak height (see details in Kanamori, 1983).

#### Surface Wave Magnitude ( $M_S$ )

The surface wave magnitude scale was developed to solve the "saturation" problem of Richter magnitude above  $M_L$  6.5. The measurement procedure is similar to measuring the



Richter magnitude, except that the peak wave amplitude is measured for surface waves that have periods of 20 sec, from long-period seismograph at teleseismic distances (Gutenberg, 1945). The surface wave magnitude calculation does not require a seismograph record within 100 km (or nearby) of the epicenter, so the teleseismic record of many large-to-moderate magnitude earthquake worldwide have been assigned surface-wave magnitudes. Because of this large data set,  $M_S$  is the typical magnitude used in empirical comparisons of magnitude versus earthquake rupture large or displacement (e.g. Bonilla et al., 1984). However, the surface-wave magnitude scale also saturates, at about  $M_S > 8$ .

#### Body-Wave Magnitude ( $M_{bLg}$ )

The short period body-wave magnitude ( $M_{bLg}$ ) is the principal magnitude used in the tectonically "stable" eastern part of North America and Canada. This magnitude is measured from peak motions recorded at distances up to 1000 km on instruments with a passband in the range 1 to 10 Hz. Peak motions usually correspond to the Lg wave. This magnitude scale is little used in paleoseismology because it saturates at magnitude levels below that of  $M_S$ . However, it is possible to convert  $m_{bLg}$  values to other magnitude scales, and vice versa (Kanamori, 1983)

#### Moment Magnitude ( $M_W$ or $M$ )

The moment magnitude scale is the most recent scale (Kanamori, 1977; Hanks and Kanamori, 1979) and is fundamentally difference from the earlier scales. Rather than relying on measured seismogram peaks, the  $M_W$  scale is tied to the seismic moment ( $M_0$ ) of an earthquake.

The seismic moment thus more directly represents the amount of energy release at the source, rather than relying on the effects of that energy on one or more seismograph at some distance from the source. Moment magnitude is calculate from seismic moment using the relation of Hanks and Kanamori (1979) for south California.

The seismic moment scale was developed to circumvent the problem of saturation in other magnitude scales, and is typically used to describe great earthquake (i.e.,  $M_S > 8$ ). Kanamori (1983) composed a graph relating  $M_W$  to  $M_L$ ,  $M_S$ ,  $m_b$  and  $m_B$  (Fig A.1.1) In the

interest of standardization, paleoearthquake magnitude should be estimated on the  $M_w$  scale; if not, then the magnitude scale used should be clearly noted.

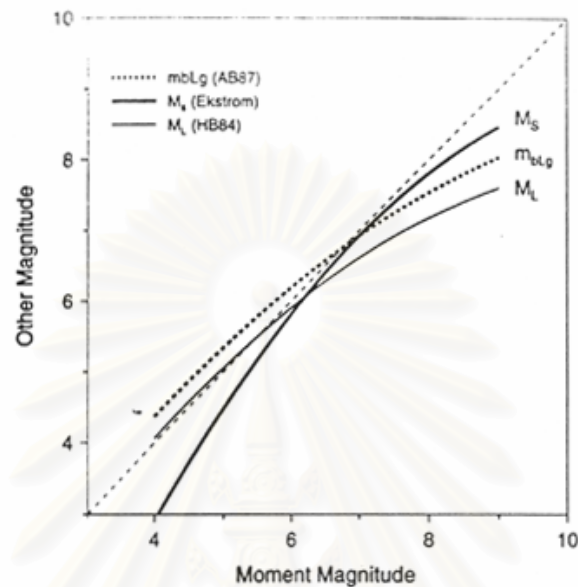
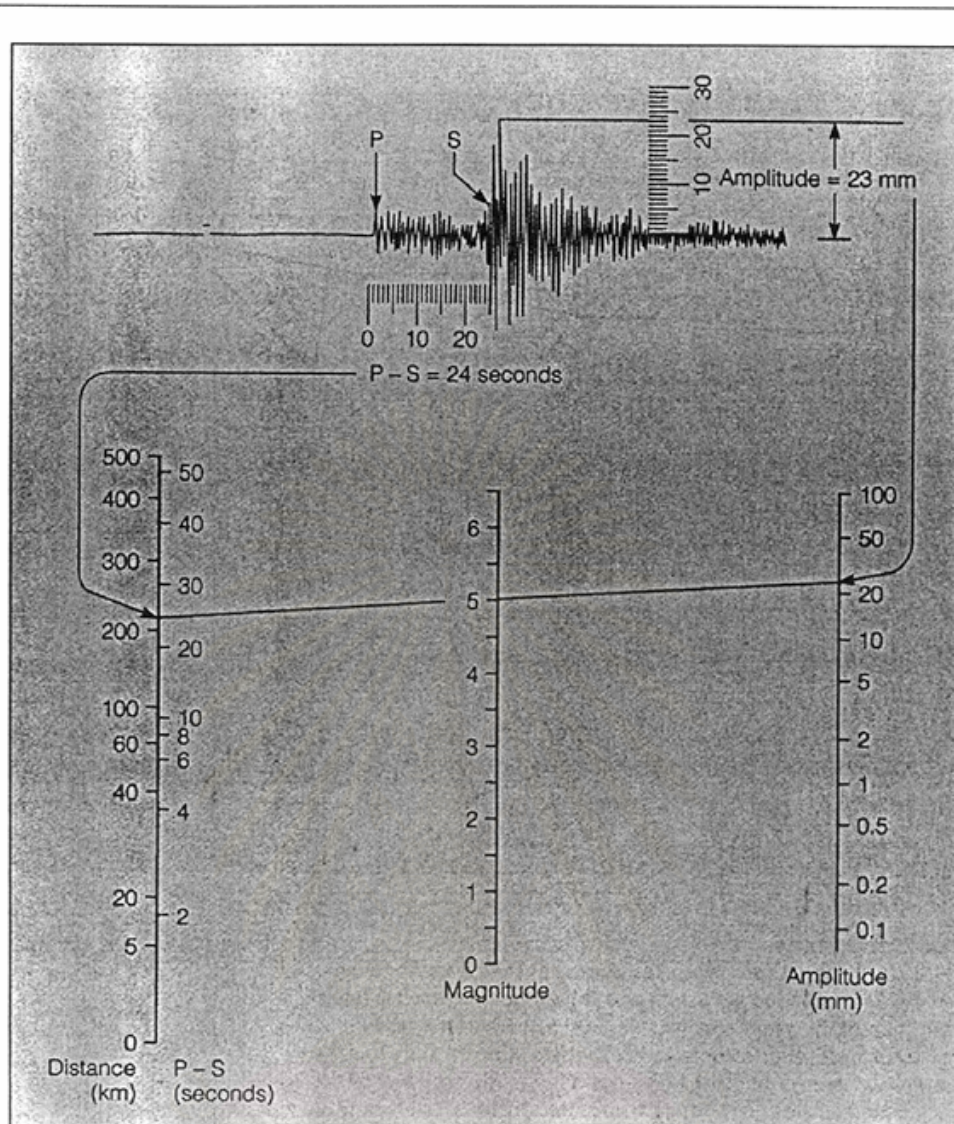


Figure A.1.1 Graph showing the relationship of various magnitudes to moment magnitude. Relation for  $m_{bLg}$  is from Atkinson and Boore (1987). For  $M_s$  and  $M_L$  the relation come from fitting a quadratic to the data compiled by Ekstrom (1987) and Hanks and Boore (1984), respectively. [From Boore and Joyner (1994); reprinted with permission of the Applied Technology Council.]

สถาบันวิทยบริการ  
จุฬาลงกรณ์มหาวิทยาลัย



Procedure for calculating local magnitude,  $M_L$

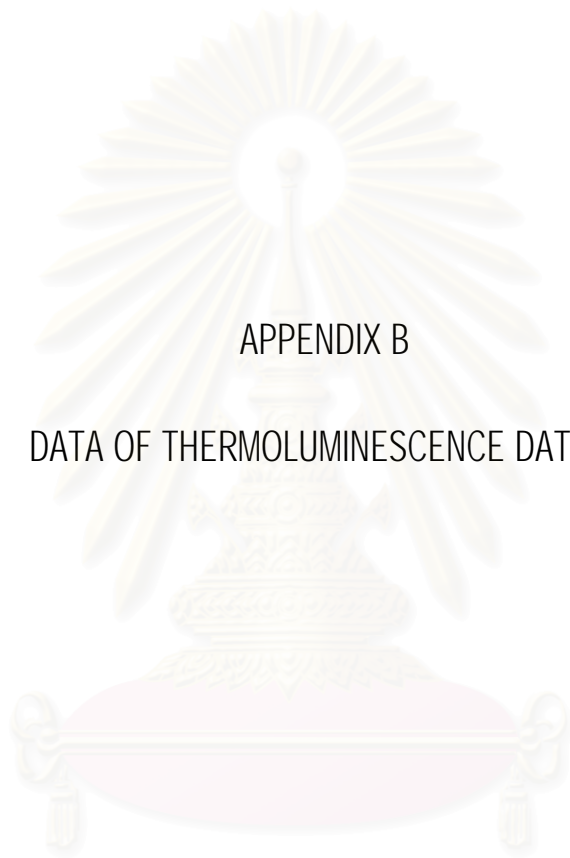
1. Measure the distance to the focus using the time interval between the S and the P waves ( $S-P = 24$  seconds).
2. Measure the height of the maximum wave motion on the seismogram (23 millimeters).
3. Place a straight edge between appropriate points on the distance (left) and amplitude (right) scale to obtain magnitude  $M_L = 5.0$ .

YOUNG FAULTING ALONG THE SOUTHERN SEGMENT OF SRI SAWAT FAULT



MR. RUTCHUT NUTTHEE  
DEPARTMENT OF GEOLOGY  
FACULTY OF SCIENCE  
CHULALONGKORN UNIVERSITY

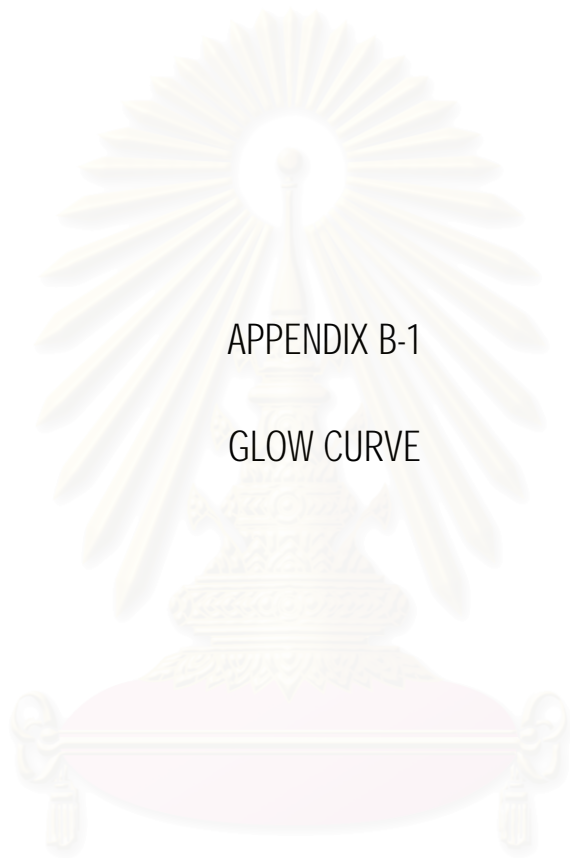
Figure A.2 Example of the calculation of the Richter magnitude ( $M_L$ ) of a local earthquake (Bolt, 1999)



APPENDIX B

DATA OF THERMOLUMINESCENCE DATING

สถาบันวิทยบริการ  
จุฬาลงกรณ์มหาวิทยาลัย



APPENDIX B-1

GLOW CURVE

สถาบันวิทยบริการ  
จุฬาลงกรณ์มหาวิทยาลัย

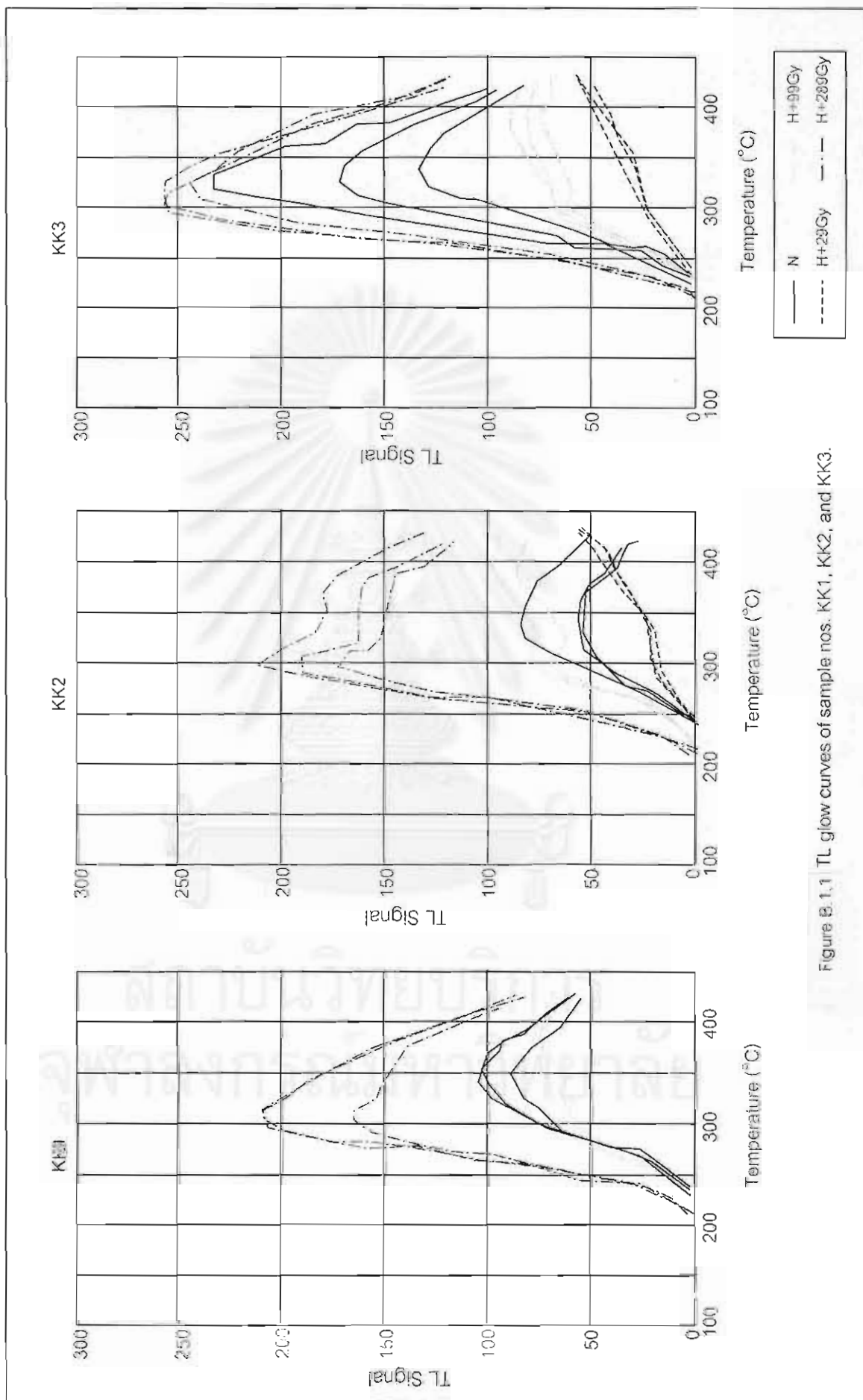


Figure B.1.1 TL glow curves of sample nos. KK1, KK2, and KK3.

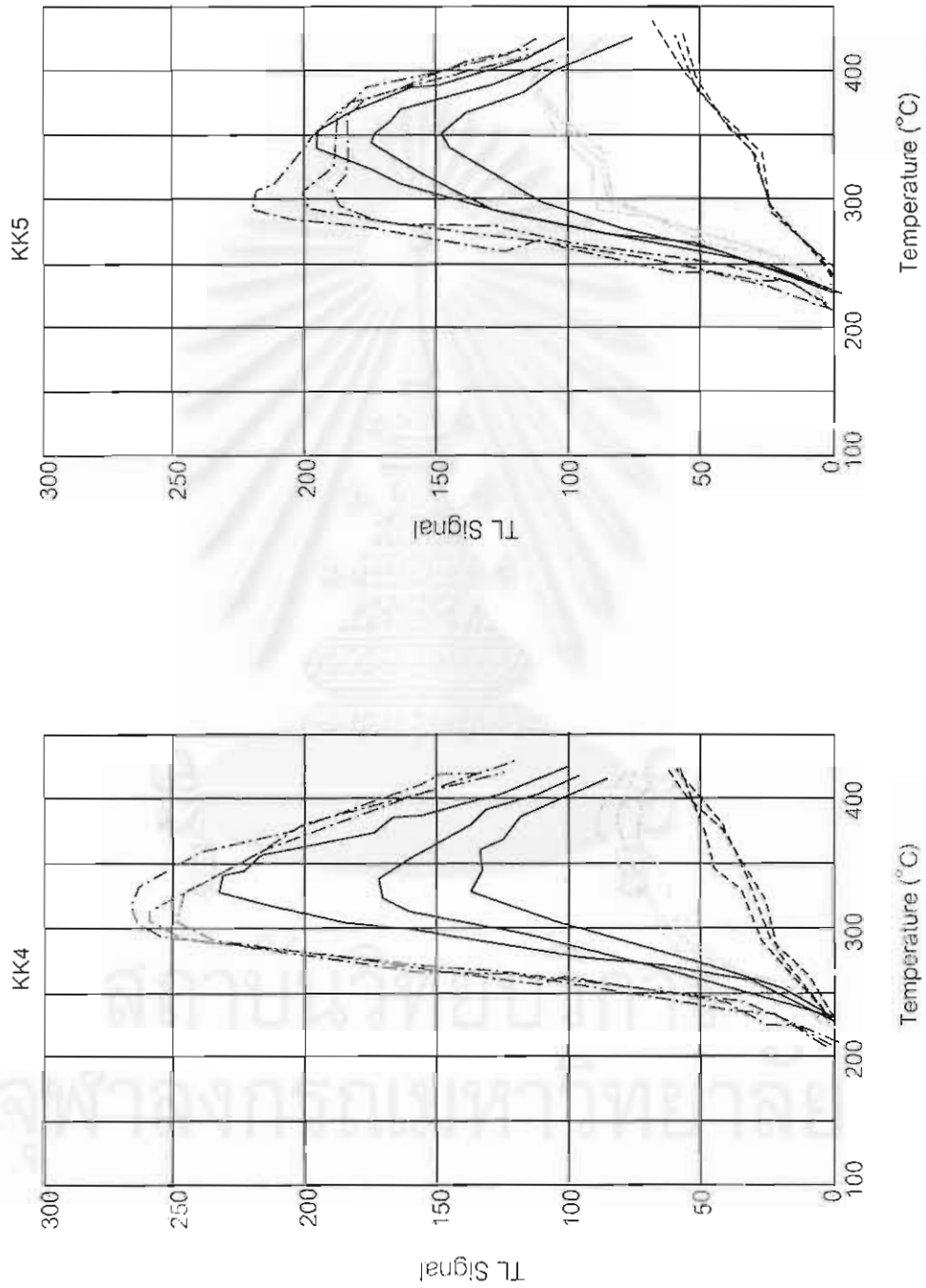


Figure B.1.2 TL glow curves of sample nos. KK4 and KK5.

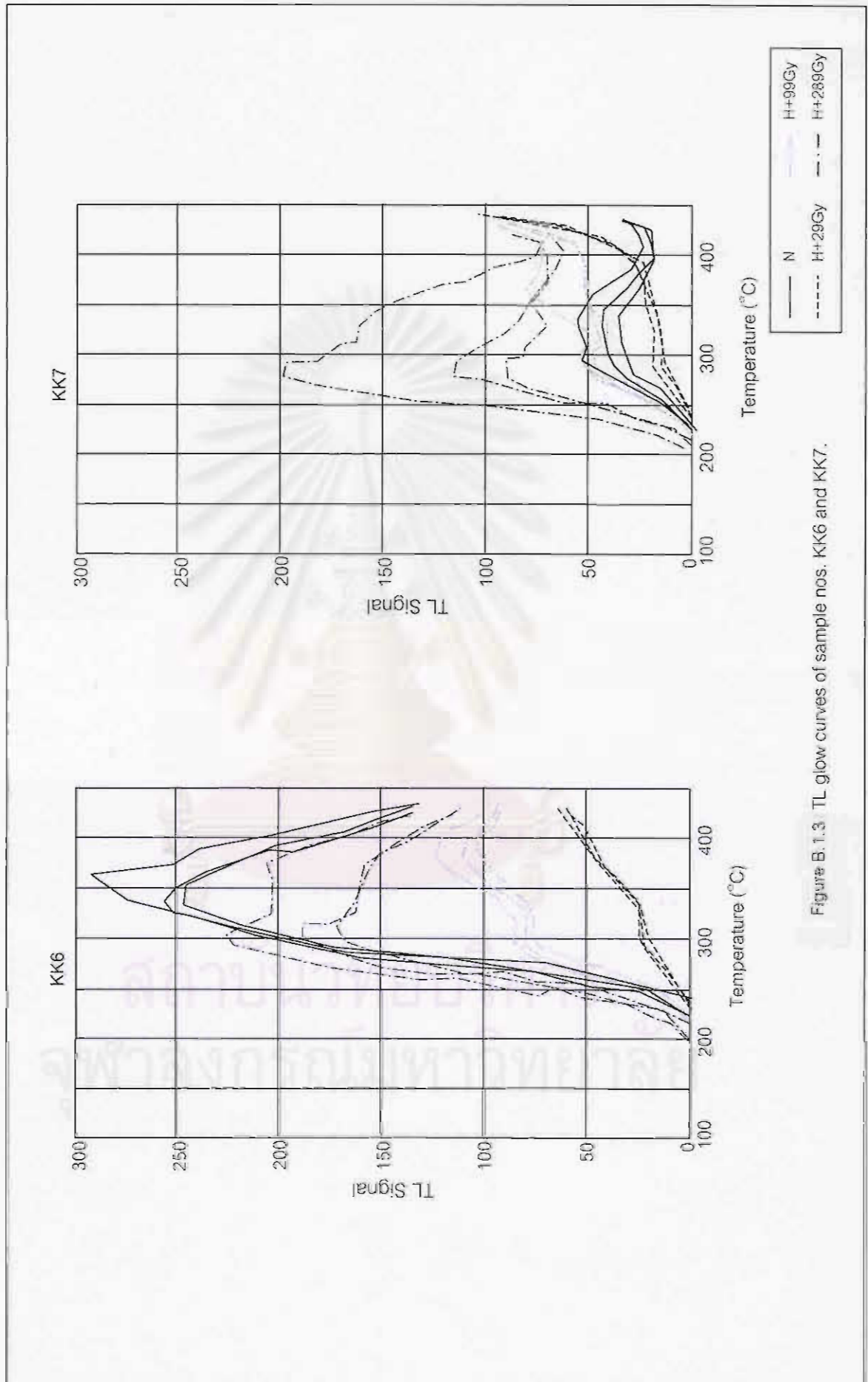


Figure B. 1.3 TL glow curves of sample nos. KK6 and KK7.



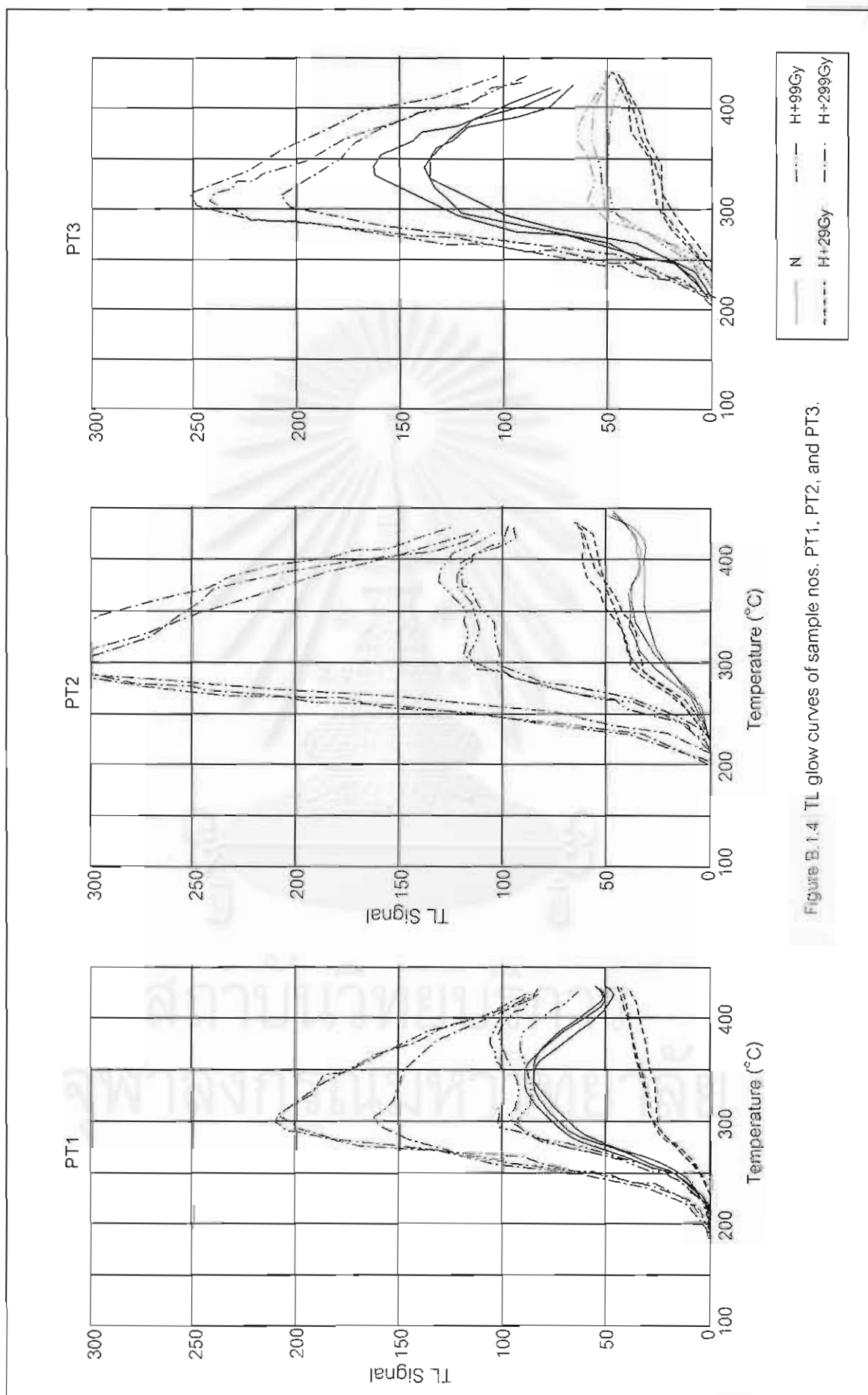


Figure B.1.4 TL glow curves of sample nos. PT1, PT2, and PT3.

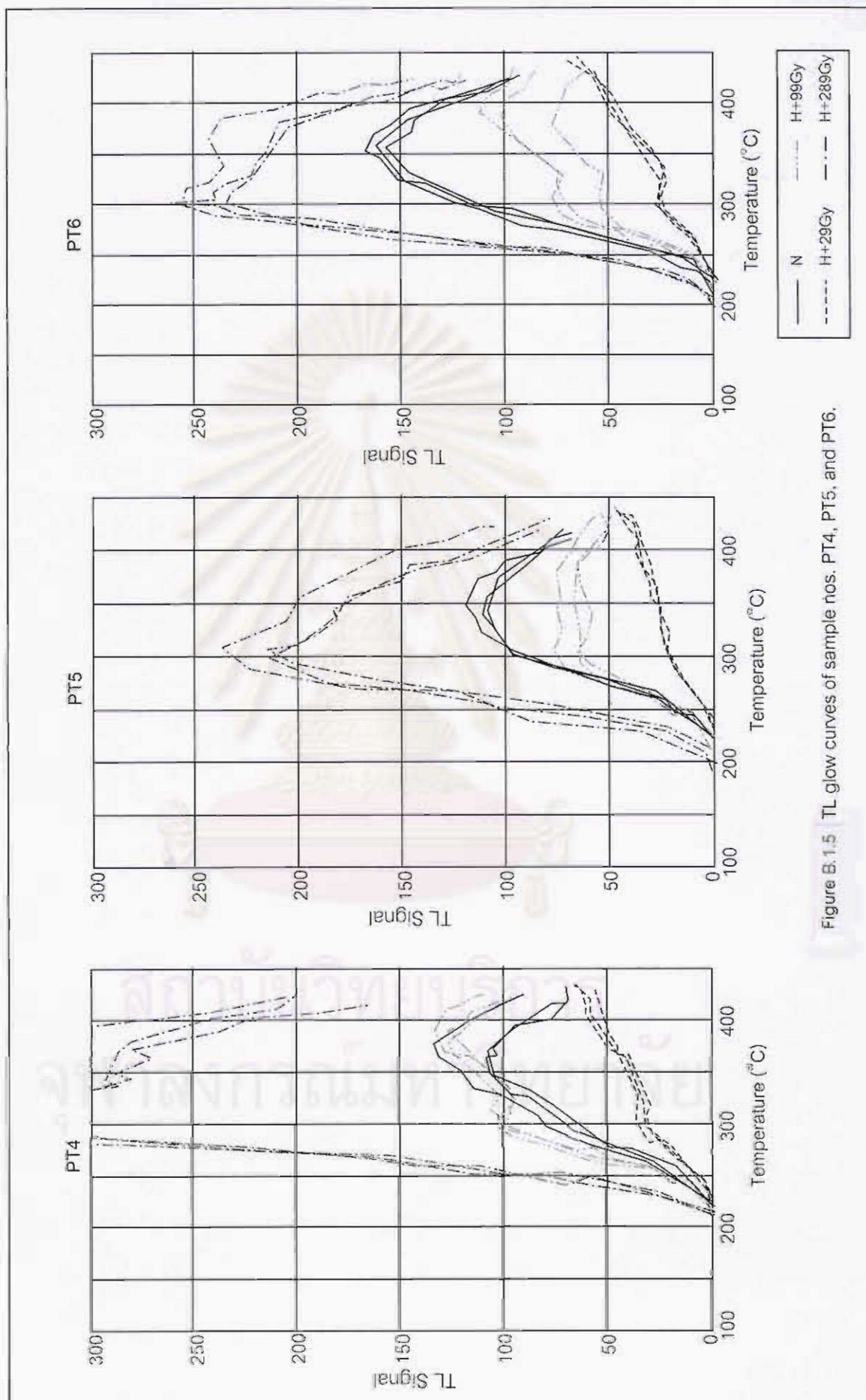


Figure B.1.5 TL glow curves of sample nos. PT4, PT5, and PT6.

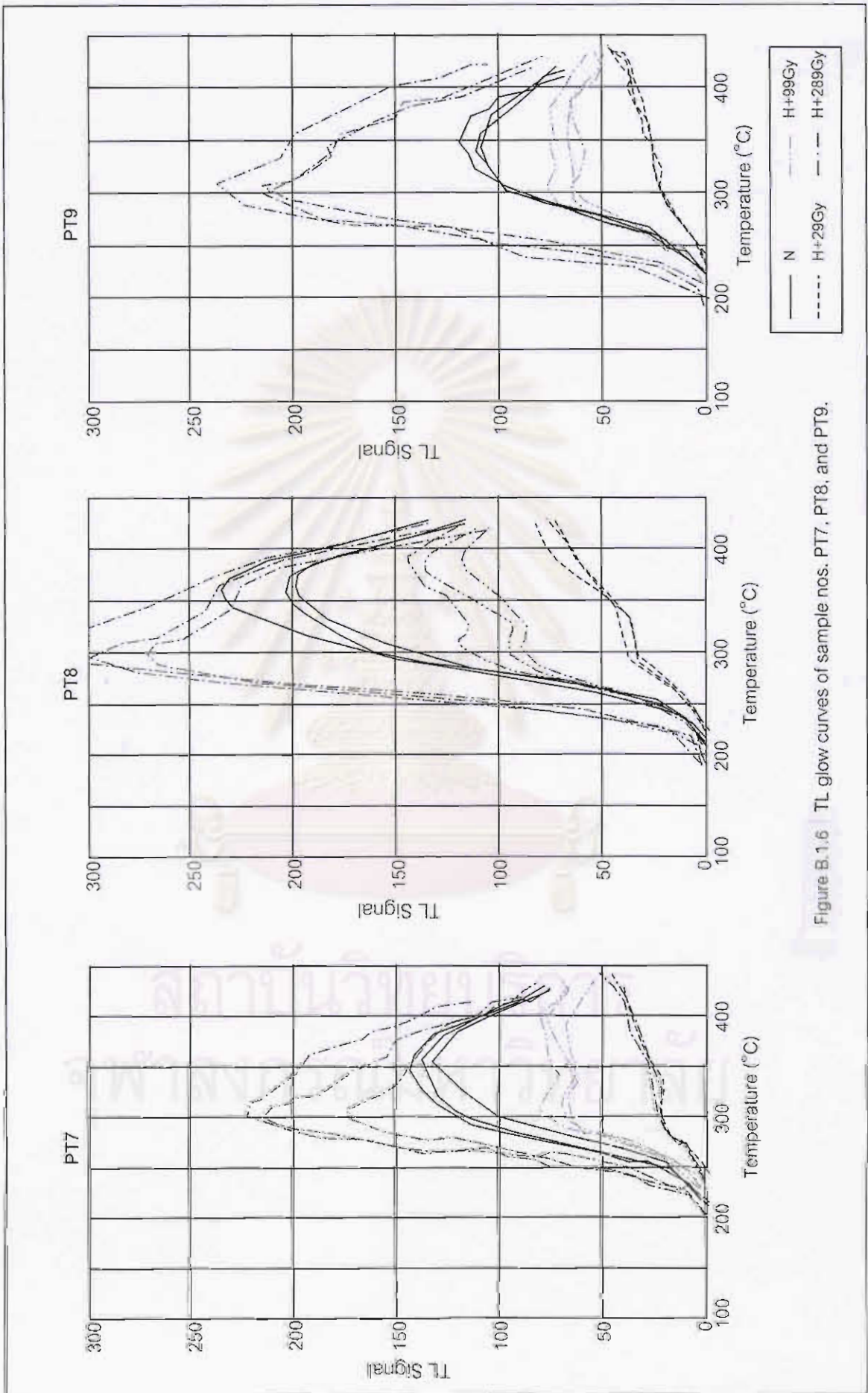


Figure B.1.6 TL glow curves of sample nos. PT7, PT8, and PT9.

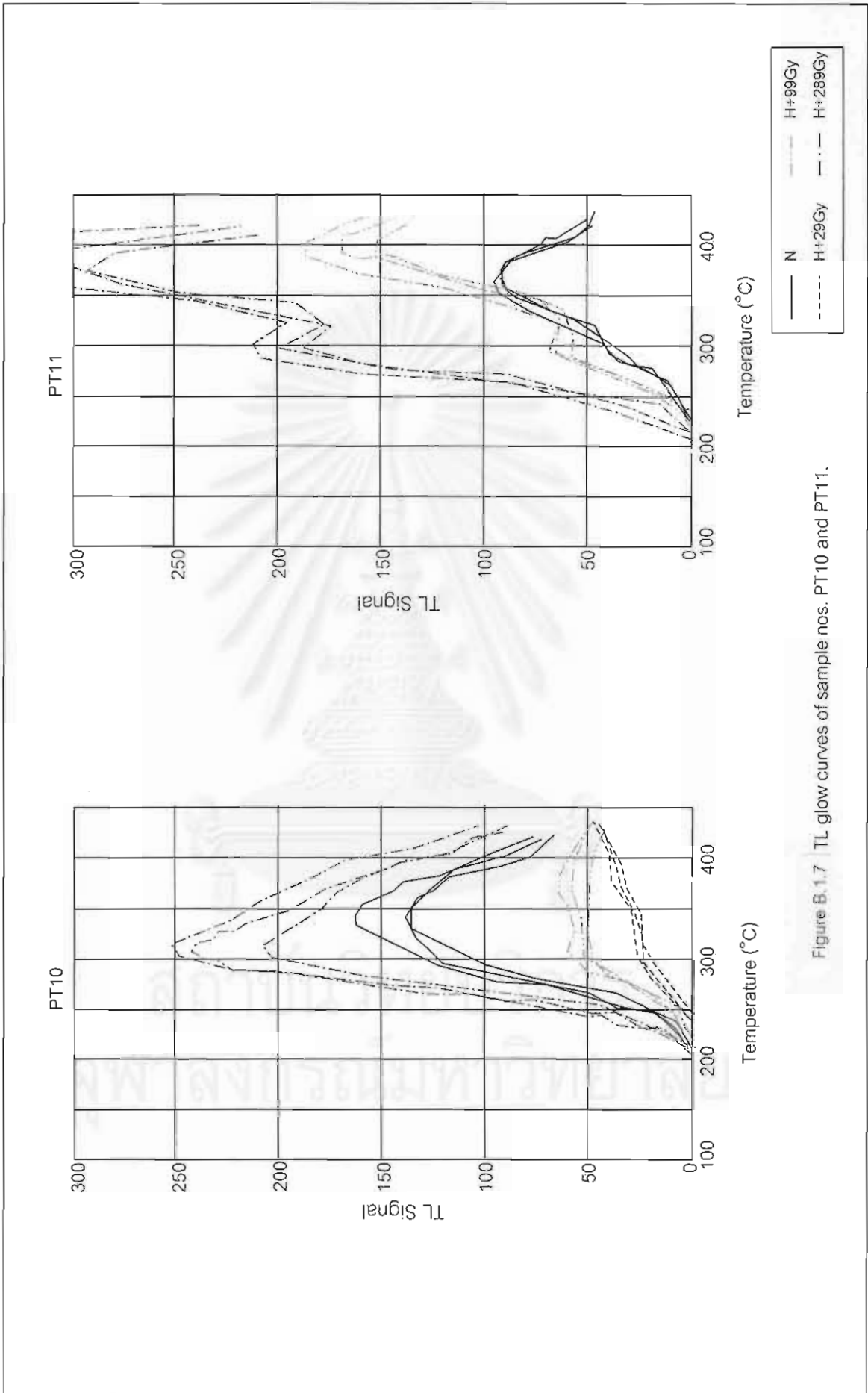
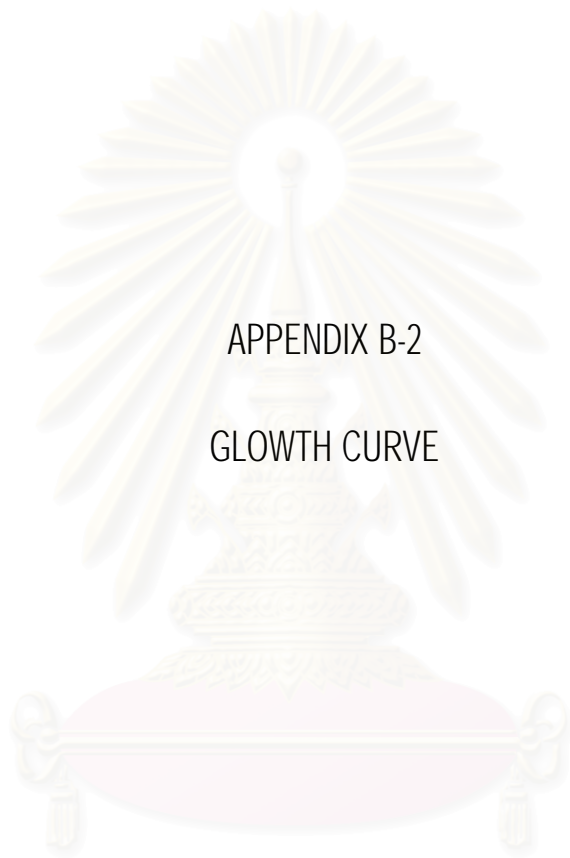


Figure B.1.7 TL glow curves of sample nos. PT10 and PT11.

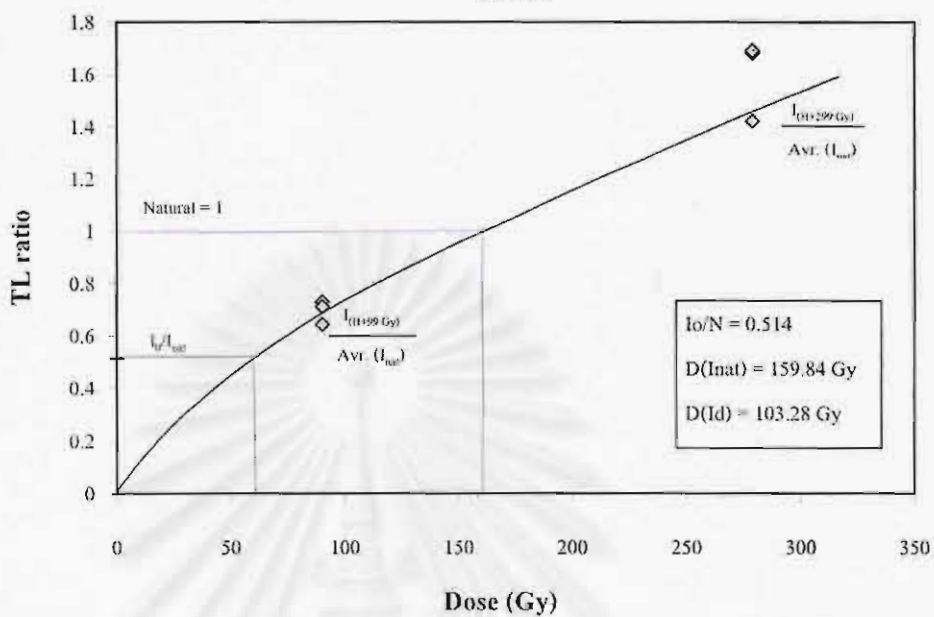


APPENDIX B-2

GROWTH CURVE

สถาบันวิทยบริการ  
จุฬาลงกรณ์มหาวิทยาลัย

### Growth Curve KK1



### Growth Curve KK2

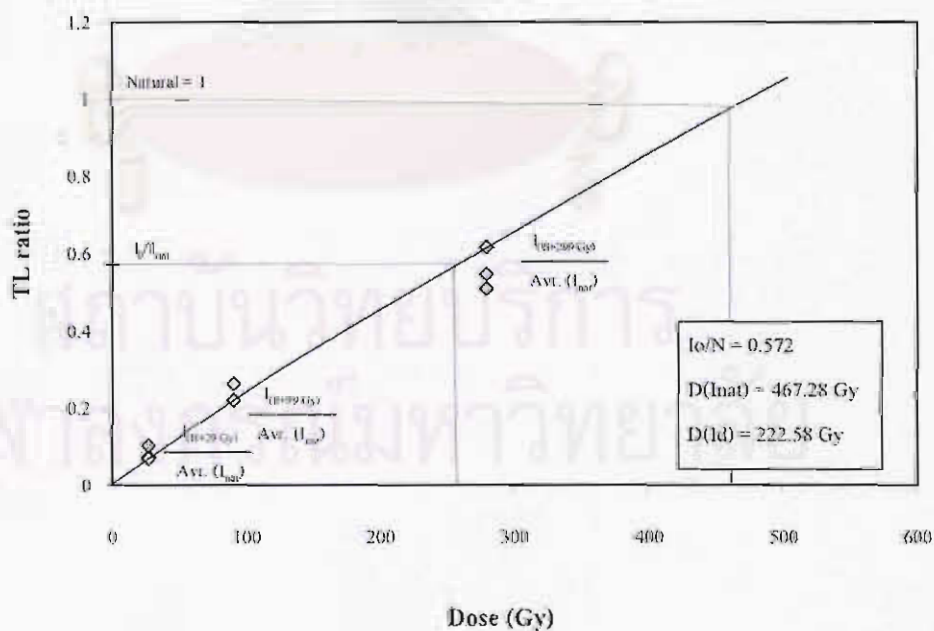


Figure B.2.1 The TL growth curve of sample nos. KK1 and KK2.

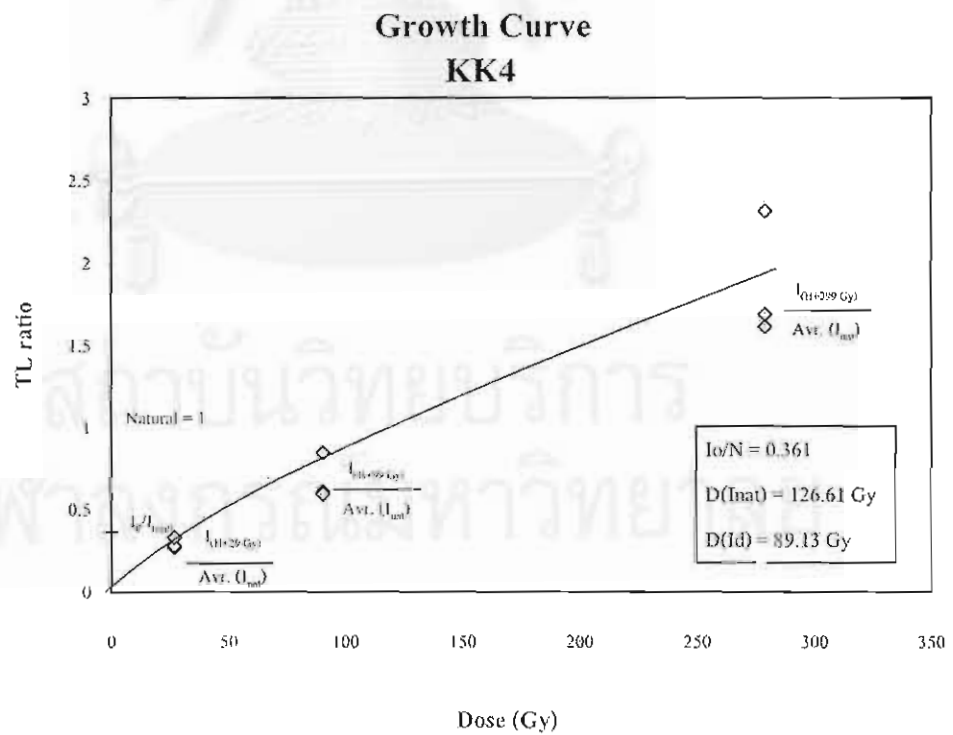
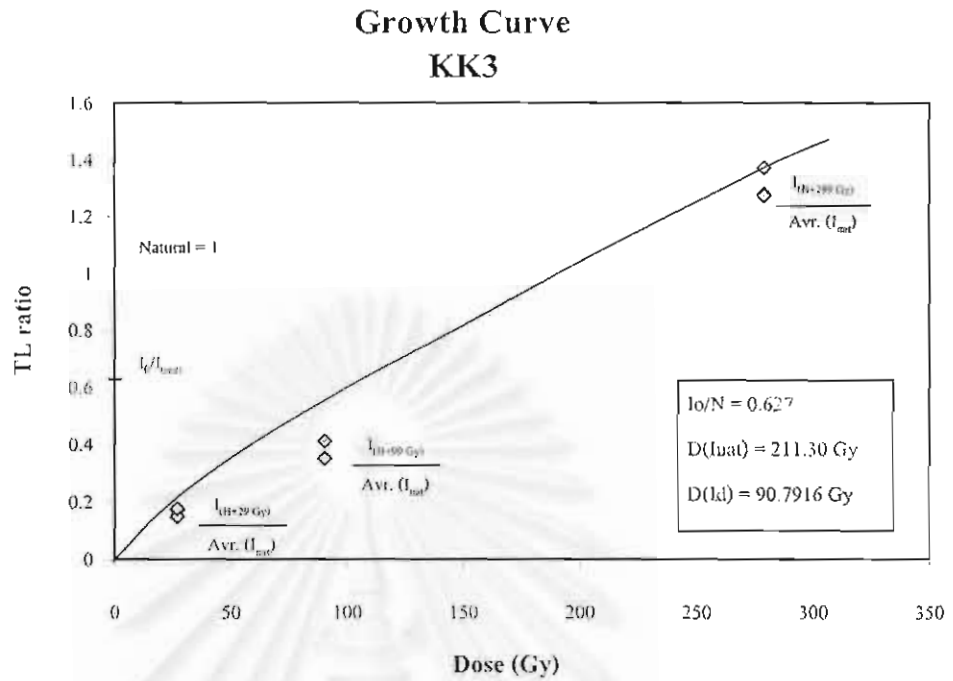


Figure B.2.2 The TL growth curve of sample nos. KK3 and KK4.

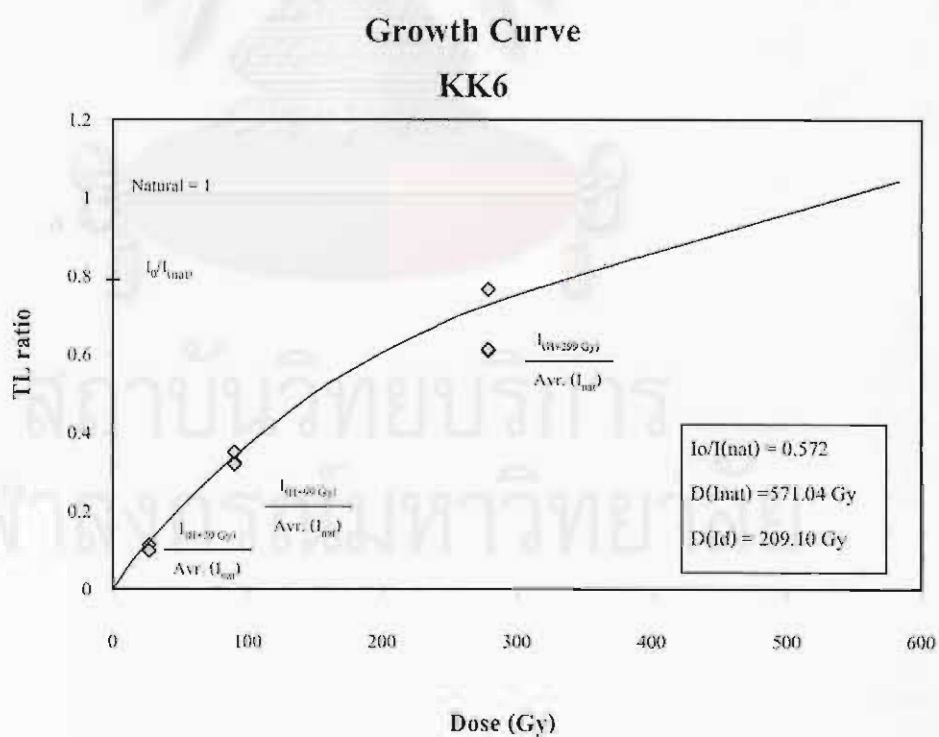
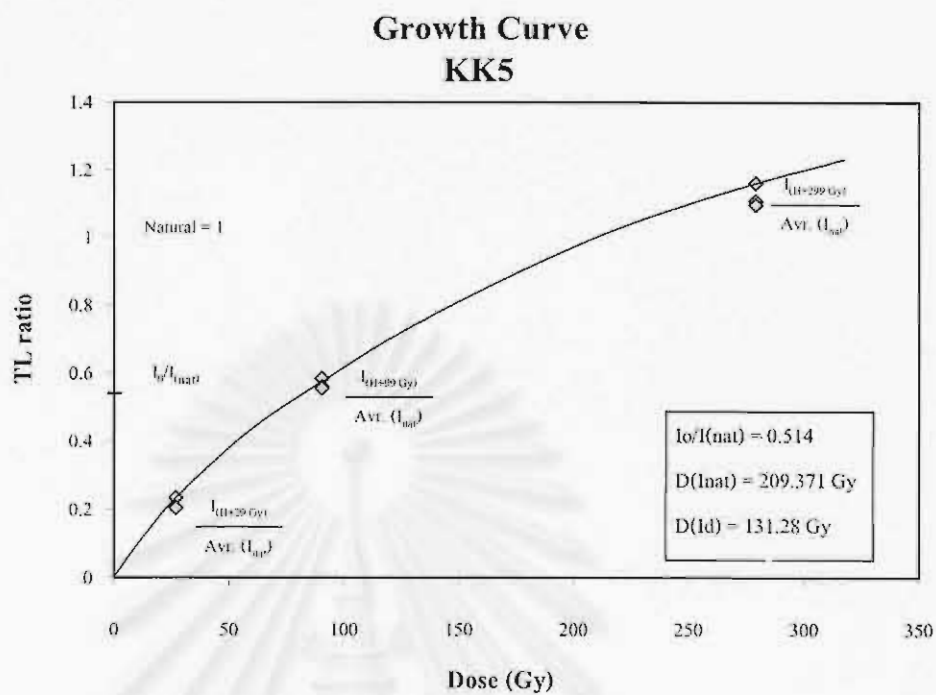


Figure B.2.3 The TL growth curve of sample nos. KK5 and KK6



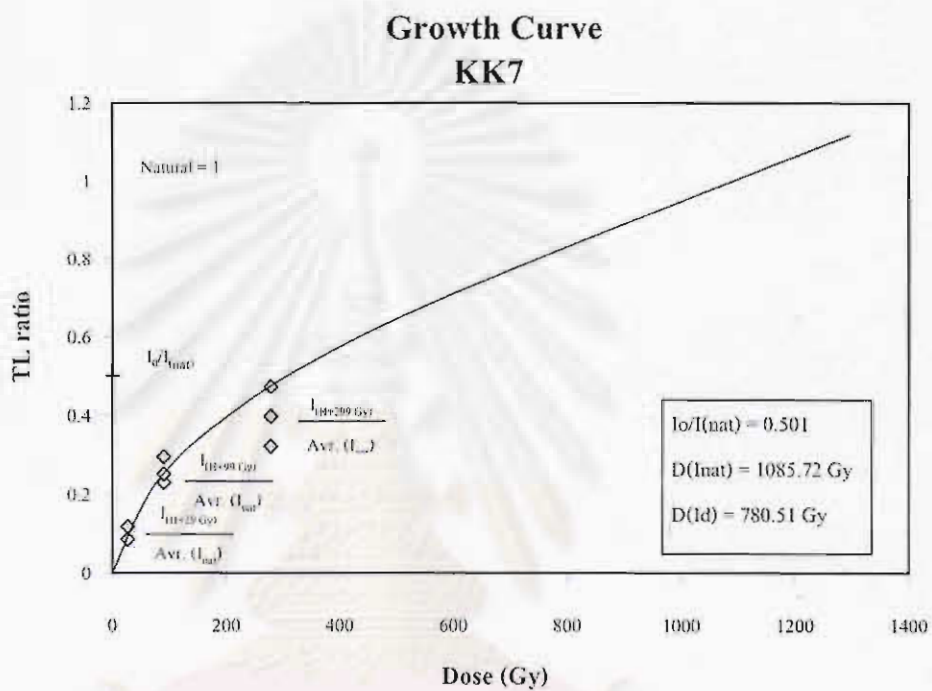


Figure B.2.4 The TL growth curve of sample no. KK7.

สถาบันวิทยุขงจักร  
จุฬาลงกรณ์มหาวิทยาลัย

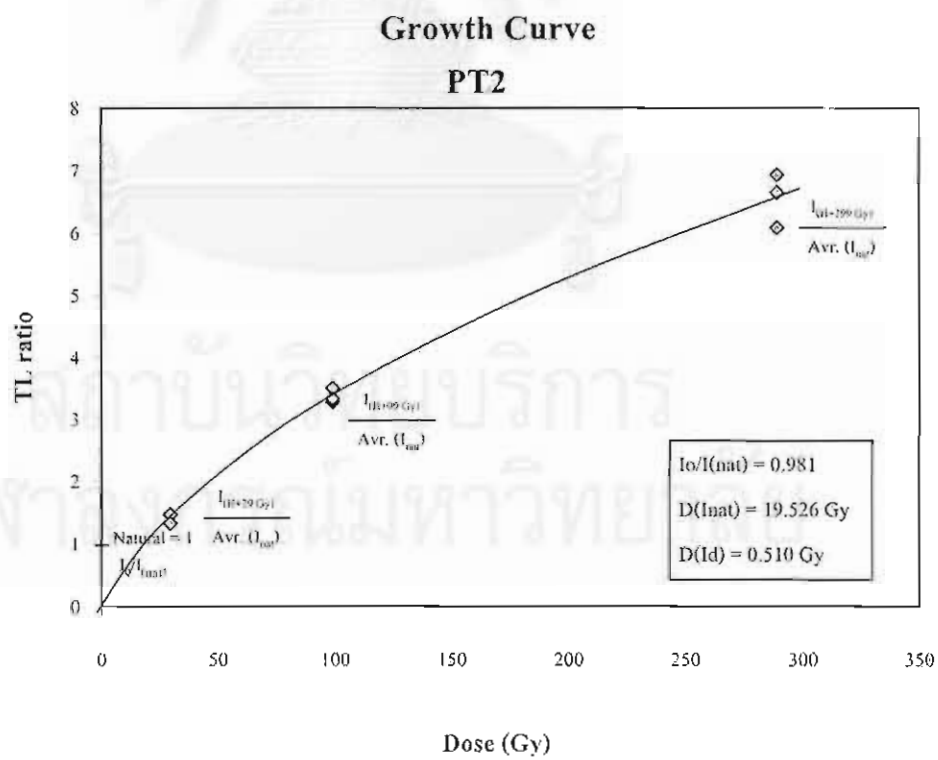
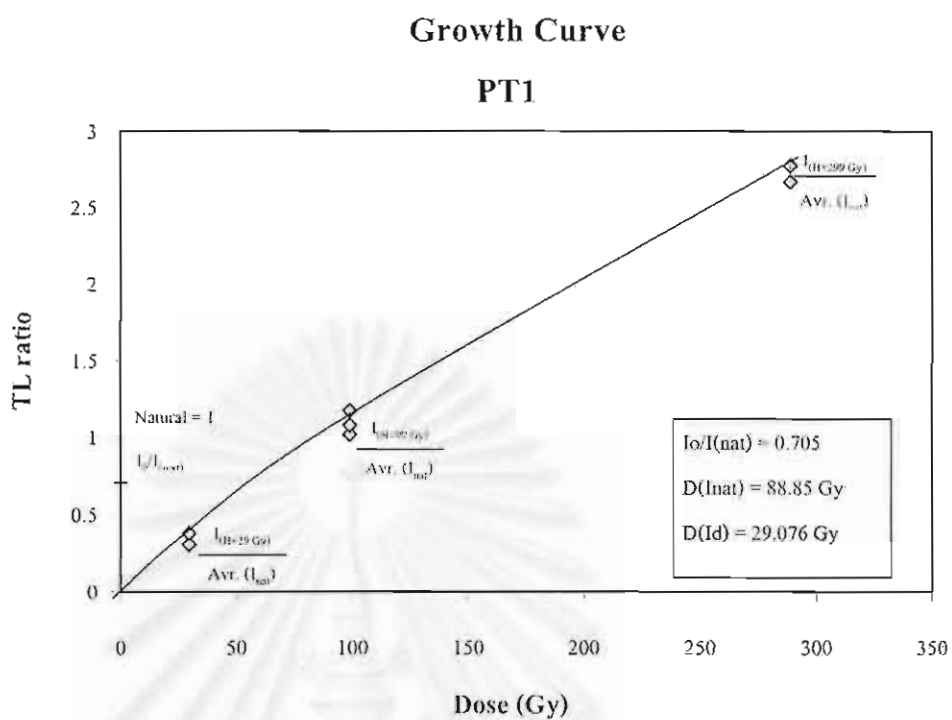


Figure B.2.5 The TL growth curve of sample nos. PT1 and PT2.

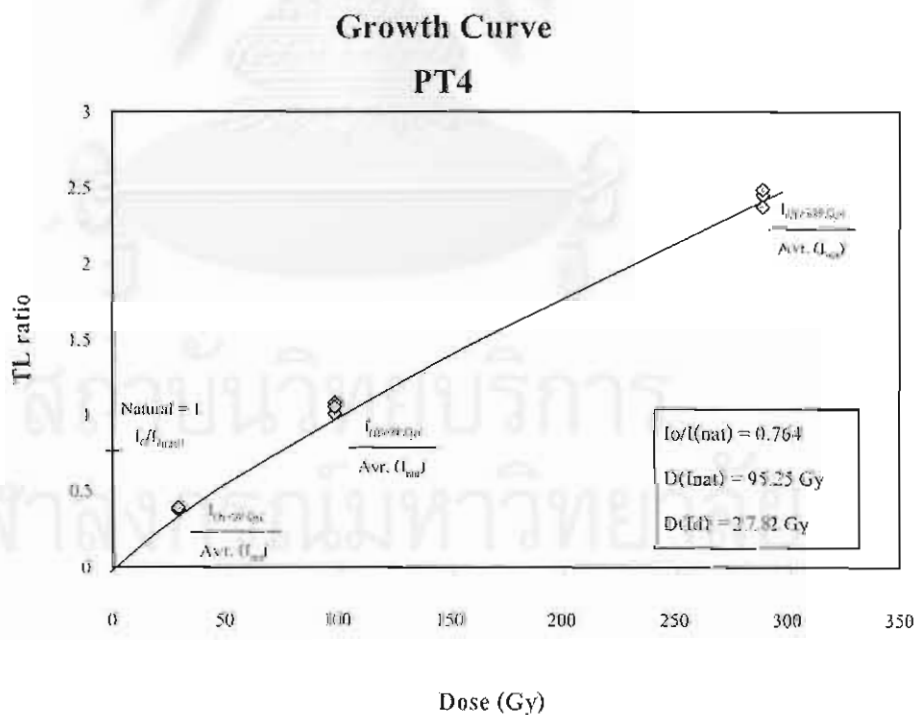
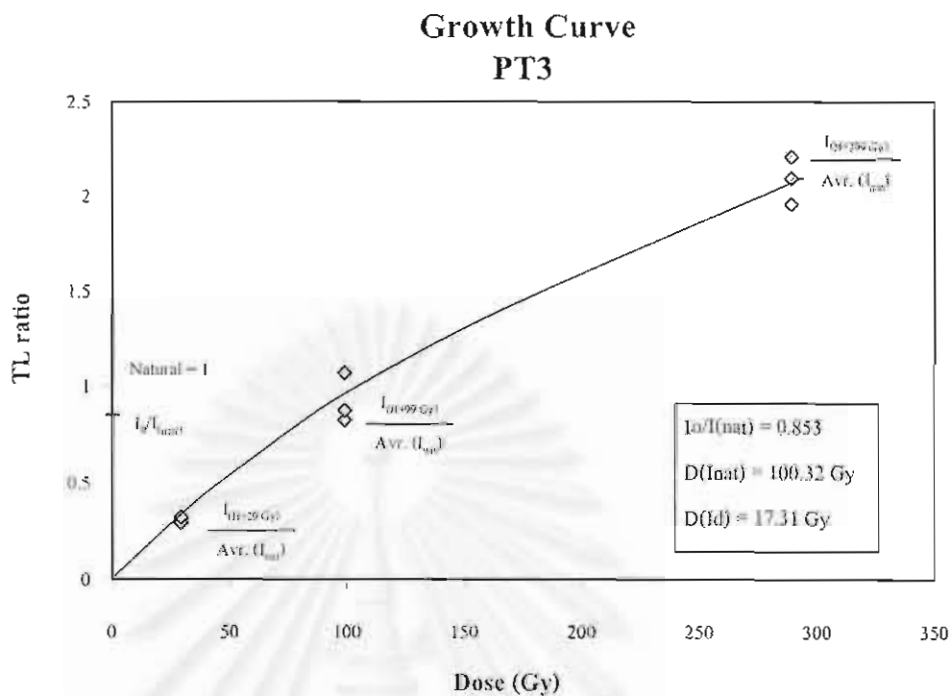
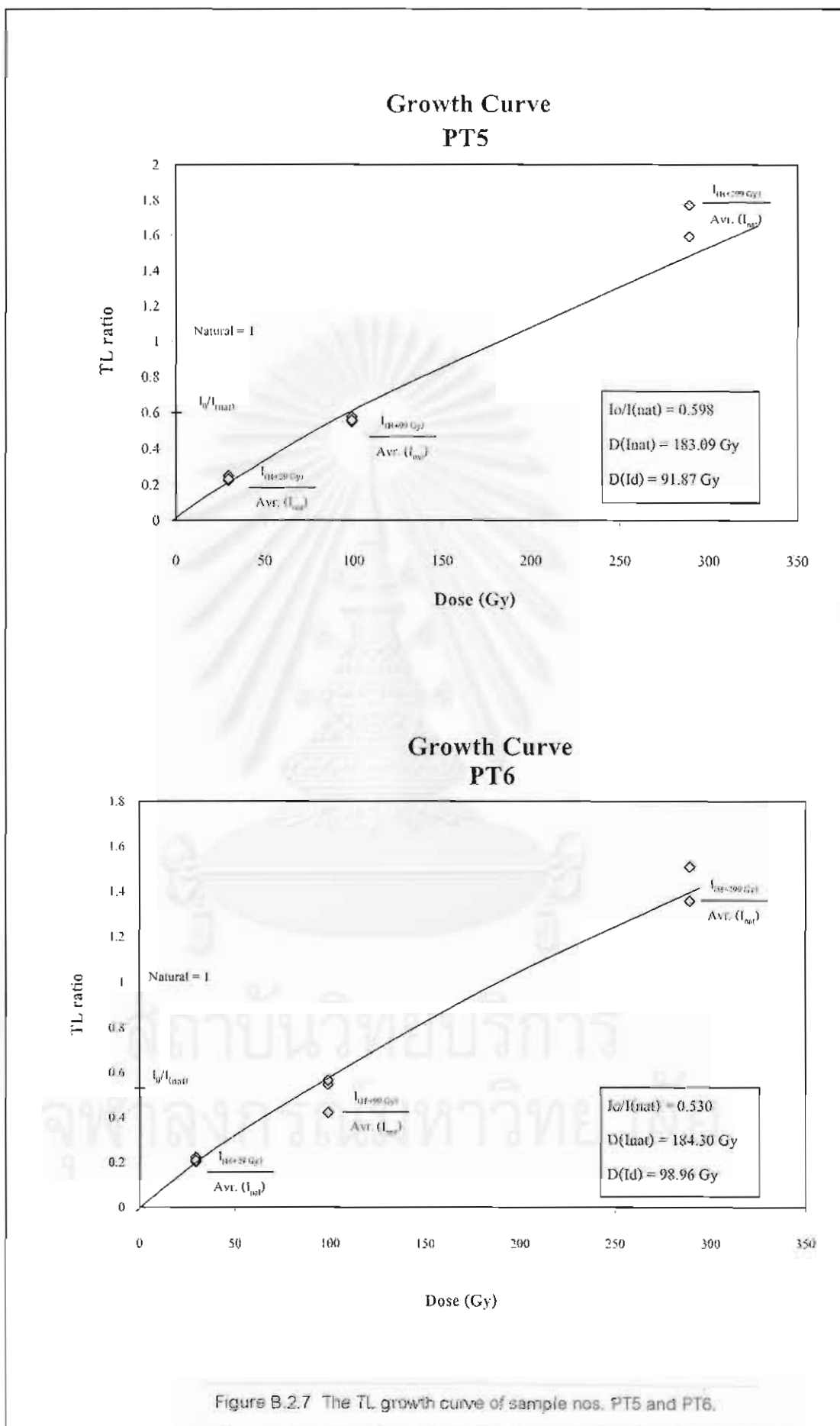
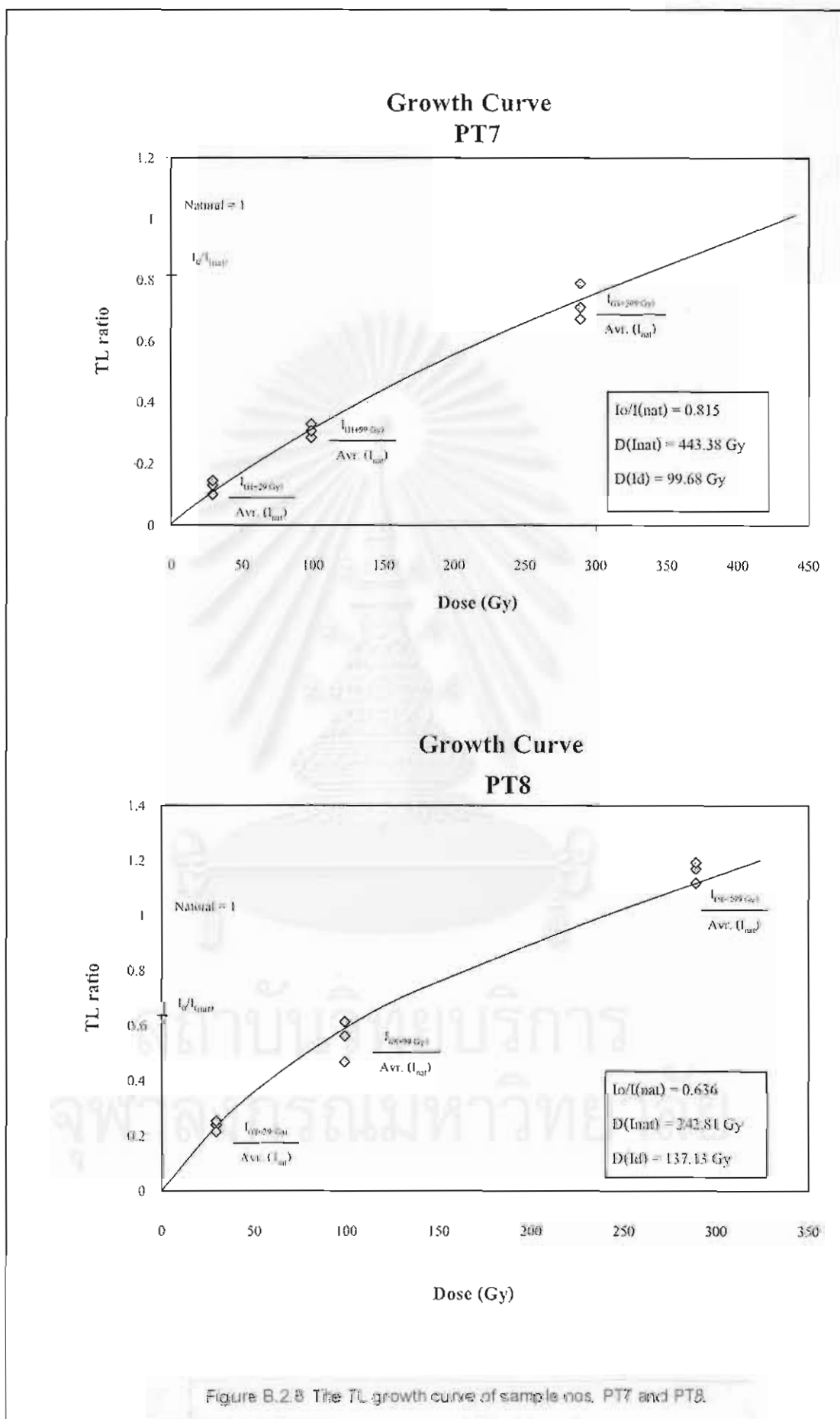
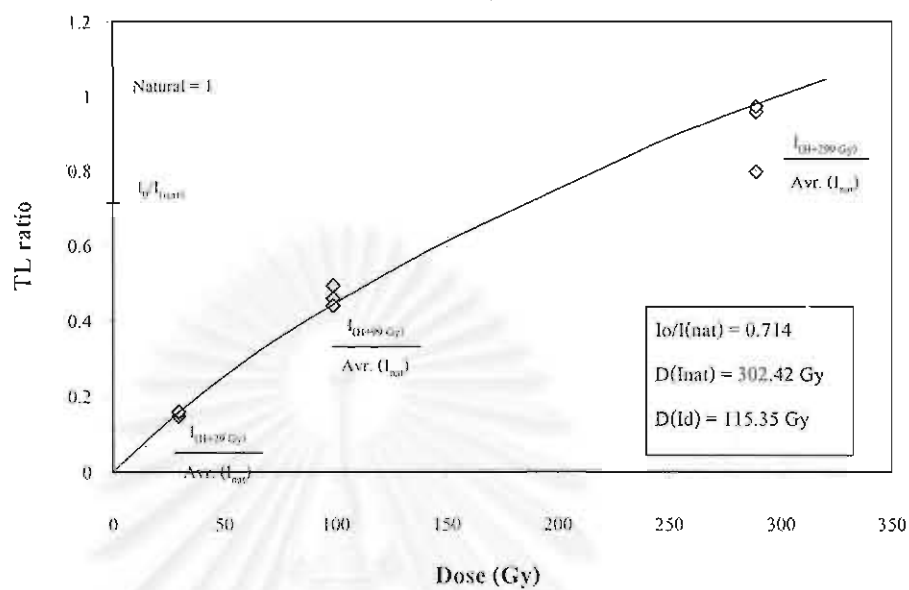


Figure 2.6 The TL growth curve of sample nos. PT3 and PT4.





### Growth Curve PT9



### Growth Curve PT10

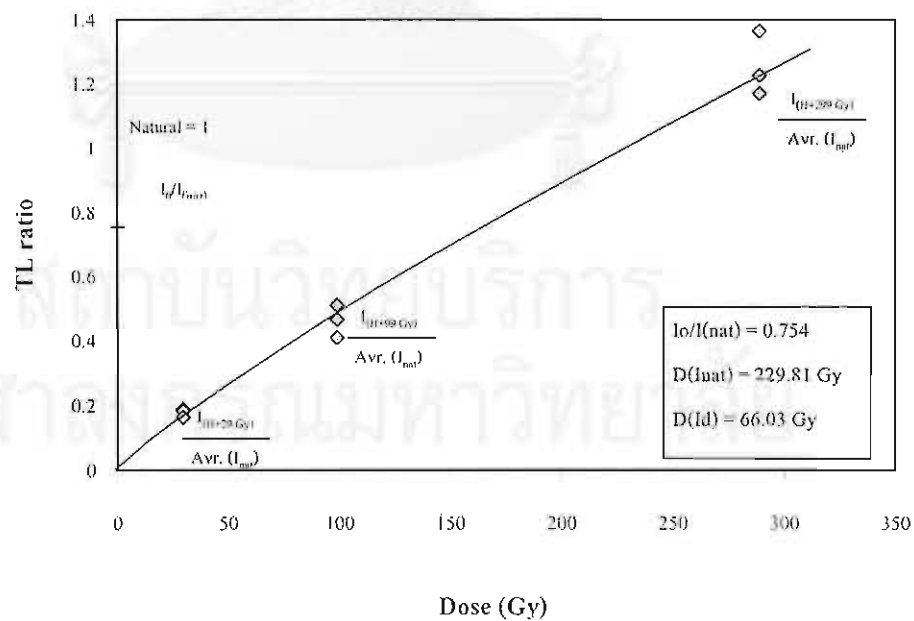


Figure B.2.9 The TL growth curve of sample nos. PT9 and PT10.

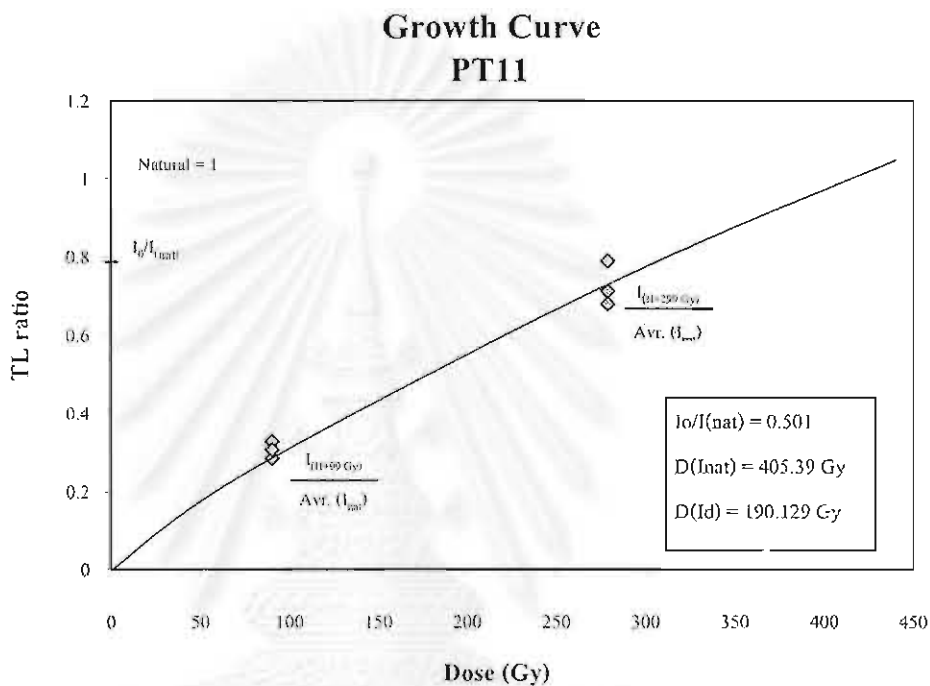
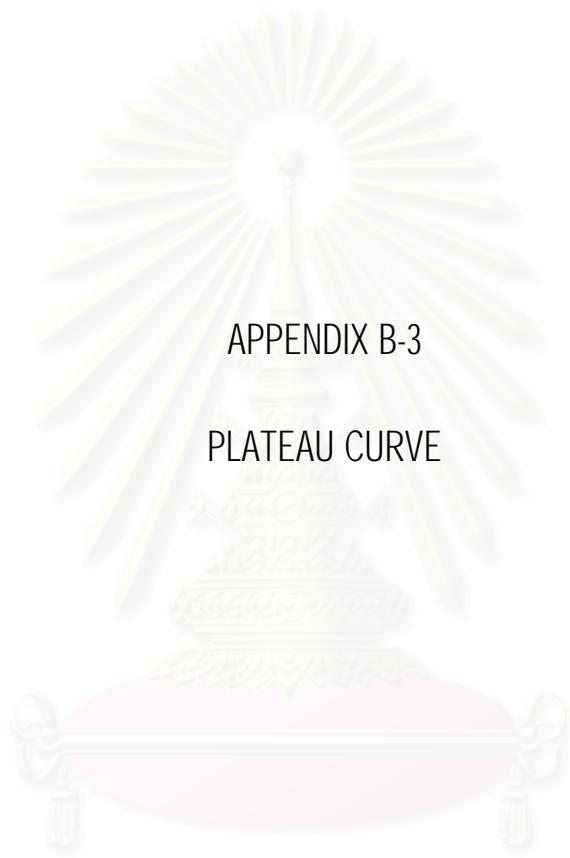


Figure B.2.10 The TL growth curve of sample no. PT11.

สถาบันวิทยบริการ  
จุฬาลงกรณ์มหาวิทยาลัย



APPENDIX B-3

PLATEAU CURVE

สถาบันวิทยบริการ  
จุฬาลงกรณ์มหาวิทยาลัย



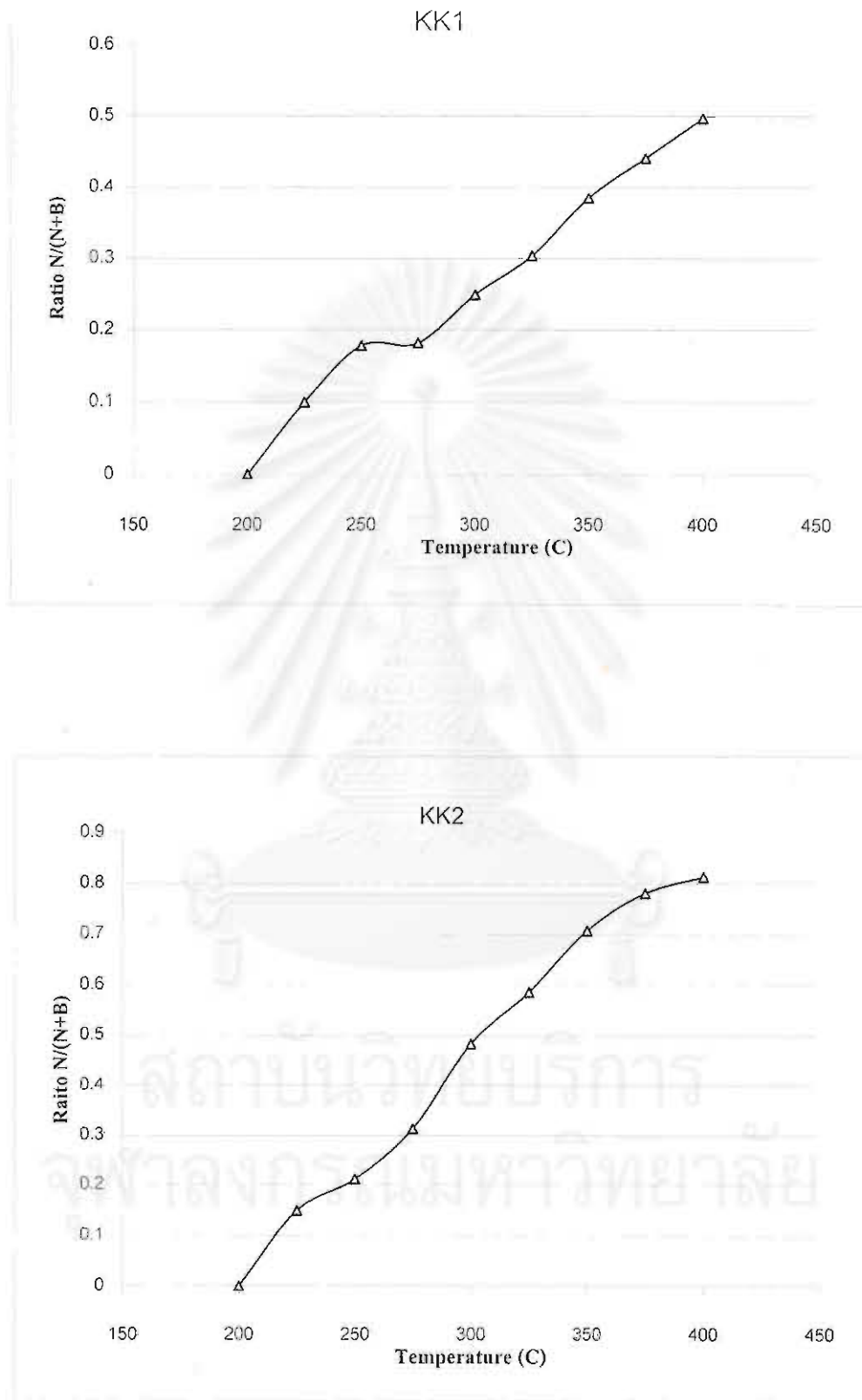


Figure B.3.1 Plateau curve of sample nos. KK1 and KK2.

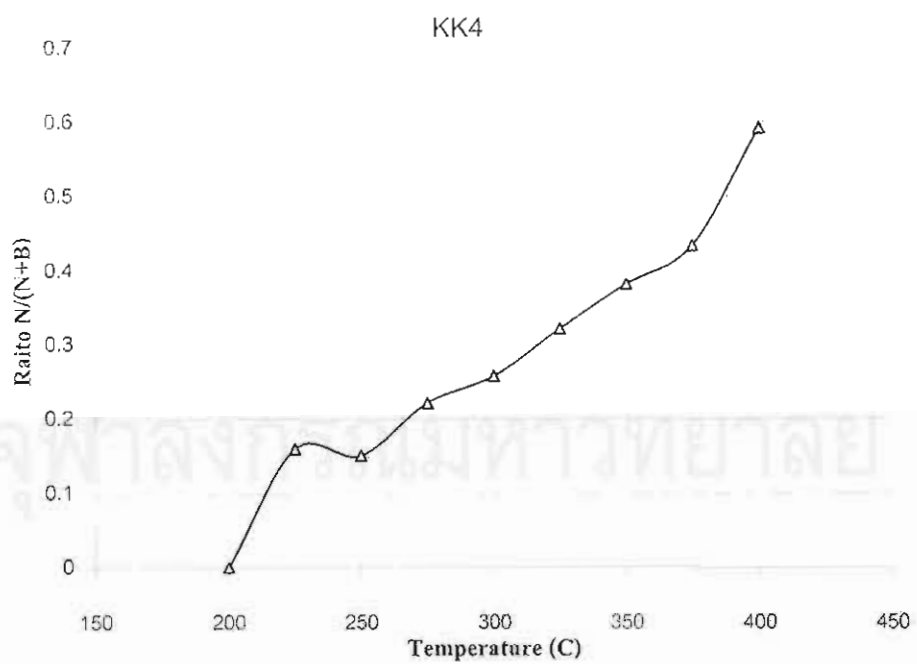
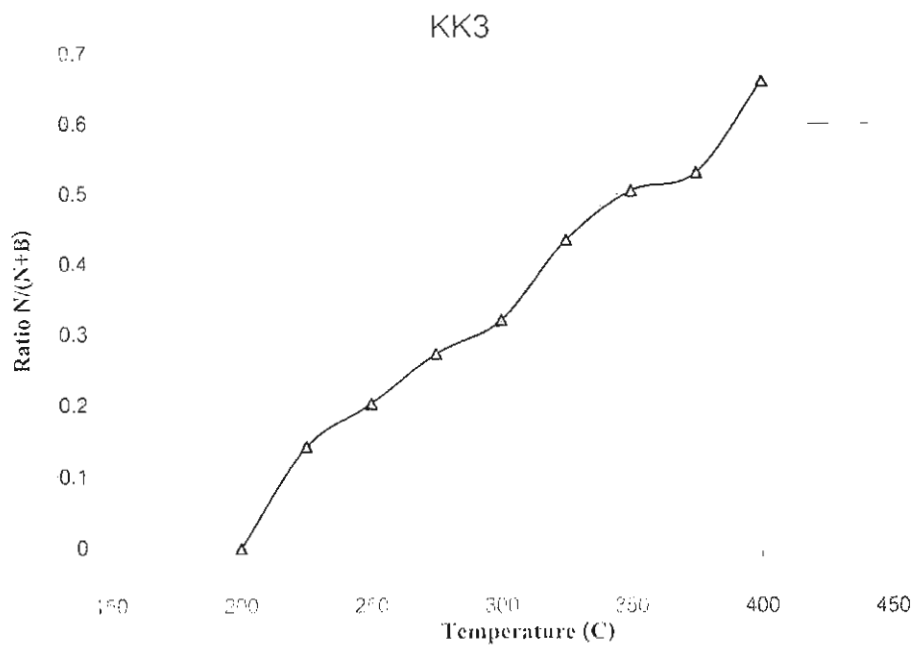


Figure B.3.2. Plateau curve of sample nos. KK3 and KK4.

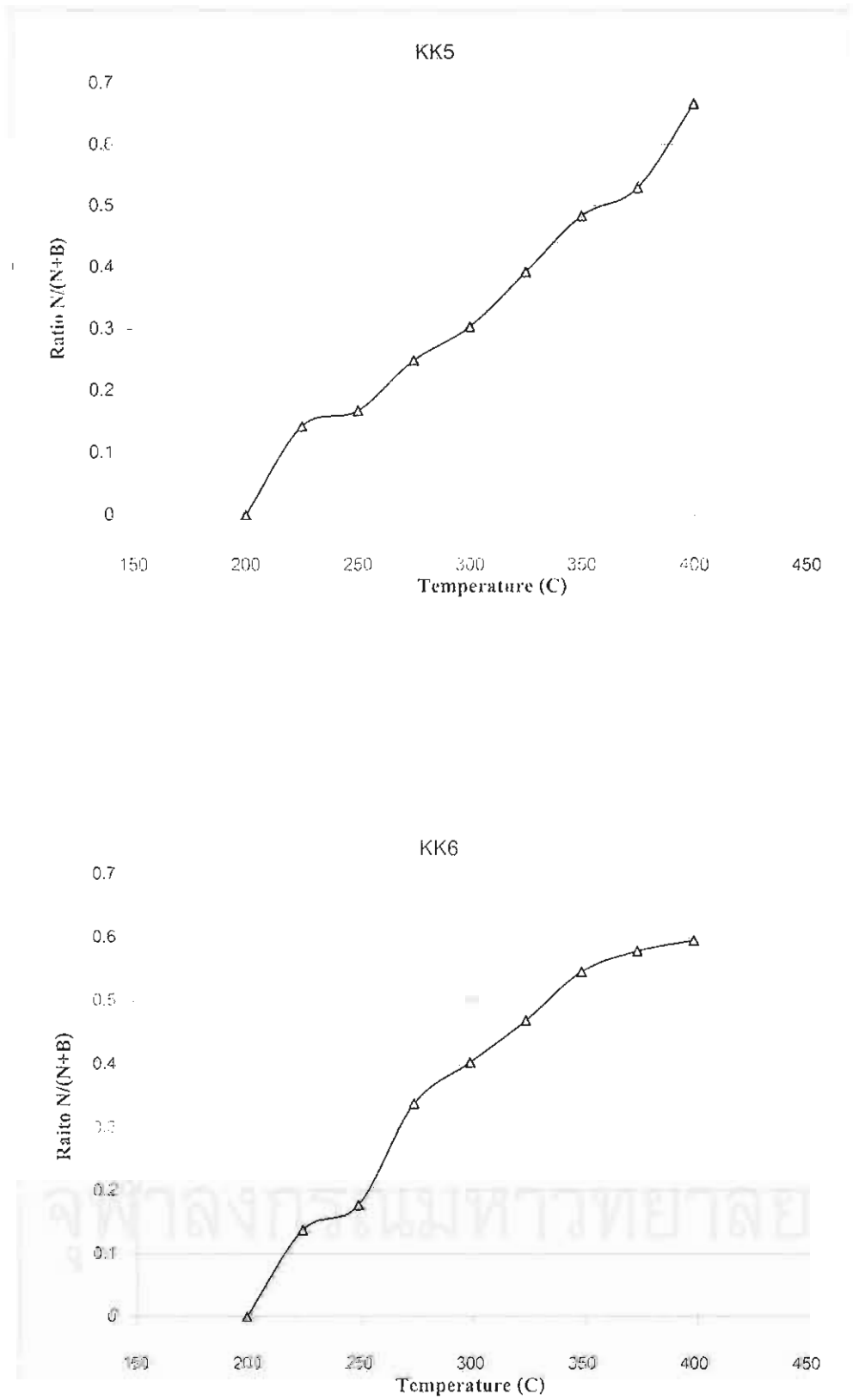


Figure B.3.3 Plateau curve of sample nos. KK5 and KK6.

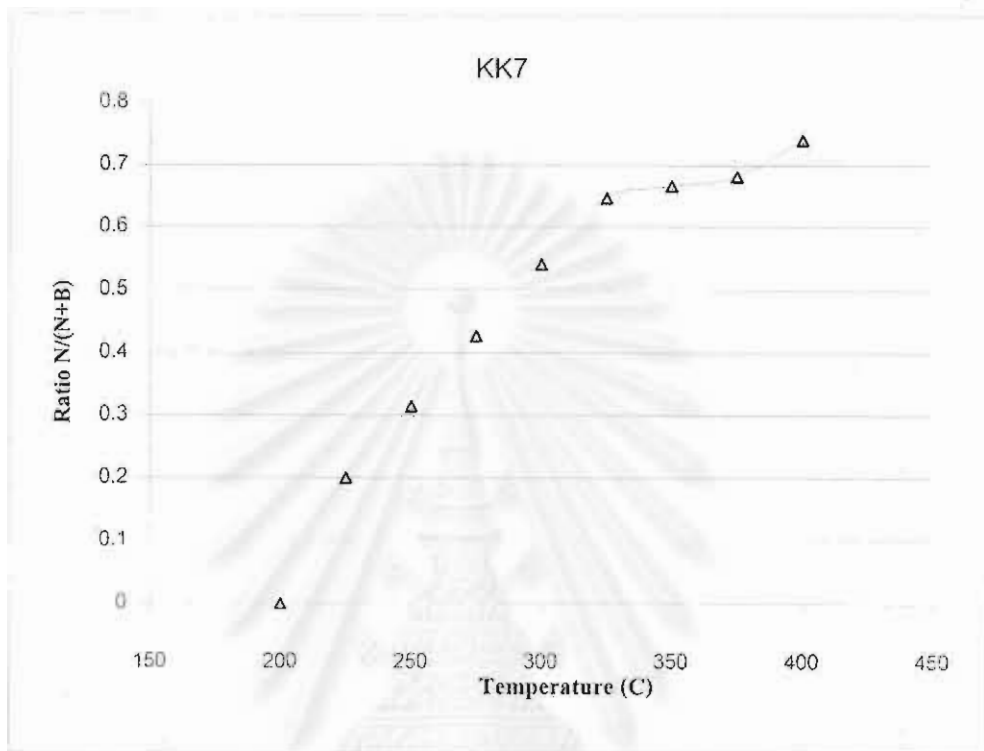


Figure B.3.4 Plateau curve of sample no. KK7.

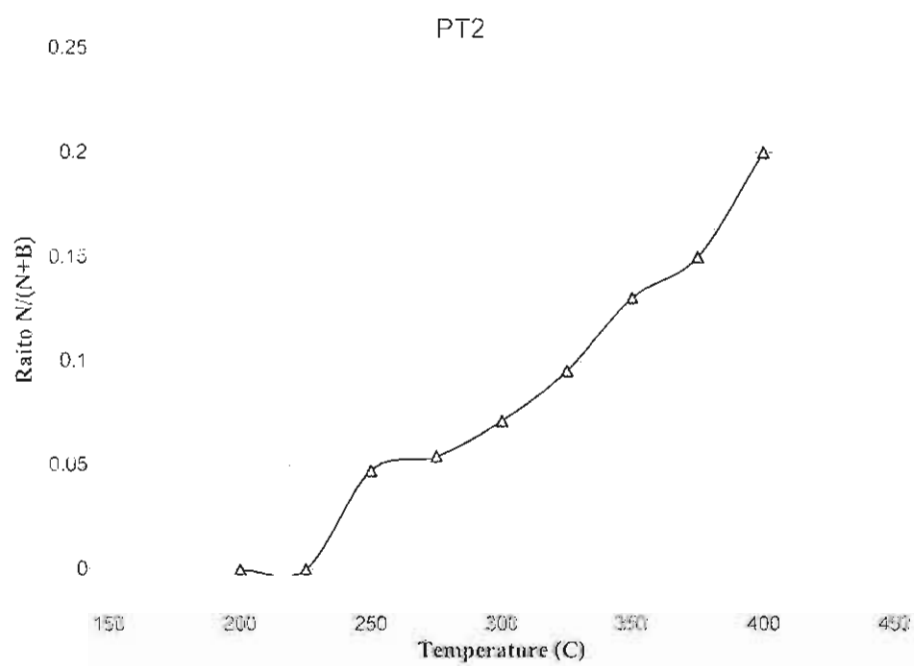
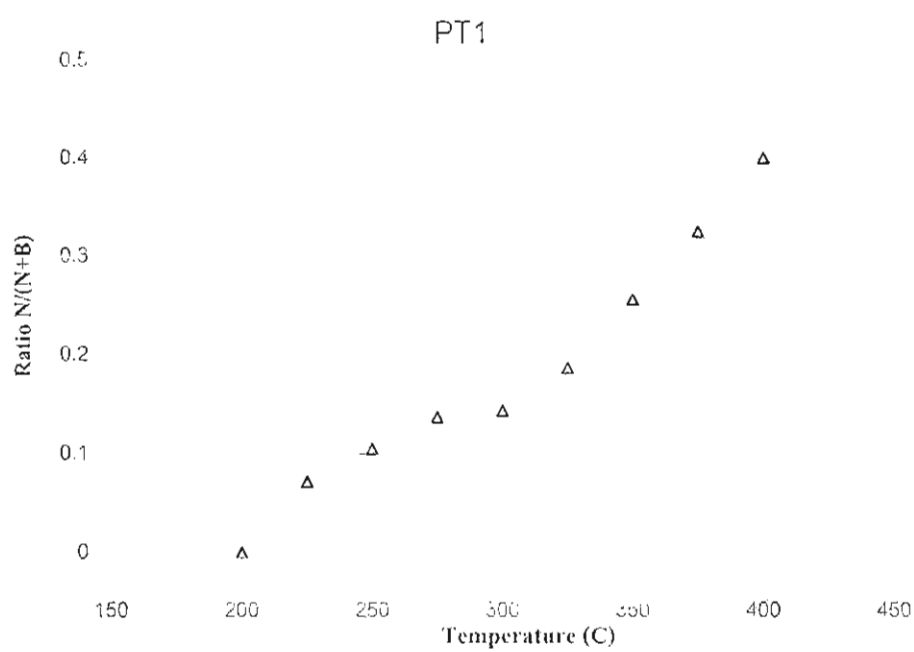


Figure B.3.5 Plateau curve of sample nos. PT1 and PT2.

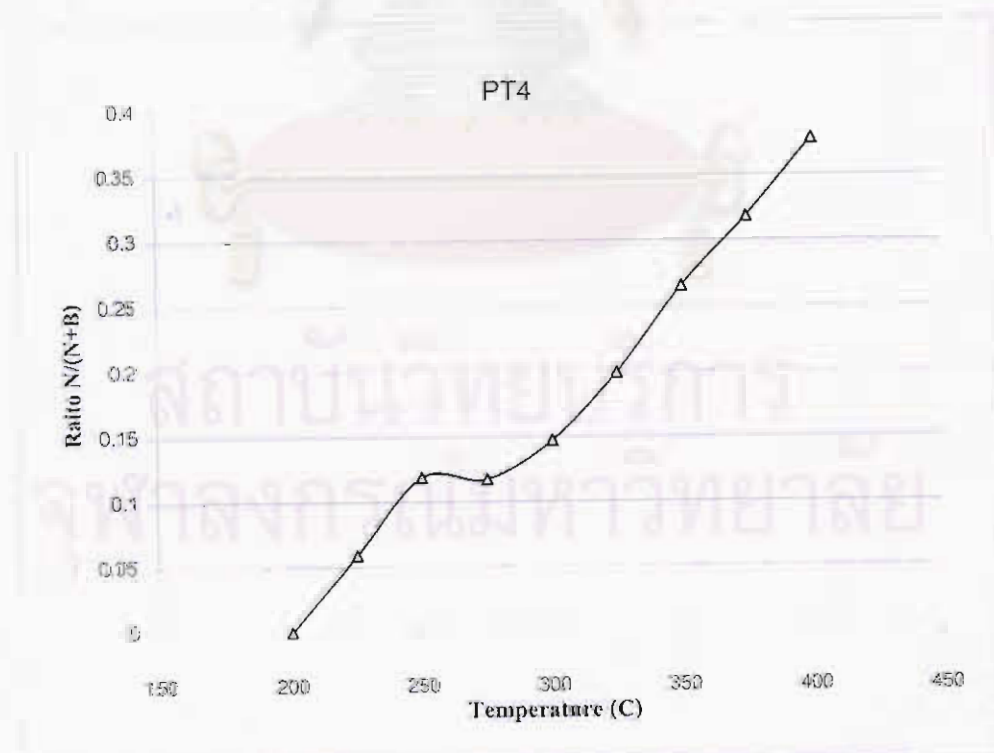
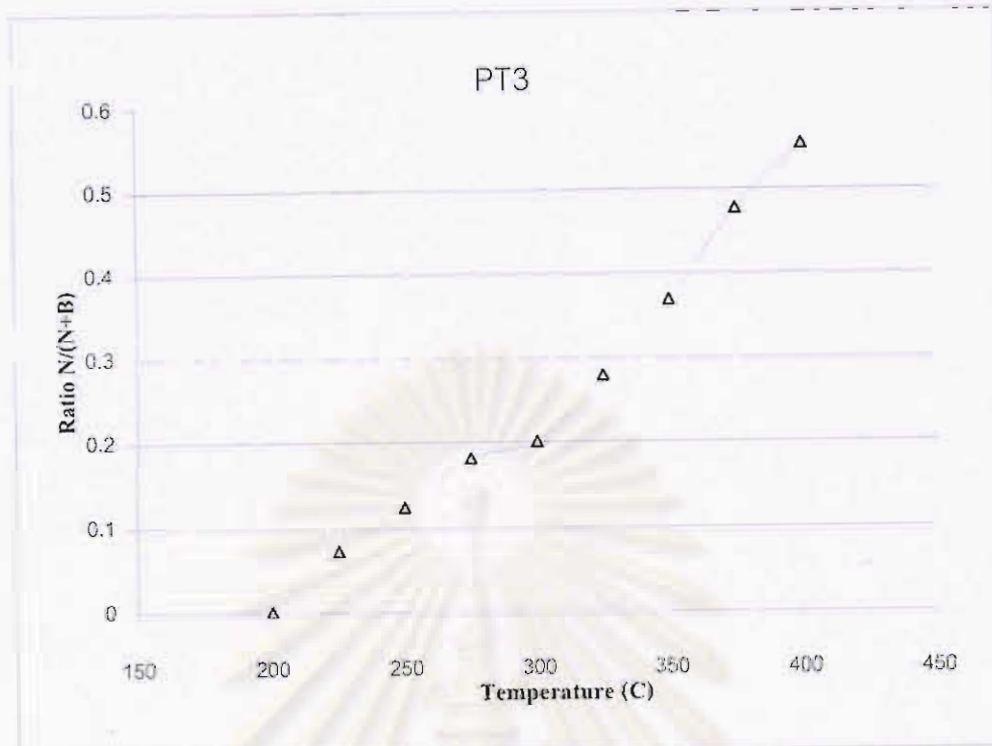


Figure B.3.6 Plateau curve of sample nos. PT3 and PT4.

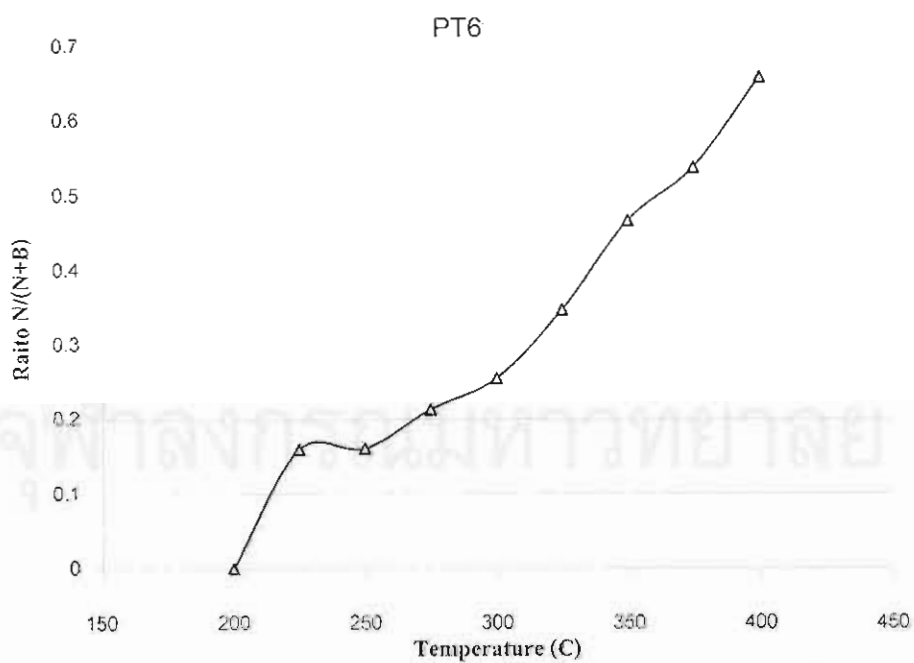
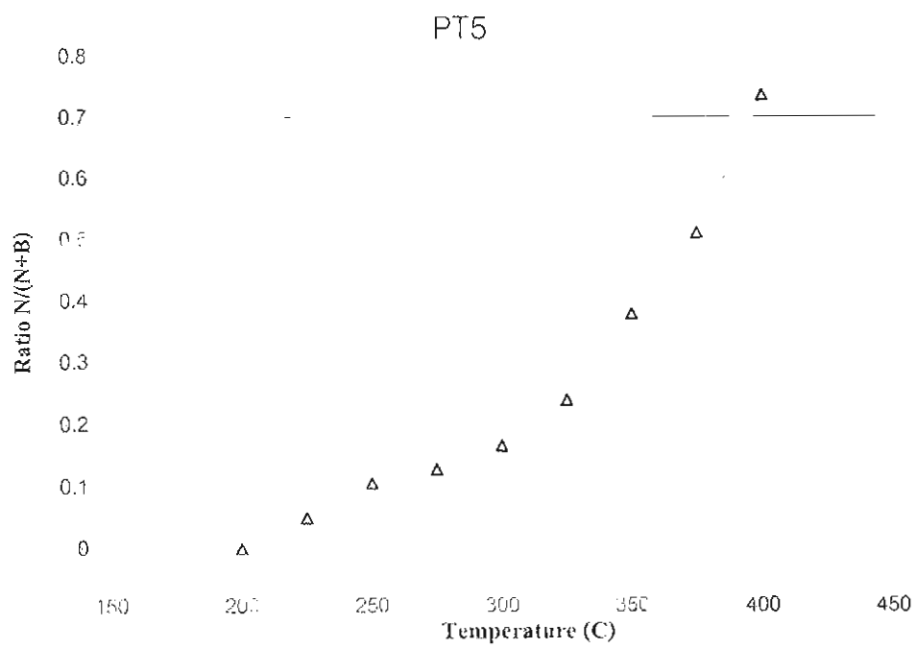


Figure B.3.7 Plateau curve of sample nos. PT5 and PT6.

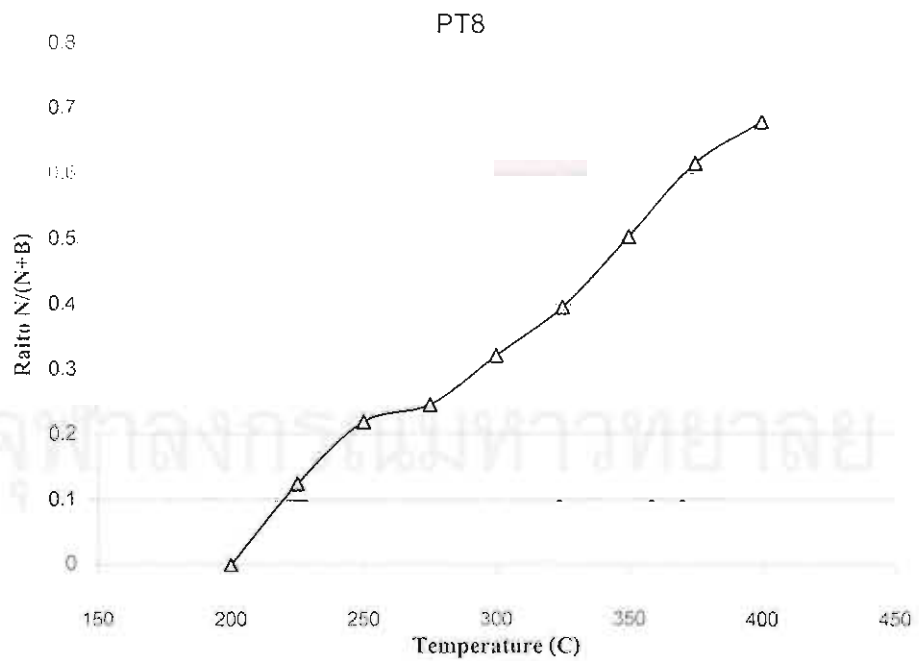
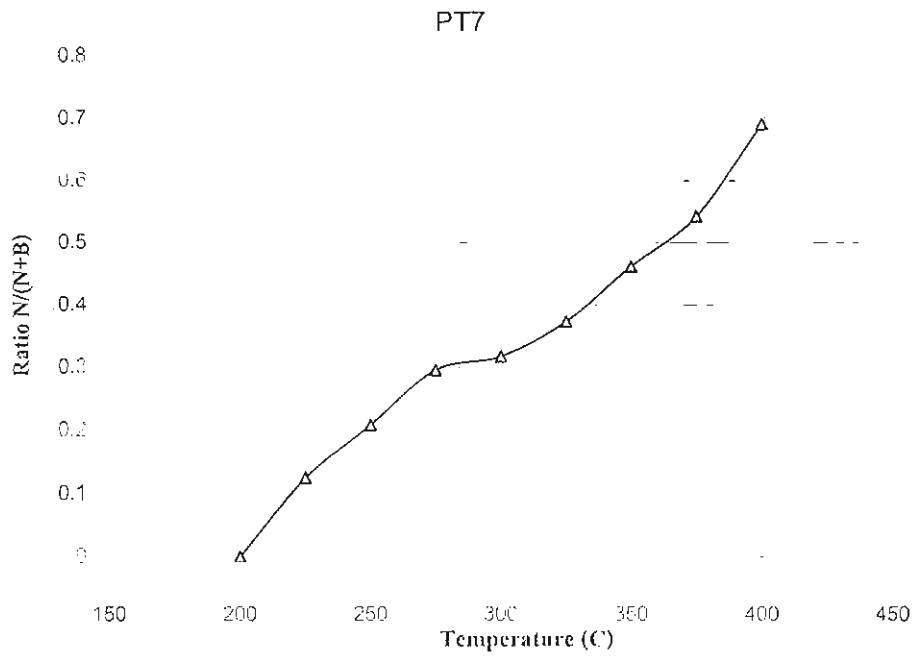


Figure B.3.8 Plateau curve of sample nos. PT7 and PT8.



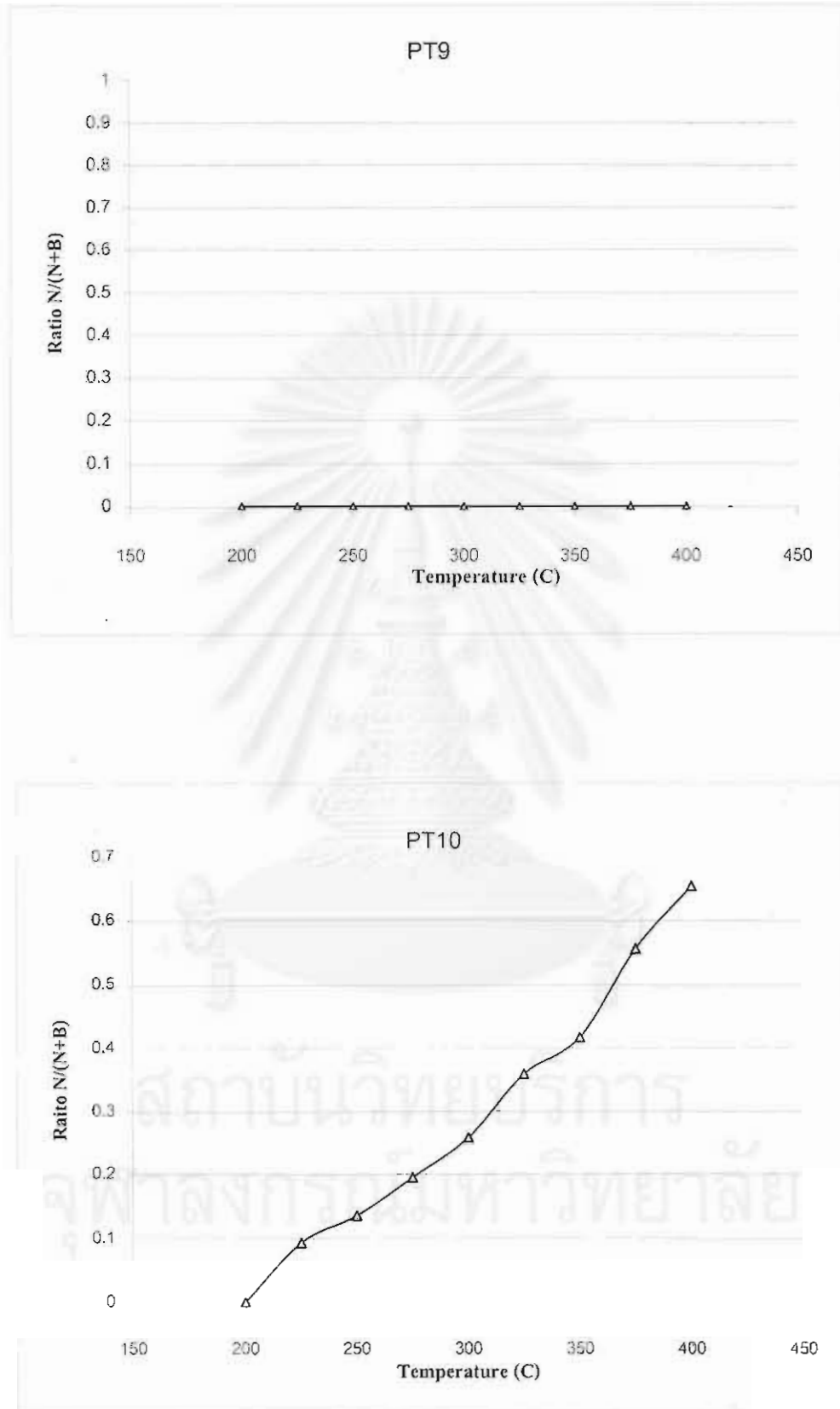


Figure B.3.9 Plateau curve of sample nos. PT9 and PT10.

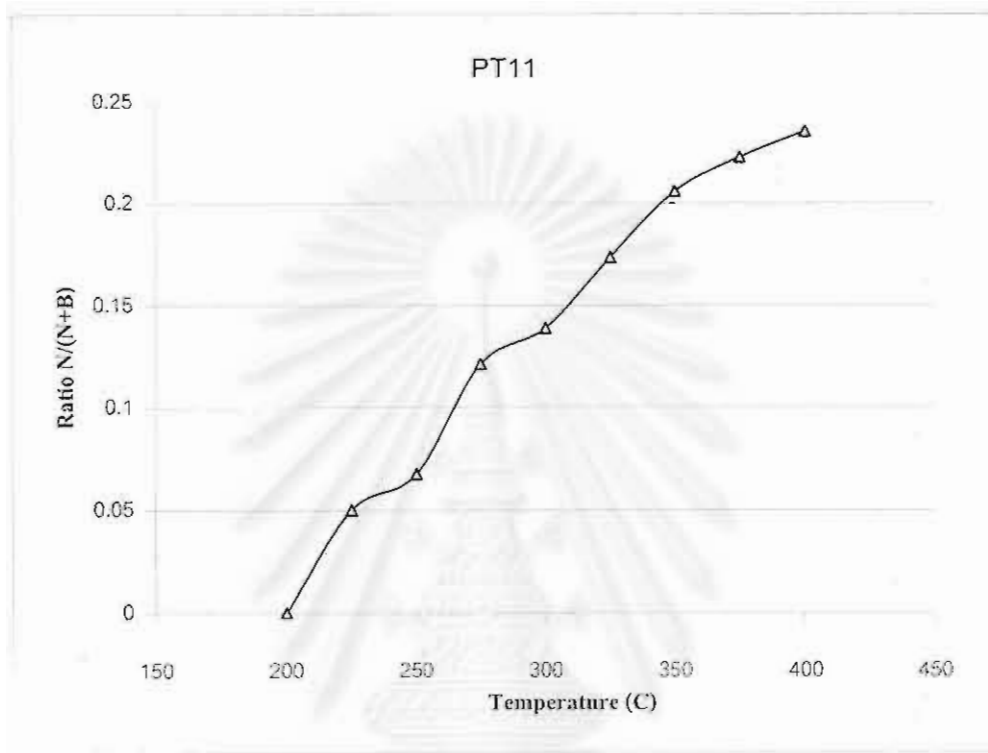
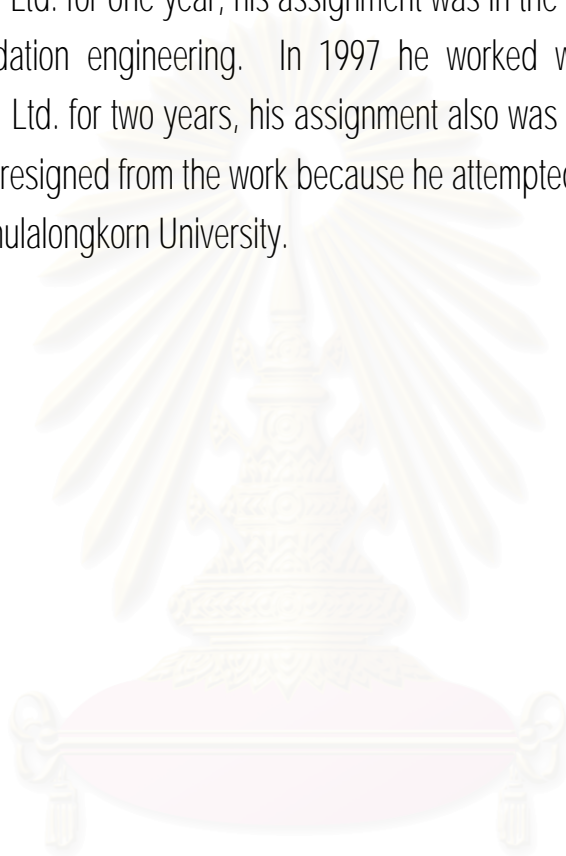


Figure B.3.10 Plateau curve of sample no. PT11.

สถาบันวิทยบริการ

## BIOGRAPHY

Mr. Rutchut Nutthee was born in Changwat Udonthani in 1972. He studied at Udon-Phitayanukul school for the pre-university education in Udonthani between 1985 to 1991. He graduated with the B.Sc. in Geotechnology from Khon Kaen University in 1995. After graduation, he worked with the Universal Engineering Consultants Co., Ltd. for one year, his assignment was in the field of geotechnical works especially foundation engineering. In 1997 he worked with the PBC Engineering Consultants Co., Ltd. for two years, his assignment also was in the field of geotechnical works. Then he resigned from the work because he attempted to study a Master degree in Geology of Chulalongkorn University.



สถาบันวิทยบริการ  
จุฬาลงกรณ์มหาวิทยาลัย